Distribution Agreement

In presenting this thesis or dissertation as a partial fulfillment of the requirements for an advanced degree from Emory University, I hereby grant to Emory University and its agents the non-exclusive license to archive, make accessible, and display my thesis or dissertation in whole or in part in all forms of media, now or hereafter known, including display on the world wide web. I understand that I may select some access restrictions as part of the online submission of this thesis or dissertation. I retain all ownership rights to the copyright of the thesis or dissertation. I also retain the right to use in future works (such as articles or books) all or part of this thesis or dissertation.

Signature:

_____ _____

Cara R. Schiavon Date

ARL2 and ELMOD2: Roles in mitochondrial morphology and localization to Rods and Rings

By

Cara R. Schiavon
Doctor of Philosophy

Graduate Division of Biological and Biomedical Sciences
Cancer Biology

Richard A. Kahn, Ph.D.
Advisor

Lawrence H. Boise, Ph.D.
Committee Member

Anna M. Kenney, Ph.D.
Committee Member

Adam I. Marcus, Ph.D.
Committee Member

Nicholas T. Seyfried, Ph.D.
Committee Member

Accepted:

Lisa A. Tedesco, Ph.D.
Dean of the James T. Laney School of Graduate Studies

Date

ARL2 and ELMOD2: Roles in mitochondrial morphology and localization to Rods and Rings

By

Cara R. Schiavon
B.S., University of Florida, 2013

Advisor: Richard A. Kahn, Ph.D.

An abstract of
A dissertation submitted to the Faculty of the
James T. Laney School of Graduate Studies of Emory University
in partial fulfillment of the requirements for the degree of
Doctor of Philosophy
in Graduate Division of Biological and Biomedical Sciences
Cancer Biology
2018

Abstract

ARL2 and ELMOD2: Roles in mitochondrial morphology and localization to Rods and Rings
By Cara R. Schiavon

The Kahn lab studies the role of ARF family GTPases in the regulation of basic cellular processes. One of my projects focused on ELMOD2, and by extent, ARL2 and their role in mitochondrial dynamics. While studying ARL2, ELMOD2, and mitochondria, I came across an unexpected cellular localization of ARL2 and ELMOD2 which we eventually identified as Rods and Rings (RR). As a result, I developed a second project focusing on the role of ARL2, ELMOD2, and RRs. The results of both projects are described herein.

Mitochondria are essential, dynamic organelles that respond to a number of stressors with changes in morphology that are linked to several mitochondrial functions, though the mechanisms involved are poorly understood. Laura Newman and I worked together to develop a set of plasmids for the expression of ARL2 and other proteins in specific compartments of the mitochondria under varying levels of expression. We also documented changes in the staining intensity of endogenous, mitochondrial ARL2 and ELMOD2 under a variety of growth conditions and stressors. Following up on Laura's work with ARL2 and mitochondria, I determined that ELMOD2 functions in a pathway downstream of ARL2 and upstream of the mitofusins promoting mitochondrial fusion. I also demonstrated evidence of a novel complex at mitochondria composed of ARL2, ELMOD2, the mitofusins, and the miros.

Rods and rings (RRs) are large linear- or circular-shaped structures typically described as polymers of IMPDH. RRs are thought to play a role in the regulation of *de novo* guanine nucleotide synthesis, however, the function and regulation of RRs is poorly understood. I have demonstrated that ARL2, a subset of its binding partners, and several resident proteins at the ER, also localize to RRs. I also have identified two new inducers of RR formation, AICAR and glucose deprivation. I demonstrated that RRs can be disassembled if guanine nucleotides can be generated by salvage synthesis regardless of the inducer. Finally, I showed that there is an ordered addition of components as RRs mature, with IMPDH first forming aggregates, followed by ARL2, and only later calnexin, a marker of the ER.

ARL2 and ELMOD2: Roles in mitochondrial morphology and localization to Rods and Rings

By

Cara R. Schiavon
B.S., University of Florida, 2013

Advisor: Richard A. Kahn

A dissertation submitted to the Faculty of the
James T. Laney School of Graduate Studies of Emory University
in partial fulfillment of the requirements for the degree of
Doctor of Philosophy
in Graduate Division of Biological and Biomedical Sciences
Cancer Biology
2018

Table of Contents

Chapter 1: Introduction

The Kahn lab studies the role of ARF family GTPases in the regulation of basic cellular processes. When I joined the lab, my project was focused on ELMOD2 (an ARL2 GAP, see below) and its role in mitochondrial dynamics. This work built upon previous studies of ARL2 and mitochondria carried out by Laura Newman. While studying ARL2, ELMOD2, and mitochondria, I came across an unexpected cellular localization of ARL2 and ELMOD2 which we eventually identified as Rods and Rings (RRs). As a result, my studies branched into two projects – one focusing on the role of ELMOD2 at mitochondria, and the other on the compositional complexity of RRs. Based upon our studies of ARL2's role at mitochondria and similarities between ARL2 and ELMOD2, I hypothesized that ***ELMOD2 regulates mitochondrial fusion upstream of the mitofusins in the same pathway as ARL2***. The observation that ARL2 and ELMOD2 localize to RRs suggests that RRs are not simple polymers of IMPDH as they are often described, and so, I hypothesized that ***RRs are more complex than previously appreciated with potential links to cell signaling***. Chapter 1 contains relevant background information in relation to ARL2, ELMOD2, mitochondria (particularly mitochondrial morphology), and RRs.

ARL2 and ELMOD2

ARL2 is ancient (predicted to be present in the last eukaryotic common ancestor (1)), very highly conserved, ubiquitously expressed in eukaryotes, and is an essential gene in *S. pombe*, *A. thaliana*, and *C. elegans* (2-4). ARL2 is the only member of the ARF or RAS superfamilies shown to function inside mitochondria. Interestingly, ARL2 is also found in other locations including the cytosol, centrosomes, and the nucleus. Previous work has shown that ARL2 in the cytosol is bound to the tubulin specific co-chaperone cofactor D and is capable of regulating the biogenesis of αβ-tubulin, with expression of mutants causing centrosomal and mitotic spindle defects (5-7). In the nucleus, ARL2 regulates STAT3 signaling (8). ARL2 has also been implicated in the transport of N-myristoylated protein cargos (1,9). The ability of one regulatory GTPase to control distinct essential functions is highly unusual and led us to propose a signaling and integrative function for ARL2 between these roles (10,11).

ARL2 and mitochondria

Alterations in ARL2 activity affect the morphology, motility, and energy metabolism of mitochondria. Expression of a dominant negative ARL2 mutant (T30N) causes mitochondrial fragmentation and perinuclear clustering (10). Conversely, expression of a dominant active ARL2 mutant (Q70L) causes mitochondria to appear more elongated and interconnected (12). ARL2 siRNA also causes fragmentation, the loss of cellular ATP to <50% of controls, and ultimately cell death (10). Other data reveal that ARL2 regulates mitochondrial fusion specifically from the IMS (13). This places ARL2 in a position to interact with OPA1 or MFN1/2 as both are exposed to the IMS and are required for fusion (14,15).

The Chan lab at Cal Tech has generated and analyzed immortalized mouse embryonic fibroblasts (MEFs) deleted for OPA1, MFN1, MFN2, or both MFN1/2. Each of these cell lines has fusion defects and fragmented mitochondria (15-17) (**Figure 1**). Using these lines, we previously showed that ARL2 is acting upstream of the MFNs because the mitochondrial fusion defect seen in *mfn1*$^{-/-}$ and *mfn2*$^{-/-}$ cells is partially rescued by expression of ARL2[Q70L] but is not when both MFNs or OPA1 are deleted. High-resolution structured illumination microscopy (SIM) reveals alignment of ARL2 and MFN1 or MFN2 at puncta that display periodicity in spacing along mitochondria, consistent with their shared actions (13).

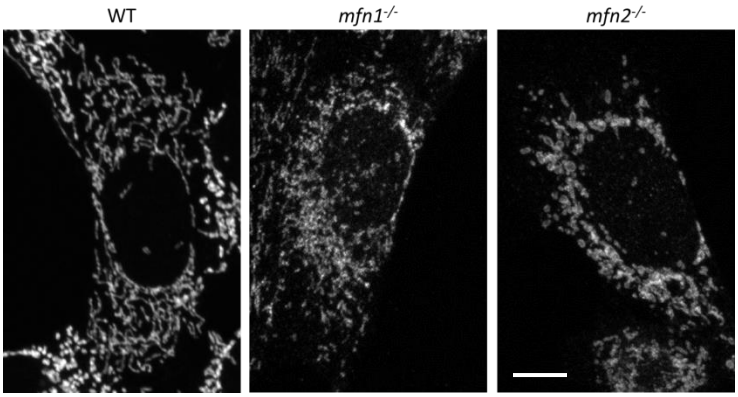

Figure 1: MEFs lacking MFN1 or 2 have fragmented mitochondria. The figure shows MEFs obtained from the Chan lab, fixed and stained for TOM20 (a mitochondrial marker). Scale bar = 10 μm. The wild-

type MEF on the left is from the parent population that was used to generate the MFN1-null (center) and MFN2-null (right) MEFs. MEFs lacking either mitofusin are fragmented compared to the MEFs they were derived from due to fusion defects.

ARL2 and disease

Several lines of evidence suggest a role for ARL2 in response to cellular stress and disease. ARL2 was found to regulate p53 localization, chemosensitivity, and microtubule dynamics in breast cancer cells (18,19). ARL2 also influences breast tumor aggressivity in mice (20). ARL2 is down-regulated by microRNA-16 and microRNA-214 in lung adenocarcinoma and colon cancer respectively (21,22). Four different microRNAs down-regulate ARL2 expression in rat cardiac myocytes leading to a drop in ATP levels and degeneration of mitochondria (23). Two of these microRNAs are up-regulated in cardiac hypertrophy and heart failure (24,25). Also, deletion of the mitochondrial ATP/ADP transporter ANT1 causes muscle wasting and cardiomyopathy in mice (26), and is accompanied by large increases in import of ARL2 into mitochondria, specifically in these affected organs (27).

ELMOD2

Like all regulatory GTPases, ARL2 activity is predicted to be controlled by the actions of guanine nucleotide exchange factors (GEFs), that catalyze exchange of bound GDP for GTP leading to activation of the GTPase, and GTPase activating proteins (GAPs), that speed the hydrolysis of bound GTP and thus GTPase inactivation (**Figure 2**). Effectors are the immediate downstream targets of regulatory GTPases that preferentially bind to the activated form to initiate biological responses and consequently have been the first focus in studies of GTPase-regulated pathways. In the ARF family, GAPs have consistently been found to have effector functions (28). Some examples are ARFGAP2 and ARFGAP3 which function in the formation of COPI-coated vesicles downstream of ARF1 to promote the interaction between COPI and SNARE proteins (29). ELMOD2 was purified in our lab based on its ARL2 GAP activity and found to be a member of a protein family, with three members in humans (30). Mutations in ELMOD1 and

ELMOD3 have been linked to deafness and defects in stereocilia in mice and humans (31,32). To date, there have been few studies on ELMOD2. ELMOD2 has been found to localize to the ER, lipid droplets, and mitochondria (10,33,34). ELMOD2 has been reported to be palmitoylated which regulates its recruitment to lipid droplets (34). It has also been identified as a candidate gene in idiopathic pulmonary fibrosis and the antiviral response (35,36). There are several parallels between the ARL2 and ELMOD2 data which support the model that ARL2 and ELMOD2 can act in a common pathway or even in a complex. ELMOD2 is the only ELMOD protein that localizes to mitochondria (10), and ARL2 is the only ARF family member (out of ~30 in mammals) similarly found in mitochondria. Like ARL2 siRNA, ELMOD2 siRNA causes mitochondrial fragmentation and perinuclear clustering (10). Finally, like ARL2, ELMOD2 is ancient – predicted to be present in the last eukaryotic common ancestor (33).

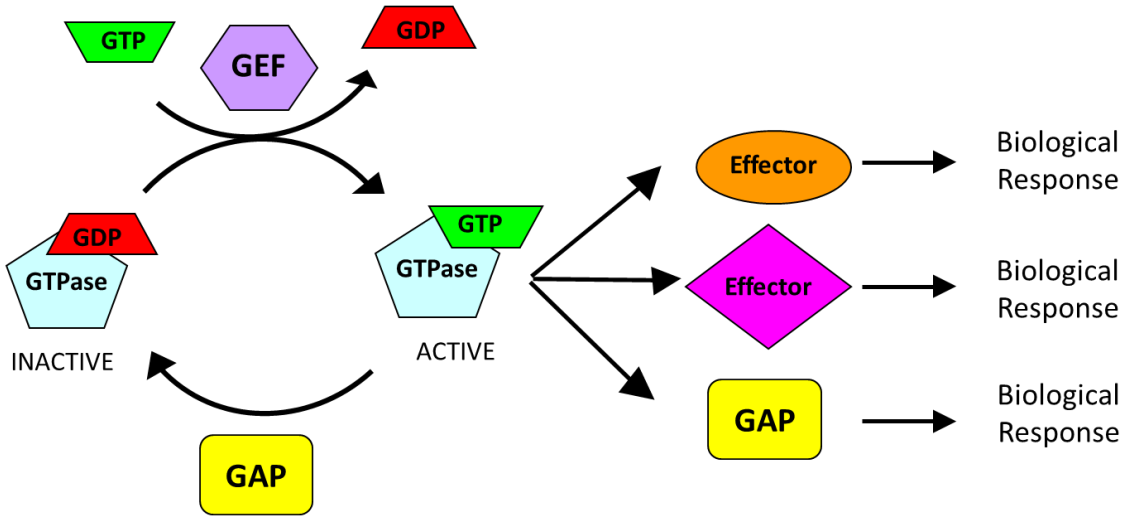

Figure 2: The canonical GTPase cycle. GTPases function as "molecular switches" which cycle between an inactive, GDP-bound state and an active GTP-bound state. The active GTPase interacts with effectors which mediate downstream biological responses. GEFs speed up the exchange of GDP to GTP, converting the GTPase to its active state. GAPs speed the hydrolysis of GTP to GDP, converting the GTPase to its inactive state. Because GAPs interact with the active GTPase, they can also serve as effectors if they mediate a response aside from inactivating the GTPase, as is the case for all ARF GAPs. GEF = guanine nucleotide exchange factor. GAP = GTPase activating protein.

Mitochondrial dynamics

Mitochondria are central to a variety of cellular functions in all eukaryotes, notably the generation of ATP but also maintenance of calcium levels, lipid metabolism, apoptosis, and cell signaling. Mitochondria are highly dynamic organelles capable of changing overall morphology between small, almost spherical organelles to a highly connected, branched network as a result of changes in the rate of mitochondrial fission and fusion (14) and these changes are highly correlated with altered functions (**Figure 3**). Mitochondrial fusion occurs to boost ATP production (37,38) and is also important for mixing of mtDNA and other mitochondrial contents (15,39-41) which is necessary to maintain the homogeneity of the mitochondrial network. On the other hand, mitochondrial fission is necessary for efficient traffic of mitochondria within the cell (42), proper distribution of mitochondria into daughter cells during mitosis (43), apoptosis regulation (44), and removal of dysfunctional mitochondria by mitophagy (45).

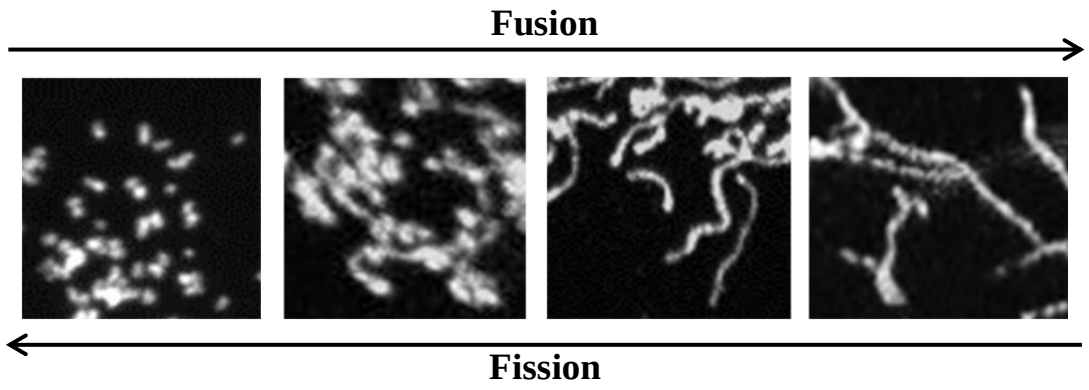

Figure 3: Examples of variation in mitochondrial morphology. Cropped images of MEF mitochondria fixed and stained for HSP60 (a mitochondrial marker protein) are pictured. The mitochondria appear increasingly tubular from left to right. Tubulation results from an increase in the rate of fusion or a decrease in the rate of fission while the opposite is true for fragmentation.

The key proteins involved in control of mitochondrial morphology are all GTPases; the two mitofusins MFN1/2, OPA1 (optic atrophy 1), and DRP1 (dynamin-related protein 1), though details of

their actions are all incomplete (**Figure 4**). MFN1/2 are essential for outer mitochondrial membrane (OMM) fusion by tethering apposing mitochondria (16,46,47). MFN1/2 are large GTPases that localize to the OMM and their activity is dependent on their oligomerization both in *cis* (within the same mitochondrion) and *trans* (across mitochondria) (47,48). MFN1 has more fusogenic activity *in vitro* (49), while MFN2 has been found to have additional signaling functions as well as tethering to the ER (17,50-53). OPA1 is necessary for inner mitochondrial membrane (IMM) fusion (54). Conversely, Drp1 is required for mitochondrial fission (55). Loss or mutation of any of these proteins has been linked to altered morphology, functions, and human diseases. While roles for each of these large GTPases in mitochondrial biology are established, the mechanisms by which they act are incompletely understood and the means of regulating them even less so.

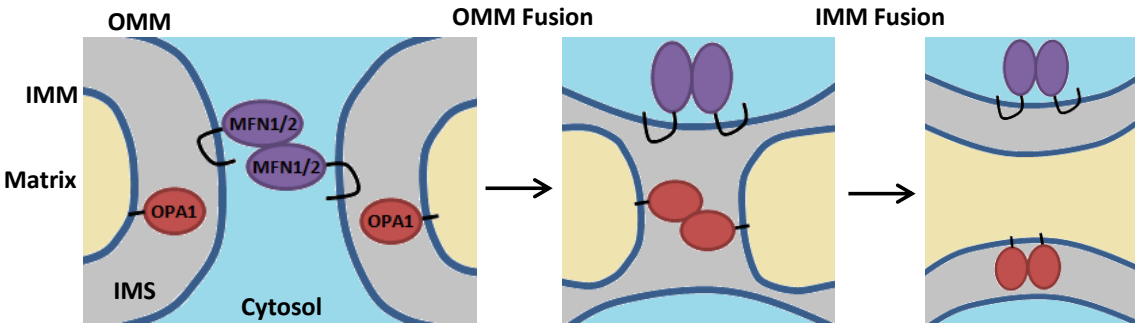

Figure 4: A simplified schematic of mitochondrial fusion. First, MFN1/2 homo- or hetero-oligomerize, leading to fusion of the OMM. Then, fusion of the IMM is mediated by OPA1. OMM = Outer mitochondrial membrane. IMM = Inner mitochondrial membrane. IMS = Intermembrane space.

Mitochondria also move about within the cell. Mitochondria primarily move along microtubules although they have also been reported to move along actin filaments and interact with intermediate filaments (56). Attachment to microtubules is mediated by two more GTPases, Miro1 and Miro2 which localize to the OMM, and the adapter protein Milton (57). Milton interacts with kinesins responsible for plus-end directed motility (58). Minus-end directed motility is carried out by dyneins and dynactin (59).

Regulation of mitochondrial dynamics

Few proteins have been found to regulate the key players in mitochondrial fusion. MIB interacts with MFN1 and negatively regulates its activity, however, the mechanism is unknown (60). Bax and SMAD2 stimulate MFN2 activity, but not MFN1 (61,62). The MFNs are also regulated by post-translational modifications. They form disulfide bonds which promote oligomerization and fusion during oxidative stress (63). They can also be ubiquitinated by Parkin during mitophagy, leading to their degradation and decreased fusion (45). MFN1 can also be phosphorylated during apoptosis leading to mitochondrial fragmentation (64), or deacetylated during glucose starvation to promote fusion (65). All of these regulatory mechanisms occur from the cytosolic face of the OMM. OPA1 is regulated by proteolytic cleavage. Cleavage by OMA1 leads to inactivation of OPA1 (66-68), while YME1L cleavage results in a cleaved form of OPA1 that promotes fusion (37,69). Mitochondrial fission occurs by recruitment of DRP1 to the OMM. DRP1 is primarily recruited by MFF but can also be recruited by FIS1, MiD49, and MiD51 (70-73). DRP1 activity is regulated by phosphorylation which can either activate or deactivate DRP1 depending on the site of phosphorylation (43,74). The ER makes contacts with the mitochondria at future sites of DRP1 recruitment and fission (75). Actin also accumulates at these sites (76), suggesting a role for the ER and actin in the events leading to mitochondrial fission. Finally, the Miros are regulated by local calcium concentration (77).

Mitochondria and disease

Mitochondrial dysfunction is associated with a broad range of human diseases. Various cardiomyopathies have been linked to dysfunctional mitochondria. Deregulation of OPA1 (78) or MFN2 (79) causes cardiomyocyte apoptosis and heart failure while a mutation in or conditional knockout of DRP1 causes dilated cardiomyopathy in mice (80) and knock-out of MFN1 and MFN2 caused eccentric hypertrophy (81). Mitochondria are also important for neurological function. Mitochondrial dysfunction is linked to a range of neurodegenerative diseases (82) particularly Parkinson's disease (83). Mutations in

MFN2 lead to Charcot-Marie Tooth syndrome (84) and mutations in OPA1 cause dominant optic atrophy (85). Finally, alterations in mitochondrial morphology and function effecting cellular metabolism, proliferation, and apoptosis have been associated with cancer (74,86,87).

Rods and Rings

As mentioned previously, I discovered that ARL2 and ELMOD2 localize to structures termed Rods and Rings. RRs are linear- or circular-shaped cellular structures whose only currently known components include enzymes involved in *de novo* nucleotide biosynthesis. Interest in RRs peaked when it was discovered that patients being treated for hepatitis C with certain antiviral therapies (a combination of Ribavirin and interferon-α) developed autoantibodies against RRs (88,89). RRs are highly variable in shape including the most common rod shape, circles/ovals, and intermediate shapes including curves, lassos, and figures-eights (**Figure 5**). It has been proposed that RRs are capable of interconverting between these shapes, however, this has never been directly observed. RRs can be observed anywhere in the cytosol although they are typically in the center of the cell (*i.e.*, not necessarily at the cell surface) and can commonly be observed next to or even inside the nucleus. There are typically 1-2 RRs per cell, however, the quantity is highly dependent on cell type and growth conditions.

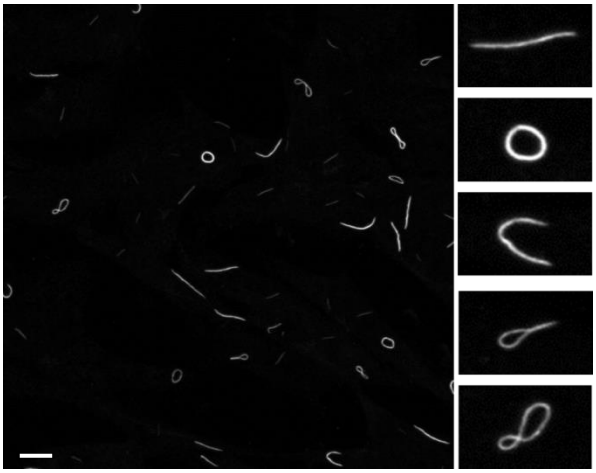

Figure 5: RR location, size, and shape variability. MEFs treated with MPA and stained for IMPDH2 are pictured. The larger image to the left shows a field of cell (scale bar = 10μm) while the smaller images

to the right show close-ups of RRs of various shapes (rod, ring, curve, lasso, figure-eight). Rods are the most common shape.

IMPDH

By far the most commonly identified component of RRs is IMPDH (inosine-5'-monophosphate dehydrogenase) (88,90-92). IMPDH catalyzes the conversion of IMP to XMP, the rate-limiting step in the *de novo* synthesis of guanine nucleotides (**Figure 6**). In addition to localization at RRs, inhibition of IMPDH with drugs such as Ribavirin (one of the antivirals mentioned above) or MPA (mycophenolic acid - a commonly used immunosuppressant to prevent organ transplant rejection) causes a dramatic increase in the quantity and size of RRs (88,90,93-96) , strongly implying a relationship between RR formation and IMPDH activity, and consequently guanine nucleotide metabolism. This is further supported by the fact that addition of guanosine to cell cultures results in the prevention of MPA-induced RRs and losses of RRs in cell lines that normally display them in the absence of drug (95,97). There are two isoforms of IMPDH in mammals, IMPDH1 and IMPDH2. IMPDH1 and 2 share 84% sequence identity and both have been found at RRs (98). The function of IMPDH is very highly conserved as nucleotide biosynthesis is essential. RRs are also highly conserved as they have been observed in a wide variety of cell types and species. In fact, RRs have been observed in every cell line tested to date including various human cancer cell lines (88,90,99,100), MEFs (88), rat retina (98), CHO (98), primary cardiomyocytes (88), rat neurons (101), mouse embryonic stem cells (88), *S. cerevisiae* (102), *D. melanogaster* (102,103), and several types of bacteria (104).

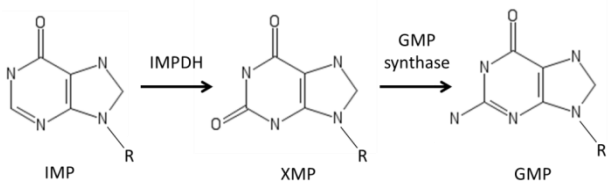

Figure 6: IMPDH catalyzes the rate-limiting step in *de novo* guanine nucleotide synthesis. IMPDH (inosine monophosphate dehydrogenase) catalyzes the conversion of IMP (inosine monophosphate) to

XMP (xanthosine monophosphate). This is the rate-limiting step in the *de novo* synthesis of guanine nucleotides. XMP is then converted to GMP (guanosine monophosphate) by GMP synthase. GMP can then be converted to GDP and GTP (guanosine di- and triphosphate).

Inducers of RRs

As previously mentioned, the quantity and size of RRs varies widely depending on growth conditions and drug treatments. The IMPDH inhibitors Ribavirin and MPA are the most commonly reported inducers of RR formation (88,90,93-96) (**Figure 7**) but other drugs also increase the quantity of RRs; including the cytidine triphosphate synthase (CTPS) inhibitors 6-diazo-5-oxo-L-norleucine (DON) and Acivicin (88,93,95). CTPS is also central to nucleotide metabolism as it catalyzes the rate-limiting step in the conversion of UTP to CTP. Glutamine deprivation also increases the formation of RRs (95). RR formation is typically rapid but the time course is dependent on the method of induction. RRs can usually be observed within an hour of most treatments and peak (*i.e.*, at or near 100% of cells have visible RRs) within 24hr (88,94). IMPDH inhibitors are particularly potent, with all cells displaying large RRs by 4hr (88,94). The formation of RRs can also be reversed or prevented by the addition of guanosine either during or following drug treatment or by removal of the drug. Disassembly of RRs is also quite rapid with complete elimination of RRs 1hr after addition of guanosine (95,97). This reversal upon addition of guanosine is further evidence of the relationship between RR formation and guanine nucleotide pools.

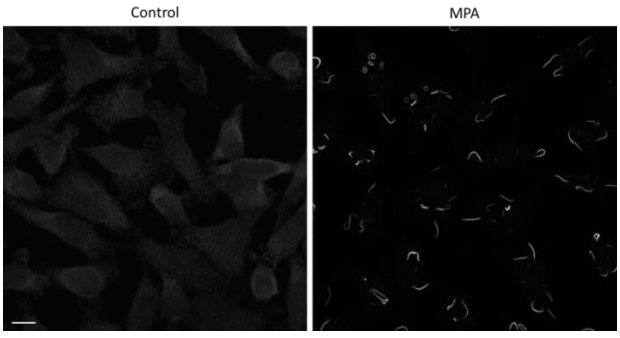

Figure 7: MPA robustly triggers the formation of RRs. HeLa cells treated with 1 μM MPA (mycophenolic acid) or vehicle control for two hours and stained for IMPDH2 are pictured. HeLa cells do

not display RRs under control conditions, but 100% of cells form large RRs within a few hours of MPA treatment. Other IMPDH inhibitors result in a similar induction of RRs.

Cytoophidia

Cytoophidia are large protein complexes which are also linked to nucleotide metabolism and share several similarities with RRs (105,106). In fact, the terms cytoophidia and RRs are often used interchangeably. CTPS1 (cytidine triphosphate synthase) is the best established component of cytoophidia (88,102,104,107). CTPS1 catalyzes the rate-limiting step in the synthesis of cytidine triphosphate (CTP). Some of the same drugs that induce RR formation also induced cytoophidia formation (mainly glutamine analogs) (88,108,109). There is also evidence of partial overlap between RRs and cytoophidia (88,108,109). However, this overlap is not consistently observed and the IMPDH inhibitors commonly used to induce RR formation do not induce the formation of cytoophidia, suggesting that RRs and cytoophidia are different structures (109).

References

1. Watzlich, D., Vetter, I., Gotthardt, K., Miertzschke, M., Chen, Y. X., Wittinghofer, A., and Ismail, S. (2013) The interplay between RPGR, PDEdelta and Arl2/3 regulate the ciliary targeting of farnesylated cargo. *EMBO reports* **14**, 465-472
2. Radcliffe, P. A., Vardy, L., and Toda, T. (2000) A conserved small GTP-binding protein Alp41 is essential for the cofactor-dependent biogenesis of microtubules in fission yeast. *FEBS Lett* **468**, 84-88
3. McElver, J., Patton, D., Rumbaugh, M., Liu, C., Yang, L. J., and Meinke, D. (2000) The TITAN5 gene of Arabidopsis encodes a protein related to the ADP ribosylation factor family of GTP binding proteins. *Plant Cell* **12**, 1379-1392

4. Antoshechkin, I., and Han, M. (2002) The C. elegans evl-20 gene is a homolog of the small GTPase ARL2 and regulates cytoskeleton dynamics during cytokinesis and morphogenesis. *Developmental cell* **2**, 579-591

5. Bhamidipati, A., Lewis, S. A., and Cowan, N. J. (2000) ADP ribosylation factor-like protein 2 (Arl2) regulates the interaction of tubulin-folding cofactor D with native tubulin. *The Journal of cell biology* **149**, 1087-1096

6. Shern, J. F., Sharer, J. D., Pallas, D. C., Bartolini, F., Cowan, N. J., Reed, M. S., Pohl, J., and Kahn, R. A. (2003) Cytosolic Arl2 is complexed with cofactor D and protein phosphatase 2A. *The Journal of biological chemistry* **278**, 40829-40836

7. Tian, G., Thomas, S., and Cowan, N. J. (2010) Effect of TBCD and its regulatory interactor Arl2 on tubulin and microtubule integrity. *Cytoskeleton* **67**, 706-714

8. Muromoto, R., Sekine, Y., Imoto, S., Ikeda, O., Okayama, T., Sato, N., and Matsuda, T. (2008) BART is essential for nuclear retention of STAT3. *Int Immunol* **20**, 395-403

9. Ismail, S. A., Chen, Y. X., Rusinova, A., Chandra, A., Bierbaum, M., Gremer, L., Triola, G., Waldmann, H., Bastiaens, P. I., and Wittinghofer, A. (2011) Arl2-GTP and Arl3-GTP regulate a GDI-like transport system for farnesylated cargo. *Nature chemical biology* **7**, 942-949

10. Newman, L. E., Zhou, C. J., Mudigonda, S., Mattheyses, A. L., Paradies, E., Marobbio, C. M., and Kahn, R. A. (2014) The ARL2 GTPase is required for mitochondrial morphology, motility, and maintenance of ATP levels. *PloS one* **9**, e99270

11. Francis, J. W., Turn, R. E., Newman, L. E., Schiavon, C., and Kahn, R. A. (2016) Higher order signaling: ARL2 as regulator of both mitochondrial fusion and microtubule dynamics allows integration of two essential cell functions. *Small GTPases*, 0

12. Newman, L. E., Schiavon, C. R., Turn, R. E., and Kahn, R. A. (2017) The ARL2 GTPase regulates mitochondrial fusion from the intermembrane space. *Cellular logistics* **7**, e1340104

13. Zhang, S., Lu, Z., Unruh, A. K., Ivan, C., Baggerly, K. A., Calin, G. A., Li, Z., Bast, R. C., Jr., and Le, X. F. (2014) Clinically Relevant microRNAs in Ovarian Cancer. *Molecular cancer research : MCR*

14. Campello, S., and Scorrano, L. (2010) Mitochondrial shape changes: orchestrating cell pathophysiology. *EMBO reports* **11**, 678-684

15. Song, Z., Ghochani, M., McCaffery, J. M., Frey, T. G., and Chan, D. C. (2009) Mitofusins and OPA1 mediate sequential steps in mitochondrial membrane fusion. *Molecular biology of the cell* **20**, 3525-3532

16. Chen, H., Detmer, S. A., Ewald, A. J., Griffin, E. E., Fraser, S. E., and Chan, D. C. (2003) Mitofusins Mfn1 and Mfn2 coordinately regulate mitochondrial fusion and are essential for embryonic development. *The Journal of cell biology* **160**, 189-200

17. Chen, H., Chomyn, A., and Chan, D. C. (2005) Disruption of fusion results in mitochondrial heterogeneity and dysfunction. *The Journal of biological chemistry* **280**, 26185-26192

18. Beghin, A., Matera, E. L., Brunet-Manquat, S., and Dumontet, C. (2008) Expression of Arl2 is associated with p53 localization and chemosensitivity in a breast cancer cell line. *Cell cycle* **7**, 3074-3082

19. Beghin, A., Honore, S., Messana, C., Matera, E. L., Aim, J., Burlinchon, S., Braguer, D., and Dumontet, C. (2007) ADP ribosylation factor like 2 (Arl2) protein influences microtubule dynamics in breast cancer cells. *Experimental cell research* **313**, 473-485

20. Beghin, A., Belin, S., Hage-Sleiman, R., Brunet Manquat, S., Goddard, S., Tabone, E., Jordheim, L. P., Treilleux, I., Poupon, M. F., Diaz, J. J., and Dumontet, C. (2009) ADP ribosylation factor like 2 (Arl2) regulates breast tumor aggressivity in immunodeficient mice. *PloS one* **4**, e7478

21. Wang, K., Li, P., Dong, Y., Cai, X., Hou, D., Guo, J., Yin, Y., Zhang, Y., Li, J., Liang, H., Yu, B., Chen, J., Zen, K., Zhang, J., Zhang, C. Y., and Chen, X. (2011) A microarray-based approach identifies ADP ribosylation factor-like protein 2 as a target of microRNA-16. *The Journal of biological chemistry* **286**, 9468-9476

22. Long, L. M., He, B. F., Huang, G. Q., Guo, Y. H., Liu, Y. S., and Huo, J. R. (2015) microRNA-214 functions as a tumor suppressor in human colon cancer via the suppression of ADP-ribosylation factor-like protein 2. *Oncology letters* **9**, 645-650

23. Nishi, H., Ono, K., Iwanaga, Y., Horie, T., Nagao, K., Takemura, G., Kinoshita, M., Kuwabara, Y., Mori, R. T., Hasegawa, K., Kita, T., and Kimura, T. (2010) MicroRNA-15b modulates cellular ATP levels and degenerates mitochondria via Arl2 in neonatal rat cardiac myocytes. *The Journal of biological chemistry* **285**, 4920-4930

24. Sayed, D., Hong, C., Chen, I. Y., Lypowy, J., and Abdellatif, M. (2007) MicroRNAs play an essential role in the development of cardiac hypertrophy. *Circ Res* **100**, 416-424

25. van Rooij, E., Sutherland, L. B., Liu, N., Williams, A. H., McAnally, J., Gerard, R. D., Richardson, J. A., and Olson, E. N. (2006) A signature pattern of stress-responsive microRNAs that can evoke cardiac hypertrophy and heart failure. *Proceedings of the National Academy of Sciences of the United States of America* **103**, 18255-18260

26. Graham, B. H., Waymire, K. G., Cottrell, B., Trounce, I. A., MacGregor, G. R., and Wallace, D. C. (1997) A mouse model for mitochondrial myopathy and cardiomyopathy resulting from a deficiency in the heart/muscle isoform of the adenine nucleotide translocator. *Nat Genet* **16**, 226-234

27. Sharer, J. D., Shern, J. F., Van Valkenburgh, H., Wallace, D. C., and Kahn, R. A. (2002) ARL2 and BART enter mitochondria and bind the adenine nucleotide transporter. *Molecular biology of the cell* **13**, 71-83

28. East, M. P., and Kahn, R. A. (2011) Models for the functions of Arf GAPs. *Semin Cell Dev Biol* **22**, 3-9

29. Weimer, C., Beck, R., Eckert, P., Reckmann, I., Moelleken, J., Brugger, B., and Wieland, F. (2008) Differential roles of ArfGAP1, ArfGAP2, and ArfGAP3 in COPI trafficking. *The Journal of cell biology* **183**, 725-735

30. Bowzard, J. B., Cheng, D., Peng, J., and Kahn, R. A. (2007) ELMOD2 is an Arl2 GTPase-activating protein that also acts on Arfs. *The Journal of biological chemistry* **282**, 17568-17580

31. Johnson, K. R., Longo-Guess, C. M., and Gagnon, L. H. (2012) Mutations of the mouse ELMO domain containing 1 gene (Elmod1) link small GTPase signaling to actin cytoskeleton dynamics in hair cell stereocilia. *PloS one* **7**, e36074

32. Jaworek, T. J., Richard, E. M., Ivanova, A. A., Giese, A. P., Choo, D. I., Khan, S. N., Riazuddin, S., Kahn, R. A., and Riazuddin, S. (2013) An alteration in ELMOD3, an Arl2 GTPase-activating protein, is associated with hearing impairment in humans. *PLoS genetics* **9**, e1003774

33. East, M. P., Bowzard, J. B., Dacks, J. B., and Kahn, R. A. (2012) ELMO domains, evolutionary and functional characterization of a novel GTPase-activating protein (GAP) domain for Arf protein family GTPases. *The Journal of biological chemistry* **287**, 39538-39553

34. Suzuki, M., Murakami, T., Cheng, J., Kano, H., Fukata, M., and Fujimoto, T. (2015) ELMOD2 is anchored to lipid droplets by palmitoylation and regulates adipocyte triglyceride lipase recruitment. *Molecular biology of the cell* **26**, 2333-2342

35. Hodgson, U., Pulkkinen, V., Dixon, M., Peyrard-Janvid, M., Rehn, M., Lahermo, P., Ollikainen, V., Salmenkivi, K., Kinnula, V., Kere, J., Tukiainen, P., and Laitinen, T. (2006) ELMOD2 is a candidate gene for familial idiopathic pulmonary fibrosis. *American journal of human genetics* **79**, 149-154

36. Pulkkinen, V., Bruce, S., Rintahaka, J., Hodgson, U., Laitinen, T., Alenius, H., Kinnula, V. L., Myllarniemi, M., Matikainen, S., and Kere, J. (2010) ELMOD2, a candidate gene for idiopathic pulmonary fibrosis, regulates antiviral responses. *FASEB journal : official publication of the Federation of American Societies for Experimental Biology* **24**, 1167-1177

37. Mishra, P., Carelli, V., Manfredi, G., and Chan, D. C. (2014) Proteolytic cleavage of Opa1 stimulates mitochondrial inner membrane fusion and couples fusion to oxidative phosphorylation. *Cell metabolism* **19**, 630-641

38. Gomes, L. C., Di Benedetto, G., and Scorrano, L. (2011) During autophagy mitochondria elongate, are spared from degradation and sustain cell viability. *Nature cell biology* **13**, 589-598

39. Chen, H., McCaffery, J. M., and Chan, D. C. (2007) Mitochondrial fusion protects against neurodegeneration in the cerebellum. *Cell* **130**, 548-562

40. Chen, H., Vermulst, M., Wang, Y. E., Chomyn, A., Prolla, T. A., McCaffery, J. M., and Chan, D. C. (2010) Mitochondrial fusion is required for mtDNA stability in skeletal muscle and tolerance of mtDNA mutations. *Cell* **141**, 280-289

41. Chan, D. C. (2012) Fusion and fission: interlinked processes critical for mitochondrial health. *Annual review of genetics* **46**, 265-287

42. Saotome, M., Safiulina, D., Szabadkai, G., Das, S., Fransson, A., Aspenstrom, P., Rizzuto, R., and Hajnoczky, G. (2008) Bidirectional Ca2+-dependent control of mitochondrial dynamics by the Miro GTPase. *Proceedings of the National Academy of Sciences of the United States of America* **105**, 20728-20733

43. Taguchi, N., Ishihara, N., Jofuku, A., Oka, T., and Mihara, K. (2007) Mitotic phosphorylation of dynamin-related GTPase Drp1 participates in mitochondrial fission. *The Journal of biological chemistry* **282**, 11521-11529

44. Frank, S., Gaume, B., Bergmann-Leitner, E. S., Leitner, W. W., Robert, E. G., Catez, F., Smith, C. L., and Youle, R. J. (2001) The role of dynamin-related protein 1, a mediator of mitochondrial fission, in apoptosis. *Developmental cell* **1**, 515-525

45. Tanaka, A., Cleland, M. M., Xu, S., Narendra, D. P., Suen, D. F., Karbowski, M., and Youle, R. J. (2010) Proteasome and p97 mediate mitophagy and degradation of mitofusins induced by Parkin. *The Journal of cell biology* **191**, 1367-1380

46. Eura, Y. (2003) Two Mitofusin Proteins, Mammalian Homologues of FZO, with Distinct Functions Are Both Required for Mitochondrial Fusion. *Journal of Biochemistry* **134**, 333-344

47. Koshiba, T., Detmer, S. A., Kaiser, J. T., Chen, H., McCaffery, J. M., and Chan, D. C. (2004) Structural basis of mitochondrial tethering by mitofusin complexes. *Science* **305**, 858-862

48. Rojo, M., Legros, F., Chateau, D., and Lombes, A. (2002) Membrane topology and mitochondrial targeting of mitofusins, ubiquitous mammalian homologs of the transmembrane GTPase Fzo. *Journal of cell science* **115**, 1663-1674

49. Ishihara, N., Eura, Y., and Mihara, K. (2004) Mitofusin 1 and 2 play distinct roles in mitochondrial fusion reactions via GTPase activity. *Journal of cell science* **117**, 6535-6546

50. Mourier, A., Motori, E., Brandt, T., Lagouge, M., Atanassov, I., Galinier, A., Rappl, G., Brodesser, S., Hultenby, K., Dieterich, C., and Larsson, N. G. (2015) Mitofusin 2 is required to maintain mitochondrial coenzyme Q levels. *The Journal of cell biology* **208**, 429-442

51. Bach, D., Pich, S., Soriano, F. X., Vega, N., Baumgartner, B., Oriola, J., Daugaard, J. R., Lloberas, J., Camps, M., Zierath, J. R., Rabasa-Lhoret, R., Wallberg-Henriksson, H., Laville, M., Palacin, M., Vidal, H., Rivera, F., Brand, M., and Zorzano, A. (2003) Mitofusin-2 determines mitochondrial network architecture and mitochondrial metabolism. A novel regulatory mechanism altered in obesity. *The Journal of biological chemistry* **278**, 17190-17197

52. Pich, S., Bach, D., Briones, P., Liesa, M., Camps, M., Testar, X., Palacin, M., and Zorzano, A. (2005) The Charcot-Marie-Tooth type 2A gene product, Mfn2, up-regulates fuel oxidation through expression of OXPHOS system. *Human molecular genetics* **14**, 1405-1415

53. de Brito, O. M., and Scorrano, L. (2008) Mitofusin 2 tethers endoplasmic reticulum to mitochondria. *Nature* **456**, 605-610

54. Zanna, C., Ghelli, A., Porcelli, A. M., Karbowski, M., Youle, R. J., Schimpf, S., Wissinger, B., Pinti, M., Cossarizza, A., Vidoni, S., Valentino, M. L., Rugolo, M., and Carelli, V. (2008) OPA1 mutations associated with dominant optic atrophy impair oxidative phosphorylation and mitochondrial fusion. *Brain* **131**, 352-367

55. Smirnova, E., Griparic, L., Shurland, D. L., and van der Bliek, A. M. (2001) Dynamin-related protein Drp1 is required for mitochondrial division in mammalian cells. *Molecular biology of the cell* **12**, 2245-2256

56. Boldogh, I. R., and Pon, L. A. (2007) Mitochondria on the move. *Trends Cell Biol* **17**, 502-510

57. Glater, E. E., Megeath, L. J., Stowers, R. S., and Schwarz, T. L. (2006) Axonal transport of mitochondria requires milton to recruit kinesin heavy chain and is light chain independent. *The Journal of cell biology* **173**, 545-557

58. Hirokawa, N., and Takemura, R. (2005) Molecular motors and mechanisms of directional transport in neurons. *Nat Rev Neurosci* **6**, 201-214

59. Varadi, A., Johnson-Cadwell, L. I., Cirulli, V., Yoon, Y., Allan, V. J., and Rutter, G. A. (2004) Cytoplasmic dynein regulates the subcellular distribution of mitochondria by controlling the recruitment of the fission factor dynamin-related protein-1. *Journal of cell science* **117**, 4389-4400

60. Eura, Y., Ishihara, N., Oka, T., and Mihara, K. (2006) Identification of a novel protein that regulates mitochondrial fusion by modulating mitofusin (Mfn) protein function. *Journal of cell science* **119**, 4913-4925

61. Hoppins, S., Edlich, F., Cleland, M. M., Banerjee, S., McCaffery, J. M., Youle, R. J., and Nunnari, J. (2011) The soluble form of Bax regulates mitochondrial fusion via MFN2 homotypic complexes. *Molecular cell* **41**, 150-160

62. Kumar, S., Pan, C. C., Shah, N., Wheeler, S. E., Hoyt, K. R., Hempel, N., Mythreye, K., and Lee, N. Y. (2016) Activation of Mitofusin2 by Smad2-RIN1 Complex during Mitochondrial Fusion. *Molecular cell* **62**, 520-531

63. Shutt, T., Geoffrion, M., Milne, R., and McBride, H. M. (2012) The intracellular redox state is a core determinant of mitochondrial fusion. *EMBO reports* **13**, 909-915

64. Pyakurel, A., Savoia, C., Hess, D., and Scorrano, L. (2015) Extracellular regulated kinase phosphorylates mitofusin 1 to control mitochondrial morphology and apoptosis. *Molecular cell* **58**, 244-254

65. Lee, J. Y., Kapur, M., Li, M., Choi, M. C., Choi, S., Kim, H. J., Kim, I., Lee, E., Taylor, J. P., and Yao, T. P. (2014) MFN1 deacetylation activates adaptive mitochondrial fusion and protects metabolically challenged mitochondria. *Journal of cell science* **127**, 4954-4963

66. Griparic, L., van der Wel, N. N., Orozco, I. J., Peters, P. J., and van der Bliek, A. M. (2004) Loss of the intermembrane space protein Mgm1/OPA1 induces swelling and localized constrictions along the lengths of mitochondria. *The Journal of biological chemistry* **279**, 18792-18798

67. Ehses, S., Raschke, I., Mancuso, G., Bernacchia, A., Geimer, S., Tondera, D., Martinou, J. C., Westermann, B., Rugarli, E. I., and Langer, T. (2009) Regulation of OPA1 processing and mitochondrial fusion by m-AAA protease isoenzymes and OMA1. *The Journal of cell biology* **187**, 1023-1036

68. Head, B., Griparic, L., Amiri, M., Gandre-Babbe, S., and van der Bliek, A. M. (2009) Inducible proteolytic inactivation of OPA1 mediated by the OMA1 protease in mammalian cells. *The Journal of cell biology* **187**, 959-966

69. Song, Z., Chen, H., Fiket, M., Alexander, C., and Chan, D. C. (2007) OPA1 processing controls mitochondrial fusion and is regulated by mRNA splicing, membrane potential, and Yme1L. *The Journal of cell biology* **178**, 749-755

70. Palmer, C. S., Osellame, L. D., Laine, D., Koutsopoulos, O. S., Frazier, A. E., and Ryan, M. T. (2011) MiD49 and MiD51, new components of the mitochondrial fission machinery. *EMBO reports* **12**, 565-573

71. Yoon, Y., Krueger, E. W., Oswald, B. J., and McNiven, M. A. (2003) The mitochondrial protein hFis1 regulates mitochondrial fission in mammalian cells through an interaction with the dynamin-like protein DLP1. *Mol Cell Biol* **23**, 5409-5420

72. Yu, T., Fox, R. J., Burwell, L. S., and Yoon, Y. (2005) Regulation of mitochondrial fission and apoptosis by the mitochondrial outer membrane protein hFis1. *Journal of cell science* **118**, 4141-4151

73. Otera, H., Wang, C., Cleland, M. M., Setoguchi, K., Yokota, S., Youle, R. J., and Mihara, K. (2010) Mff is an essential factor for mitochondrial recruitment of Drp1 during mitochondrial fission in mammalian cells. *The Journal of cell biology* **191**, 1141-1158

74. Kashatus, J. A., Nascimento, A., Myers, L. J., Sher, A., Byrne, F. L., Hoehn, K. L., Counter, C. M., and Kashatus, D. F. (2015) Erk2 Phosphorylation of Drp1 Promotes Mitochondrial Fission and MAPK-Driven Tumor Growth. *Molecular cell* **57**, 537-551

75. Friedman, J. R., Lackner, L. L., West, M., DiBenedetto, J. R., Nunnari, J., and Voeltz, G. K. (2011) ER tubules mark sites of mitochondrial division. *Science* **334**, 358-362

76. De Vos, K. J., Allan, V. J., Grierson, A. J., and Sheetz, M. P. (2005) Mitochondrial function and actin regulate dynamin-related protein 1-dependent mitochondrial fission. *Current biology : CB* **15**, 678-683

77. Wang, X., and Schwarz, T. L. (2009) The mechanism of Ca2+ -dependent regulation of kinesin-mediated mitochondrial motility. *Cell* **136**, 163-174

78. Chen, L., Gong, Q., Stice, J. P., and Knowlton, A. A. (2009) Mitochondrial OPA1, apoptosis, and heart failure. *Cardiovasc Res* **84**, 91-99

79. Shen, T., Zheng, M., Cao, C., Chen, C., Tang, J., Zhang, W., Cheng, H., Chen, K. H., and Xiao, R. P. (2007) Mitofusin-2 is a major determinant of oxidative stress-mediated heart muscle cell apoptosis. *The Journal of biological chemistry* **282**, 23354-23361

80. Ashrafian, H., Docherty, L., Leo, V., Towlson, C., Neilan, M., Steeples, V., Lygate, C. A., Hough, T., Townsend, S., Williams, D., Wells, S., Norris, D., Glyn-Jones, S., Land, J., Barbaric, I., Lalanne, Z., Denny, P., Szumska, D., Bhattacharya, S., Griffin, J. L., Hargreaves, I., Fernandez-Fuentes, N., Cheeseman, M., Watkins, H., and Dear, T. N. (2010) A mutation in the mitochondrial fission gene Dnm1l leads to cardiomyopathy. *PLoS genetics* **6**, e1001000

81. Song, M., Mihara, K., Chen, Y., Scorrano, L., and Dorn, G. W., 2nd. (2015) Mitochondrial fission and fusion factors reciprocally orchestrate mitophagic culling in mouse hearts and cultured fibroblasts. *Cell metabolism* **21**, 273-285

82. Lin, M. T., and Beal, M. F. (2006) Mitochondrial dysfunction and oxidative stress in neurodegenerative diseases. *Nature* **443**, 787-795

83. Abou-Sleiman, P. M., Muqit, M. M., and Wood, N. W. (2006) Expanding insights of mitochondrial dysfunction in Parkinson's disease. *Nat Rev Neurosci* **7**, 207-219

84. Stuppia, G., Rizzo, F., Riboldi, G., Del Bo, R., Nizzardo, M., Simone, C., Comi, G. P., Bresolin, N., and Corti, S. (2015) MFN2-related neuropathies: Clinical features, molecular pathogenesis and therapeutic perspectives. *J Neurol Sci*

85. Carelli, V., Ross-Cisneros, F. N., and Sadun, A. A. (2004) Mitochondrial dysfunction as a cause of optic neuropathies. *Prog Retin Eye Res* **23**, 53-89

86. Gottlieb, E., and Tomlinson, I. P. (2005) Mitochondrial tumour suppressors: a genetic and biochemical update. *Nat Rev Cancer* **5**, 857-866

87. Serasinghe, M. N., Wieder, S. Y., Renault, T. T., Elkholi, R., Asciolla, J. J., Yao, J. L., Jabado, O., Hoehn, K., Kageyama, Y., Sesaki, H., and Chipuk, J. E. (2015) Mitochondrial Division Is Requisite to RAS-Induced Transformation and Targeted by Oncogenic MAPK Pathway Inhibitors. *Molecular cell* **57**, 521-536

88. Carcamo, W. C., Satoh, M., Kasahara, H., Terada, N., Hamazaki, T., Chan, J. Y., Yao, B., Tamayo, S., Covini, G., von Muhlen, C. A., and Chan, E. K. (2011) Induction of cytoplasmic rods and rings structures by inhibition of the CTP and GTP synthetic pathway in mammalian cells. *PloS one* **6**, e29690

89. Covini, G., Carcamo, W. C., Bredi, E., von Muhlen, C. A., Colombo, M., and Chan, E. K. (2012) Cytoplasmic rods and rings autoantibodies developed during pegylated interferon and ribavirin therapy in patients with chronic hepatitis C. *Antiviral therapy* **17**, 805-811

90. Ji, Y., Gu, J., Makhov, A. M., Griffith, J. D., and Mitchell, B. S. (2006) Regulation of the interaction of inosine monophosphate dehydrogenase with mycophenolic Acid by GTP. *The Journal of biological chemistry* **281**, 206-212

91. Juda, P., Smigova, J., Kovacik, L., Bartova, E., and Raska, I. (2014) Ultrastructure of cytoplasmic and nuclear inosine-5'-monophosphate dehydrogenase 2 "rods and rings" inclusions. *J Histochem Cytochem* **62**, 739-750

92. Calise, S. J., Keppeke, G. D., Andrade, L. E., and Chan, E. K. (2015) Anti-rods/rings: a human model of drug-induced autoantibody generation. *Front Immunol* **6**, 41

93. Keppeke, G. D., Andrade, L. E., Grieshaber, S. S., and Chan, E. K. (2015) Microinjection of specific anti-IMPDH2 antibodies induces disassembly of cytoplasmic rods/rings that are primarily stationary and stable structures. *Cell & bioscience* **5**, 1

94. Keppeke, G. D., Prado, M. S., Nunes, E., Perazzio, S. F., Rodrigues, S. H., Ferraz, M. L., Chan, E. K., and Andrade, L. E. (2016) Differential capacity of therapeutic drugs to induce Rods/Rings structures in vitro and in vivo and generation of anti-Rods/Rings autoantibodies. *Clin Immunol* **173**, 149-156

95. Calise, S. J., Carcamo, W. C., Krueger, C., Yin, J. D., Purich, D. L., and Chan, E. K. (2014) Glutamine deprivation initiates reversible assembly of mammalian rods and rings. *Cellular and molecular life sciences : CMLS* **71**, 2963-2973

96. Thomas, E. C., Gunter, J. H., Webster, J. A., Schieber, N. L., Oorschot, V., Parton, R. G., and Whitehead, J. P. (2012) Different characteristics and nucleotide binding properties of inosine monophosphate dehydrogenase (IMPDH) isoforms. *PloS one* **7**, e51096

97. Calise, S. J., Purich, D. L., Nguyen, T., Saleem, D. A., Krueger, C., Yin, J. D., and Chan, E. K. (2016) 'Rod and ring' formation from IMP dehydrogenase is regulated through the one-carbon metabolic pathway. *Journal of cell science* **129**, 3042-3052

98. Gunter, J. H., Thomas, E. C., Lengefeld, N., Kruger, S. J., Worton, L., Gardiner, E. M., Jones, A., Barnett, N. L., and Whitehead, J. P. (2008) Characterisation of inosine monophosphate dehydrogenase expression during retinal development: differences between variants and isoforms. *The international journal of biochemistry & cell biology* **40**, 1716-1728

99. Willingham, M. C., Richert, N. D., and Rutherford, A. V. (1987) A novel fibrillar structure in cultured cells detected by a monoclonal antibody. *Experimental cell research* **171**, 284-295

100. Chen, K., Zhang, J., Tastan, O. Y., Deussen, Z. A., Siswick, M. Y., and Liu, J. L. (2011) Glutamine analogs promote cytoophidium assembly in human and Drosophila cells. *Journal of genetics and genomics = Yi chuan xue bao* **38**, 391-402

101. Ramer, M. S., Cruz Cabrera, M. A., Alan, N., Scott, A. L., and Inskip, J. A. (2010) A new organellar complex in rat sympathetic neurons. *PloS one* **5**, e10872

102. Noree, C., Sato, B. K., Broyer, R. M., and Wilhelm, J. E. (2010) Identification of novel filament-forming proteins in Saccharomyces cerevisiae and Drosophila melanogaster. *The Journal of cell biology* **190**, 541-551

103. Liu, J. L. (2010) Intracellular compartmentation of CTP synthase in Drosophila. *Journal of genetics and genomics = Yi chuan xue bao* **37**, 281-296

104. Ingerson-Mahar, M., Briegel, A., Werner, J. N., Jensen, G. J., and Gitai, Z. (2010) The metabolic enzyme CTP synthase forms cytoskeletal filaments. *Nature cell biology* **12**, 739-746

105. Chang, C. C., Lin, W. C., Pai, L. M., Lee, H. S., Wu, S. C., Ding, S. T., Liu, J. L., and Sung, L. Y. (2015) Cytoophidium assembly reflects upregulation of IMPDH activity. *Journal of cell science* **128**, 3550-3555

106. Liu, J. L. (2016) The Cytoophidium and Its Kind: Filamentation and Compartmentation of Metabolic Enzymes. *Annual review of cell and developmental biology* **32**, 349-372

107. Liu, J. L. (2011) The enigmatic cytoophidium: compartmentation of CTP synthase via filament formation. *Bioessays* **33**, 159-164

108. Calise, S. J., Carcamo, W. C., Ceribelli, A., Dominguez, Y., Satoh, M., and Chan, E. K. L. (2014) Antibodies to Rods and Rings. 161-168

109. Keppeke, G. D., Calise, S. J., Chan, E. K., and Andrade, L. E. (2015) Assembly of IMPDH2-based, CTPS-based, and mixed rod/ring structures is dependent on cell type and conditions of induction. *Journal of genetics and genomics* **42**, 287-299

Chapter 2: Plasmids for variable expression of proteins targeted to the mitochondrial matrix or intermembrane space

This chapter was published as:

Laura E. Newman*, Cara Schiavon*, Richard A. Kahn. Plasmids for variable expression of proteins targeted to the mitochondrial matrix or intermembrane space. Cellular logistics. 2016

* These authors contributed equally to this work

Abstract

We describe the construction of a collection of plasmids for varied expression of proteins targeted to the mitochondrial matrix or intermembrane space, using previously defined targeting sequences and strength CMV promoters. The limited size of these compartments makes them particularly vulnerable to artifacts from over-expression. We found that different proteins display different kinetics of expression and import that should be considered when analyzing results from this approach. Finally, this collection of plasmids has been deposited in the Addgene plasmid repository to facilitate the ready access and use of these tools.

Introduction

Mitochondria are structurally complex, morphologically heterogeneous, and essential organelles best known for their roles in ATP production via respiration and apoptosis. They are also critical to a number of other essential housekeeping and regulatory processes, including calcium metabolism, signaling via reactive oxygen species, phospholipid metabolism, and more generally in cell metabolism. There are clear links to a host of human diseases that result from defects in mitochondrial proteins and processes (1-9). Depending on cell type and conditions mitochondria can appear as many small, almost spherical puncta, as one highly inter-connected network or anywhere in between these extremes as a result of differences in the net fusion and fission. This morphological diversity and close connection to other structures contribute to the technical difficulties inherent in studies of mitochondrial signaling and functions. A primary source of structural complexity derives from the fact that mitochondria have two membranes; an inner membrane that surrounds the mitochondrial matrix, and an outer membrane that is exposed to cytosol and the intermembrane space (IMS). The matrix and inner membrane contain the electron transport chain (ETC) complexes that use the proton gradient to synthesize ATP. The IMS houses proteins that may regulate the ETC or apoptosis, *e.g.*, cytochrome c or Bax (10, 11). Despite the existence of a mitochondrial genome and protein synthetic machineries, the overwhelming majority of

mitochondrial proteins are encoded in the nuclear genome, and must be imported to their sites of action. Specific sub-mitochondrial localization of imported proteins is achieved through the actions of the translocases of the outer and inner membranes, which are distinct, multi-subunit complexes that recognize mitochondria localization sequences (MLS) (12-14) on target proteins and transport them across their respective membranes. Strong MLSs have been identified and shown capable of driving other proteins to specific compartments when fused on their N-termini. A second means of mitochondrial import makes use of disulfide bond formation between the cysteines in a "twin cysteine motif" (C-X_3-C or C-X_9-C) and Mia40, located in the IMS to aid in targeting to the IMS or matrix (15). This mechanism of Mia40-dependent mitochondrial import can be slower than that driven by a strong MLS and rates are sensitive to Mia40 or glutathione levels (16). Our studies focus on the roles of soluble proteins that localize to the matrix, or IMS, and thus we focus here on the use of MLSs proven to drive fusion proteins to one compartment or the other.

MLSs have low primary sequence conservation, though most form an amphipathic α-helix at the N-terminus. MLSs are typically cleaved by mitochondrial proteases after import and arrival at their destination. Thus, this cleavage is often used to monitor maturation and targeting (12, 17, 18). A few MLSs have been extensively studied and shown to target proteins to the matrix or IMS, with known sites of cleavage by mitochondrial proteases (19). These strong MLSs can also target other proteins to specific compartments when fused at their N-terminus. Among these strong MLSs are the 32 residue N-terminus of human ornithine carbamoyltransferase (OCT) that drives proteins to the mitochondrial matrix (20, 21), or the 59 residue leader sequence from human Smac (aka Diablo) that targets the IMS (22-26).

There is also a group of proteins that are present and active in other parts of the cell that also contain a smaller pool inside mitochondria. Included in this list are STAT3 (27, 28), MEF2D (29), ARL2 (30-32), ELMOD2 (30), and several DNA damage repair proteins (33). Notable about this list of proteins with dual localizations is their importance to cell signaling and regulation.

Indirect immunofluorescence or GFP tagging are essential tools for determining protein localization(s) but even the highest resolution fluorescent microscopes are challenged to resolve the compartments or structures within mitochondria. And these techniques are challenged further by high "background" non-mitochondrial staining when the target protein is more abundant in cytosol than in mitochondria. The use of targeting vectors that drive exogenous proteins to specific sub-mitochondrial compartments provides a useful complement to high resolution imaging.

We recognized that the matrix and IMS are small, saturable compartments that may be altered non-specifically by excessive protein accumulation. Thus, we used the system described by Morita, et al. (34), that allows control over the strength of the promoter driving protein expression, in combination with previously described mitochondrial targeting leader sequences. The N-termini of SMAC/Diablo and OCT are used to target fusion proteins to the IMS or matrix, respectively. Each of these leader sequences is cleaved by proteases located in the appropriate compartment, which allows an easy way to monitor the import process. We designed into our collection unique restriction sites that allows for ready sub-cloning and the optional use of the HA epitope, to facilitate immunolocalization of exogenously expressed proteins.

Methods

Antibodies & Reagents

The rabbit polyclonal antibody directed against human ARL2 has been previously described (32, 35). Antibodies directed against the following antigens were also used in this study: GFP (Abcam ab290), HSP60 (Enzo Life Sciences ADI-SPA-807), cytochrome C (BD Biosciences 556432), alpha-tubulin (Sigma T9026).

Cloning and Constructs

A plasmid containing the open reading frame of rat OCT, pOCT:GFP, was a gift from Heidi McBride (McGill University) and that of human SMAC/Diablo, SMAC-GFP, a gift from Doug Green (Addgene plasmid #40881), were used as templates in PCR reactions as the sources of the OCT and SMAC leader sequences. The seven plasmids carrying a series of truncations in the CMV promoter, pCMVΔ0 - pCMVΔ6, and resulting in decreasing levels of exogenous protein expression, were described in Morita, et al. (34) and obtained from DNASU.

Into each of the parental CMVΔ0-6 plasmids we inserted OCT or SMAC leader sequences between the KpnI and BamHI sites, then the HA epitope (YPYDVPDYA) between BamHI and EcoRI sites, and ORFs of interest between EcoRI and XhoI sites (see Figure 1). This allows one to include (or not) the HA epitope. Note that the addition of unique restriction sites and short linkers results in proteins, after cleavage of leader sequences, which are still slightly larger than the untagged or only HA-tagged proteins. Into these we inserted the open reading frame of eGFP (accession #U55762) or human ARL2 (NP_001658).

The N-terminal leader sequence used for targeting fusion proteins to the mitochondrial matrix is that derived from human ornithine carbamoyltransferase (OCT; aka ornithine trans-carbamylase), as initially described in Horwich, et al (20, 21). We used the 96 nt sequence: ATGCTGTCTAATTTGAGAATCCTGCTCAACAAGGCAGCTCTTAGAAAGGCTCACACTTCCATGGTTCGAAATTTTCGGTATGGGAAGCCAGTCCAG, which encodes the 32-residue sequence: MLSNLRILLNKAALRKAHTSMVRNFRYGKPVQ.

And for the IMS leader sequence we used that described by Ozawa, et al (25) and Sabharwal, et al (26) from human SMAC (aka Diablo), which is 177 nt:

ATGGCGGCTCTGAAGAGTTGGCTGTCGCGCAGCGTAACTTCATTCTTCAGGTACAGACAGTGTTTGTGTGTTCCTGTTGTGGCTAACTTTAAGAAGCGGTGTTTCTCAGAATTGATAAGACCATGGCACAAAACTGTGACGATTGGCTTTGGAGTAACCCTGTGTGCGGTTCCTATT, which encodes

the 59 residue leader:

MAALKSWLSRSVTSFFRYRQCLCVPVVANFKKRCFSELIRPWHKTVTIGFGVTLCAVPI.

PCR reactions were designed to amplify each component, using specific primers, and sub-cloned into the parent vectors by standard restriction digestions and ligations. All inserts were verified by DNA sequencing. Note that the pCMVΔ0-6 plasmids are in the pcDNA3.1 backbone and thus contain both Amp^R and Neo^R selectable markers.

Cell culture

Human cervical carcinoma (HeLa) cells were obtained from ATCC and grown in DMEM medium (supplemented with 10% fetal bovine serum (Invitrogen, Carlsbad, CA) and 2 mM glutamine) at 37°C in the presence of 5% CO_2. Cells are screened monthly for mycoplasma and were not cultured for more than 30 passages.

Transfection

Cells at ~90% density were transfected while attached in 6 well plates. Each plasmid (1 μg) was diluted in 250 μl Optimem (Invitrogen). Lipofectamine 2000 (2 μg; Invitrogen) was diluted in a separate tube containing 250 μl Optimem, vortexed briefly, and incubated at room temperature for 5 minutes. The tubes were then mixed and incubated another 20 minutes at room temperature. Following incubation, cell culture medium was changed to 1.5 ml of Optimem, and transfection complexes (500 μl) were added drop wise to the wells. After 4 hours, the medium was changed back to DMEM growth medium. For imaging experiments, cells were split 1:3 after the four hour transfection onto matrigel (BD Biosciences) coated coverslips in a new 6 well plate.

Western blots and data reproducibility

Cells were harvested by rinsing twice with PBS, collected by incubation in 5 mM EDTA in phosphate buffered saline (PBS; 140 mM NaCl, 3 mM KCl, 10 mM Na_2HPO_4, 2 mM KH_2PO_4, pH 6.75),

and pelleted in a microfuge (14,000 rpm, 4°C). Cells were lysed in 1% CHAPS, 25 mM HEPES pH 7.4, 100 mM NaCl, and protease inhibitors (Sigma #P-2714) on ice for 30 minutes, and the S14 was obtained by clarifying lysates by centrifugation for 30 minutes (14,000 rpm, 4°C). Protein concentrations were determined by Bradford Assay (Bio-Rad) using bovine serum albumin as standard. Protein samples (20 µg/well) were separated on 15% polyacrylamide gels and wet-transferred to nitrocellulose membranes (Bio-Rad #162-0112) at 70V for 2.5 hours. Western blotting procedures were carried out at room temperature. Membranes were blocked in blotto (5% (w/v) dry milk, 50 mM Tris pH 8, 2 mM $CaCl_2$, 80 mM NaCl, 0.2% (v/v) Tween-20, 0.02% sodium azide) for 1 hour. When probing for ARL2, membranes were blocked in an alternate blocking buffer (10% goat serum, 5% Tween-20 in PBS), freshly filtered through a 0.2µm membrane. Membranes were then incubated with primary antibody in blocking buffer at 4°C overnight. Removal of excess primary antibody was carried out by washing the membranes in PBST (PBS with 0.1% Tween-20) three times for 10 min each. The anti-rabbit 790 secondary antibody (Invitrogen A11374) or anti-mouse 800 secondary antibody (Rockland 610-745-002) was diluted 1:10,000 in PBST and incubated with the membrane for 1 hour at room temperature. The membrane was protected from light from this point on. Excess secondary antibody was removed by washing the membranes in PBST 3 times for 10 min each. Excess Tween-20 was removed by quickly rinsing membranes 3 times in PBS, followed by 2x5 minute washes in PBS. Data were collected using the Odyssey Infrared Imager. For CCCP and ARL2 competition experiments, western blotting was performed as described above, with the exception that HRP-conjugated secondary antibodies were used (GE cat #NA934V, #NA931V), and blots were incubated in luminol containing solution (0.1 mM Tris-HCl pH 8.0, 1.2 mM luminol, 0.2 mM p-coumaric acid, 0.009% hydrogen peroxide) for 1 min prior to exposure to film. The following antibody dilutions were used for western blotting: ARL2 (1:1000), GFP (1:1000), alpha tubulin (1:2500).

Every experiment described herein has been repeated at least twice with similar results. Immunoblotting with antibodies to alpha tubulin was performed in each case as a loading control to confirm equal total protein loaded per lane, in agreement with total protein assays.

Immunofluorescence

Cells were grown on Matrigel (BD Biosciences #356231) coated coverslips. Cells were fixed for 15 minutes in a pre-warmed (37°C) solution of 4% paraformaldehyde in PBS, and then permeabilized with 0.1% (v/v) Triton X-100 in PBS for 10 minutes at room temperature. Alternatively, for differential permeabilization of outer and inner mitochondrial membranes, cells were permeabilized with either 0.02% or 0.1% (w/v) digitonin in PBS for 10 minutes at room temperature. Incubation with primary antibodies was carried out in PBS containing 1% (w/v) BSA, filtered, at 4°C overnight. Secondary antibodies (Alexa fluorophores, Invitrogen) were incubated in the same buffer for 1 hour at room temperature at a 1:500 dilution, following 4 x 5 min washes in PBS. Coverslips were then rinsed twice for 5 minutes each, stained with Hoechst 33342 for 4 min, rinsed twice again for 5 min, and mounted onto slides using Prolong Antifade (Invitrogen). The following antibody dilutions were used: ARL2 (1:1000), HSP60 (1:5000), cytochrome C (1:1000). Images were acquired using an Olympus FV1000 microscope, using 488 and 543 laser excitation and a 100x objective (1.45 NA). Image processing was carried out using ImageJ.

CCCP treatment

The time of CCCP addition to cells following transfection differed based on whether the cells were expressing OCT-GFP or SMAC-GFP because they were found to display different import kinetics. All cells were transfected as described above and were exposed to 10 µM CCCP. OCT-HA-GFP cells were exposed to 4 hours of CCCP treatment 4 hours after transfection, while SMAC-HA-GFP cells were exposed to 4 hours of CCCP treatment 12 hours after transfection. Empty vector and GFP controls were included in each case. Cells were then collected and processed for immunoblotting as described above.

Timing was designed to minimize cell toxicity resulting from the drug treatment and maximize drug exposure during the peak of protein expression and potential import.

Results and Discussion

Plasmid construction and controls

This paper describes the generation of two series of plasmids that are each based upon the original CMV promoter truncation series described by Morita, et al (34). We have inserted N-terminal leader sequences that direct the fusion proteins to either the mitochondrial matrix or the IMS. The 32-residue, mitochondrial matrix localization tag is that described by Horwich, et al. (20, 21) for the human ornithine carbamoyltransferase (OCT, aka ornithine trans-carbamylase) protein. The 59-residue, IMS-directing leader is that derived from the human SMAC/Diablo protein, as previously described (25, 26). We also included in our constructs the HA epitope (YPYDVPDYA), between the leader sequences and proteins of interest (see Fig. 1). This allows monitoring of protein expression to which no antibody is available and comparisons of levels of different expressed proteins. The construction of these plasmids is described under Methods and a plasmid map showing key features is shown in Fig. 1.

Here we describe the use of these series of plasmids, using primarily eGFP[1] as the exogenous protein, to highlight issues surrounding their use in targeting proteins to each compartment of mitochondria. We also generated a parallel series of plasmids as controls that express GFP that remains in cytosol. No differences from controls were noted in overall mitochondrial morphologies in cells expressing SMAC- or OCT-GFP from even the strongest (CMVΔ0) promoter. Thus, forcing import of GFP (*e.g.*, see Fig. 2) to the matrix or IMS alone is not sufficient to alter the overall morphology of mitochondria.

[1] Note that all constructs described herein use the same enhanced green fluorescent protein (eGFP) open reading frame but for simplicity and in agreement with common usage is referred to as simply GFP.

It is clear from Fig. 2 that GFP lacking a leader sequence is cytosolic and excluded from mitochondria. In contrast, that with either leader is primarily mitochondrial, as visualized with the marker of the matrix (HSP60, Fig. 2) or IMS (cytochrome c, Fig. 3). In work described in detail elsewhere (Newman, et al.; manuscript submitted), we also generated the series of CMVΔ0-6 plasmids to express variable levels of SMAC- or OCT-HA-ARL2, a regulatory GTPase that we are currently studying for its role in mitochondrial biology. We have earlier reported the presence of endogenous ARL2 inside mitochondria, though typically only a small fraction of total cellular ARL2 is imported into mitochondria (30, 32). The addition of the leader sequences used here allowed us to target each compartment for the vast majority of the exogenously expressed proteins and allowed functional studies of its site of action and mechanisms.

Testing the targeting and processing of SMAC and OCT driven import

The use of these two N-terminal leader sequences to drive exogenous proteins to the matrix or IMS has been well documented previously (20, 21, 25, 26). But to ensure that they were acting as predicted in this system, we first used selective permeabilization of the outer and inner mitochondrial membranes of cultured cells, to document specificity in protein import (Fig. 3). The SMAC-HA-ARL2 (Fig. 3A) or OCT-HA-ARL2 (Fig. 3B) proteins were expressed in HeLa cells and one day after transfection cells were fixed in 4% paraformaldehyde. Cells were then permeabilized with different concentrations of digitonin to selectively permeabilize mitochondrial membranes, as described previously (30, 36, 37) and under Methods. At low (0.02%) detergent the outer, but not inner, mitochondrial membrane was permeabilized, allowing staining of IMS but not matrix proteins. This resulted in staining of cytochrome c (Fig. 3) or Tom20 (not shown), as positive controls, and SMAC-HA-ARL2 (Fig. 3A), but not OCT-HA-ARL2 or HSP60, as each of these was in the matrix. In contrast, permeabilization with higher (0.1%) digitonin resulted in staining of either SMAC- or OCT-tagged ARL2 as well as HSP60 (Fig. 3B). These results are completely consistent with previous evidence demonstrating specificity in targeting exogenous proteins to the matrix or IMS using these leader sequences.

Further evidence of import and specific localization within mitochondria was evident by the fact that each of the leader sequences was efficiently cleaved upon import, as seen by shifts in electrophoretic mobility in immunoblots and as described previously (20, 21, 25). To further confirm that the cleavage observed was dependent upon mitochondrial import, we examined effects of the proton ionophore, carbonyl cyanide m-chlorophenylhydrazone (CCCP) on the processing of the expressed proteins. CCCP reduces the proton gradient that is required to drive protein import that is dependent upon leader sequences (17, 18), though not that driven by Mia40 (16, 38, 39). We compared the processing of OCT-HA-GFP (data not shown), SMAC-HA-GFP, or untagged GFP (Fig. 4) in control (untreated) cells and those treated with CCCP, as described under Methods. The GFP control was expressed to the same levels with or without CCCP and migrated in SDS gels at the expected size of ~26 kDa (Fig. 4, lanes 3 and 4). The SMAC-HA-GFP was imported into the IMS, as evidenced by cleavage of the 4 kDa leader, migrating just above the untagged GFP as a result of the 1.2 kDa HA tag (Fig. 4, lane 5 vs 4). However, in marked contrast to the GFP controls, the cleavage of SMAC-HA-GFP to form HA-GFP was essentially completely prevented by CCCP (Fig. 4, lane 6). The absence of the full-length protein is thought to result from its instability in cytosol, as found in similar experiments in previous publications. Thus, as expected, the efficient import of proteins driven to the IMS or matrix by SMAC or OCT leaders is dependent upon the proton gradient across the inner mitochondrial membrane.

Expression of OCT-HA-GFP actually resulted in the appearance of three bands when lysates were probed in immunoblots, using antibodies directed against GFP (Fig. 5A, B). This was most evident upon over-exposure of immunoblots (Fig. 5, middle). Expression of untagged GFP (Fig. 5, lane 2) is used as a marker of the 26 kDa, full-length GFP that is excluded from mitochondria. This control yielded only one band. The major band observed with expression of OCT-HA-GFP migrates just above the GFP control, consistent with the addition of the HA tag. With the strongest CMV promoters and/or longer exposure of immunoblots, a band that co-migrates with GFP is evident. This is thought to result from protease activity at the N-terminus, beyond that of the leader sequence, as that lowest band stains positive

for GFP but not for HA (Fig. 5B). And the third band, migrating at ~31 kDa in SDS gels, is consistent with it being the full length OCT-HA-GFP. This species too is most evident with the strongest promoters or longest exposures of the blots. The weaker CMVΔ4-6 promoters (Fig. 5A, last three lanes) yield exclusively the cleaved, imported HA-GFP protein and thus are optimal for studies in which incomplete targeting complicates interpretations. Finally, we inconsistently observed a minor, fourth band, running just above the major HA-GFP band (*e.g.*, see Fig. 8A). We believe this to be an incompletely processed, imported species, perhaps comparable to that described earlier by Horwich, et al (20, 21) that may result from two sites of proteolysis in the leader sequence or even roles for two different proteases.

Effects of varying the levels of protein expression

An immunoblot from cells expressing OCT-HA-GFP using the different strength promoters (CMVΔ0-6) gives a good indication of the range of expression achieved (e.g., Fig. 5A). The levels of GFP achieved in cytosol (Fig. 5A, lane 2) and of the cleaved OCT-HA-GFP (and thus predominantly HA-GFP; Fig. 5A, lane 3) in the matrix are similar. While this might be expected as a result of the use of the same (CMVΔ0) promoter, this suggests that the imported protein is not rapidly degraded and that one can achieve comparable total cellular levels despite sequestration to a compartment of limited size. Note also the decreasing levels of expression in going from CMVΔ0 to CMVΔ6, as described by Morita, et al (34) but shown here for a protein that is almost exclusively localized to the matrix.

A completely analogous experiment was conducted to test the SMAC leader sequence, and results are shown in Fig. 5C. Again, the total levels of protein expressed were comparable for cytosolic GFP and for SMAC-HA-GFP that targets to the IMS. However, in this case the uncleaved protein was more prominent and there was a larger difference in size of the cleaved and uncleaved proteins as a result of the SMAC leader being almost twice as long as the OCT leader (6.8 kDa). We again observed three bands in the SMAC-HA-GFP expressing lanes with decreasing overall protein expression in moving from CMVΔ0-CMVΔ6. And again, we interpret the three bands to be uncleaved SMAC-HA-GFP, cleaved

HA-GFP, and further digested GFP that lacks the HA tag (Fig. 5D). Note that in neither case does the proteolysis appear to continue beyond the size of GFP, based upon mobility compared to the cytosolic GFP (lane 2).

We have now used this system to target a number of different proteins to sub-mitochondrial compartments and find that each construct should be tested for extent of processing. That is, the apparently higher extent of processing of SMAC-HA-GFP (Fig. 5A), compared to OCT-HA-GFP (Fig. 5C) is not a consistent result of using the SMAC vs OCT leaders. Another important variable to consider when it is important to achieve the greatest extent of specific targeting is the length of time of expression.

The levels of protein expression and rates of import can differ

Additional testing of this system to express different proteins revealed variations in the levels of protein expressed and in the rate of import/cleavage. We developed this system to assist in our studies of the ARL2 GTPase pathway inside mitochondria. In contrast to our control, GFP, we found that the levels of HA-ARL2 inside the IMS, driven there by the SMAC leader, were substantially lower than ARL2 localizing to cytosol (Fig. 6, compare lanes 2 and 3) despite being driven off the same promoter. We believe it is likely that the amount of ARL2 and SMAC-HA-ARL2 proteins expressed were similar but that the half-life of ARL2 is shorter in the IMS than in cytosol. This conclusion is supported by the observation that the levels of ARL2 and OCT-HA-ARL2, again driven off the same promoters, resulted in very similar levels of recombinant ARL2 proteins (data not shown). Previously published (32) and unpublished data (Newman, Schiavon, and Kahn; unpublished observations) from our lab further suggest that the fraction of total cellular ARL2 imported into mitochondria and/or half-life of mitochondrial ARL2 are regulated. Thus, based upon these findings we encourage anyone considering using the system described herein to take into account possible effects of targeting on the half-life or stability of your protein.

In contrast to the results with SMAC-HA-GFP, we failed to observe the uncleaved SMAC-HA-ARL2 band (predicted MW ~28.6 kDa; Fig. 6, lanes 3-9), indicating that there are also differences in the rate of import/cleavage depending upon the protein fused to the SMAC-HA leader. Note that because of the lower levels of mitochondrial ARL2 achieved from expression of SMAC-HA-ARL2, longer exposure times were needed, resulting in increased appearance of non-specific bands in immunoblots. Antigen competition (Fig. 7) was used to confirm that the bands indicated are indeed ARL2 and those identified in Fig. 6 as non-specific (N.S.) are based upon their presence in all samples, including negative controls (lane 1 and 2).

We further examined the kinetics of protein expression and import/cleavage by comparing different leader sequences as a function of time after transfection. Although it appeared in several instances that expression of the OCT fusion proteins was more evident at the earliest time point (12 hr; Fig. 8A, lane 2) than the same proteins fused to the SMAC leader (Fig. 8B, lane 2), this is not a large effect and would require extensive quantitation to confirm, so was not pursued further. In contrast, it appears that ARL2 was imported/cleaved more rapidly than was GFP when the two were expressed off the same promoter, with either leader (compare Fig. 8C to 8A, 8D to 8B). While the full length OCT-HA-GFP or SMAC-HA-GFP were evident in each case (more so with longer exposures), the full-length ARL2 fusion proteins were virtually never seen for SMAC-HA-ARL2 and only faintly, and with over-exposure, for OCT-HA-ARL2 (Fig. 8C). While a small fraction of total cellular ARL2 has been found inside mitochondria of all cells and tissues examined (32), this is not the case for GFP. Thus, ARL2 is expected to contain its own targeting information that we believe includes its N-terminus (unpublished observations). ARL2 is unique among the ARF family of regulatory GTPases in its ability to localize to mitochondria, and shares with a subset of this family the lack of N-myristoylation at the N-terminus that is important to the biology of the ARFs (40-42). Thus, we cannot exclude the possibility that the innate ARL2 MLS contributes to the faster rate of import than seen for GFP.

Finally, when these plasmids were used with a wider range of proteins some larger differences in the apparent half-lives were evident. This difference was much more marked for ELMOD2 (data not shown), an ARL2 GAP, as its level peaked at 24 hr and was essentially undetectable at later time points. Thus, the nature of the protein being examined can clearly influence the apparent kinetics of mitochondrial import as well as stability of the targeted protein and this should be taken into account.

Summary

We describe here a collection of plasmids designed for the variable expression of exogenous proteins targeted to either the mitochondrial matrix or IMS. The combination of the previously described series of CMV promoter truncations (34) with the mitochondrial leader sequences, OCT (20, 21) and SMAC (24-26), provide a powerful means of targeting exogenous proteins to either compartment. Importantly to the study of the biology of any protein(s) targeted to mitochondria, we did not observe any evident changes to mitochondria morphology upon forced import of GFP or ARL2 using this system. Thus, the presence of these proteins alone does not appear to be sufficient to trigger a response that may confound functional studies. However, this is clearly an important issue that must be addressed for each protein under study. A number of uses are envisioned for such tools, including but not limited to testing sub-mitochondrial compartments as sites of action of regulatory proteins. We expect these reagents to be perhaps most useful in analyses of proteins that are incompletely targeted to mitochondria, *e.g.*, ARL2 or STAT3. And as protein proximity assays are becoming increasingly powerful and specific (11, 43, 44) it is essential to have tools that allow as complete as possible targeting so as to minimize off-target interactors or background. It was for such studies that we emphasize the need to investigate the kinetics of protein expression and processing as residual cytosolic, full-length protein is expected to confound or complicate such datasets. While the strong MLSs employed here were shown to strongly target the designed compartment we expect residual fusion protein to be in cytosol. Thus, we expect the optimal use of these reagents in defining a protein's site of action will include targeting multiple compartments, with demonstrated functional specificity to a single compartment. Other uses are likely to be found for these

series of plasmids and to assist in such developments we have deposited them in Addgene, to make them more readily available to all researchers.

Acknowledgments

We thank Heidi McBride and Doug Green for the gifts of plasmids. This work was supported in part by grants to R.A.K (R01-GM090158), L.E.N. (American Heart Association pre-doctoral fellowship (14PRE18840040) and NIH pre-doctoral fellowship F31-GM111047) and by the Integrated Cellular Imaging Microscopy Core of the Emory Neuroscience NINDS Core Facilities grant, P30-NS055077.

References

1. Chan DC. Mitochondria: dynamic organelles in disease, aging, and development. Cell 2006;125(7):1241-1252.

2. Baloyannis SJ. Mitochondrial alterations in Alzheimer's disease. Journal of Alzheimer's disease : JAD 2006;9(2):119-126.

3. Valentine JS, Doucette PA, Zittin Potter S. Copper-zinc superoxide dismutase and amyotrophic lateral sclerosis. Annu Rev Biochem 2005;74:563-593.

4. Zhao C, Takita J, Tanaka Y, Setou M, Nakagawa T, Takeda S, Yang HW, Terada S, Nakata T, Takei Y, Saito M, Tsuji S, Hayashi Y, Hirokawa N. Charcot-Marie-Tooth disease type 2A caused by mutation in a microtubule motor KIF1Bbeta. Cell 2001;105(5):587-597.

5. Kroemer G, Reed JC. Mitochondrial control of cell death. Nat Med 2000;6(5):513-519.

6. Esposito LA, Melov S, Panov A, Cottrell BA, Wallace DC. Mitochondrial disease in mouse results in increased oxidative stress. Proc Natl Acad Sci U S A 1999;96(9):4820-4825.

7. Graham BH, Waymire KG, Cottrell B, Trounce IA, MacGregor GR, Wallace DC. A mouse model for mitochondrial myopathy and cardiomyopathy resulting from a deficiency in the heart/muscle isoform of the adenine nucleotide translocator. Nat Genet 1997;16(3):226-234.

8. Dimauro S, Davidzon G. Mitochondrial DNA and disease. Ann Med 2005;37(3):222-232.

9. Mishra P, Chan DC. Mitochondrial dynamics and inheritance during cell division, development and disease. Nat Rev Mol Cell Biol 2014;15(10):634-646.

10. Vogtle FN, Burkhart JM, Rao S, Gerbeth C, Hinrichs J, Martinou JC, Chacinska A, Sickmann A, Zahedi RP, Meisinger C. Intermembrane space proteome of yeast mitochondria. Mol Cell Proteomics 2012;11(12):1840-1852.

11. Hung V, Zou P, Rhee HW, Udeshi ND, Cracan V, Svinkina T, Carr SA, Mootha VK, Ting AY. Proteomic mapping of the human mitochondrial intermembrane space in live cells via ratiometric APEX tagging. Mol Cell 2014;55(2):332-341.

12. Chacinska A, Koehler CM, Milenkovic D, Lithgow T, Pfanner N. Importing mitochondrial proteins: machineries and mechanisms. Cell 2009;138(4):628-644.

13. Neupert W, Herrmann JM. Translocation of proteins into mitochondria. Annu Rev Biochem 2007;76:723-749.

14. Emanuelsson O, von Heijne G, Schneider G. Analysis and prediction of mitochondrial targeting peptides. Methods Cell Biol 2001;65:175-187.

15. Stojanovski D, Milenkovic D, Muller JM, Gabriel K, Schulze-Specking A, Baker MJ, Ryan MT, Guiard B, Pfanner N, Chacinska A. Mitochondrial protein import: precursor oxidation in a ternary complex with disulfide carrier and sulfhydryl oxidase. J Cell Biol 2008;183(2):195-202.

16. Fischer M, Horn S, Belkacemi A, Kojer K, Petrungaro C, Habich M, Ali M, Kuttner V, Bien M, Kauff F, Dengjel J, Herrmann JM, Riemer J. Protein import and oxidative folding in the mitochondrial intermembrane space of intact mammalian cells. Mol Biol Cell 2013;24(14):2160-2170.

17. Geissler A, Krimmer T, Bomer U, Guiard B, Rassow J, Pfanner N. Membrane potential-driven protein import into mitochondria. The sorting sequence of cytochrome b(2) modulates the deltapsi-dependence of translocation of the matrix-targeting sequence. Mol Biol Cell 2000;11(11):3977-3991.

18. Reid GA, Schatz G. Import of proteins into mitochondria. Yeast cells grown in the presence of carbonyl cyanide m-chlorophenylhydrazone accumulate massive amounts of some mitochondrial precursor polypeptides. J Biol Chem 1982;257(21):13056-13061.

19. van Loon AP, Brandli AW, Schatz G. The presequences of two imported mitochondrial proteins contain information for intracellular and intramitochondrial sorting. Cell 1986;44(5):801-812.

20. Horwich AL, Kalousek F, Mellman I, Rosenberg LE. A leader peptide is sufficient to direct mitochondrial import of a chimeric protein. EMBO J 1985;4(5):1129-1135.

21. Horwich AL, Kalousek F, Fenton WA, Pollock RA, Rosenberg LE. Targeting of pre-ornithine transcarbamylase to mitochondria: definition of critical regions and residues in the leader peptide. Cell 1986;44(3):451-459.

22. Du C, Fang M, Li Y, Li L, Wang X. Smac, a Mitochondrial Protein that Promotes Cytochrome c–Dependent Caspase Activation by Eliminating IAP Inhibition. Cell 2000;102(1):33-42.

23. Verhagen AM, Ekert PG, Pakusch M, Silke J, Connolly LM, Reid GE, Moritz RL, Simpson RJ, Vaux DL. Identification of DIABLO, a Mammalian Protein that Promotes Apoptosis by Binding to and Antagonizing IAP Proteins. Cell 2000;102(1):43-53.

24. Burri L, Strahm Y, Hawkins CJ, Gentle IE, Puryer MA, Verhagen A, Callus B, Vaux D, Lithgow T. Mature DIABLO/Smac Is Produced by the IMP Protease Complex on the Mitochondrial Inner Membrane. Molecular Biology of the Cell 2005;16(6):2926-2933.

25. Ozawa T, Natori Y, Sako Y, Kuroiwa H, Kuroiwa T, Umezawa Y. A Minimal Peptide Sequence That Targets Fluorescent and Functional Proteins into the Mitochondrial Intermembrane Space. ACS Chemical Biology 2007;2(3):176-186.

26. Sabharwal SS, Waypa GB, Marks JD, Schumacker PT. Peroxiredoxin-5 targeted to the mitochondrial intermembrane space attenuates hypoxia-induced reactive oxygen species signalling. Biochem J 2013;456(3):337-346.

27. Wegrzyn J, Potla R, Chwae YJ, Sepuri NB, Zhang Q, Koeck T, Derecka M, Szczepanek K, Szelag M, Gornicka A, Moh A, Moghaddas S, Chen Q, Bobbili S, Cichy J, *et al.* Function of mitochondrial Stat3 in cellular respiration. Science 2009;323(5915):793-797.

28. Gough DJ, Corlett A, Schlessinger K, Wegrzyn J, Larner AC, Levy DE. Mitochondrial STAT3 supports Ras-dependent oncogenic transformation. Science 2009;324(5935):1713-1716.

29. She H, Yang Q, Shepherd K, Smith Y, Miller G, Testa C, Mao Z. Direct regulation of complex I by mitochondrial MEF2D is disrupted in a mouse model of Parkinson disease and in human patients. The Journal of clinical investigation 2011;121(3):930-940.

30. Newman LE, Zhou CJ, Mudigonda S, Mattheyses AL, Paradies E, Marobbio CM, Kahn RA. The ARL2 GTPase is required for mitochondrial morphology, motility, and maintenance of ATP levels. PloS one 2014;9(6):e99270.

31. Nishi H, Ono K, Iwanaga Y, Horie T, Nagao K, Takemura G, Kinoshita M, Kuwabara Y, Mori RT, Hasegawa K, Kita T, Kimura T. MicroRNA-15b modulates cellular ATP levels and degenerates mitochondria via Arl2 in neonatal rat cardiac myocytes. J Biol Chem 2010;285(7):4920-4930.

32. Sharer JD, Shern JF, Van Valkenburgh H, Wallace DC, Kahn RA. ARL2 and BART enter mitochondria and bind the adenine nucleotide transporter. Mol Biol Cell 2002;13(1):71-83.

33. Bauer NC, Corbett AH, Doetsch PW. The current state of eukaryotic DNA base damage and repair. Nucleic Acids Res 2015;43(21):10083-10101.

34. Morita E, Arii J, Christensen D, Votteler J, Sundquist WI. Attenuated protein expression vectors for use in siRNA rescue experiments. BioTechniques 2012;0(0):1-5.

35. Zhou C, Cunningham L, Marcus AI, Li Y, Kahn RA. Arl2 and Arl3 regulate different microtubule-dependent processes. Mol Biol Cell 2006;17(5):2476-2487.

36. Jeyaraju DV, Xu L, Letellier MC, Bandaru S, Zunino R, Berg EA, McBride HM, Pellegrini L. Phosphorylation and cleavage of presenilin-associated rhomboid-like protein (PARL) promotes changes in mitochondrial morphology. Proc Natl Acad Sci U S A 2006;103(49):18562-18567.

37. Otera H, Ohsakaya S, Nagaura Z, Ishihara N, Mihara K. Export of mitochondrial AIF in response to proapoptotic stimuli depends on processing at the intermembrane space. EMBO J 2005;24(7):1375-1386.

38. Gutscher M, Pauleau AL, Marty L, Brach T, Wabnitz GH, Samstag Y, Meyer AJ, Dick TP. Real-time imaging of the intracellular glutathione redox potential. Nat Methods 2008;5(6):553-559.

39. Bose HS, Lingappa VR, Miller WL. The steroidogenic acute regulatory protein, StAR, works only at the outer mitochondrial membrane. Endocrine research 2002;28(4):295-308.

40. Randazzo PA, Terui T, Sturch S, Fales HM, Ferrige AG, Kahn RA. The myristoylated amino terminus of ADP-ribosylation factor 1 is a phospholipid- and GTP-sensitive switch. J Biol Chem 1995;270(24):14809-14815.

41. Kahn RA, Goddard C, Newkirk M. Chemical and immunological characterization of the 21-kDa ADP-ribosylation factor of adenylate cyclase. J Biol Chem 1988;263(17):8282-8287.

42. Weiss O, Holden J, Rulka C, Kahn RA. Nucleotide binding and cofactor activities of purified bovine brain and bacterially expressed ADP-ribosylation factor. J Biol Chem 1989;264(35):21066-21072.

43. Lam SS, Martell JD, Kamer KJ, Deerinck TJ, Ellisman MH, Mootha VK, Ting AY. Directed evolution of APEX2 for electron microscopy and proximity labeling. Nat Methods 2015;12(1):51-54.

44. Rhee HW, Zou P, Udeshi ND, Martell JD, Mootha VK, Carr SA, Ting AY. Proteomic mapping of mitochondria in living cells via spatially restricted enzymatic tagging. Science 2013;339(6125):1328-1331.

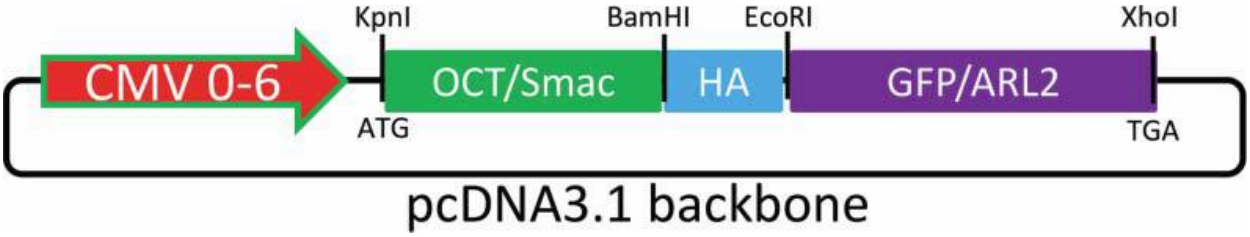

Figure 1: Schematic of constructs The parent plasmids are the collection of seven pcDNA3.1-based vectors with decreasing length and strength CMV promoters, going from pCMVΔ0-pCMVΔ6, as described in Morita, et al (34). Unique KpnI, BamHI, EcoRI, and XhoI sites were used for insertion of OCT or SMAC leaders, an HA epitope, and GFP or ARL2 open reading frames, as described under Methods.

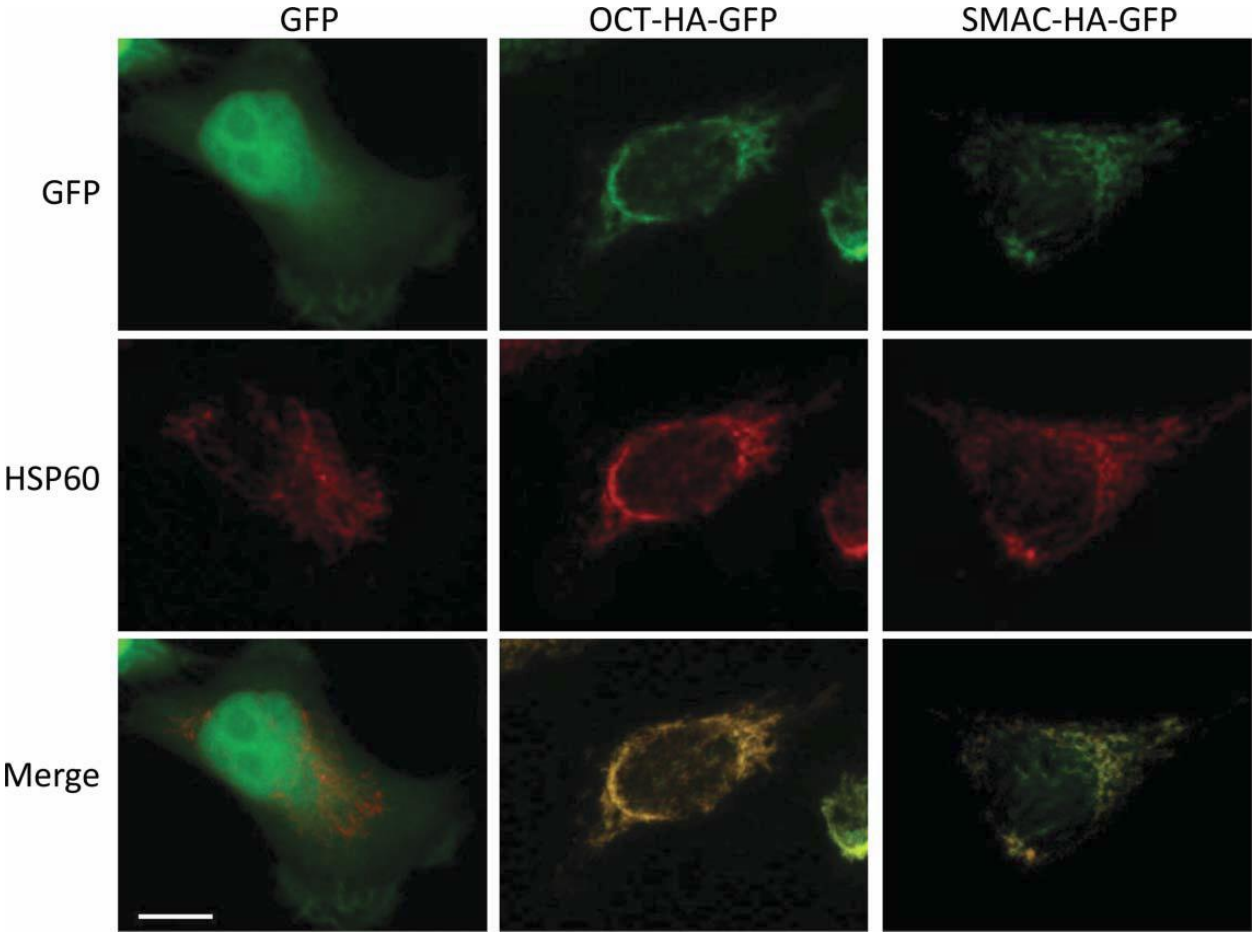

Figure 2: Neither OCT-HA-GFP nor SMAC-HA-GFP alter mitochondrial morphology. HeLa cells were transfected with GFP, OCT-HA-GFP, or SMAC-HA-GFP, fixed in 4% paraformaldehyde 24 hours later, and stained for HSP60. Z stack projections of representative cells are shown. Scale bar = 10 µm. Similar results were obtained at 48 hours after transfection (data not shown).

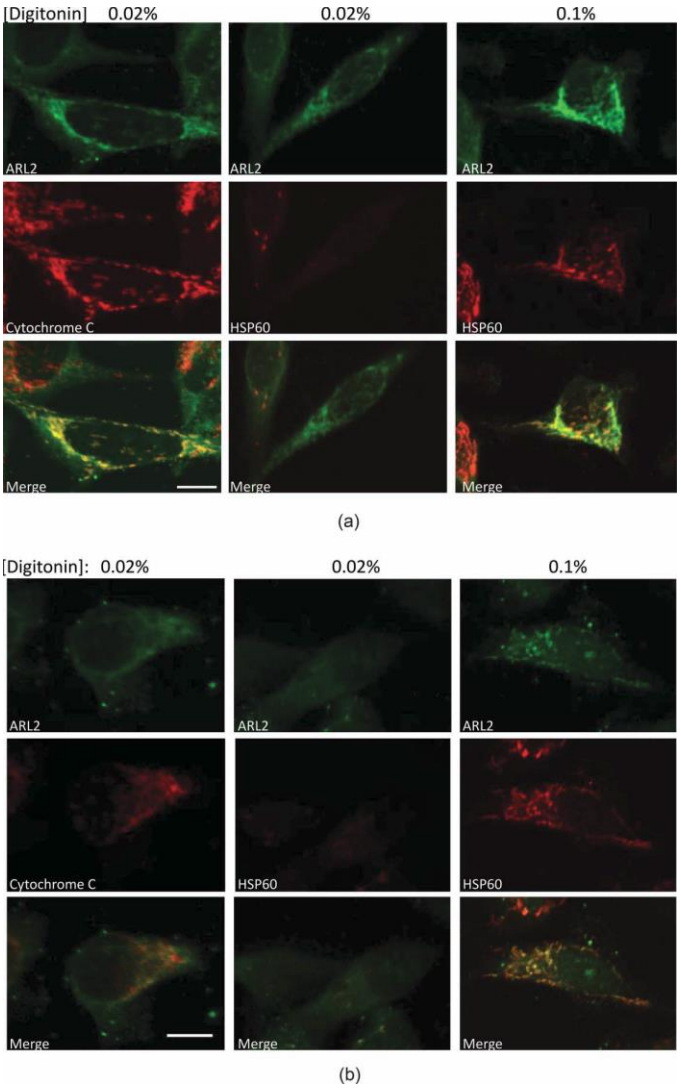

Figure 3: SMAC-HA-ARL2 and OCT-HA-ARL2 are correctly localized to the IMS or matrix, respectively. HeLa cells were transfected with plasmids directing expression of either SMAC-HA-ARL2 (**A**) or OCT-HA-ARL2 (**B**) and fixed in 4% paraformaldehyde prior to permeabilization in either 0.02% (left two columns) or 0.1% w/v digitonin (right column) for 10 minutes at room temperature, as described under Methods. Cells were then processed for immunofluorescence using dual labeling for ARL2 (green, top row) and either cytochrome c (middle row, left panel) or HSP60 (middle row, middle and right panels), as markers of the IMS and matrix, respectively. Merged images are shown in the bottom row in each case. Z stack projections are shown. Scale bar = 10 µm.

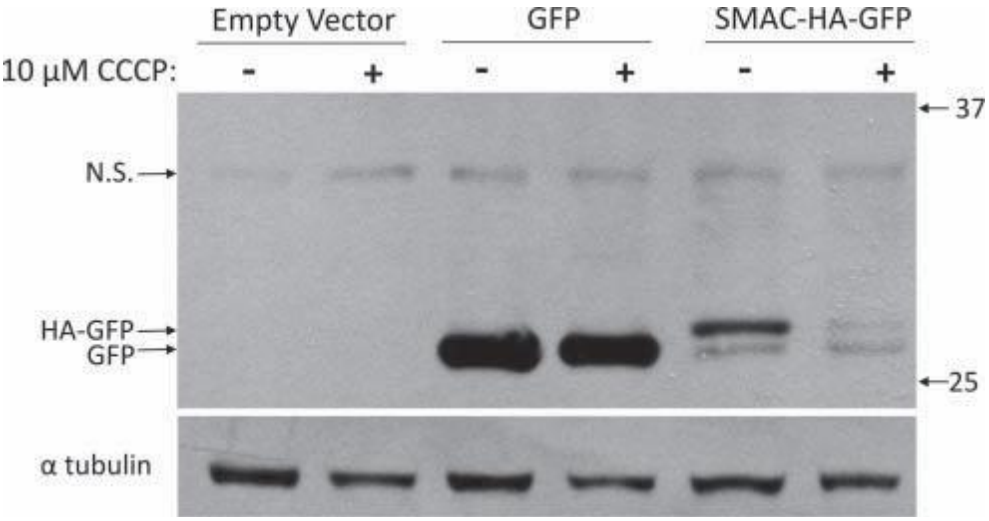

Figure 4: CCCP treatment prevents the import and cleavage of SMAC-HA-GFP. HeLa cells transfected with 1 μg of either parental plasmid (pcDNA3.1, lanes 1 and 2), or that directing expression of cytosol-localizing, untagged GFP (lane 3 and 4), or IMS-localizing SMAC-HA-GFP (lanes 5 and 6). Twelve hours after transfection, 10 μM CCCP (+) or vehicle control (-) was added to the cells, which were then harvested 4 hours later. Total cell lysates were prepared and proteins (20 μg/lane) were resolved in SDS polyacrylamide gels before transfer to nitrocellulose filters and immunoblotted using antibodies directed against GFP (top panel) or α-tubulin (bottom panel), as described under Methods. CCCP treatment had no effect on expression of cytosolic GFP (lanes 3 and 4) but decreased the expression of the cleaved protein (~28 kDa) (lanes 5 and 6). Size markers (in kDa) are shown on the right.

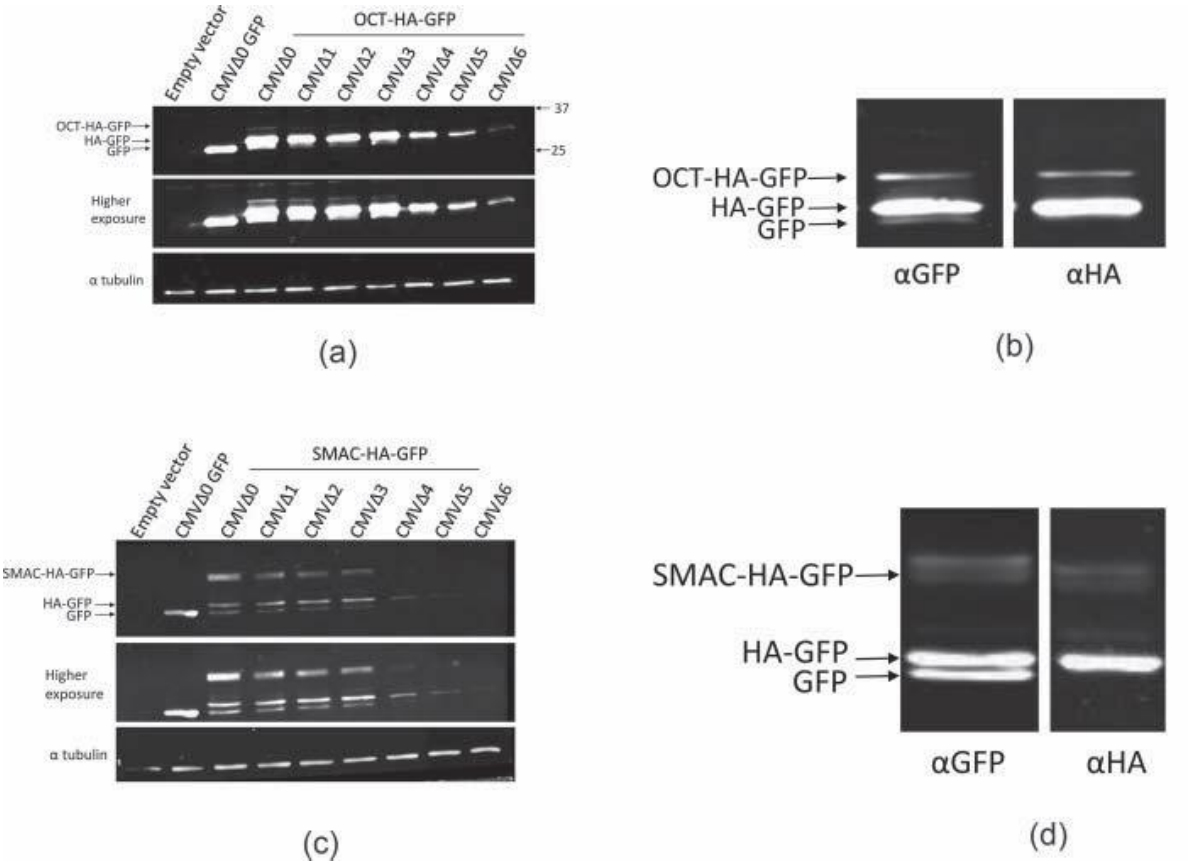

Figure 5: Comparing OCT-HA-GFP and SMAC-HA-GFP expressed with decreasing strength CMV promoters. HeLa cells transfected with 1 μg of either parental plasmid (pcDNA3.1, lane 1), or directing expression of untagged GFP (lane 2), or matrix localizing **(A)** OCT-HA-GFP under control of CMV promoters CMVΔ0-6 (lanes 3-9) or SMAC-HA-GFP **(C)** were harvested 24 hr post-transfection. Total cell lysates were prepared and proteins (20 μg/lane) were resolved in SDS polyacrylamide gels before transfer to nitrocellulose filters and immunoblotted using antibodies directed against GFP (top two panels) or α-tubulin (bottom panel), as described under Methods. A single, strong band of immunoreactivity is seen with untagged, cytosolic, GFP (lane 2) while the presence of the HA tag (lanes 3-9) results in a slightly larger protein of similar intensity. The presence of bands of higher apparent molecular weight are consistent with the full length proteins; OCT-HA-GFP predicted to be 31 kDa and SMAC-HA-GFP 34 kDa. Duplicate samples of CMV0-OCT-HA-GFP (**B**) or CMV0-SMAC-HA-GFP **(D)** were analyzed, one probed for GFP and the other for HA. Size markers (in kDa) are shown on the right.

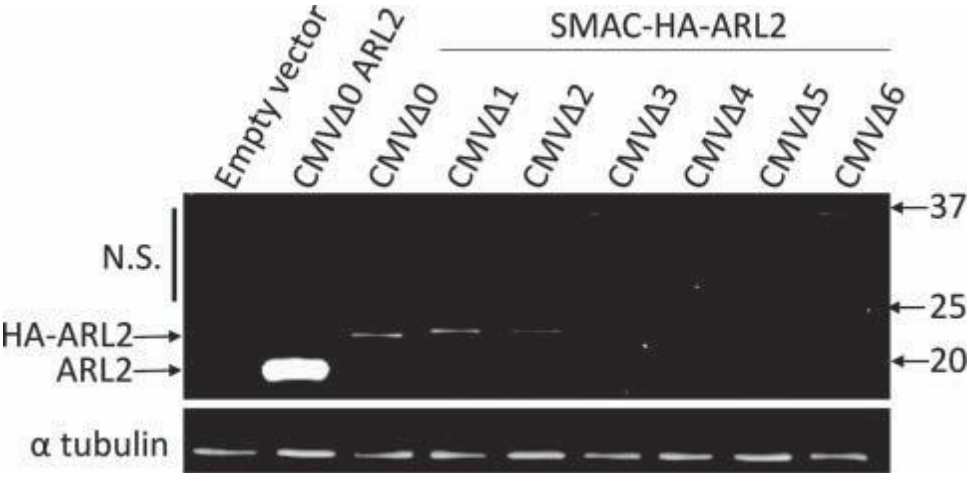

Figure 6: SMAC-HA-ARL2 is expressed to lower levels than is ARL2 and cleavage appears to be complete at every level of expression. HeLa cells were transfected with the series of 7 different strength CMV promoters to express SMAC-HA-ARL2, as described in the legend to Figure 2 and under Methods, with blotting for either ARL2 or α-tubulin. Empty pcDNA3.1 (lane 1) or expressing untagged ARL2 (lane 2) were included as controls. In contrast to results from SMAC-HA-GFP (see Figure 3), we could detect no evidence of uncleaved SMAC-HA-ARL2, indicating it is very efficiently processed to HA-ARL2, consistent with its mobility in SDS gels. SMAC-HA-ARL2 was also expressed to much lower levels than untagged ARL2, even when each used the same (CMVΔ0) promoter. Note that because of the lower levels of expression it was necessary to use longer exposure times, resulting in the more evident appearance of non-specific bands (N.S.), as seen even in control lanes (1 and 2).

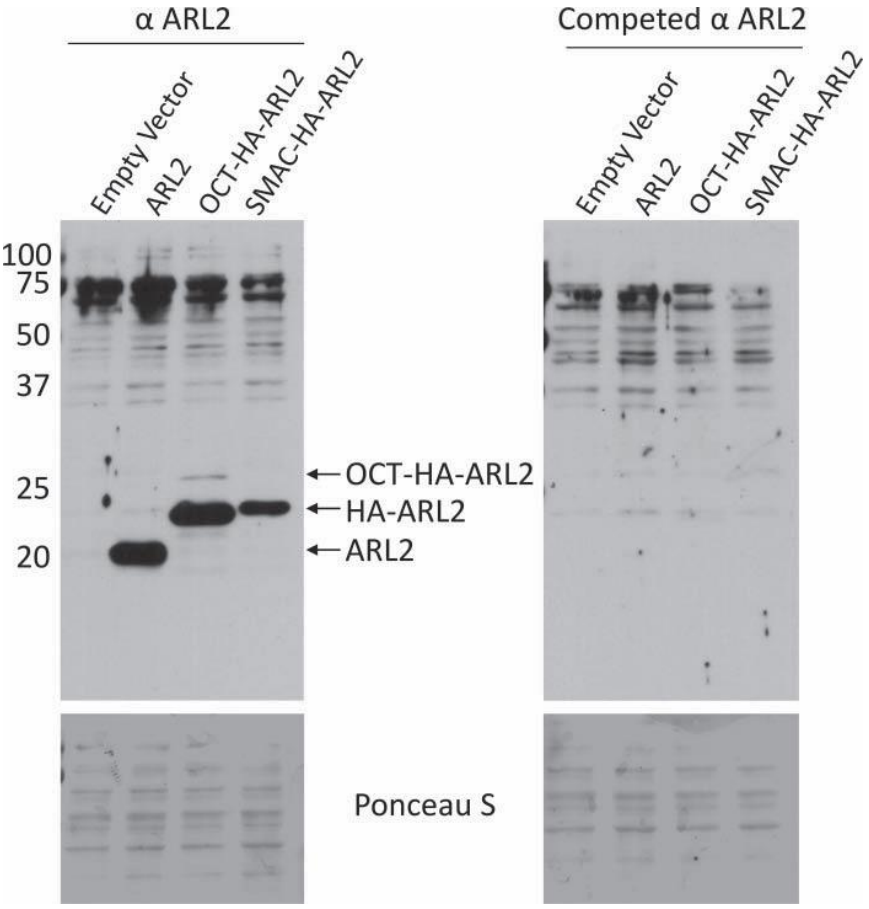

Figure 7: Antigen competition confirms the identity of ARL2 fusion proteins and specificity of the ARL2 antibody. HeLa cells transfected with 1 μg of either parental plasmid (pcDNA3.1, lane 1), or directing expression of untagged ARL2 (lane 2), OCT-HA-ARL2 (lane 3), or SMAC-HA-ARL2 (lane 4) and harvested 24 hr post-transfection. Total cell lysates were prepared and two sets of identical samples (5 μg/lane) were resolved in one SDS polyacrylamide gel before transfer to nitrocellulose filters, as described under Methods. The two sets of identical samples were separated and probed with our rabbit polyclonal antibody directed against ARL2 at 1:7,000 dilution, either without (left panel) or with (right panel) prior incubation with 20 μg purified, recombinant ARL2. Bands corresponding to untagged ARL2 (lane 2), uncleaved and cleaved OCT-HA-ARL2 (lane 3), and cleaved SMAC-HA-ARL2 (lane 4) are all absent from the competition blot. Ponceau S staining of the blots immediately after transfer shows that equal protein was present on both blots.

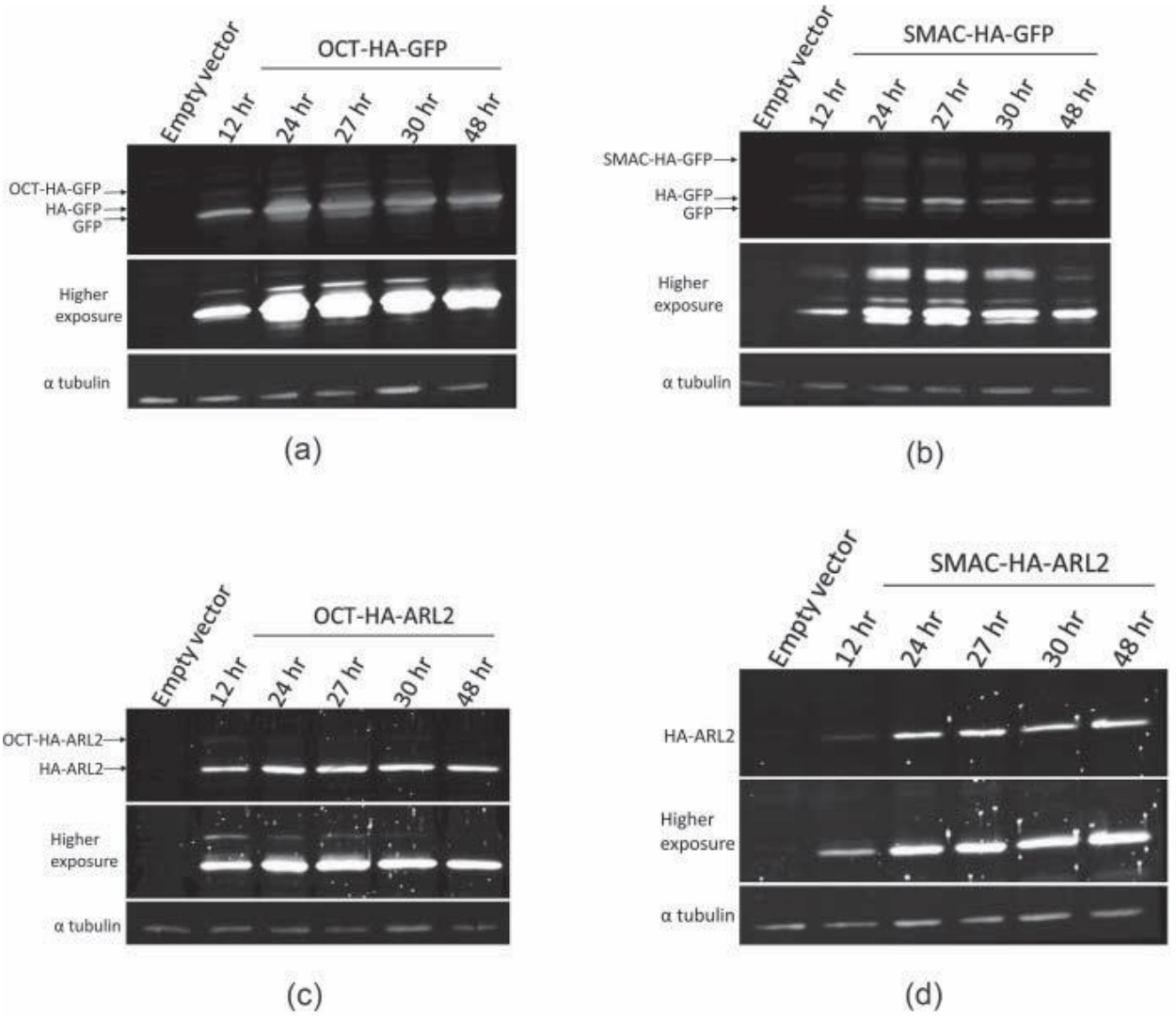

Figure 8: Different proteins expressed off the same promoters and leader sequences are expressed to different levels and with differing extents or kinetics of import/processing. ALL PANELS: HeLa cells were transfected with 1 μg pCMVΔ0 plasmids directing expression of no exogenous protein (Empty vector), OCT-HA-GFP, SMAC-HA-GFP, OCT-HA-ARL2, or SMAC-HA-ARL2, as described under Methods. Cells were harvested at the indicated times, lysates prepared, and total cellular proteins (20 μg) were resolved in SDS gels. Immunoblotting was performed with antibodies to GFP, ARL2 or α-tubulin (loading control). (**A**) Processed OCT-HA-GFP is readily apparent within 12 hours after transfection and the level is fairly constant over the 48 hrs of this study. With longer exposure the full length protein is evident though is greatly reduced by 48 hrs, at which point new protein expression is expected to be

clearly diminished. Some partially processed or further processed proteins may be seen above or below the major band of HA-GFP, which migrates at the expected 28 kDa. (**B**) SMAC-HA-GFP expression may be slightly delayed, in comparison to the OCT-HA-GFP, with a larger fraction of the recombinant protein migrating as the uncleaved ~35 kDa protein. Partially cleaved and further processed proteins are again evident. (**C**) OCT-HA-ARL2 expression is evident as the imported/cleaved protein is readily observed within 12 hr after transfection and is quite stable over the 48 hr time course. Small amounts of the uncleaved or partially cleaved protein can be seen with over-exposure but these are essentially gone by 48 hrs. (**D**) SMAC-HA-ARL2 is the most efficiently imported/cleaved protein tested, with difficulty seeing the uncleaved protein at any time point, and is also stable over the 48 hr time course.

Chapter 3: The abundance of the ARL2 GTPase and its GAP, ELMOD2, at mitochondria are modulated by the fusogenic activity of mitofusins and stressors

This chapter was published as:

Laura E. Newman*, Cara R. Schiavon*, Chengjing Zhou, Richard A. Kahn. The abundance of the ARL2 GTPase and its GAP, ELMOD2, at mitochondria are modulated by the fusogenic activity of mitofusins and stressors. PloS one. 2017

* These authors contributed equally to this work

Abstract

Mitochondria are essential, dynamic organelles that respond to a number of stressors with changes in morphology that are linked to several mitochondrial functions, though the mechanisms involved are poorly understood. We show that the levels of the regulatory GTPase ARL2 and its GAP, ELMOD2, are specifically increased at mitochondria in immortalized mouse embryo fibroblasts deleted for Mitofusin 2 (MFN2), but not MFN1. Elevated ARL2 and ELMOD2 in MEFs deleted for MFN2 could be reversed by re-introduction of MFN2, but only when the mitochondrial fragmentation in these MEFs was also reversed, demonstrating that reversal of elevated ARL2 and ELMOD2 requires the fusogenic activity of MFN2. Other stressors with links to mitochondrial morphology were investigated and several, including glucose or serum deprivation, also caused increases in ARL2 and ELMOD2. In contrast, a number of pharmacological inhibitors of energy metabolism caused increases in ARL2 without affecting ELMOD2 levels. Together we interpret these data as evidence of two ARL2-sensitive pathways in mitochondria, one affecting ATP levels that is independent of ELMOD2 and the other leading to mitochondrial fusion involving MFN2 that does involve ELMOD2.

Introduction

Mitochondria are essential organelles that are hubs for several important cellular functions, including ATP production, lipid metabolism, calcium regulation, and apoptosis. This diversity of essential functions is accompanied by diversity in morphology as mitochondria are highly dynamic organelles that can range in size and shape from many small spheres to one large inter-connected network. The linkages between function and morphology must be sensitive to cues coming from other parts of the cell [1-3]. Mitochondrial morphology is the result of a balance between fission and fusion, which are mediated by four large dynamin-related GTPases. Mitochondrial fission is mediated by DRP1 [4, 5], while fusion is controlled by three GTPases: MFN1 and MFN2 regulate outer membrane fusion [6, 7], and OPA1

promotes inner membrane fusion [8]. Mitochondria elongate during several types of stress as a result of increased fusion [9, 10] and also elongate during starvation, protecting them from autophagy [11, 12].

To date, only a handful of proteins have been shown to regulate either mitofusins or OPA1, and how these regulators promote fusion under stress is an area of ongoing research.

We recently discovered that ARL2 plays a role in the regulation of mitochondrial fusion (Newman et al., submitted). ARL2, a ~20 kDa member of the ARF family of regulatory GTPases, is very highly conserved throughout eukaryotic evolution, ubiquitously expressed, predicted to be present in the last eukaryotic common ancestor [13], and is essential in eukaryotes [14-16]. ARL2 plays essential roles in the biogenesis of tubulin and in microtubule dynamics, as well as traffic of farnesylated proteins [17-24]. Only later was ARL2 found to also localize specifically to mitochondria, where it also plays essential roles. ARL2 siRNA causes mitochondrial fragmentation, a loss in plus-end directed mitochondrial motility, and a dramatic (~50%) loss in cellular ATP [25]. ARL2 also regulates mitochondrial fusion from the IMS, acting upstream to increase fusion requiring either MFN1 or MFN2 (Newman, et al. submitted).

We also identified and purified the ARL2 GAP, ELMOD2, and found that it too localizes to mitochondria [26]. ELMOD2 siRNA results in fragmentation and perinuclear clustering but has no effect on ATP levels. As a result, we currently model ARL2 as having at least two distinguishable actions in mitochondria: one leading to regulation of ATP production and a separate one that involves ELMOD2 and impacting fusion and motility.

Mitochondria play crucial roles in several essential cellular processes and must be sensitive to inputs from different parts of the cell to maintain homeostasis or respond to a changing environment. With the identification of a regulatory GTPase and an effector/GAP implicated as regulators of fusion and motility, we sought to examine whether they may be responsive to stressors that are known to impact mitochondrial morphology and functions. Here, we show that the levels of mitochondrial ARL2 and

ELMOD2 are highly sensitive to mitochondrial stress and changes in the levels of MFN2. These results further the model that ARL2 and ELMOD2 are components in a system of communication between mitochondria and other parts of the cell.

Methods

Antibodies & reagents

Rabbit polyclonal antibodies directed against human ARL2, ARL3, and ELMOD2 were generated in our lab and have been described previously [25, 30, 47]. Characterization of the specificity of these reagents has included comparisons to pre-immune serum and antigen competition in both immunoblots and indirect immunofluorescence. Each of these methods has been optimized for specificity and sensitivity of these antibodies. The following antibodies were obtained from commercial sources: HA (Covance MMS-101P), HSP60 (Enzo Life Sciences ADI-SPA-807), cytochrome c (BD Biosciences 556432), myc (Invitrogen R950-25), TOM20 (BD Biosciences 61228), OPA1 (BD Biosciences 612606), Complex V subunit alpha (Mitosciences MS502), NDUFA9 (Mitosciences MS111), UQCRC2 (Mitosciences MS304), alpha tubulin (Sigma T9026), ELMOD2 (St. John's Laboratory STG27186). We used a commercial ELMOD2 antibody for western blotting because it generated immunoblots with fewer nonspecific bands (as determined by antigen competition). The following antibody dilutions were used in our studies for immunofluorescence: ARL2 (1:2000), ELMOD2 (1:500), ARL3 (1:1000), HSP60 (1:5000), myc (1:1000), HA (1:2000), cytochrome c (1:2000), TOM20 (1:5000), OPA1 (1:100), Complex V subunit alpha (1:200), NDUFA9 (1:200), UQCRC2 (1:2000). The following antibody dilutions were used for immunoblotting: ARL2 (1:2000), ELMOD2 (1:500), OPA1 (1:1000), alpha tubulin (1:2500), myc (1:1000).

Cloning and constructs

The following plasmids were generously provided by David Chan: MFN1-10xmyc and MFN2-16xmyc in pcDNA3.1, and MFN2 CMT2A mutations [V69F], [L76P], [R94Q], and [R274Q] in MFN2-

7xmyc in pcDNA3.1 [6, 34]. The MFN2[K109A]-16xmyc plasmid (in pcDNA3.1) was generated in the lab of David Chan and obtained through Addgene (plasmid 26051). CMVΔ6 SMAC-HA-ARL2 and OCT-HA-ARL2 have been described and characterized previously [43].

Cell culture

Human cervical carcinoma (HeLa), mouse embryonic fibroblast (MEF) and African green monkey kidney (COS7) cell lines were used in our studies to allow comparisons between them, ensure against a phenomenon that may be unique to one line, and to allow comparisons between cells displaying different mitochondrial morphologies. All were used as they are relatively flat, making them good for imaging. Additionally, we routinely obtain high transfection efficiencies (50-90%) and can readily detect endogenous ARL2 and ELMOD2 in HeLa and COS7 cell lines. Most experiments described here were performed in each of the different cell lines and we obtained very similar results. Cells were grown in DMEM medium, supplemented with 10% fetal bovine serum (FBS; cat# 11965-092, Invitrogen, Carlsbad, CA) and 2mM glutamine at 37°C in the presence of 5% CO2. For imaging, cells were grown on matrigel (BD Biosciences #356231) coated coverslips. HeLa and COS7 cells were originally obtained from the ATCC. Immortalized MEFs from wild type, *mfn1-/-*, *mfn2-/-*, or *mfn1-/-mfn2-/-*, mice were a generous gift from Dr. David Chan [6, 7, 32, 33].

Treatment with metabolic stressors

Prior to exposure to stressors, cells were plated on matrigel-coated coverslips and allowed to attach for at least four hours in standard DMEM medium. For growth in medium containing different carbon sources, the medium was exchanged after cells had attached. Cells were then fixed 24 or 48 hours later. Our normal DMEM medium contains 25 mM glucose supplemented with 10% FBS. No glucose medium is DMEM with no added glucose (cat# 11966-025, Invitrogen) supplemented with 10% FBS. Low serum medium is DMEM (25 mM glucose) supplemented with 2% FBS. Galactose medium was

previously described [39] and was made with DMEM containing no glucose but with 10 mM galactose, 10 mM HEPES pH 7.4, and 10% FBS.

For other treatments, cells were plated and maintained in standard (25 mM glucose) DMEM with 10% FBS. One day after plating, cells were treated with the following drugs for the following times: 25 mM 2-deoxyglucose (Sigma cat#D8375, 16 hours), 10 μM oligomycin (Seahorse cat#101706-100, 16 hours), 10 μM antimycin A (Seahorse cat#101706-100, 16 hours), 10 μM rotenone (Seahorse cat#101706-100, 16 hours).

Mitochondrial fractionation

Mitochondria were fractionated using a previously published protocol [65]. Cells were washed twice in PBS, incubated for 10 minutes in 5 mM EDTA in PBS, and collected. Cells were pelleted and washed in TD buffer (25 mM Tris-HCl, pH 7.4, 0.7 mM Na2HPO4, 133 mM NaCl, 5 mM KCl). Cells were resuspended in RSB buffer (10 mM Tris-HCl pH 7.4, 10 mM NaCl, 1.5 mM CaCl2, protease inhibitors (Sigma #P-2714), to a final volume of about 10x the volume of the cell pellet, and incubated on ice for 20 minutes prior to homogenization with a Dounce glass/glass tight homogenizer (30 strokes). Lysis of cells was verified using trypan blue. MS buffer, prepared as a 2.5X stock, was added to yield a final concentration of 1x MS (5 mM Tris-HCl pH 7.4, 210 mM mannitol, 70 mM sucrose, 5mM EDTA pH 8). Unbroken cells and nuclei were removed by centrifugation (10 min., 1000xg), after which mitochondria were pelleted from the post-nuclear supernatant (20 min., 14,000xg). Mitochondria were then solubilized for 30 minutes on ice in 1% CHAPS, 25 mM HEPES pH 7.4, 100 mM NaCl, and protease inhibitors.

Western blotting

Cells were harvested by rinsing twice with PBS, collected by incubation in 5mM EDTA in phosphate buffered saline (PBS; 140 mM NaCl, 3 mM KCl, 10 mM Na2HPO4, 2 mM KH2PO4, pH 6.75), and pelleted in a microfuge (14,000 rpm, 4ÊC). Cells were lysed in 1% CHAPS, 25 mM HEPES

pH 7.4, 100 mM NaCl, and protease inhibitors (Sigma #P-2714) on ice for 30 minutes, and the S14 was obtained by clarifying lysates by centrifugation for 30 minutes (14,000 rpm, 4ÊC). Protein concentrations were determined by Bradford Assay (Bio-Rad) using bovine serum albumin as standard. Samples were separated on 13% polyacrylamide gels and wet-transferred to nitrocellulose membranes (Bio-Rad #162-0112) at 70V for 2.5 hours. Western blotting procedures were carried out at room temperature. Membranes were blocked in blotto (5% (w/v) dry milk, 50 mM Tris pH 8, 2 mM CaCl2, 80 mM NaCl, 0.2% (v/v) Tween-20, 0.02% sodium azide) for 1 hour. When probing for ARL2, membranes were blocked in an alternate blocking buffer (10% goat serum, 5% Tween-20 in PBS), freshly filtered through a 0.2 μm membrane. Membranes were then incubated with primary antibody in blocking buffer at 4°C overnight. Removal of excess primary antibody was carried out by washing the membranes in PBST (PBS with 0.1% Tween-20) three times for 10 min each. HRP-conjugated secondary antibodies (GE cat #NA934V, #NA931V) were diluted 1:5,000 in PBST and incubated with the membrane for 1 hour at room temperature. Excess secondary antibody was removed by washing the membranes in PBST 3 times for 10 min each, then incubated in luminol containing solution (0.1 mM Tris-HCl pH 8.0, 1.2 mM luminol, 0.2 mM p-coumaric acid, 0.009% hydrogen peroxide) for 1 min prior to exposure to film.

Transfections

Cells at 90% density or higher were transfected in 6 well plates using the following protocols. Both the amount of DNA and the ratio of Lipofectamine: DNA were separately optimized for ARL2 expression in HeLa and COS7 cells. A ratio of 2 μg Lipofectamine: 1 μg DNA yielded the highest transfection efficiency. ARL2 plasmids (2 μg) were diluted in 250 μL Optimem (Invitrogen). Lipofectamine 2000 (4 μg; Invitrogen) was diluted in a separate tube containing 250 μL Optimem, vortexed briefly, and incubated at room temperature for 5 minutes. The tubes were mixed and incubated 20 minutes. Cell culture medium was changed to 1.5 ml of Optimem, and transfection complexes (500 μL) were added dropwise to the cells. After 4 hours, cells were trypsinized and replated onto coverslips,

typically at a 1:3 (24 hour time point) or 1:4 (48 hour time point) split. This transfection typically resulted in at least 70% of cells overexpressing ARL2.

MEFs were transfected using a similar protocol. Both the amount of DNA and the ratio of Lipofectamine: DNA were optimized for expression in MEFs. A ratio of 3 μg Lipofectamine: 1 μg DNA yielded the highest percentage of transfected cells, based upon immunofluorescent staining. Plasmids (5 μg) and Lipofectamine 2000 (15 μg; Invitrogen) were diluted in separate tubes, each containing 250 μL Optimem. The tube containing Lipofectamine was vortexed briefly, and incubated at room temperature for 5 minutes. The tubes were then mixed and incubated 20 minutes at room temperature. Cell culture medium was changed to 1.5 ml of Optimem, and transfection complexes (500 μL) were added dropwise to the cells. After 4 hours, cells were trypsinized and replated onto matrigel-coated coverslips, typically at a 1:4 split, and allowed to attach overnight. This transfection protocol typically resulted in ~40% of MEFs expressing MFN1-myc or MFN2-myc.

Immunofluorescence

Cells grown on matrigel-coated coverslips were fixed in a pre-warmed (37°C) solution of 4% paraformaldehyde in PBS (10 mM Na2HPO4, 2 mM KH2PO4, pH 6.75, 140 mM NaCl, 3mM KCl) for 15 minutes at room temperature, and then permeabilized with 0.1% (v/v) Triton X-100 in PBS for 10 minutes at room temperature. Incubation with primary antibodies was carried out in filtered PBS containing 1% (w/v) BSA at 4°C overnight, followed by 4 x 5 minute washes in PBS. Secondary antibodies (1:500, Alexa fluorophores 488 and 546, Invitrogen) were incubated in PBS containing 1% BSA for 1 hour at room temperature. Secondary antibody was removed by 2 x 5 minute washes in PBS. DNA was then stained with Hoechst 33342 (1 μM) (excitation max = 350 nm, emission max = 461 nm) for 4 minutes, followed by 2 x 5 minute washes in PBS. Coverslips were then mounted onto slides using Prolong Antifade (Invitrogen). To perform pre-permeabilization fixation, cells were treated with ice-cold 0.5% saponin in PBS for 1 minute on ice and immediately fixed with ice cold 4% PFA. Staining was then

performed as described above. We routinely perform staining with only secondary antibody incubation, to ensure that the signal we observe is specific to our primary antibodies.

Imaging

Images were acquired using an Olympus FV1000 microscope and Olympus Fluoview v1.7 software, using a 100x oil objective (1.45 NA). Alexa 488 (excitation maximum = 496 nm, emission maximum = 519 nm) and 546 (excitation maximum = 556 nm, emission maximum = 573 nm) fluorophores were imaged using 488 and 543 laser excitation, respectively. We ensured that the signal we observe while double labeling was not due to bleed through by labeling cells separately with each fluorophore and imaging with each laser line. Images were acquired with a resolution of 1024x1024 pixels and 16 bit depth. Z-stacks were acquired with a step size of 0.37 μm, which were converted to average image intensity projections using ImageJ, where indicated. Whenever ARL2 or ELMOD2 staining was compared between different experimental conditions, imaging settings were held constant between slides and conditions. Cells were plated using coverslips from the same batch, fixed the same day, stained with the same dilution of antibody at the same time, and imaged the same day using the same parameters (laser power, gain, pinhole, and offset). No adjustments to ARL2/ELMOD2 staining were made post-acquisition (other than increasing brightness and contrast of images for easier visualization, which was applied uniformly to all images in any comparison), and post-imaging processing of ARL2 and ELMOD2 staining was limited to generation of z-stack projections. We noted that z-stack projections of ELMOD2 stained cells resulted in higher quality images, so are used for ELMOD2 images. No such improvement was noted with z stack projections of ARL2 stained cells, so single focal planes are shown in order to minimize image processing. Focal planes selected for presentation were chosen with regard to bringing the most mitochondria in focus.

Imaging quantification

Image quantification was performed using ImageJ. Individual cells were cropped from a field, and 8 bit average z stack projections were generated. Automatic thresholding was performed on the mitochondrial channel (HSP60 or cytochrome c) using Otsu's method [66], to generate a mask. The mean pixel intensity in the ARL2 or ELMOD2 channel was then measured within the mask. For each condition, at least 10 cells were analyzed from one representative experiment, and each experiment quantified here has been repeated at least three times. Data represented are an average, normalized using the average of the control condition. Error bars represent standard error of the mean (SEM). To determine if increases in ARL2/ELMOD2 staining were significant, one tailed t tests were performed using Prism. One asterisk (*) denotes $p<0.05$, two (**) denotes $p<0.01$, three (***) denotes $p<0.001$, and four (****) denotes $p<0.0001$.

Structured Illumination Microscopy (SIM)

Cells were imaged on a Nikon N-SIM using a 100X (NA 1.49) oil objective. For each cell, a widefield image was obtained in addition to raw SIM data. Reconstruction was achieved using the Nikon Elements software, and reconstruction parameters suggested by the software were adjusted with reference to the widefield image, to avoid previously described artifacts (http://www.gelifesciences.com/gehcls_images/GELS/Pdf%20documents/2015-05-06-Pellett-Bitesizebio-Seminar.pdf).

Authentication of key reagents and data reproducibility

All cell lines used in our studies were originally obtained from ATCC, with the exception of mouse embryo fibroblast (MEF) lines that were either made by collaborators or colleagues who publish them and send them directly to us. All cell lines are routinely (approximately monthly) screened for the presence of mycoplasma, using DNA staining or PCR protocols. Records are maintained of cell line sources and passage number for each cryopreserved sample and no cells are used beyond passage 30. Every experiment was repeated at least twice, yielding similar results, and typically several more than two

times. Because cell lines are clonal they are not viewed as biological replicates but technical ones when plated on multiple cover slips or dishes. The numbers of cells analyzed is stated for each condition, when quantification of pixel intensities was performed, as described above.

Antibodies used in these studies that were generated by contracts to companies for animal injections using our purified proteins (ARL2, ARL3, and ELMOD2) and characterized by us *at a minimum* for specificity in immunoblotting and immunofluorescence assays by comparison of immune to pre-immune sera and using (purified) antigen competition. When possible we also use antigen competition to confirm/test for specificity of antibodies obtained from other researchers or vendors. All antibodies are tested for recognition of a protein of the expected molecular weight in immunoblots. When an appropriate plasmid is available we also use transient over-expression in immunoblotting to confirm band with correct electrophoretic mobility.

Results

Mitochondrial ARL2 staining is sensitive to re-plating and cell density

Studies of ARL2 began in the 1990's with a focus on its role in microtubules as a result of data from genetic studies in several model organisms [14-16, 27-29]. In contrast, studies in our lab during and since that period have consistently pointed to mitochondria as an important site of action for ARL2 [25, 30, 31]. Characterization of our specific rabbit polyclonal antibody directed against ARL2 allowed immunofluorescent and immunoblotting evidence of the existence of a mitochondrial pool of ARL2, estimated at ~5% of total cellular ARL2 [30]. Throughout our studies we have noted that the intensity of mitochondrial staining of ARL2 varied between experiments and cell lines. With our long term goal of understanding the mechanisms of both ARL2 regulation of mitochondrial fusion (Newman et al., submitted) and actions in other parts of the cell, we sought to better understand the sources of variation in staining of mitochondrial ARL2. Systematic and careful analysis of imaging data allowed us to identify a number of conditions that contribute to variations in the intensity of imaging data for ARL2 in

mitochondria. These are described below and provide further support for our conclusion that ARL2 and its GAP, ELMOD2, regulate mitofusins and mitochondrial fusion and are themselves regulated in abundance at mitochondria.

The first variable identified was the time between plating of cells and fixation prior to imaging. When HeLa cells were fixed and stained within 24 hours of plating, the ARL2 staining profiles were diffuse and only weakly reminiscent of mitochondria, though double labeling with mitochondrial markers confirmed that some ARL2 was indeed overlapping with markers of mitochondria and represented mitochondrial ARL2 (Fig 1A and 1B). Mitochondrial ARL2 staining became stronger and as a result more clearly overlapping with that of the intermembrane space (IMS) marker cytochrome c or matrix marker HSP60 (Fig 1B) after two days and even more so by the third day. This does not appear to be the result of depletion of nutrients from culture medium as more frequent feeding with fresh medium did not alter this time course. By the fourth day after plating or if the initial plating was at a higher cell density (Fig 1B), cells were typically near confluence and we found that mitochondrial staining of ARL2 was clearly decreased. When the time after plating was held constant but the cell density was varied it was quite clear that higher cell density resulted in decreased mitochondrial staining; typically, this was evident as cells approached ~90% confluence. Note that the effects of time after plating and cell density are quite obvious by visual inspection and consistent throughout the cell population, as seen in the view shown in Fig 1A and quantified in Fig 1C, but are more evident as mitochondrial-specific in the enlarged view of single cells, shown in Fig 1B and later figures. The effects of days after plating on ARL2 staining at mitochondria was evident in HeLa and MEFs but not COS7 cells, although the effects of cell density on ARL2 was observed in all three cell lines. Mitochondrial staining of ELMOD2, an ARL2 GAP, also diminished with approach to confluence (Fig 1D) but was unchanged with different days after plating (Fig 1E). When quantified, we observed no statistically significant change in mitochondrial ELMOD2 staining with different days after plating, unlike ARL2. While consistent and highly reproducible, the effects of time after plating and cell density on ARL2 staining were weaker than other effects on ARL2 staining,

described below. All immunofluorescence data described used fixation with 4% paraformaldehyde and permeabilization with 0.1% Triton X-100. These conditions were chosen as optimal for visualization of mitochondrial proteins, particularly ARL2 as its larger cytosolic pool is expected to be incompletely fixed and appear as diffuse staining throughout the cell. However, it is also quite apparent that under these conditions our rabbit, polyclonal antibody raised against ELMOD2 yields a strong signal in the nucleus (Figs 1-9). This nuclear staining is present in the pre-immune serum and is not competed by prior incubation of the primary antibody with antigen (purified, recombinant ELMOD2) [25] and thus is non-specific. This is in contrast to the signal from this same antibody that overlaps with mitochondria markers, *e.g.*, HSP60 (*e.g.*, Figs 1, 2D, and 3B). All comparisons in staining intensities described below are controlled for time after plating and for cell densities.

Deletion of MFN2 increases mitochondrial staining of ARL2 and ELMOD2

Using immortalized MEFs deleted for MFN1, MFN2, or both mitofusins [6, 7, 32, 33], we found that expression of the dominant active point mutant, ARL2[Q70L], reversed mitochondrial fragmentation associated with the loss of either MFN1 or MFN2, but not the loss of both (Newman, et al., submitted). When we stained wild type, *mfn1-/-*, *mfn2-/-*, or *mfn1-/-mfn2-/-* MEFs, all grown under the same conditions (DMEM medium, 25 mM glucose, 10% FBS), we found strong differences in the levels of endogenous, mitochondrial ARL2 staining. MEFs were plated at the same density, and fixed, stained, and imaged in parallel, to control for other factors, as described above. While we observed mitochondrial staining of ARL2 in wild type MEFs, it was clearly stronger in *mfn2-/-* MEFs, and even stronger in the double null (*mfn1-/-mfn2-/-*) MEFs (Fig 2A, 2B and 2E). Though most *mfn1-/-mfn2-/-* MEFs had clearly stronger mitochondrial staining of ARL2, compared to *mfn2-/-* or wild type MEFs (Fig 2A, 2B and 2E), we noted an increase in heterogeneity in mitochondrial staining of ARL2, compared to the other two MEF lines, possibly due to the previously documented heterogeneity among mitochondria within these cells due to the complete loss of fusion [7]. Because of this greater heterogeneity, we show both a field of cells as well as an enlarged view of 1-2 cells in Fig 2A and 2B, respectively, with the latter showing double

labeling with the matrix marker HSP60. We obtained the same results when ARL2 was visualized with a mouse monoclonal antibody, detecting the increases in staining of mitochondrial ARL2 in *mfn2-/-* and *mfn1-/-mfn2-/-* MEFs. In striking contrast, mitochondrial ARL2 staining in *mfn1-/-* MEFs appeared diminished, compared to wild type MEFs, with the majority of cells in the population showing no discernable mitochondrial ARL2 signal (Fig 2A and 2B). Quantification of wild type and *mfn1-/-* MEFs revealed no significant differences between these two populations, while the *mfn2-/-* and double null cells displayed statistically significantly increases in ARL2 staining than wild type controls (Fig 2E). Fig 2 also shows, particularly when viewing HSP60 staining, the fragmentation of mitochondria that results from the loss of MFNs, as described previously [6, 7]. Because mitochondrial staining was increased in *mfn2-/-* and *mfn1-/-mfn2-/* MEFs, but unchanged in *mfn1-/-* MEFs, the increase in mitochondrial signal was clearly not simply an indirect result of mitochondrial fragmentation, but was linked to MFN2.

ELMOD2 was first identified as an ARL2 GTPase activating protein (GAP) [26] and later evidence pointed to it acting as an ARL2 effector in mitochondria [25]. Thus, we asked if mitochondrial ELMOD2 staining is also sensitive to MFN2 deletion, and found that it too is elevated in MEFs deleted for MFN2 over that seen in wild type cells (Fig 2C, 2D and 2F). The double null *mfn1-/-mfn2-/-* cells also displayed higher staining than seen in the wild type MEFs, though this was not clearly or consistently higher than that seen in *mfn2-/-* cells (Fig 2C, 2D and 2F). The ELMOD2 signal was not obviously weaker in the *mfn1-/-* cells than in wild type, perhaps due to the overall weak mitochondrial staining of ELMOD2 in wild type MEFs (Fig 2C, 2D and 2F). Thus, ARL2 and ELMOD2 staining in mitochondria are each specifically increased in cells deleted for MFN2. We observed no evident changes in HSP60 (Fig 2B and 2D) or cytochrome c signals between these MEF lines, supporting the conclusion that the changes in staining were specific to ARL2 and ELMOD2. Immunoblots of total cell lysates from wild type, *mfn1-/-*, *mfn2-/-*, or *mfn1-/-mfn2-/-* MEFs showed no differences in the levels of endogenous ARL2 or ELMOD2 between these different cell lines (Fig 2G), supporting our conclusion that the mitochondrial

pools of ARL2 and ELMOD2 were specifically altered. The effects of gene deletions on ARL2 and ELMOD2 at mitochondria are summarized in Table 1.

Increased mitochondrial staining of ARL2 and ELMOD2 in mfn1-/-mfn2-/- MEFs is reversed upon expression of MFN2 and restoration of tubular morphology

As a further test of specificity of the effects of MFN2 deletion, we performed rescue experiments. Transfection of *mfn1-/-mfn2-/-* MEFs with pcDNA3.1 (empty vector) resulted in no changes in either mitochondrial morphology or ARL2 staining (Fig 3A, left). Expression of MFN2-myc in these cells restored tubular mitochondrial morphology, as previously reported [34]. MFN2-myc also reversed the increased ARL2 staining of mitochondria (Fig 3A). The differences between the mitochondrial staining of ARL2 in *mfn1-/-mfn2-/-* cells expressing MFN2-myc, compared to empty vector control, is perhaps the strongest change in staining of ARL2 that we observed in this study. Because transient transfection yields a mixed population in terms of transfected cells and in levels of protein expression, it was quite apparent that there was a strong correlation between the ability of MFN2-myc expression to reverse mitochondrial fragmentation and elevated mitochondrial staining of ARL2. In most cells with tubular morphology, ARL2 staining was reduced to the point where it was barely detectible and lower even than ARL2 staining in wild type MEFs (Fig 2A). As mitochondrial staining of ARL2 is reduced, the cytosolic staining becomes more evident (e.g., see Fig 3A, top MFN2-myc panel), thus the loss in mitochondrial ARL2 signal is perhaps best seen in the merged image, revealing the clear loss in overlap with myc staining, which is marking MFN2 and mitochondria. Though a minority of MFN2-myc expressing cells with tubular mitochondrial morphology still displayed mitochondrial staining of ARL2, this staining was clearly diminished compared to controls. In MFN2-myc positive cells with fragmented mitochondria, ARL2 staining remained high, suggesting that the effect was correlated with reversal of fragmentation.

We next investigated effects of MFN2 expression on mitochondrial ELMOD2, and found that MFN2-myc expression could also reverse the elevated ELMOD2 (Fig 3B). MEFs deleted for both MFNs

displayed strong ELMOD2 staining that overlapped extensively with that of HSP60 (Fig 3B, left panels). In contrast, the double MFN null cells expressing MFN2-myc had clearly reduced staining of mitochondrial ELMOD2, as evidenced by the lack of overlap between the ELMOD2 and myc staining (Fig 3B). And as was true for ARL2, we observed a strong correlation between rescue of fragmentation by MFN2 and the loss of mitochondrial staining of ELMOD2. Similarly, the small percentage of *mfn1-/-mfn2-/-* MEFs that expressed low levels of MFN2-myc and retained fragmented mitochondria displayed high levels of mitochondrial ELMOD2 staining that was comparable to cells receiving empty vector. Similar results were obtained when cells were examined 24 or 48 hours after transfection.

Because the reversal of elevated mitochondrial ARL2/ELMOD2 staining in *mfn1-/-mfn2-/-* MEFs by MFN2-myc was correlated with restoration of tubular morphology, we asked if the reversal depended on the fusogenic activity of the expressed MFN2. A mutation in the GTPase domain of MFN2, [K109A], abolishes its fusogenic activity. We confirmed the failure of MFN2[K109A]-myc to reverse the fragmentation phenotype in *mfn1-/-mfn2-/-* MEFs [34] (Fig 3). No changes in the staining of ARL2 or ELMOD2 were observed in cells expressing MFN2 [K109A]-myc, compared to empty vector controls. ARL2 and ELMOD2 remained mitochondrial, indistinguishable in intensity from controls, and co-localized with myc staining (Fig 3). Results were the same when cells were fixed 24 or 48 hours after transfection. Therefore, we consistently observed close correlations between staining intensities of ARL2 and ELMOD2 in mitochondria and fusion activity of MFN2; *e.g.*, the ability of MFN2 to reverse the increased ARL2/ELMOD2 mitochondrial signal requires its fusogenic activity.

Expression of MFN1-myc also reversed fragmentation in *mfn1-/-mfn2-/-* MEFs, as previously reported [34]. But in marked contrast to MFN2-myc, MFN1-myc did not reverse the increased staining of mitochondrial ARL2 (Fig 3A) or ELMOD2 (Fig 3B). Thus, the reversal of elevated ARL2 staining seen with MFN2-myc expression was not due simply to restoration of tubular morphology but was specific to, and perhaps dependent upon, MFN2-mediated fusion.

To ensure that the changes in mitochondrial ARL2 and ELMOD2 were not simply due to differences in expression between MFN2-myc, MFN2[K109A]-myc, and MFN1-myc, we performed immunoblots, probing for the myc epitope after expression in *mfn1-/-mfn2-/-* MEFs. Immunoblots showed no differences in the levels of expression between MFN2-myc and MFN2[K109A]-myc (Fig 3C). The signal detected for MFN1-myc was lower than that seen for MFN2-myc, but the MFN1 fusion protein contains 10 myc tags on its C terminus, while each of the MFN2 proteins carries 16 myc tags. The increase in number of epitope tags is expected to increase the sensitivity in immunoblots using the myc antibody and also likely explains the slightly faster mobility of MFN1-myc in these gels (Fig 3C). Thus, though we are unable to definitively conclude that MFN1-myc and MFN2-myc express to similar levels, it is likely that they are expressed similarly as the same vector was used and they each rescue the mitochondrial morphology defects observed in the deletion strains.

Mutations in MFN2 cause Charcot Marie Tooth Type 2A, a peripheral neuropathy [35]. Though most disease-associated mutations (such as [R94Q]) interfere with the fusogenic activity of MFN2, a subset (e.g., [V69F], [L76P], [R274Q]) are still capable of fusion [34]. We asked if these MFN2 mutants, which are still capable of fusion, have differential effects on ARL2 or ELMOD2 staining at mitochondria, compared to MFN2-myc. We expressed myc-tagged MFN2 harboring [V69F], [L76P] or [R274Q] mutations in *mfn1-/-mfn2-/-* MEFs and found that each MFN2 mutant restored tubular morphology, as previously described [34]. Furthermore, each mutant also reversed the increased ARL2 (Fig 3D) or ELMOD2 (Fig 3E) staining at mitochondria, similar to wild type MFN2-myc, at both 24 and 48 hours after transfection. In contrast, MFN2[R94Q]-myc failed to rescue fragmentation, consistent with previously published data [34], and did not reverse the elevated ARL2 and ELMOD2 staining in *mfn1-/-mfn2-/-* MEFs (Fig 3E and 3F). We conclude that changes in ARL2 and ELMOD2 staining at mitochondria are closely linked to MFN2-mediated fusion.

Reversal of elevated ARL2 and ELMOD2 staining in mfn2-/- MEFs

Expression of MFN2-myc in *mfn2-/-* MEFs led to restoration of tubular mitochondria, as well as a decrease in mitochondrial ARL2/ELMOD2 (Fig 4A and 4B), similar to our results in *mfn1-/-mfn2-/-* MEFs. In contrast to results in the double null cells, expression of MFN2 [K109A]-myc in *mfn2-/-* MEFs restored tubular mitochondrial morphology in ~50% of transfected cells, consistent with previously reported data [6]. The partial rescue by MFN2[K109A]-myc in *mfn2-/-* MEFs, compared to the lack of any rescue of fragmentation in *mfn1-/-mfn2-/-* MEFs, is likely due to the presence of endogenous MFN1 in *mfn2-/-* MEFs, as MFN1 and MFN2 can hetero-oligomerize to promote fusion [6, 7, 36]. In MEFs expressing MFN2[K109A]-myc and displaying tubular morphology, we observed a decrease in ARL2 and ELMOD2 mitochondrial signal, comparable to expression of MFN2-myc (Fig 4A and 4B). However, in the remaining cells expressing MFN2[K109A]-myc that retained fragmented mitochondria, mitochondrial staining of ARL2/ELMOD2 remained high (Fig 4A and 4B right most panels). Cells expressing MFN2[K109A]-myc with fragmented mitochondria generally appeared to have lower levels of myc expression (Fig 4A and 4B), possibly explaining the lack of rescue in those cells. We conclude that the increase in mitochondrial staining of ARL2 and ELMOD2 that is so evident in cells deleted for MFN2, alone or in combination with MFN1, is dependent on the ability of MFN2 to support fusion in MEFs.

Expression of MFN2-myc in wild type MEFs does not alter mitochondrial staining of ARL2 or ELMOD2

As re-introduction of MFN2 in *mfn1-/-mfn2-/-* MEFs caused a decrease in mitochondrial staining of ARL2, we tested if MFN2-myc could also decrease endogenous mitochondrial ARL2 or ELMOD2 in wild type MEFs. Empty vector, MFN1-myc, or MFN2-myc were expressed in wild type MEFs, which were fixed and stained for HSP60 and ARL2 or ELMOD2 24 or 48 hours later. MEFs receiving empty vector displayed tubular mitochondrial morphology, whereas MFN1-myc and MFN2-myc led to elongation of mitochondria. Neither empty vector, MFN1-myc, nor MFN2-myc had any obvious effect on mitochondrial staining of ARL2 or ELMOD2 in wild type cells, which remained weak (Fig 5). Thus, there may exist minimal levels of mitochondrial ARL2 and ELMOD2 which are not subject to regulation by the levels of MFN2.

Mitochondrial ARL2 and ELMOD2 increase in response to stressors that cause mitochondrial elongation

Mitochondrial elongation occurs in response to stressors, such as glucose deprivation, as a result of increased fusion and decreased fission [10, 12, 37, 38]. We asked if mitochondrial staining of ARL2 or ELMOD2 changed in response to such conditions, and if these effects were correlated with changes to mitochondrial morphology. We found that ARL2 in mitochondria was markedly increased under a number of conditions, summarized in Table 2. Two of the conditions that yielded among the most striking changes were growth of COS7 cells in the absence of glucose (0 glucose), or in low (2%) serum (Fig 6A, 6B and 6D). Our cells are routinely maintained in DMEM that contains 25 mM glucose supplemented with 10% fetal bovine serum (FBS). Effects were evident one day after changing the medium to 0 glucose or 2% FBS and were further increased at two days. In contrast to the marked differences in ARL2 staining, no changes in intensity were observed with several other mitochondrial markers, including HSP60 (matrix), cytochrome c (IMS), TOM20 (outer membrane), Complex I subunit NDUFA9 (inner membrane), Complex III subunit UQCRC2, and Complex V subunit alpha. Similar, though somewhat less striking effects on ARL2 staining were observed when cells were cultured for 48 hours in 10 mM galactose with 0 glucose, which makes cells more dependent upon respiration instead of glycolysis [39], with no changes to mitochondrial markers.

Mitochondrial staining of ELMOD2 was also increased when cells were grown in 0 glucose or 2% serum (Fig 6C, 6D, and 6F). The kinetics of these effects were similar to those seen for ARL2, with ELMOD2 staining increased after 24 hours, and more so after 48 hours in all three cell lines. Also like ARL2, when cells were grown in galactose containing medium (10 mM, with 0 glucose), ELMOD2 staining was increased within 24 hours and further increased after 48 hours. The increase in ELMOD2 staining seen in galactose was less prominent than the effect with 0 glucose or low serum, again similar to ARL2.

In addition to the increased staining of ARL2 and ELMOD2 under the conditions described above, we also observed changes in mitochondrial morphology resulting from the treatments used. Growth in 0 glucose, 2% serum, or 10 mM galactose each resulted in an increase in mitochondrial elongation, branching, and looping structures, compared to controls (Fig 6). This effect was most obvious with 0 glucose or in galactose medium, and was observed in COS7, HeLa, and MEFs, though was most obvious in MEFs, due to mitochondria appearing more elongated in untreated COS7 and HeLa cells. These changes in mitochondrial morphology are consistent with previously published data in regards to cellular starvation [9-12, 38, 40]. We also note that mitochondrial staining of endogenous ARL2 and ELMOD2 appeared stronger in COS7 cells (Fig 6) than in HeLa (Fig 1) or MEFs (Fig 2). This may be due to different mitochondrial morphologies across the three cell lines.

ARL3 staining does not change with MFN2 deletion or cellular stressors

As ARL2 is a member of the ARF family of GTPases, we wondered if the effects of MFN2 deletion were unique to ARL2, or if MFN2 deletion could also recruit other ARF family GTPases to mitochondria. ARL3 is the closest paralog to ARL2 in humans, sharing 53% identity with ARL2. Therefore, we stained wild type or *mfn1-/-mfn2-/-* MEFs, where we had seen the largest increase in ARL2 staining, for ARL3 and did not observe any mitochondrial localization of ARL3 (Fig 7A), consistent with previously reported data [25]. We performed the same experiment staining cells for ARL13B, or ARF1-6, and saw no mitochondrial localization of any other GTPase in either wild type or *mfn1-/-mfn2-/-* MEFs. As a further test of specificity, we cultured COS7 cells in 0 glucose or low serum media, and stained cells for ARL3. While each of these conditions led to an increase in mitochondrial ARL2, no changes were observed in ARL3 staining with either condition (Fig 7B). Therefore, mitochondrial localization of ARL2 is unique among ARF family GTPases, as are the effects of MFN2 deletion and stressors on mitochondrial ARL2.

ARL2 and ELMOD2 are further increased in stressed mfn2-/- and mfn1-/-mfn2-/- MEFs, but not mfn1-/- MEFs

Given that deletion of MFN2 or starving cells each increase ARL2 staining in mitochondria, we asked if these effects were additive. We grew wild type, *mfn1-/-*, *mfn2-/-*, or *mfn1-/-mfn2-/-* MEFs in normal, 0 glucose, or low serum media for two days before fixing and processing. The wild type MEFs grown in either 0 glucose or low serum had increased ARL2 and ELMOD2 mitochondrial signal compared to those grown in normal medium (Fig 8), and displayed elongated mitochondria, as described above in COS7 and HeLa cells. MEFs deleted for MFN2 cultured in 0 glucose or 2% serum had increased ARL2 or ELMOD2 mitochondrial staining compared to normal medium (Fig 8). Similarly, *mfn1-/-mfn2-/-* MEFs grown in 0 glucose or low serum media also had stronger ARL2 (Fig 8A) and ELMOD2 (Fig 8B) mitochondrial staining over that seen in normal medium. For each of the MEF lines, 0 glucose resulted in the strongest increase in ARL2 staining, while growth in 2% serum resulted in the strongest increase in ELMOD2 staining. In contrast, there was little or no increase in ARL2 or ELMOD2 in *mfn1-/-* MEFs grown in no glucose or low serum medium for 48 hours, compared to *mfn1-/-* MEFs grown in normal medium (Fig 8).

We also observed striking differences in mitochondrial morphology in response to stress between the MEF lines. MFN2 null MEFs grown in normal medium had fragmented mitochondria, compared to wild type cells, but growth in 0 glucose or low serum resulted in a partial reversal in mitochondrial morphology, displaying an intermediate, rod-shaped morphology, with some cells displaying a tubular morphology (Fig 8). In contrast, *mfn1-/-* MEFs showed no evidence of even partial rescue of the fragmentation resulting from the absence of MFN1 when grown in 0 glucose or low serum. Finally, *mfn1-/-mfn2-/-* MEFs cultured in 0 glucose or low serum also displayed no differences in mitochondrial morphology compared to cells grown in normal medium, consistent with their inability to undergo fusion [7].

Metabolic inhibitors increase mitochondrial ARL2 but not ELMOD2

Mitochondrial fusion is linked to the activity of the electron transport chain [10]. Therefore, we tested other metabolic stressors for effects on mitochondrial ARL2 levels. Every metabolic poison acting on ATP generation that we tested resulted in increased mitochondrial ARL2. The strongest effect was observed after an overnight (16 hr) treatment with 2-deoxyglucose (25 mM), an inhibitor of glycolysis [41] (Fig 9A). Similar effects were seen when cells were treated with specific inhibitors of the electron transport chain; oligomycin (10 μM, complex V inhibitor), rotenone (10 μM, complex I inhibitor), or antimycin A (10 μM, complex III inhibitor). Time courses were performed to determine the maximal effects of 2-deoxyglucose, oligomycin, or antimycin A. We found that increased ARL2 was evident as soon as 3 hours after addition of each drug and continued to increase, peaking at 16 hours. Cells treated with rotenone did not show any obvious increase until overnight (16 hr) treatment. We also observed an increase in ARL2 staining with 1 hour of menadione treatment, which increases mitochondrial ROS [42]. These effects were observed in all three cell lines examined-COS7, HeLa, and MEFs (Table 2).

In marked contrast to ARL2, we found that ELMOD2 staining was not altered in response to the same drugs that caused mitochondrial ARL2 to increase. Overnight treatment of cells with 2-deoxyglucose (Fig 9B), oligomycin, antimycin A, rotenone, or menadione had no effect on ELMOD2 staining (Table 2). None of these drugs caused mitochondrial elongation. Oligomycin, antimycin A, and rotenone caused mitochondrial fragmentation, while 2-deoxyglucose and menadione had minimal effects on mitochondrial morphology. Therefore, mitochondrial staining of ARL2 responds to metabolic stress, but staining of ELMOD2 only changes when mitochondrial elongation is observed.

Mitochondrial ARL2 is not altered by stressors when the recombinant protein is directed to mitochondria

Western blots of whole cell lysates, comparing controls to the same cells after several of the treatments described above, failed to detect any consistent changes in the total cellular ARL2 or ELMOD2 expressed in any of the three cell lines tested; as an example data from HeLa cells are shown in

Fig 10A and 10B. When mitochondria were enriched by differential centrifugation, pelleting mitochondria at 14,000x*g* from a post-nuclear supernatant, we also could detect no consistent changes in mitochondria-associated ARL2 or ELMOD2. HeLa cells treated with 2-deoxyglucose or oligomycin or grown in low serum medium showed no increase in ARL2 (Fig 10A) or ELMOD2 (Fig 10B) in the P14. In the immunoblots shown in Fig 10A and 10B, the ARL2 and ELMOD2 immunoreactivity does appear slightly reduced in some conditions, but this is not a consistent finding and in the data shown it is under conditions in which ARL2 and ELMOD2 staining at mitochondria is *increased*. Thus, any increases in immunoreactivity observed at mitochondria by immunofluorescence is not the result of an increase in total cellular ARL2/ELMOD2 or that in the P14. Note that because only a minor fraction of total cellular ARL2 fractionates with mitochondria (P14, Fig 10A) and that ELMOD2 is expressed to only low levels, long exposures are required to monitor their levels by immunoreactivity, which results in higher backgrounds. Similarly, no differences in ARL2 or ELMOD2 were observed between the crude mitochondria fractions from wild type, *mfn1-/-*, *mfn2-/-*, or *mfn1-/-mfn2-/-* MEFs.

That immunoblots of the crude mitochondria fraction from cells that display increased staining of ARL2/ELMOD2 did not show correlated increases in the protein fractionating with mitochondria is difficult to interpret for a number of reasons. Our initial finding that simply detaching cells from the culture dish, the first step in both re-plating cells and for cell fractionation, may be sufficient to reverse any increases in staining at mitochondria (Fig 1) resulting from the treatments used, suggests that a reversible process is involved. As a result, rapid degradation or export of ARL2/ELMOD2 from mitochondria in response to cell detachment may confound fractionation results. While we believe that the increased import of ARL2 into mitochondria explains the increased ARL2 staining, there exist other possibilities that we sought to test. For example, a time-dependent incorporation of ARL2/ELMOD2 into a macromolecular complex or change in tertiary structure, resulting in altered access of antibodies to specific epitopes upon fixation, could yield the changes in staining intensities identified above.

To ask if changes in antibody recognition of the epitope were involved, we expressed ARL2 carrying a small epitope tag at its C-terminus, ARL2-HA, in HeLa cells and examined changes in HA staining in cells in response to stressors. The C-termini of ARF family proteins are not involved directly in protein-protein interactions and thus the access of antibodies to the HA epitope at that location is predicted to be unaltered by ARL2 binding to partners. Like untagged ARL2, ARL2-HA was partially imported into mitochondria, and brief permeabilization of cells prior to fixation (0.5% saponin, 1 minute) removed cytosolic ARL2 and allowed for better visualization of the mitochondrial pool (Newman, et al., submitted). Note that prefixation permeabilization results in changes in mitochondrial morphologies, as they appear smaller and more fragmented than when fixed prior to permeabilization. In addition, cells were imaged using higher laser power, due to loss of signal, so Z stack projections are shown as they average the increase in noise to yield the optimal signal to noise. ARL2-HA was expressed in cells grown in low serum. After two days, cells were permeabilized prior to fixation, and stained for ARL2 and HA. As expected, the low serum treatment increased endogenous mitochondrial ARL2 staining in cells receiving empty vector and also increased mitochondrial HA and ARL2 staining in cells expressing ARL2-HA (Fig 10C). We were unable to perform a similar experiment for ELMOD2 as we found that epitope tagging at either the N or C terminus interfered with its localization to mitochondria. These results are consistent with the low serum treatment causing an increase in the abundance of ARL2-HA at mitochondria and suggest that increased ARL2 staining at mitochondria reflects increased mitochondrial import or half-life of the imported ARL2 rather than a change in antibody access to the fixed ARL2.

We next asked if ARL2 that is strongly driven to the IMS, as a result of an N-terminal fusion with the leader sequence from SMAC (SMAC-HA-ARL2) [43] is affected by stressors. This construct is appropriately and efficiently targeted to the IMS, with rapid cleavage of the SMAC leader and retention of the HA-ARL2 in the IMS with no effects on mitochondrial morphology [43]. SMAC-HA-ARL2 was expressed in HeLa cells, which were replated onto coverslips and allowed to attach for four hours before changing to low serum medium. Two days later, cells were fixed and stained for ARL2 and HA. When

ARL2 was imaged in cells receiving empty vector, we saw the expected increase in endogenous ARL2 staining that co-localizes with mitochondrial markers, in response to growth of cells in low serum medium (data not shown). In contrast, in cells expressing SMAC-HA-ARL2, there was already a strong signal for HA or ARL2 from mitochondria and this was not further increased in response to growth in low serum (Fig 10D). Similar results were obtained with OCT-HA-ARL2, which targets ARL2 to the matrix. Taken together, these results suggest that the increased staining of ARL2 at mitochondria reflects increased levels of the protein, resulting from either increased import or decreased loss (degradation or export), rather than changes in tertiary or quaternary structure that might alter immunostaining.

Finally, mitochondrial ARL2 is found in discrete puncta along mitochondria, optimally visualized using structured illumination microscopy (SIM) (Newman et al., submitted). SIM is useful for increasing resolution of fluorescence images but less so for comparing intensities between images due to the requirements for data acquisition and processing. We asked if conditions leading to increased ARL2 in mitochondria were associated with changes in ARL2 puncta. COS7 cells were treated with 2-deoxyglucose overnight, stained for ARL2, and imaged by SIM. We observed that ARL2 still localized to puncta in 2-deoxyglucose treated cells (Fig 10E) repeating along the length of mitochondria at an interval of ~0.4 μm, as previously described for untreated cells (Newman et al., submitted). Therefore, increased mitochondrial ARL2 appears to represent increased abundance of ARL2 at puncta, though we cannot eliminate the possibility of increased amounts of soluble ARL2 inside mitochondria as well.

Discussion

ARL2 plays essential cellular roles both at mitochondria, where it regulates energy metabolism and fusion [25, 30](Newman et al., submitted), and in cytosol, where together with TBCD it regulates tubulin biogenesis, microtubules, and has links to cell division [44-47]. Because only a small fraction of total cellular ARL2 is found at mitochondria and the majority is tightly bound to TBCD in cytosol there is predicted to be a mechanism for regulating recruitment to mitochondria, though such a mechanism

remains elusive. We describe increases in mitochondrial pools of ARL2 in response to a number of environmental factors; including changes in fusogenic activity resulting from deletion of mitofusins (particularly MFN2), cell attachment, cell density, and pharmacological stressors that target energy metabolism. Many, but not all, of the changes observed in mitochondrial pools of ARL2 were also seen for the ARL2 GAP, ELMOD2, though not for any other mitochondrial proteins monitored. Once we were able to control for effects of time after cell attachment and cell density, the changes in ARL2 and ELMOD2 intensities became very clear and consistent in each of the three cell lines used in our studies (see Tables 1 and 2 for summaries). We discuss the interpretation of these results within the context of the existing literature and recent data from our lab demonstrating a role for ARL2 in the regulation of mitochondrial fusion from the IMS (Newman et al., submitted).

What is responsible for the increases in ARL2 and ELMOD2 at mitochondria described here? Previously, we showed that mitochondrial ARL2 is increased in abundance several fold, though only in the affected tissues (heart and skeletal muscle), in *ant1-/-* mice [30], which display muscle wasting and cardiomyopathy [48]. This observation was interpreted as evidence supporting the existence of a regulated mitochondrial import pathway and led us to study changes to ARL2 in response to stressors in cell culture. Our more recent studies of the effects of dominant mutants of ARL2 on mitochondrial morphology and motility, upstream of mitofusins (Newman et al., submitted), also led us to investigate effects of changes in MFN levels on mitochondrial ARL2 and ELMOD2. While we see quite strong and uniform increases in ARL2 staining at mitochondria, no changes in ARL2 or ELMOD2 were detected in crude mitochondrial fractions by immunoblotting. However, our observation that simply trypsinizing and replating cells dramatically diminished ARL2 staining at mitochondria confounds interpretation of these results. We considered changes in availability of epitopes as an alternative explanation for the changes in fluorescence intensity. To control for this, we tested whether stress induced increases were evident in cells expressing C-terminal HA tagged ARL2 and found that they were. Because HA imaging used an unrelated antibody and is directed to a tag that is not present in endogenous ARL2, and thus not likely to

be directly involved in protein-protein interactions, we interpret this as strongly supporting our conclusion that the increased immunofluorescence signal is the result of increases in the amount of protein at mitochondria. This conclusion was further supported by the observation that another recombinant protein, SMAC-HA-ARL2 [43], that is strongly driven to the IMS by the 52-residue SMAC leader sequence prior to its cleavage, did not display any changes in HA staining intensity in response to growth in low serum. Thus, it is not a change in the quaternary structure of mitochondrial ARL2 that occurs in response to stress but rather a change in the amount of ARL2 at that compartment. We performed a few experiments using a mouse monoclonal antibody to ARL2, in contrast to the widespread use of our rabbit polyclonal antibody, and found that they both yielded the same results. The epitopes are not known for either of these antibodies but as they were independently derived they further strengthen our conclusions. Finally, we believe the increases in ARL2 are inside mitochondria and not on the outer membrane for two reasons: (1) we have recently shown that ARL2 acts from the IMS to regulate fusion (Newman et al., submitted), and (2) the increased staining in response to 2-deoxyglucose seen in HeLa cells resulted in an increased signal in ARL2 puncta localized at mitochondria when visualized by structured illumination microscopy (Fig 10E). Taken together, these results suggest that changes in ARL2, and by extension ELMOD2, staining is the result of changes in protein abundance specifically at this one organelle. These results cannot distinguish between an increase in protein abundance in mitochondria resulting from increased import vs decreased export or degradation, though we currently favor the former model. Because no correlative changes were observed for any other mitochondrial proteins tested, we conclude that ARL2 and ELMOD2 are changing in a highly specific and regulated fashion in response to specific cellular demands and signals; classic hallmarks of regulatory GTPase pathways.

ARL2 and ELMOD2 levels at mitochondria are sensitive to the presence of fusion-competent MFN2. This is in marked contrast to results with ARL3, the closest ARL2 paralog, ARFs or other family members and speaks to the specificity of these observations. For example, while ARF1 has been implicated in mitochondrial morphology [49] there is currently no evidence of its specific localization or

direct actions at the organelle. MEFs deleted for MFN2 showed increased ARL2 and ELMOD2 staining at mitochondria, compared to controls. This increased staining was not due to the fragmentation observed in these MEFs, as *mfn1-/-* MEFs did not show increased ARL2/ELMOD2 staining. Though MFN1 and MFN2 share ~60% identity [50] and a level of functional redundancy regarding fusion, MFN2 is proposed to have additional metabolic roles [7, 51-54] and may play a role in mitochondria/ER tethering [55], though this is contested [56, 57]. Increased levels of ARL2 and ELMOD2, along with mitochondrial fragmentation, could be reversed by expression of MFN2-myc in either *mfn2-/-* or *mfn1-/-mfn2-/-* MEFs. Importantly, expression of MFN1-myc could reverse the fragmentation but not the elevation in ARL2 and ELMOD2 levels. This demonstrates that these changes in protein levels were not strictly correlated with the loss of fusion, *per se*, but more linked to the function(s) of MFN2. A fusion dead mutant (MFN2[K109A]), which cannot reverse fragmentation in *mfn1-/-mfn2-/-* MEFs [34], also failed to decrease ARL2/ELMOD2 levels in these cells. Perhaps the most telling linkage between ARL2/ELMOD2 levels and MFN2 fusogenic activity was found when MFN2[K109A] was expressed in *mfn2-/-* MEFs. In this case fragmentation was partially reversed, presumably a result of the presence of MFN1 that can hetero-oligomerize with the mutant MFN2 [6], as were the elevation in ARL2 and ELMOD2 at mitochondria. And there was a correlation between cells in which fusion had been restored and staining had been reversed.

Results described here also further support our earlier conclusion that ARL2 acts in at least two distinct pathways in mitochondria, one affecting ATP levels that is independent of ELMOD2 and another that involves ELMOD2 and regulates mitochondrial fusion and motility. ARL2 siRNA results in ~50% loss in cellular ATP, while ELMOD2 knockdown had no effect on ATP levels [25]. Yet knockdown of either protein caused mitochondrial fragmentation and perinuclear clustering, presumably from the loss of plus end directed motility. Despite its discovery as an ARL2 GAP, we view ELMOD2 as likely acting in mitochondria as an effector, *i.e.*, binding directly to the activated (GTP-bound) form of the GTPase and mediating aspects of its biological response, in this case fusion and motility. This is consistent with every

other known ARF family GAP, each of which have been found to have effector properties [58-61]. Note that ARL2 and ELMOD2 behave the same in response to the loss of MFNs in MEFs (summarized in Table 1), in which mitochondrial fusion is altered. Yet the stressors of energy metabolism yield clear differences in responses of ARL2 and ELMOD2 (summarized in Table 2). Treatments that lower cellular ATP (2-deoxyglucose, oligomycin, antimycin A, etc.) do not alter ELMOD2 mitochondrial staining, consistent with ELMOD2 not playing a role in regulation of ATP. However, a subset of conditions (0 glucose, low serum, and galactose) that increase mitochondrial staining of ARL2 also increase that of ELMOD2. These stressors led to mitochondrial elongation, consistent with changes in ARL2 and ELMOD2 being linked to mitochondrial fusion. Work from others has shown that mitochondria fuse during stress, and that this pathway (called stress induced mitochondrial hyperfusion, or SIMH) requires MFN1 and not MFN2 [9-12]. Growth conditions (0 glucose, low serum) that led to increased ARL2/ ELMOD2 and mitochondrial elongation promoted elongation in *mfn2-/-* but not *mfn1-/-* MEFs, consistent with previously reported data regarding SIMH [9]. Interestingly, increased ARL2/ELMOD2 occurred with stress in *mfn2-/-* but not *mfn1-/-* MEFs (Fig 8). Therefore, ARL2 and ELMOD2 may be acting upstream of MFN1 during SIMH. Based on these data and our rescue experiments with MFN2-myc, we speculate that increased MFN1 activity during SIMH may lead to increased ARL2/ELMOD2 in mitochondria, and that increased MFN2 activity may lead to decreased ARL2/ELMOD2.

The simple observations that the amounts of ARL2 and ELMOD2 at mitochondria are sensitive to cell attachment and density suggest that a signaling pathway exists to communicate information from the cell surface to mitochondria. A precedent might be seen in STAT3, best known for its role in conveying signals from the cell surface to the nucleus but more recently shown to act also inside mitochondria [62-64]. We have identified a number of conditions and reagents that activate it and thus provide the tools and assays required to further explore mechanisms.

To summarize, we conclude that ARL2 and ELMOD2 are increased at mitochondria in response to several types of cellular stress, and that this increase is correlated with MFN2 activity and fusion. These data are highly supportive of other studies (Newman, et al., submitted) in which we show that ARL2 acts from the IMS to regulate fusion upstream of the MFNs. They are also consistent with data from the *ant1-/-* mice, which showed that changes in ARL2 levels in mitochondria may be tissue specific as they were dramatically increased only in affected tissues, skeletal muscle and heart [30]. Together they support the model that ARL2 and ELMOD2 levels at mitochondria are regulated and responsive to stressors and changes in MFN2 fusogenic potential. The model that an ancient, highly conserved, and ubiquitous regulatory GTPase regulates essential aspects of mitochondrial functions, morphology, and motility has broad significance and potential impact to our understanding of the basic cell biology of this organelle and its roles in human disease.

Acknowledgments

We thank David Chan (Caltech) for the generous gift of plasmids and *mfn1-/-*, *mfn2-/-*, and *mfn1-/-mfn2-/-* MEFs. We gratefully acknowledge Drs. Heidi McBride, David Chan, Victor Faundez, Elizabeth Sztul, and Gerald Shadel for their ideas and suggestions in discussions of this work at various stages. We thank Dr. Alexa Mattheyses (Emory) for assistance with imaging quantification.

References

1. Chan DC. Mitochondrial Fusion and Fission in Mammals. Annu Rev Cell Dev Biol. 2006; 22:79-99. https://doi.org/10.1146/annurev.cellbio.22.010305.104638 PMID: 16704336

2. Karbowski M, Youle RJ. Dynamics of mitochondrial morphology in healthy cells and during apoptosis. Cell Death Differ. 2003; 10(8):870-80. Epub 2003/07/18. https://doi.org/10.1038/sj.cdd.4401260 PMID: 12867994

3. Sauvanet C, Duvezin-Caubet S, di Rago JP, Rojo M. Energetic requirements and bioenergetic modulation of mitochondrial morphology and dynamics. Semin Cell Dev Biol. 2010; 21(6):558-65. Epub 2009/12/23. https://doi.org/10.1016/j.semcdb.2009.12.006 PMID: 20025987

4. Labrousse AM, Zappaterra MD, Rube DA, van der Bliek AM. C. elegans dynamin-related protein DRP-1 controls severing of the mitochondrial outer membrane. Mol Cell. 1999; 4(5):815-26. Epub 2000/01/05. PMID: 10619028

5. Smirnova E, Griparic L, Shurland DL, van der Bliek AM. Dynamin-related protein Drp1 is required for mitochondrial division in mammalian cells. Mol Biol Cell. 2001; 12(8):2245-56. Epub 2001/08/22. PMID: 11514614

6. Chen H, Detmer SA, Ewald AJ, Griffin EE, Fraser SE, Chan DC. Mitofusins Mfn1 and Mfn2 coordinately regulate mitochondrial fusion and are essential for embryonic development. J Cell Biol. 2003; 160 (2):189-200. https://doi.org/10.1083/jcb.200211046 PMID: 12527753

7. Chen H, Chomyn A, Chan DC. Disruption of fusion results in mitochondrial heterogeneity and dysfunction. J Biol Chem. 2005; 280(28):26185-92. Epub 2005/05/19. https://doi.org/10.1074/jbc.M503062200 PMID: 15899901

8. Cipolat S, de Brito OM, Dal Zilio B, Scorrano L. OPA1 requires mitofusin 1 to promote mitochondrial fusion. Proc Natl Acad Sci U S A. 2004; 101(45):15927-32. https://doi.org/10.1073/pnas.0407043101 PMID: 15509649

9. Tondera D, Grandemange S, Jourdain A, Karbowski M, Mattenberger Y, Herzig S, et al. SLP-2 is required for stress-induced mitochondrial hyperfusion. EMBO J. 2009; 28(11):1589-600. Epub 2009/04/11. https://doi.org/10.1038/emboj.2009.89 PMID: 19360003

10. Mishra P, Carelli V, Manfredi G, Chan David C. Proteolytic Cleavage of Opa1 Stimulates Mitochondrial Inner Membrane Fusion and Couples Fusion to Oxidative Phosphorylation. Cell Metabolism. 2014; 19 (4):630-41. https://doi.org/10.1016/j.cmet.2014.03.011 PMID: 24703695

11. Gomes LC, Di Benedetto G, Scorrano L. During autophagy mitochondria elongate, are spared from degradation and sustain cell viability. Nat Cell Biol. 2011; 13(5):589-98. Epub 2011/04/12. https://doi.org/10.1038/ncb2220 PMID: 21478857

12. Rambold AS, Kostelecky B, Elia N, Lippincott-Schwartz J. Tubular network formation protects mitochondria from autophagosomal degradation during nutrient starvation. Proc Natl Acad Sci U S A. 2011; 108(25):10190-5. https://doi.org/10.1073/pnas.1107402108 PMID: 21646527

13. Li Y, Kelly WG, Logsdon JM Jr, Schurko AM, Harfe BD, Hill-Harfe KL, et al. Functional genomic analysis of the ADP-ribosylation factor family of GTPases: phylogeny among diverse eukaryotes and function in C. elegans. FASEB J. 2004; 18(15):1834-50. Epub 2004/12/04. https://doi.org/10.1096/fj.04-2273com PMID: 15576487

14. Antoshechkin I, Han M. The C. elegans evl-20 gene is a homolog of the small GTPase ARL2 and regulates cytoskeleton dynamics during cytokinesis and morphogenesis. Dev Cell. 2002; 2(5):579-91. Epub 2002/05/23. PMID: 12015966

15. Radcliffe PA, Vardy L, Toda T. A conserved small GTP-binding protein Alp41 is essential for the cofactor-dependent biogenesis of microtubules in fission yeast. FEBS Lett. 2000; 468(1):84-8. PMID: 10683446

16. McElver J, Patton D, Rumbaugh M, Liu C, Yang LJ, Meinke D. The TITAN5 gene of Arabidopsis encodes a protein related to the ADP ribosylation factor family of GTP binding proteins. Plant Cell.

2000; 12(8):1379-92. Epub 2000/08/19. PMID: 10948257

17. Fansa EK, Wittinghofer A. Sorting of lipidated cargo by the Arl2/Arl3 system. Small GTPases. 2016:1-9.

18. Jaiswal M, Fansa EK, KoÈsling SK, Mejuch T, Waldmann H, Wittinghofer A. Novel Biochemical and Structural Insights into the Interaction of Myristoylated Cargo with Unc119 Protein and Their Release by Arl2/3. J Biol Chem. 2016; 291(39):20766-78. https://doi.org/10.1074/jbc.M116.741827 PMID: 27481943

19. Fansa EK, Kosling SK, Zent E, Wittinghofer A, Ismail S. PDE6delta-mediated sorting of INPP5E into the cilium is determined by cargo-carrier affinity. Nat Commun. 2016; 7:11366. https://doi.org/10.1038/ncomms11366 PMID: 27063844

20. Ismail SA, Chen Y-X, Rusinova A, Chandra A, Bierbaum M, Gremer L, et al. Arl2-GTP and Arl3-GTP regulate a GDI-like transport system for farnesylated cargo. Nat Chem Biol. 2011; 7(12):942-9. http://www.nature.com/nchembio/journal/v7/n12/abs/nchembio.686.html#supplementary-information. https://doi.org/10.1038/nchembio.686 PMID: 22002721

21. Watzlich D, Vetter I, Gotthardt K, Miertzschke M, Chen YX, Wittinghofer A, et al. The interplay between RPGR, PDEdelta and Arl2/3 regulate the ciliary targeting of farnesylated cargo. EMBO Rep. 2013; 14 (5):465-72. https://doi.org/10.1038/embor.2013.37 PMID: 23559067

22. Hanzal-Bayer M, Renault L, Roversi P, Wittinghofer A, Hillig RC. The complex of Arl2-GTP and PDE delta: from structure to function. EMBO J. 2002; 21(9):2095-106. Epub 2002/05/01. https://doi.org/10.1093/emboj/21.9.2095 PMID: 11980706

23. Hanzal-Bayer M, Linari M, Wittinghofer A. Properties of the interaction of Arf-like protein 2 with PDEdelta. J Mol Biol. 2005; 350(5):1074-82. https://doi.org/10.1016/j.jmb.2005.05.036 PMID: 15979089

24. Ismail SA, Chen YX, Miertzschke M, Vetter IR, Koerner C, Wittinghofer A. Structural basis for Arl3-specific release of myristoylated ciliary cargo from UNC119. EMBO J. 2012; 31(20):4085-94. https://doi.org/10.1038/emboj.2012.257 PMID: 22960633

25. Newman LE, Zhou C-j, Mudigonda S, Mattheyses AL, Paradies E, Marobbio CMT, et al. The ARL2 GTPase Is Required for Mitochondrial Morphology, Motility, and Maintenance of ATP Levels. PLoS One. 2014; 9(6):e99270. https://doi.org/10.1371/journal.pone.0099270 PMID: 24911211

26. Bowzard JB, Cheng D, Peng J, Kahn RA. ELMOD2 is an Arl2 GTPase-activating protein that also acts on Arfs. J Biol Chem. 2007; 282(24):17568-80. Epub 2007/04/25. https://doi.org/10.1074/jbc.M701347200 PMID: 17452337

27. Hoyt MA, Stearns T, Botstein D. Chromosome instability mutants of Saccharomyces cerevisiae that are defective in microtubule-mediated processes. Mol Cell Biol. 1990; 10(1):223-34. Epub 1990/01/01. PMID: 2403635

28. Stearns T, Hoyt MA, Botstein D. Yeast mutants sensitive to antimicrotubule drugs define three genes that affect microtubule function. Genetics. 1990; 124(2):251-62. PMID: 2407611

29. Liu CM, Meinke DW. The titan mutants of Arabidopsis are disrupted in mitosis and cell cycle control during seed development. The Plant J: for cell and molecular biology. 1998; 16(1):21-31.

30. Sharer JD, Shern JF, Van Valkenburgh H, Wallace DC, Kahn RA. ARL2 and BART enter mitochondria and bind the adenine nucleotide transporter. Mol Biol Cell. 2002; 13(1):71-83. Epub 2002/01/26. https://doi.org/10.1091/mbc.01-05-0245 PMID: 11809823

31. Sharer JD, Kahn RA. The ARF-like 2 (ARL2)-binding protein, BART. Purification, cloning, and initial characterization. J Biol Chem. 1999; 274(39):27553-61. Epub 1999/09/17. PMID: 10488091

32. Song Z, Chen H, Fiket M, Alexander C, Chan DC. OPA1 processing controls mitochondrial fusion and is regulated by mRNA splicing, membrane potential, and Yme1L. J Cell Biol. 2007; 178(5):749-55. Epub 2007/08/22. https://doi.org/10.1083/jcb.200704110 PMID: 17709429

33. Koshiba T, Detmer SA, Kaiser JT, Chen H, McCaffery JM, Chan DC. Structural basis of mitochondrial tethering by mitofusin complexes. Science. 2004; 305(5685):858-62. Epub 2004/08/07. https://doi.org/10.1126/science.1099793 PMID: 15297672

34. Detmer SA, Chan DC. Complementation between mouse Mfn1 and Mfn2 protects mitochondrial fusion defects caused by CMT2A disease mutations. J Cell Biol. 2007; 176(4):405-14. Epub 2007/02/14. https://doi.org/10.1083/jcb.200611080 PMID: 17296794

35. Zuchner S, Mersiyanova IV, Muglia M, Bissar-Tadmouri N, Rochelle J, Dadali EL, et al. Mutations in the mitochondrial GTPase mitofusin 2 cause Charcot-Marie-Tooth neuropathy type 2A. Nat Genet. 2004; 36(5):449-51. Epub 2004/04/06. https://doi.org/10.1038/ng1341 PMID: 15064763

36. Eura Y, Ishihara N, Yokota S, Mihara K. Two mitofusin proteins, mammalian homologues of FZO, with distinct functions are both required for mitochondrial fusion. J Biochem. 2003; 134(3):333-44. Epub 2003/10/17. PMID: 14561718

37. Gomes LC, Scorrano L. Mitochondrial elongation during autophagy: a stereotypical response to survive in difficult times. Autophagy. 2011; 7(10):1251-3. Epub 2011/07/12. https://doi.org/10.4161/auto.7.10. 16771 PMID: 21743300

38. Lee J-Y, Kapur M, Li M, Choi M-C, Choi S, Kim H-J, et al. MFN1 deacetylation activates adaptive mitochondrial fusion and protects metabolically challenged mitochondria. J Cell Science. 2014; 127 (22):4954-63. Epub September 30, 2014.

39. Benard G, Bellance N, James D, Parrone P, Fernandez H, Letellier T, et al. Mitochondrial bioenergetics and structural network organization. J Cell Sci. 2007; 120(5):838-48.

40. Toyama EQ, Herzig S, Courchet J, Lewis TL, LosoÂn OC, Hellberg K, et al. AMP-activated protein kinase mediates mitochondrial fission in response to energy stress. Science. 2016; 351(6270):275-81. https://doi.org/10.1126/science.aab4138 PMID: 26816379

41. Wick AN, Drury DR, Nakada HI, Wolfe JB, Britton WttaoB, Grabowski R. Localization of the primary metabolic block produced by 2-deoxyglucose. J Biol Chem. 1957; 224(2):963-9. PMID: 13405925

42. Castro FA, Mariani D, Panek AD, Eleutherio EC, Pereira MD. Cytotoxicity mechanism of two naphthoquinones (menadione and plumbagin) in Saccharomyces cerevisiae. PLoS One. 2008; 3(12):e3999. Epub 2008/12/23. https://doi.org/10.1371/journal.pone.0003999 PMID: 19098979

43. Newman LE, Schiavon C, Kahn RA. Plasmids for variable expression of proteins targeted to the mitochondrial matrix or intermembrane space. Cellular Logistics. 2016; 6(4):e1247939. Epub 2017/01/04.

https://doi.org/10.1080/21592799.2016.1247939 PMID: 28042516

44. Cunningham LA, Kahn RA. Cofactor D functions as a centrosomal protein and is required for the recruitment of the gamma-tubulin ring complex at centrosomes and organization of the mitotic spindle. J Biol Chem. 2008; 283(11):7155-65. Epub 2008/01/04. https://doi.org/10.1074/jbc.M706753200 PMID:

18171676

45. Bhamidipati A, Lewis SA, Cowan NJ. ADP ribosylation factor-like protein 2 (Arl2) regulates the interaction of tubulin-folding cofactor D with native tubulin. J Cell Biol. 2000; 149(5):1087-96. Epub 2000/06/01. PMID: 10831612

46. Tian G, Thomas S, Cowan NJ. Effect of TBCD and its regulatory interactor Arl2 on tubulin and microtubule integrity. Cytoskeleton (Hoboken). 2010; 67(11):706-14. Epub 2010/08/27.

47. Zhou C, Cunningham L, Marcus AI, Li Y, Kahn RA. Arl2 and Arl3 regulate different microtubule-dependent processes. Mol Biol Cell. 2006; 17(5):2476-87. Epub 2006/03/10. https://doi.org/10.1091/mbc.E05-10-0929 PMID: 16525022

48. Graham BH, Waymire KG, Cottrell B, Trounce IA, MacGregor GR, Wallace DC. A mouse model for mitochondrial myopathy and cardiomyopathy resulting from a deficiency in the heart/muscle isoform of the adenine nucleotide translocator. Nat Genet. 1997; 16(3):226-34. Epub 1997/07/01. https://doi.org/10.1038/ng0797-226 PMID: 9207786

49. Ackema KB, Hench J, Bockler S, Wang SC, Sauder U, Mergentaler H, et al. The small GTPase Arf1 modulates mitochondrial morphology and function. EMBO J. 2014; 33(22):2659-75. Epub 2014/09/06. https://doi.org/10.15252/embj.201489039 PMID: 25190516

50. Santel A, Frank S, Gaume B, Herrler M, Youle RJ, Fuller MT. Mitofusin-1 protein is a generally expressed mediator of mitochondrial fusion in mammalian cells. J Cell Sci. 2003; 116(Pt 13):2763-74. Epub 2003/05/22. https://doi.org/10.1242/jcs.00479 PMID: 12759376

51. Pich S, Bach D, Briones P, Liesa M, Camps M, Testar X, et al. The Charcot-Marie-Tooth type 2A gene product, Mfn2, up-regulates fuel oxidation through expression of OXPHOS system. Hum Mol Genet. 2005; 14(11):1405-15. Epub 2005/04/15. https://doi.org/10.1093/hmg/ddi149 PMID: 15829499

52. Bach D, Pich S, Soriano FX, Vega N, Baumgartner B, Oriola J, et al. Mitofusin-2 determines mitochondrial network architecture and mitochondrial metabolism. A novel regulatory mechanism altered

in obesity. J Biol Chem. 2003; 278(19):17190-7. Epub 2003/02/25. https://doi.org/10.1074/jbc.M212754200 PMID: 12598526

53. Mourier A, Motori E, Brandt T, Lagouge M, Atanassov I, Galinier A, et al. Mitofusin 2 is required to maintain mitochondrial coenzyme Q levels. J Cell Biol. 2015; 208(4):429-42. Epub 2015/02/18. https://doi.org/10.1083/jcb.201411100 PMID: 25688136

54. Schrepfer E, Scorrano L. Mitofusins, from Mitochondria to Metabolism. Mol Cell. 2016; 61(5):683-94.Epub 2016/03/05. https://doi.org/10.1016/j.molcel.2016.02.022 PMID: 26942673

55. de Brito OM, Scorrano L. Mitofusin 2 tethers endoplasmic reticulum to mitochondria. Nature. 2008; 456 (7222):605-10. Epub 2008/12/05. https://doi.org/10.1038/nature07534 PMID: 19052620

56. Cosson P, Marchetti A, Ravazzola M, Orci L. Mitofusin-2 independent juxtaposition of endoplasmic reticulum and mitochondria: an ultrastructural study. PLoS One. 2012; 7(9):e46293. Epub 2012/10/03. https://doi.org/10.1371/journal.pone.0046293 PMID: 23029466

57. Filadi R, Greotti E, Turacchio G, Luini A, Pozzan T, Pizzo P. Mitofusin 2 ablation increases endoplasmic reticulum-mitochondria coupling. Proc Natl Acad Sci U S A. 2015; 112(17):E2174±81. Epub 2015/04/15. https://doi.org/10.1073/pnas.1504880112 PMID: 25870285

58. Zhang CJ, Bowzard JB, Anido A, Kahn RA. Four ARF GAPs in Saccharomyces cerevisiae have both overlapping and distinct functions. Yeast. 2003; 20(4):315-30. Epub 2003/03/11. https://doi.org/10.1002/yea.966 PMID: 12627398

59. Zhang CJ, Cavenagh MM, Kahn RA. A family of Arf effectors defined as suppressors of the loss of Arf function in the yeast Saccharomyces cerevisiae. J Biol Chem. 1998; 273(31):19792-6. Epub 1998/07/25. PMID: 9677411

60. East MP, Bowzard JB, Dacks JB, Kahn RA. ELMO domains, evolutionary and functional characterization of a novel GTPase-activating protein (GAP) domain for Arf protein family GTPases. J Biol Chem. 2012; 287(47):39538-53. Epub 2012/09/28. https://doi.org/10.1074/jbc.M112.417477 PMID: 23014990

61. East MP, Kahn RA. Models for the functions of Arf GAPs. Semin Cell Dev Biol. 2011; 22(1):3-9. Epub 2010/07/20. https://doi.org/10.1016/j.semcdb.2010.07.002 PMID: 20637885

62. Gough DJ, Corlett A, Schlessinger K, Wegrzyn J, Larner AC, Levy DE. Mitochondrial STAT3 supports Ras-dependent oncogenic transformation. Science. 2009; 324(5935):1713-6. Epub 2009/06/27. https://doi.org/10.1126/science.1171721 PMID: 19556508

63. Wegrzyn J, Potla R, Chwae YJ, Sepuri NB, Zhang Q, Koeck T, et al. Function of mitochondrial Stat3 in cellular respiration. Science. 2009; 323(5915):793-7. Epub 2009/01/10. https://doi.org/10.1126/science.1164551 PMID: 19131594

64. Tammineni P, Anugula C, Mohammed F, Anjaneyulu M, Larner AC, Sepuri NB. The import of the transcription factor STAT3 into mitochondria depends on GRIM-19, a component of the electron transport chain. J Biol Chem. 2013; 288(7):4723-32. Epub 2012/12/29. https://doi.org/10.1074/jbc.M112.378984 PMID: 23271731

65. Tapper DP, Van Etten RA, Clayton DA. Isolation of mammalian mitochondrial DNA and RNA and cloning of the mitochondrial genome. Methods Enzymol. 1983; 97:426-34. Epub 1983/01/01. PMID: 6197614

66. Otsu N. Threshold Selection Method from Gray-Level Histograms. Ieee T Syst Man Cyb. 1979; 9 (1):62-6.

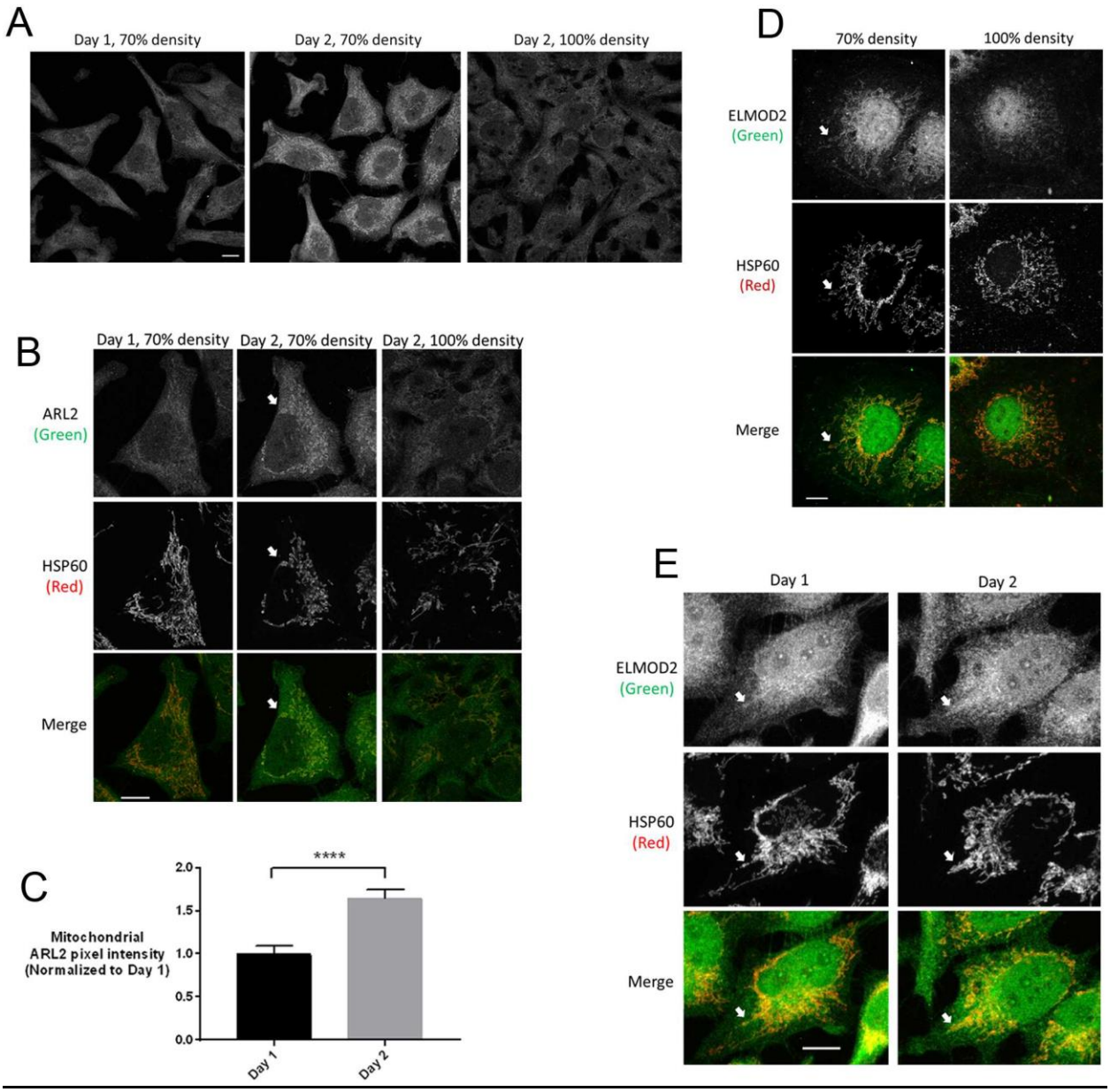

Figure 1. Mitochondrial staining of ARL2 and ELMOD2 vary in intensity with cell density and days after plating. (**A**) HeLa cells were fixed at ~70% confluence either one (left) or two days (middle) after plating, or seeded at higher density and fixed at 100% confluence at 2 days (right). Cells were fixed and stained for ARL2 and HSP60, as described under Methods. (**B**) One cell from each field in panel A was selected and enlarged. ARL2 (top) and HSP60 staining (middle) are shown separately, with merged images on the bottom. Images are single planes acquired by confocal microscopy. Images in A and B are single planes acquired by confocal microscopy; scale bars = 10 μm. (**C**) Mitochondrial ARL2 pixel

intensity was quantified in cells plated one or two days, as described under Materials and Methods. For each condition, 10 cells were analyzed, and the increase in ARL2 signal in Day 2 cells was statistically significant ($p<0.0001$). (**D**) COS7 cells at either 70% or 100% density were fixed 2 days after plating and stained for ELMOD2 and HSP60. (**E**) HeLa cells were fixed at 70% confluence and stained for ELMOD2 and HSP60. ELMOD2 (top) and HSP60 staining (middle) are shown, with merged images on the bottom. Images are z stack projections, and scale bars = 10 μm. Nuclear staining of ELMOD2 is non-specific, as described in the text.

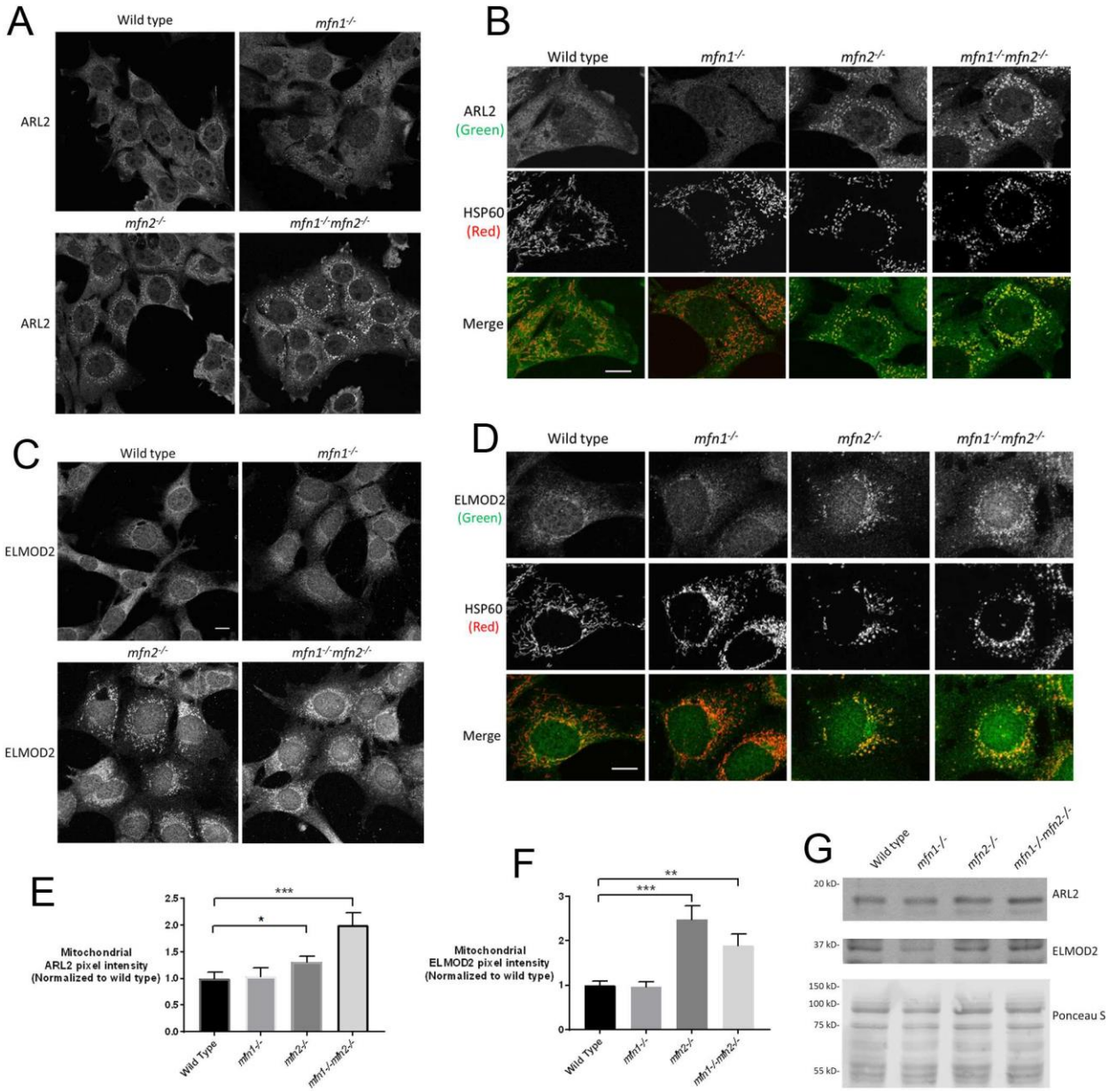

Figure 2. Mitochondrial ARL2 and ELMOD2 are increased in *mfn2-/-* and *mfn1-/-mfn2-/-* MEFs.

Wild type, *mfn1-/-*, *mfn2-/-*, or *mfn1-/-mfn2-/-* MEFs were fixed (50% density) one day after plating and stained for ARL2 or HSP60. (**A**) ARL2 is shown for each line. (**B**) Single cells stained for ARL2 (top) and HSP60 (middle) are shown and merged (bottom). Single z planes are shown. (**C**) Same as A, except cells were stained for ELMOD2. Z stack projections are shown. (**D**) Same as B, except staining for ELMOD2 and HSP60. Scale bar = 10 μm. (**E**) Mitochondrial ARL2 pixel intensity was quantified in wild type, *mfn1-/-*, *mfn2-/-*, or *mfn1-/-mfn2-/-* MEFs, as described under Materials and Methods. For each

condition,10 cells were analyzed, with the exception of wild type cells, where 11 cells were analyzed. The increases in ARL2 signal in *mfn2-/-* and *mfn1-/-mfn2-/-* MEFs were statistically significant ($p<0.05$ and $p<0.001$, respectively). (**F**) Same as E, except quantified for ELMOD2. Increases in *mfn2-/-* and *mfn1-/-mfn2-/-* MEFs were statistically significant ($p<0.001$ and $p<0.01$, respectively). (**G**) Lysates from wild type, *mfn1-/-*, *mfn2-/-*, or *mfn1-/-mfn2-/-* MEFs were resolved by SDS-PAGE and transferred to nitrocellulose, as described under Methods. Ponceau S staining (lower panel) was performed immediately after transfer. The membrane was then cut and probed for ARL2 (top panel) or ELMOD2 (middle panel).

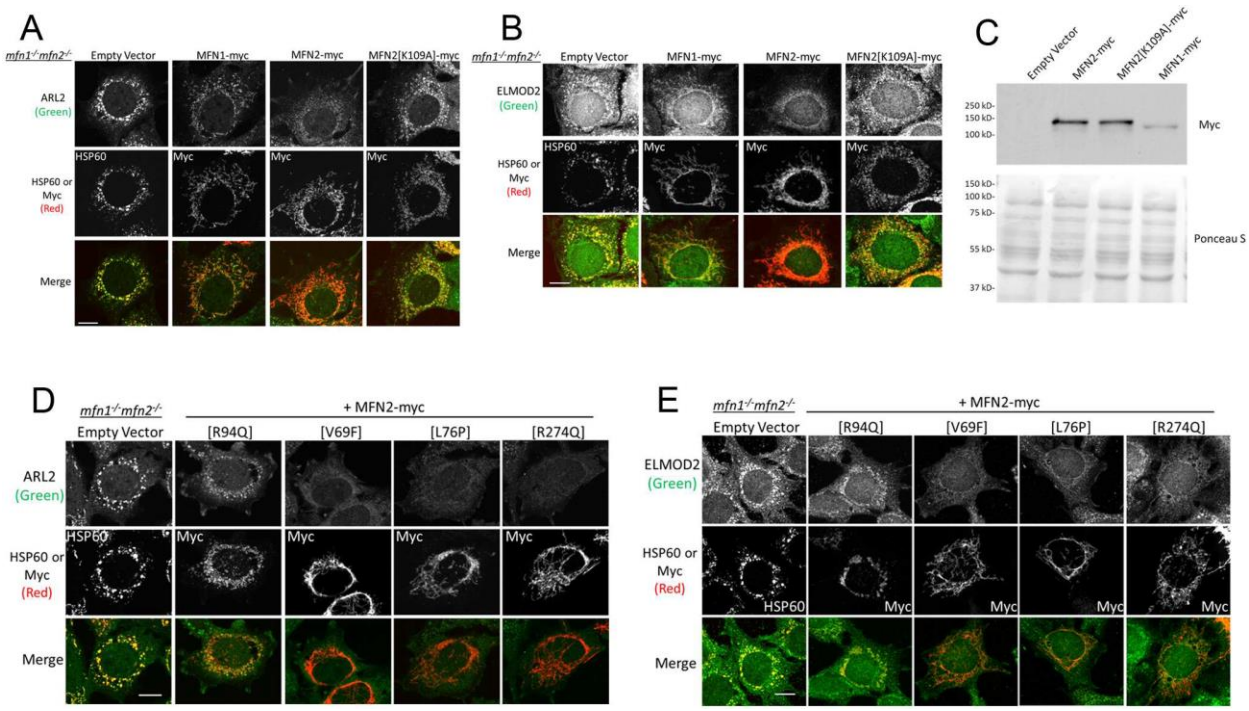

Figure 3. Elevated mitochondrial ARL2 and ELMOD2 is reversed in *mfn1-/-mfn2-/-* MEFs with restoration of fusion by MFN2. (**A**) *mfn1-/-mfn2-/-* MEFs were transfected with empty vector, or the same vector directing expression of MFN1-myc, MFN2-myc, or MFN2[K109A]-myc. MEFs were fixed 48 hours later and stained for ARL2 (top) and either HSP60 (empty vector) or myc (MFN1-myc, MFN2-myc, MFN2[K109A]-myc) (middle). Merged images are shown at the bottom. Single planes are shown. (**B**) Same as A, except cells were stained for ELMOD2. Z stack projections are shown. (**C**) Cells treated as in A but after 24 hours total cell lysates were obtained, resolved by SDS-PAGE, transferred to nitrocellulose, and probed with anti-myc (upper panel), as described under Methods. Ponceau S staining (lower panel) was performed immediately after transfer. (**D**) *mfn1-/-mfn2-/-* MEFs were transfected with empty vector, or the same vector directing expression of MFN2[R94Q]-myc, MFN2[V69F]-myc, MFN2[L76P]-myc, or MFN2[R274Q]-myc. MEFs were fixed 48 hours later and stained for ARL2 (top) and either HSP60 (empty vector) or myc (MFN2-myc) (middle). Merged images are shown (bottom). Single planes are shown. (**E**) Same as D, except cells were stained for ELMOD2. Z stack projections are shown. Scale bars = 10 μm.

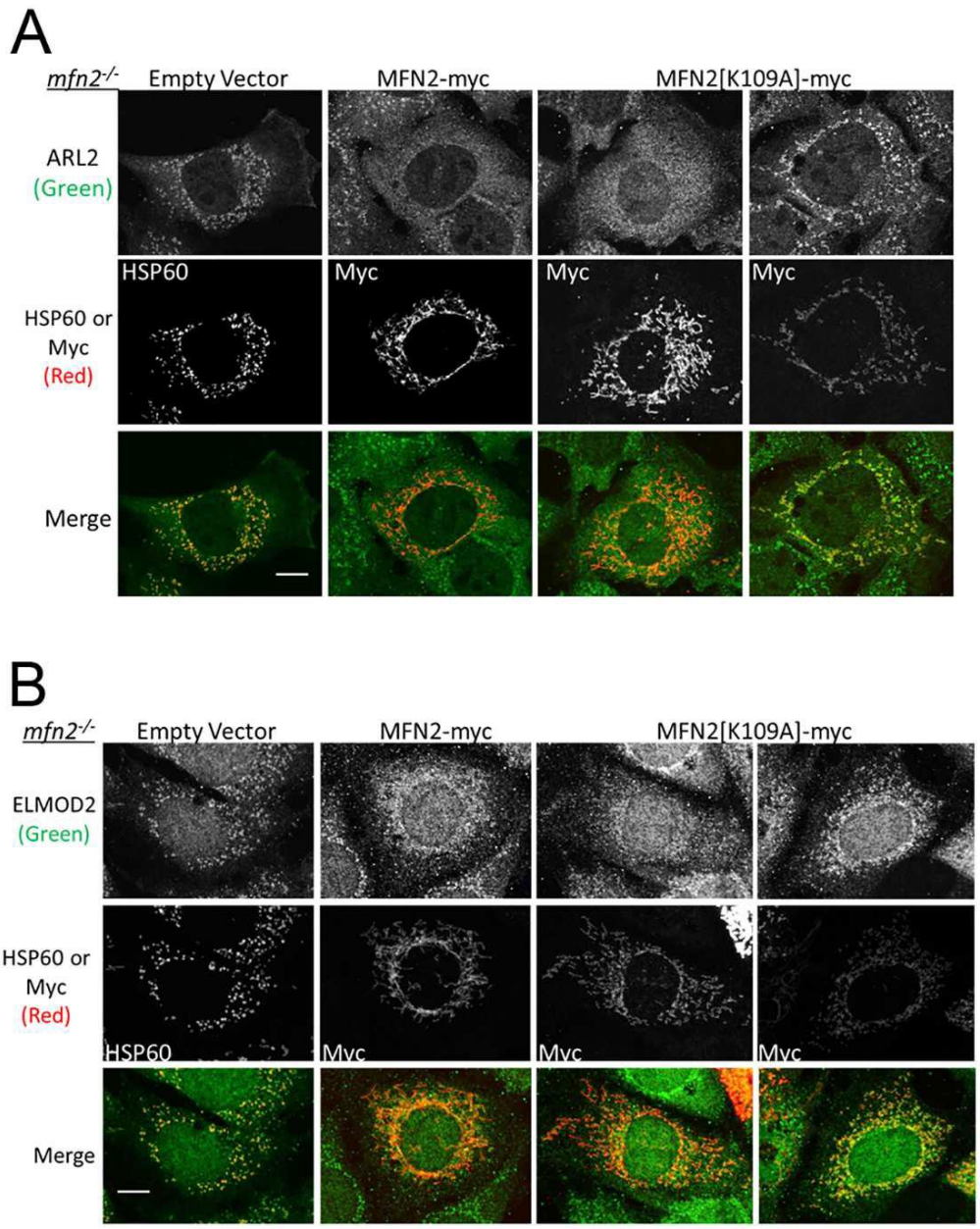

Figure 4. Elevated mitochondrial ARL2 and ELMOD2 are reversed with expression of MFN2-myc or MFN2[K109A]-myc in *mfn2-/-* MEFs. (**A**) MFN2-myc or MFN2[K109A]-myc were expressed in *mfn2-/-* MEFs, fixed 48 hours later and stained for ARL2 (top) and either HSP60 (empty vector) or myc (MFN2-myc, MFN2[K109A]-myc) (middle). Merged images are shown at the bottom. Single planes are shown. (**B**) Same as A, except cells were stained for ELMOD2. Z stack projections are shown. Scale bar = 10 μm.

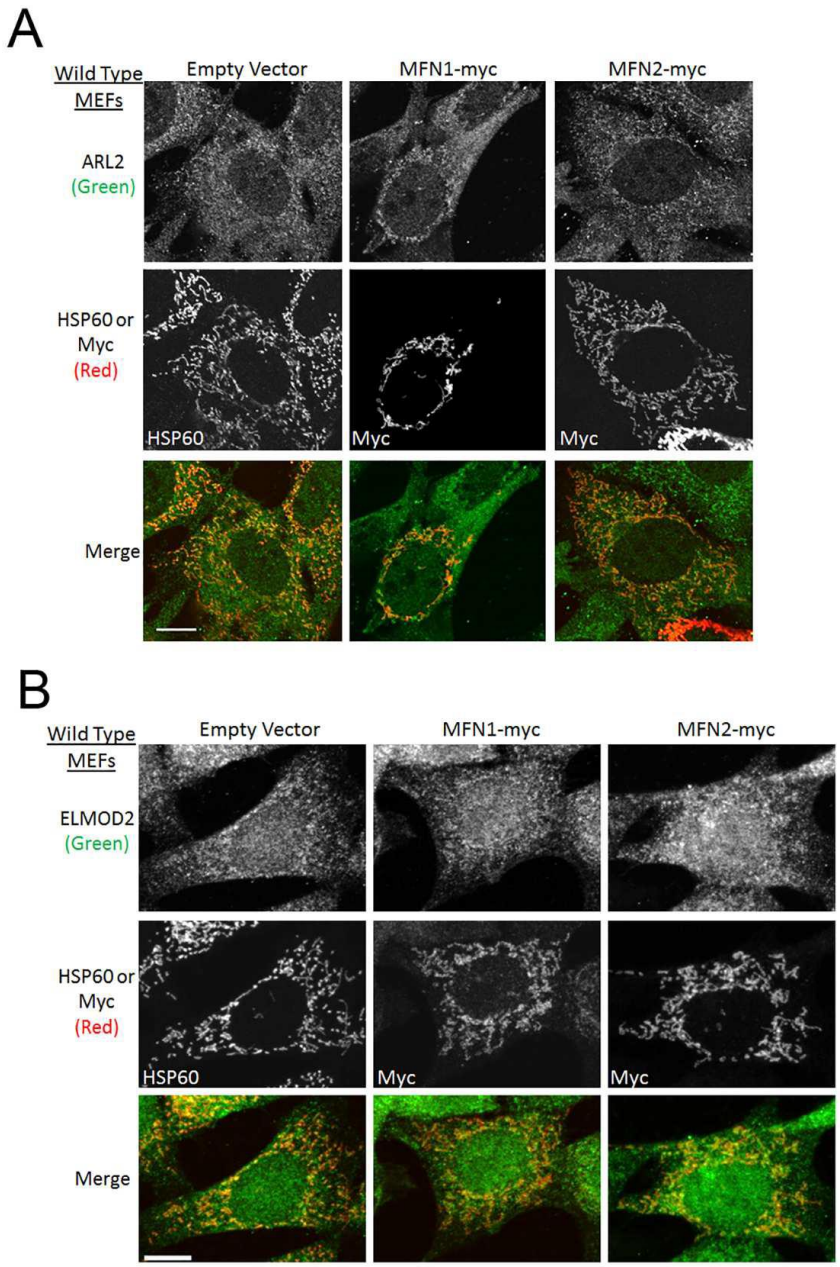

Figure 5. Expression of MFN1-myc or MFN2-myc does not affect ARL2 or ELMOD2 staining intensity inwild type MEFs. (**A**) Wild type MEFs were transfected with empty vector, MFN1-myc, or MFN2-myc. Cells were fixed 48 hours later and stained for ARL2 (top) and either HSP60 (empty vector) or myc (MFN1-myc, MFN2-myc) (middle). Merged images are shown at the bottom. Single planes are shown. (**B**) Same as A, except cells were stained for ELMOD2. Z stack projections are shown. Scale bar = 10 μm.

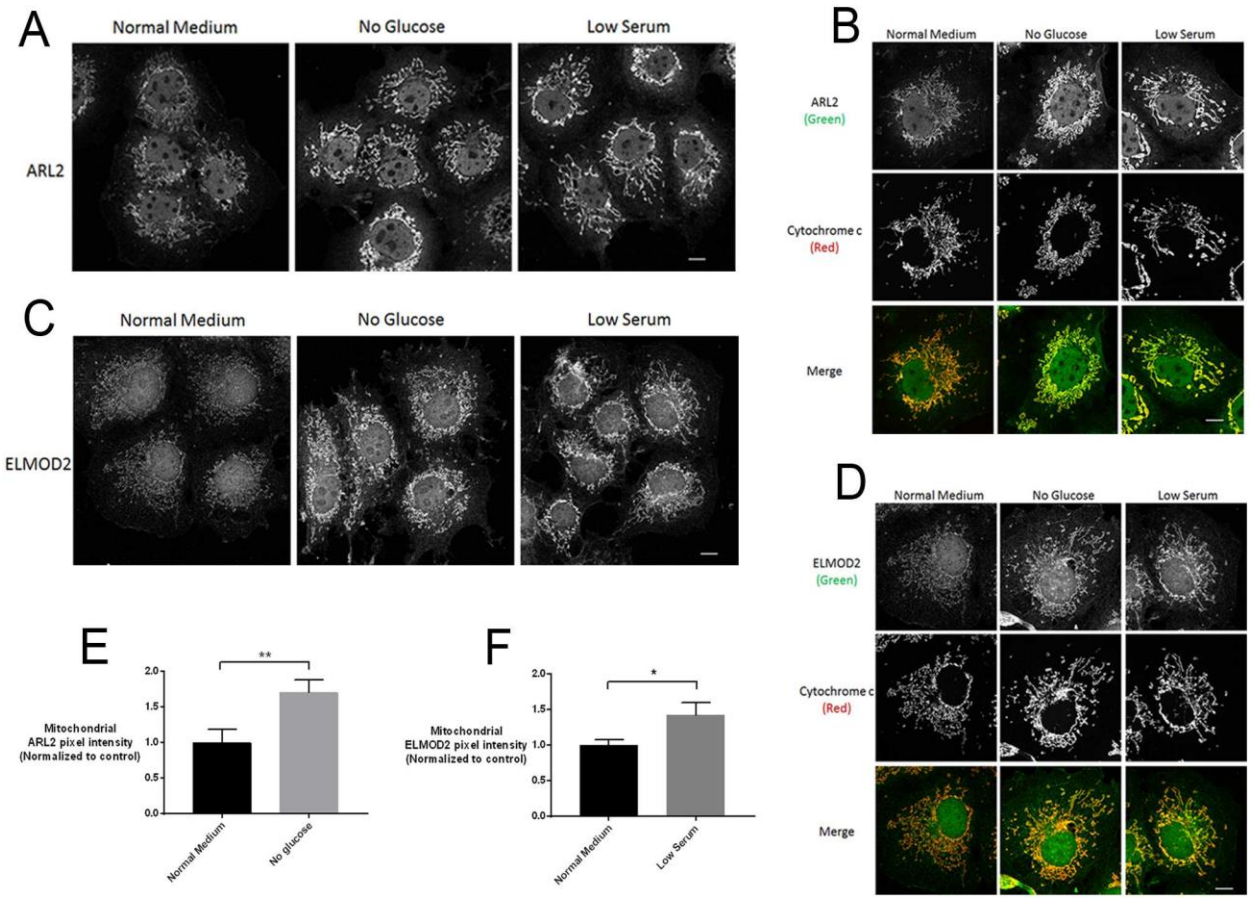

Figure 6. Mitochondrial ARL2 and ELMOD2 increase in cells cultured in 0 glucose or 2% serum.

(**A**) COS7 cells cultured for 48 hours in normal, 0 glucose, or 2% serum medium were fixed and stained for ARL2 (top). (**B**) Individual cells stained for ARL2 (top) and cytochrome c (middle) are shown. Merged images are shown at the bottom. Images in A and B are single planes. (**C**) Same as A, except cells were stained for ELMOD2. (**D**) Individual cells stained for ELMOD2 (top) and cytochrome c (middle) are shown, with merged images at the bottom. Images in C and D are z stack projections. **(E)** Mitochondrial ARL2 pixel intensity was quantified in images of cells cultured in normal or no glucose media, as described in Materials and Methods, and the increase was statistically significant ($p<0.01$). (**F**) Mitochondrial ELMOD2 pixel intensity was quantified in images of cells cultured in normal or low serum media, as described in Materials and Methods, and the increase was statistically significant ($p<0.05$). All scale bars = 10 μm.

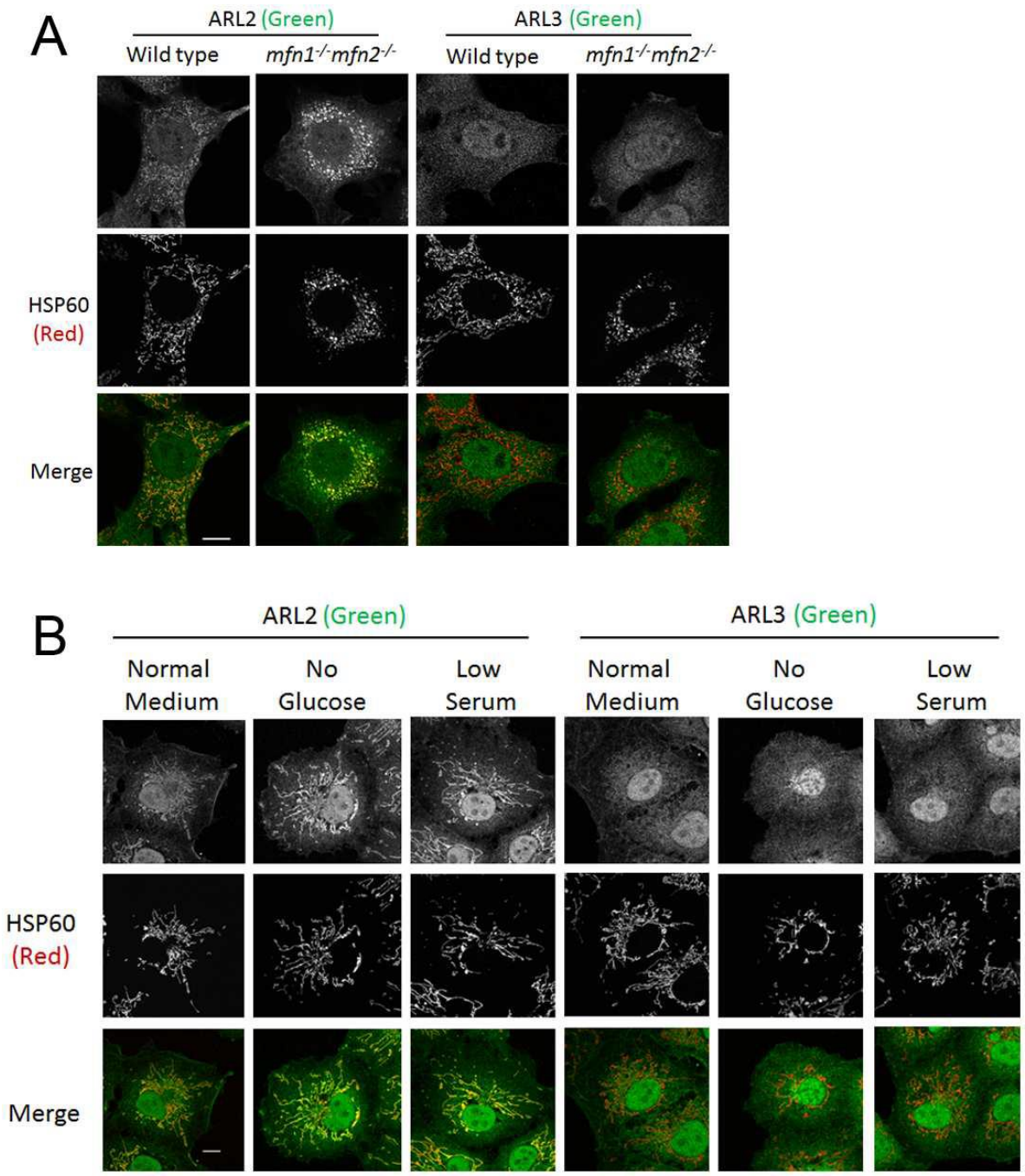

Figure 7. ARL3 staining is unchanged with MFN2 deletion, glucose starvation, or serum starvation. (**A**) Wild type or *mfn1-/-mfn2-/-* MEFs were fixed (50%) one day after plating and stained for HSP60 (middle) and either ARL2 (left two columns) or ARL3 (right two columns). Single planes are shown. (**B**) COS7 cells were cultured for 48 hours in normal medium, 0 glucose medium, or 2% serum medium then fixed and stained for HSP60 (middle) and either ARL2 (left three columns) or ARL3 (right three columns). Single planes are shown. All scale bars = 10 μm.

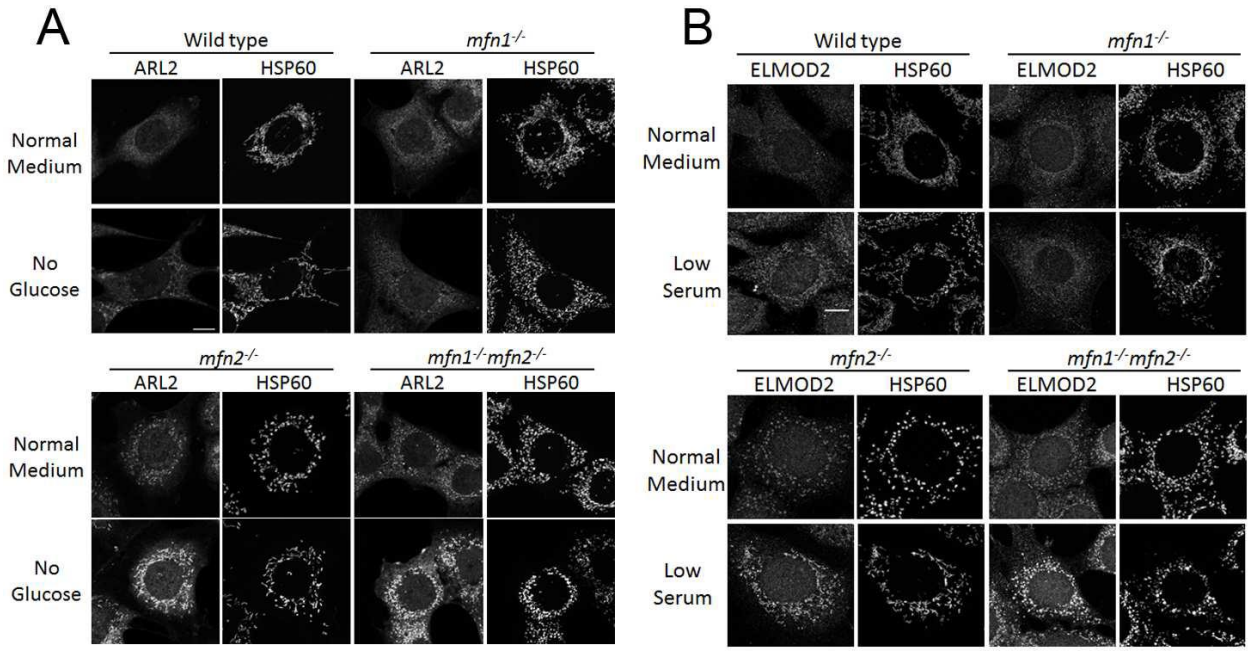

Figure 8. Glucose or serum deprivation increases mitochondrial ARL2 in wild type, *mfn2-/-*, or *mfn1-/-mfn2-/-*, but not *mfn1-/-* MEFs. MEFs were cultured for 48 hours in normal, 0 glucose, or low serum medium, and fixed and stained for ARL2 (**A**) or ELMOD2 (**B**) as well as HSP60. Single planes are shown in (A) and z stack projections in (B). Scale bar = 10 μm.

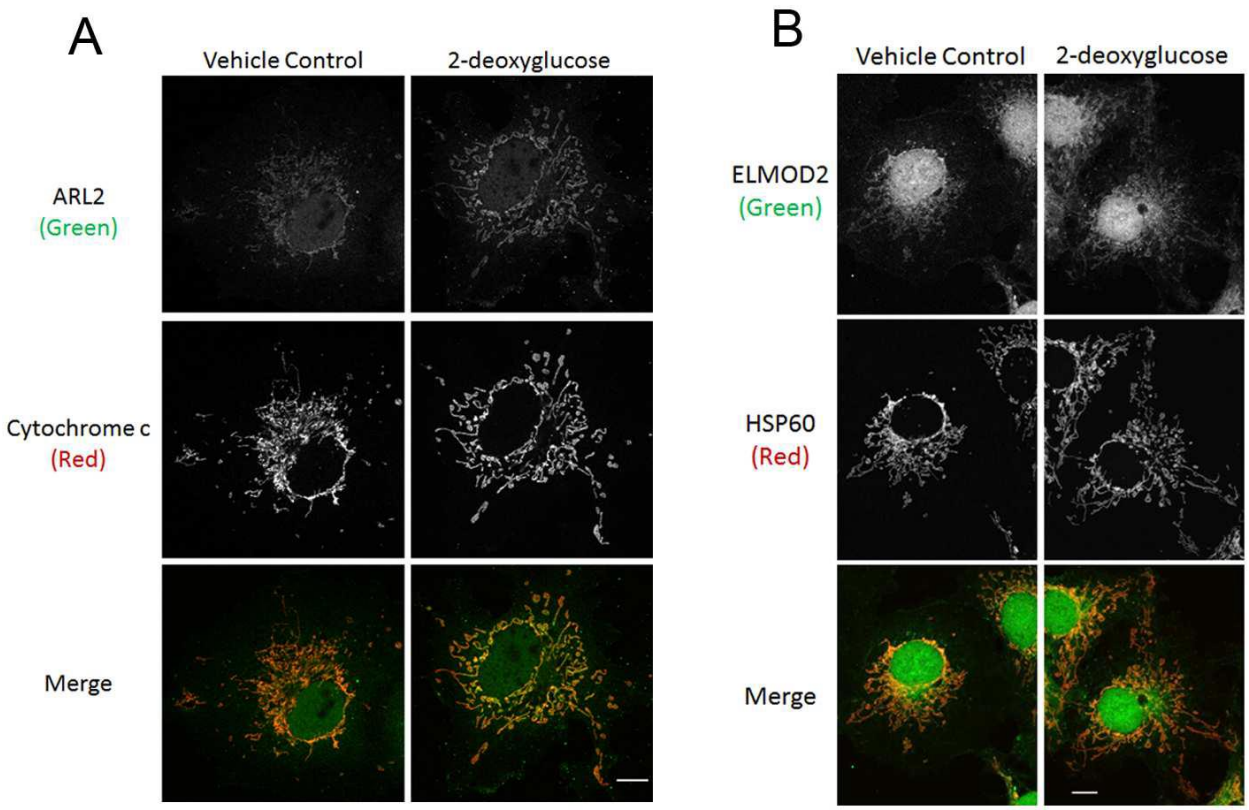

Figure 9. Mitochondrial ARL2, but not ELMOD2, is increased by 2-deoxyglucose. (**A**) COS7 cells were cultured in glucose or 2-deoxyglucose (25 mM) medium. Cells were fixed 16 hours later and stained for ARL2 (top) and cytochrome c (middle). Merged images are shown at the bottom. Images are single planes. (**B**) Same as (A), except cells were stained for ELMOD2. Images are z stack projections. Scale bar = 10 μm.

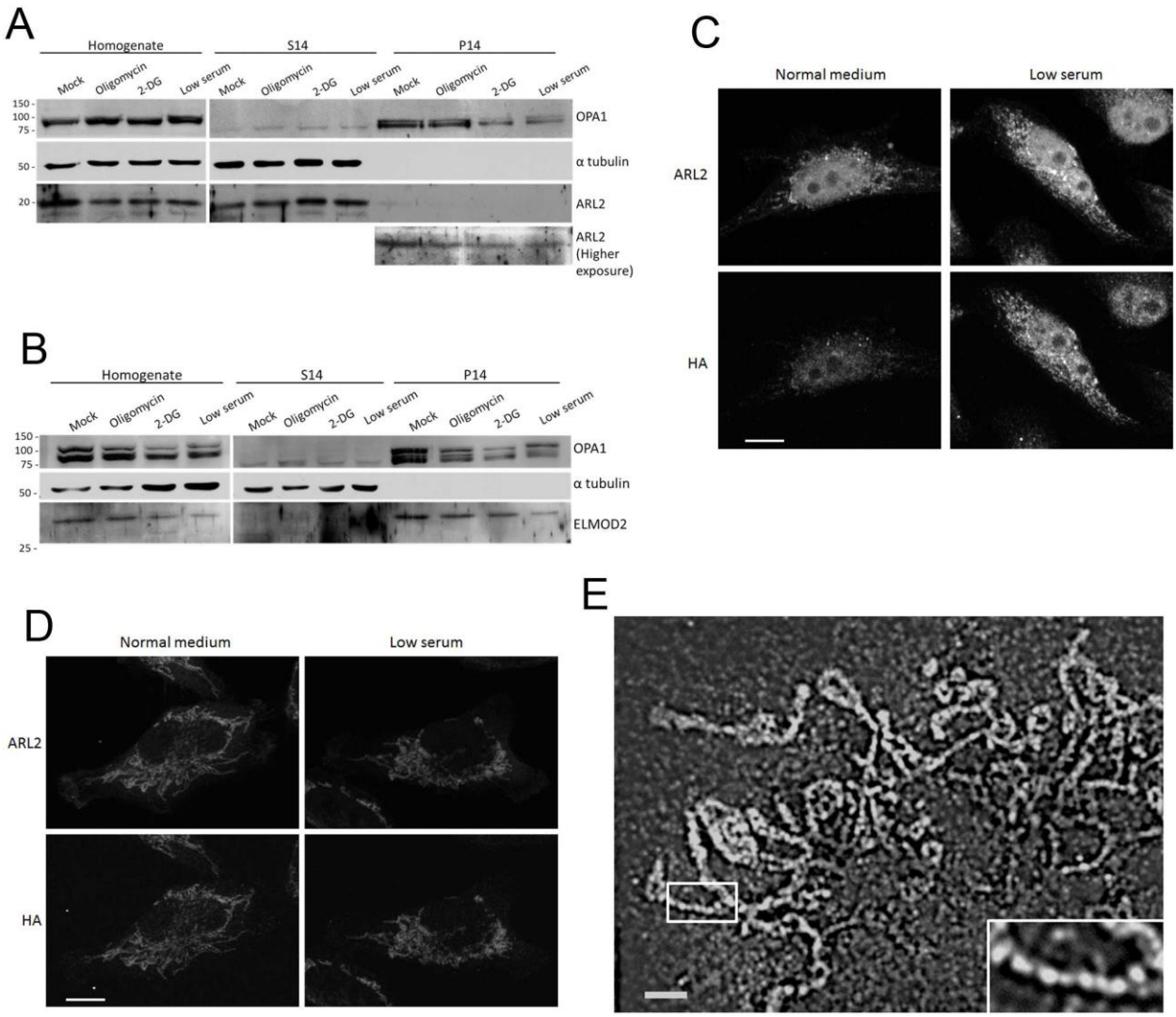

Figure 10. ARL2 and HA staining increase in stressed cells expressing ARL2-HA, but not in cells expressing SMAC-HA-ARL2. (**A**) HeLa cells were treated overnight with 25 mM 2-deoxyglucose, 10 μM oligomycin or vehicle control, or grown in medium with 2% serum for 48 hours. Cells were then harvested and fractionated as described under Materials and Methods. Homogenate, S14, and P14 fractions were immunoblotted for ARL2, alpha tubulin (cytosolic marker), and OPA1 (mitochondrial marker). Equal volumes were loaded. (**B**) Same as A except fractions were immunoblotted for ELMOD2.(**C**) HeLa cells were transfected with ARL2-HA and allowed to attach to coverslips for 4 hours, before the medium was replaced with normal or 2% serum medium. Two days later, cells were permeabilized prior to fixation, to remove cytosolic ARL2, then stained for ARL2 and HA. Images are z stack projections. (**D**) HeLa cells expressing SMAC-HA-ARL2 were treated as in A but without pre-

fixation permeabilization. Cells were fixed and stained for ARL2 and HA. Images are single planes acquired by confocal microscopy. Scale bar = 10 μm. (**E**) COS7 cells were treated with 25 mM 2-deoxyglucose for 16 hr, fixed and stained for ARL2 and imaged using SIM. A representative cell is shown. The blowup (bottom right) is 2.5x the size of the larger image shown. Scale bar = 2 μm.

MEF line	Transfected plasmid (Protein expressed)	ARL2 staining relative to wild type MEFs	ELMOD2 staining relative to wild type MEFs
Wild type	N/A	NC	NC
mfn1$^{-/-}$	N/A	NC	NC
mfn2$^{-/-}$	N/A	+	+
mfn1$^{-/-}$*mfn2*$^{-/-}$	N/A	+	+
mfn2$^{-/-}$	Empty vector	+	+
mfn2$^{-/-}$	MFN1-myc	+	+
mfn2$^{-/-}$	MFN2-myc	-	-
mfn2$^{-/-}$	MFN2[K109A]-myc	-	-
mfn1$^{-/-}$*mfn2*$^{-/-}$	Empty vector	+	+
mfn1$^{-/-}$*mfn2*$^{-/-}$	MFN1-myc	+	+
mfn1$^{-/-}$*mfn2*$^{-/-}$	MFN2-myc	-	-
mfn1$^{-/-}$*mfn2*$^{-/-}$	MFN2[K109A]-myc	+	+
mfn1$^{-/-}$*mfn2*$^{-/-}$	MFN2[R94Q]-myc	+	+
mfn1$^{-/-}$*mfn2*$^{-/-}$	MFN2[V69F]-myc	-	-
mfn1$^{-/-}$*mfn2*$^{-/-}$	MFN2[L76P]-myc	-	-
mfn1$^{-/-}$*mfn2*$^{-/-}$	MFN2[R274Q]-myc	-	-

Table I. Summary of effects of MFN deletions on ARL2/ELMOD2 staining in MEF lines. See text for details. NC, no change compared to wild type MEFs. +, - indicate clearly increased or decreased mitochondrial staining, respectively.

Stressor	Duration of stress	ARL2 staining	ELMOD2 staining	Effect on mitochondrial morphology	Cell lines
0 mM glucose + 10% FBS	24, 48 hours	+	+	Elongation	COS7, HeLa, MEFs
25 mM glucose + 2% FBS	24, 48 hours	+	+	Elongation	COS7, HeLa, MEFs
10 mM galactose	24, 48 hours	+	+	Elongation	COS7, HeLa, MEFs
25mM 2-deoxyglucose	16 hours	+	NC	Partial fragmentation	COS7, HeLa, MEFs
10 µM oligomycin	16 hours	+	NC	Fragmentation	COS7, HeLa, MEFs
10 µM antimycin A	16 hours	+	NC	Fragmenation	COS7, HeLa, MEFs
10 µM rotenone	16 hours	+	NC	Fragmentation	COS7, HeLa, MEFs
10 µM menadione	1 hour	+	NC	No change	COS7, HeLa

Table II. Summary of the effects of energetic stressors on mitochondrial staining of ARL2 or ELMOD2. See text for details. + indicates an increase in staining intensity, over that seen in cells grown in DMEM medium with 25 mM glucose and 10% FBS. NC indicates no changes in staining intensities were evident.

Chapter 4: ELMOD2 regulates mitochondrial fusion in a mitofusin-dependent manner downstream of ARL2

Cara R. Schiavon, Rachel E. Turn, Laura E. Newman, Richard A. Kahn

Abstract

Mitochondria are dynamic organelles vital to the function of all eukaryotic cells. The primary players in mitochondrial morphology have been identified but their mechanism(s) of regulation are still being elucidated. ARL2 is a regulatory GTPase which has previously been shown to play a role in the regulation of mitochondrial morphology. Here we demonstrate that ELMOD2, an ARL2 GTPase activating protein (GAP), is necessary for ARL2 to promote mitochondrial elongation. We show that loss of ELMOD2 causes mitochondrial fragmentation and a lower rate of mitochondrial fusion, while ELMOD2 overexpression promotes mitochondrial tubulation and increases the rate of fusion in a mitofusin-dependent fashion. We also show that a GAP-dead mutant of ELMOD2 is capable of promoting fusion. Finally, we show that ELMOD2, ARL2, mitofusins 1 and 2, and miros 1 and 2 localize to discrete puncta along mitochondria and that these puncta repeat at a regular interval. These results suggest that ELMOD2 is functioning as an effector downstream of ARL2 and upstream of the mitofusins to promote mitochondrial fusion and that ARL2, ELMOD2, mitofusins, and miros may be part of a mitochondrial complex important for regulation of mitochondrial morphology.

Introduction

Mitochondria are vital for a variety of cellular functions in all eukaryotes. Most well-known is the generation of ATP but they are also involved in maintenance of calcium levels, lipid metabolism, apoptosis, and cell signaling. Mitochondria are highly dynamic organelles capable of changing overall morphology between small, spherical organelles to a highly connected, branched network as a result of changes in the rate of mitochondrial fission and fusion (1). These changes are highly correlated with altered functions.

The key proteins involved in control of mitochondrial morphology are MFN1/2, (mitofusin 1 and 2) OPA1 (optic atrophy 1), and DRP1 (dynamin-related protein 1). MFN1/2 are essential for outer mitochondrial membrane (OMM) fusion by tethering apposing mitochondria (2-4). MFN1/2 are large

GTPases that localize to the OMM and their activity is dependent on their oligomerization both in *cis* (within the same mitochondrion) and *trans* (across mitochondria) (4,5). OPA1 is necessary for inner mitochondrial membrane (IMM) fusion (6). Conversely, Drp1 is required for mitochondrial fission (7). While roles for each of these large GTPases in mitochondrial biology are established, the mechanisms by which they act are incompletely understood and the ways in which they are regulated are still being determined.

ARL2 is an ancient (8), very highly conserved, ubiquitously expressed small regulatory GTPase. ARL2 has been found to localize to the cytosol, centrosomes, the nucleus, and mitochondria. Previous work has shown that ARL2 in the cytosol is bound to the tubulin specific co-chaperone cofactor D and is capable of regulating the biogenesis of αβ-tubulin (9-11). In the nucleus, ARL2 regulates STAT3 signaling (12). ARL2 has also been implicated in the transport of N-myristoylated protein cargos (8,13).

ARL2 is the only member of the ARF or RAS superfamilies shown to function inside mitochondria. We have previously shown that alterations in ARL2 activity affect the morphology, motility, and energy metabolism of mitochondria. Expression of a dominant negative ARL2 mutant causes mitochondrial fragmentation and perinuclear clustering (14). Conversely, expression of a dominant active ARL2 mutant causes mitochondria to appear more elongated (15). ARL2 siRNA also causes fragmentation, the loss of cellular ATP to <50% of controls, and ultimately cell death (14). Other data reveal that ARL2 regulates mitochondrial fusion specifically from the IMS, upstream of the MFNs, and that ARL2 and MFN1 /2 localize to puncta that display the same periodicity in spacing along mitochondria (15).

Like all regulatory GTPases, ARL2 activity is predicted to be controlled by the actions of guanine nucleotide exchange factors (GEFs) and GTPase activating proteins (GAPs). Additionally, effectors are the immediate downstream targets of regulatory GTPases that preferentially bind to the activated form to initiate biological responses and consequently have been the first focus in studies of GTPase-regulated

pathways. In the ARF family, GAPs have consistently been found to have effector functions (16), further highlighting their importance. ELMOD2 was purified in our lab based on its ARL2 GAP activity and found to be a member of a protein family, with three members in humans (17). ELMOD2 has been found to localize to the ER, lipid droplets, and mitochondria (14,18,19).

There are several parallels between ARL2 and ELMOD2. ELMOD2 is the only ELMOD protein that localizes to mitochondria (14), and ARL2 is the only ARF family member (out of ~30 in mammals) similarly found in mitochondria. Like ARL2 siRNA, ELMOD2 siRNA causes mitochondrial fragmentation and perinuclear clustering (14). Like ARL2, ELMOD2 is ancient – predicted to be present in the last eukaryotic common ancestor (18). Finally, we previously demonstrated that ARL2 mitochondrial staining intensity changes as a result of various growth conditions and stressors and that mitochondrial ELMOD2 staining follows the same trends (20). These similarities between ARL2 and ELMOD2 led us to further study the potential role of ELMOD2 at mitochondria.

Methods

Antibodies and reagents:

The following antibodies were used in this study: rabbit monoclonal TOM20 (Cell Signaling #42406S), myc (Invitrogen #R950-25), HSP60 (Stressgen #ADI-SPA-807), mouse monoclonal TOM20 (BD Biosciences #61228), and cytochrome c (BD Biosciences #556432). ARL2 and ELMOD2 antibodies were generated in our lab and raised against their corresponding recombinant, full length, human proteins and have been described previously (1,8).

Cloning and constructs:

The following plasmids were generously gifted or commercially obtained and used in this study: MFN1-10xmyc and MFN2-16xmyc in pcDNA3.1 (Dr. David Chan, California Institute of Technology, (3)), myc-Miro1 (Addgene plasmid #47888) and myc-Miro2 (Addgene plasmid #4789, Dr. Pontus

Aspenstrom, Karolinska Institute (9)), human mitoPLD-GFP (Dr. Michael Frohman, Stony Brook University (10)), mito-PAGFP (Dr. Richard Youle, NIH, Addgene plasmid #23348, (11)), mito-dsRed (Dr. James Zheng, Emory), and pSpCas9(BB)-2A-Puro (PX459) V2.0 (Addgene plasmid #62988). ARL2[Q70L], ELMOD2-myc/his, and ELMOD2[R167K]-myc/his in pcDNA3.1 were described previously (6,12). ELMOD2-myc/DDK in pCMV6 was purchased from OriGene (#MR204034). ELMOD2[R167K]-myc/DDK was generated by site-directed mutagenesis using the QuickChange mutagenesis kit (Agilent Technologies #210518) and sequence-verified. Note that ELMOD2-myc/his directs expression of human ELMOD2 while ELMOD2-myc/DDK directs expression of mouse ELMOD2. Human and mouse ELMOD2 share 87% sequence identity and both are equally capable of influencing mitochondrial morphology, however, mouse ELMOD2 expresses to higher levels than human ELMOD2. Lentiviruses directing expression of mouse ELMOD2 or ELMOD3 were generated and purified in the Emory Lentiviral Vector Core Facility, after the ELMOD open reading frames were cloned into the pFUGW vector.

Cell lines:

COS7 cells were originally obtained from ATCC. WT (parental; ATCC CRL-2991), MFN1-null, MFN2-null, OPA1-null, and MFN1/MFN2 double knock-out (DKO) MEFs were a generous gift from Dr. David Chan (California Institute of Technology) (3,13,14).

The immortalized WT cells served as the parental population for CRISPR-Cas9 knockout of ELMOD2. To ensure that any phenotypes studied were not the product of off-target effects of CRISPR or random selection of clonal lines, we generated at least 2 null lines from at least two different guide RNAs (a minimum of 4 lines). Guides (20 nt) were designed using Benchling (https://benchling.com/) and cloned into the pSpCas9(BB)-2A-Puro (PX459) V2.0 vector. WT MEFs were transfected with guide plasmids and one day later puromycin (3 µg/mL, Sigma #P8833) was added for four days, to enrich for

transfected cells. Clonal isolation via limited dilution was then performed in 96 well plates, each clone was expanded and genomic DNA obtained for screening of indels by Sanger sequencing.

Cell culture:

Cells were grown in DMEM (ThermoFisher #11965) supplemented with 10% fetal bovine serum (Atlanta Biologicals #S11150) at 37°C in the presence of 5% CO_2 and in the absence of antibiotics. No cells were cultured beyond 30 passages (all ELMOD2 null lines were analyzed pre-passage 10). Cell density, feeding, and plating were kept constant between conditions and experiments, with a target of ~70% confluence for cell imaging. Cells were screened for mycoplasma regularly by staining with Hoechst 33342 DNA dye.

Transfection and transduction:

Cells at 90% density or higher were transfected in 6 well plates using the following protocol. COS7 cells were transfected with a ratio of 2 µg Lipofectamine 2000: 1 µg DNA. MEFs were transfected using a similar protocol, though we found optimal expression was obtained using a 3:1 µg ratio of Lipofectamine 2000: DNA. Cells were transfected with 0.5 µg MFN1-myc, MFN2-myc, mitoPLD-GFP, myc-Miro1, or myc-Miro2, 2 µg ARL2[Q70L], or 4 µg of any ELMOD2-expressing plasmid. Plasmids were diluted in 250 µL Opti-MEM (Invitrogen #31985). Lipofectamine 2000 (Invitrogen #11668) was diluted in a separate tube containing 250 µL Opti-MEM, vortexed briefly, and incubated at room temperature for 5 minutes. The tubes were mixed and incubated 20 minutes. Cell culture medium was changed to 1.5 ml of Opti-MEM, and transfection complexes (500 µL) were added dropwise to the cells. After 4 hours, cells were trypsinized and replated into fresh wells or onto coverslips.

For lentiviral transduction for expression of ELMOD2-myc or ELMOD3-myc, 10,000 cells were plated into 24 well plates and allowed to settle for 1-2 hours. Cells were transduced with virus (MOI of $2x10^9$) at a 150:1 ratio of lentivirus to cells. After 48 hours of treatment, medium was swapped with fresh DMEM.

For transfection of ELMOD2-null lines, cells were transfected with PEI at a 3:1 ratio of PEI to DNA. These complexes were diluted in 0% FBS DMEM and incubated at room temperature for 20 minutes before being added dropwise to cells immersed in 2% FBS DMEM (medium swapped to 2% FBS DMEM from 10% FBS DMEM immediately before transfection). Cells grew for 24 hours before being replated onto coverslips. After 48 hours, cells were fixed and prepared for immunofluorescence experiments (see below).

Immunoblotting:

Cells were harvested by rinsing twice with PBS, collected by incubation in 5 mM EDTA in PBS and pelleted in a microfuge (14,000 rpm, 4°C). Cells were lysed in 1% CHAPS, 25 mM HEPES pH 7.4, 100 mM NaCl, and 0.1% protease inhibitors (Sigma #P-2714) on ice for 30 minutes, and the S14 was obtained by clarifying lysates by centrifugation for 30 minutes (14,000 rpm, 4°C). Protein concentrations were determined by Bradford Assay (Bio-Rad #5000006) using bovine serum albumin (Thermo Scientific #23209) as standard. Protein samples (20 μg/well) were separated on 11% polyacrylamide gels and transferred to nitrocellulose membranes (Bio-Rad #162–0112) at 20V overnight. Membranes were blocked in PBST (PBS with 0.1% Tween-20) containing 5% (w/v) dry milk (Bio-Rad #170-6404) for 1 hour. Membranes were then incubated with primary antibody in blocking buffer at 4°C overnight, followed by washing in PBST 3 times for 10 min each. HRP-conjugated secondary antibody (GE #NA931V) was diluted in PBST and incubated for 1 hour at room temperature, followed by washing 3 times in PBST for 10 min each. Excess Tween-20 was removed by quickly rinsing membranes in PBS. Blots were incubated in luminol containing solution (0.1 mM Tris-HCl pH 8.0, 1.2 mM luminol, 0.2 mM p-coumaric acid, 0.009% hydrogen peroxide) for 1 min before exposure to film. Myc antibody was used at a dilution of 1:1000 for immunoblotting experiments.

Immunofluorescence:

Cells were grown on matrigel (BD Biosciences #356231) coated coverslips, fixed in a pre-warmed (37°C) solution of 4% paraformaldehyde in PBS (140 mM NaCl, 3 mM KCl, 10 mM Na_2HPO_4, 2 mM KH_2PO_4, pH 6.75) for 15 minutes at room temperature and permeabilized with 0.1% (v/v) Triton X-100 in PBS for 10 minutes at room temperature. Coverslips were blocked for 1 hour at room temperature using filtered PBS containing 1% (w/v) BSA (Sigma #A3059). Primary antibodies were incubated in blocking solution at 4°C overnight, followed by 4 x 5 minute washes in PBS. Secondary antibodies (1:500, Alexa fluorophores, ThermoFisher) were incubated in blocking solution for 1 hour at room temperature. Secondary antibody was removed by 2 x 5 minute washes in PBS. DNA was then stained with Hoechst 33342 for 4 minutes, followed by 2 x 5 minutes washes in PBS. Stained coverslips were mounted onto slides using Mowiol. Bleed through of secondary antibodies between channels was monitored by regularly staining cells with only secondary antibody.

Confocal images were acquired using an Olympus FV1000 microscope and Olympus Fluoview v1.7 software, using 488 and 543 laser excitation and a 100x oil objective (1.45 NA). Z-stacks were acquired with a step size of 0.37 µm, which were converted to maximum image intensity projections using ImageJ where indicated. The following antibody dilutions were used: rabbit monoclonal TOM20 (1:200), myc (1:2000), HSP60 (1:5000), mouse monoclonal TOM20 (1:5000), cytochrome c (1:2000), ARL2 (1:2000), and ELMOD2 (1:500).

Live-cell imaging (mito-PAGFP assay):

For MFN null experiments, cells were transfected with 2 µg mito-PAGFP, 1 µg mito-dsRed, and 3 µg of the indicated plasmid and replated onto 35 mm MatTek dishes (#P35GC-1.5-14-C) following 4 hours of transfection, as described above. For ELMOD2 null experiments, cells were transfected using the previously described PEI protocol. Cells were transfected directly onto glass bottom dishes for 24 hours with 4 µg mito-PAGFP, 2 µg of mitodsRed, and 18 µg PEI the day before imaging. At least two hours prior to imaging, the medium was changed to prewarmed DMEM with 25 mM HEPES plus 10% FBS and

without phenol red (Invitrogen #21063). Live cell imaging was performed using a Nikon A1R confocal microscope, enclosed in a temperature control chamber at 37°C, using a 100X (NA 1.49) oil objective. A circular ROI (4 μm diameter) for photoactivation was selected near the nucleus (2). Photoactivation was achieved by excitation with 405 nm laser (45% power) for six cycles for a total duration of 2.16 seconds. Images were acquired at 1024 x 1024 pixels at 0.5 frames/second during photoactivation. Images were then acquired every 10 minutes over 40 minutes. GFP and dsRed were sequentially excited with 488 and 561 laser lines. Imaging data were collected using Nikon Elements software.

Quantification of the mito-PAGFP mitochondrial fusion assay was performed as previously described (15) using FIJI. A cell was excluded from analysis if it had less than a 10-fold increase in GFP signal following photoactivation or moved from the field of view during imaging. Masks for each channel were created, and thresholding was performed using "Otsu dark" in ImageJ. The number of pixels within each mask for both GFP and dsRed was measured, and calculated as a ratio of GFP signal to dsRed signal. The difference in this ratio between 0 min. (immediately after photoactivation) and 10, 20, 30, or 40 min after photoactivation is reported as percent increase in GFP-positive mitochondria.

Gated Stimulated Emission Depletion (gSTED) microscopy:

Cells were imaged on a Leica gSTED 3X microscope using a 100X (NA 1.4) oil objective. Cells were selected based on an apparently normal mitochondrial morphology, and a range of expression for each construct was examined. Fluorophores were excited by 488 and 561 laser lines which were depleted with 592 and 660 laser lines, respectively. Z-stacks were acquired with a step size of 0.22 μm, which were converted to maximum image intensity projections using ImageJ where indicated. For each cell, a confocal image was obtained in addition to gSTED data. Images were acquired using Leica X software and deconvoluted using Huygens software. Deconvolution was carried out based on…

To quantify gSTED data, the red and green channels for each gSTED image were merged and z-stacks were converted to maximum intensity projections in ImageJ to yield a single image per cell per

condition. ImageJ's segmented line tool (line width of 5) was used to manually draw as many linear ROIs as necessary to cover all easily discernable mitochondria in the cell. Mitochondria that were clustered such that individual mitochondria could not be distinguished and out of focus mitochondria were excluded. ImageJ was then used to measure the red and green pixel intensities within these ROIs. These raw data were then used to generate plot profiles for graphical comparisons of staining periodicity, to generate scatter plots and calculate the correlation coefficient between the red and green signals (Microsoft Excel), and to measure the distance between peaks in pixel intensities (MATLAB R2018a).

Reproducibility/statistics:

Every experiment described has been independently repeated at least twice. For quantification of immunofluorescence experiments, at least 100 cells per condition were analyzed per experiment. For live-cell experiments, 10 cells were analyzed per condition. For gSTED analysis, pixel intensities were measured across a total ROI length (mitochondrial length) of at least 100 μm per cell and at least 3 cells were analyzed per condition. Error bars represent standard error of the mean (SEM).

Results

Knockout of ELMOD2 causes mitochondrial fragmentation

We previously demonstrated that knockdown of ELMOD2 using siRNAs results in mitochondrial fragmentation (1). However, knockdown via siRNA is inherently incomplete and transient. To test the effect of complete loss of ELMOD2, we generated clonal ELMOD2-null lines using CRISPR-Cas9 in immortalized mouse embryonic fibroblasts (MEFs). As described in detail under Methods, we used two different guide RNAs to generate short indels in exons encoding ELMOD2 near the N-terminus that result in frame-shifting mutations in both alleles. Screening was done by DNA sequencing. For simplicity's sake, we will refer to these lines as nulls, recognizing the possibility that a short N-terminal fragment, completely lacking the ELMO domain, may be expressed and could even exert a cellular effect. We obtained 10 ELMOD2-null lines, 1 heterozygous line (only one allele frameshifted), and 3 clonal wild-

type (WT) lines (lines that went through the CRISPR and cloning process but were found to have no mutations in the region of the ELMOD2 gene sequenced). After confirming the genotype of each of these lines via Sanger sequencing, we observed the mitochondrial morphology in these lines as well as the original WT MEF line used to generate them (hereafter referred to as the "parental WT" line) (**Fig 1**).

In all clonal WT and parental WT lines, the vast majority (average of all 4 lines = 87%) of cells have mitochondria with a tubular morphology. In these lines, only a small proportion of cells display mitochondria that appear short (average = 6%) or fragmented (average = 2%). The mitochondria in the ELMOD2 heterozygous line were similar to those observed in WT lines, with only a modest increase in the proportion of cells with short mitochondria (15%). Across the ELMOD2-null lines, mitochondrial morphology was far more variable but consistently displayed higher levels of fragmentation. Mitochondrial morphology appeared short in 14-42% of cells (average of all 10 lines = 28%) while the proportion of cells with fragmented mitochondria varied even more widely at 9-71% (average of all lines = 30%). On average, only 42% of ELMOD2-null cells showed mitochondria with a tubular morphology, down from the 87% seen in WT lines. Conversely, mitochondria were short or fragmented in 58% of ELMOD2-null lines (averages across all 10 lines), while the average proportion of WT lines with short or fragmented mitochondria was only 8%. Thus, despite this variability, there was a marked increase in the percentages of cells displaying less tubular and shorter or more fragmented mitochondria in cells lacking ELMOD2.

To confirm that the mitochondrial fragmentation observed in the ELMOD2-null lines results from the loss of ELMOD2, rather than an off-target effect(s), we re-introduced ELMOD2 into 4 of these lines (2 from each of 2 guides) by lentiviral transduction of mouse ELMOD2-myc. Expression of ELMOD2-myc resulted in a consistent reversal of the mitochondrial fragmentation with the mitochondrial morphology in transduced cells appearing very similar to those in WT cells. The proportion of cells with fragmented or short mitochondria dropped to an average of 10% and 9%, respectively, while the fraction with tubular mitochondria increased to 76%. Expression of ELMOD2-myc in the parental WT, one of the

clonal WTs, or the ELMOD2 heterozygous line had little to no effect on mitochondrial morphology. Thus, increased levels of ELMOD2 activity over that found in WT cells does not appear to alter mitochondrial morphologies, while expression of the tagged form of ELMOD2 reverses these effects of deletion on mitochondrial morphology. All together, these results are in agreement with the previously published data showing that loss of ELMOD2 leads to mitochondrial fragmentation.

Loss of ELMOD2 reduces the rate of mitochondrial fusion

The mitochondrial fragmentation observed in ELMOD2-null lines may be caused by an increase in fission, a decrease in fusion, or some combination of the two. To begin to address this, we used the strongest assay available, in which mitochondrially-targeted photoactivatable GFP (mito-PAGFP) is co-expressed with a photostable mitochondrial marker (mito-DsRed) (2). Photoactivation of a small region of interest (4μm diameter; circles in **Fig. 2A**), was followed by monitoring the spread of the activated fluor (green) over time and is expressed as the percent increase in pixels having signal from both fluors (green and red) (**Fig. 2B**).

Figure 2A shows examples of a WT line, an ELMOD2-null line, and an ELMOD2-null line expressing ELMOD2-myc. By visual inspection it is clear that there is much less spread of the activated fluor in the ELMOD2-null line compared to WT 40min after photo-activation, and that this is reversed upon expression of ELMOD2-myc. To account for consistency, two WT lines, two ELMOD2-null lines, and two ELMOD2-null lines transduced with ELMOD2-myc were tested and the results were quantified and averaged together (**Fig. 2B**). This confirms that the rate of mitochondrial fusion is decreased in cells lacking ELMOD2. We carried out the same analysis on MEFs null for MFN2, which have documented defects in mitochondrial fusion as a comparison. Surprisingly, loss of ELMOD2 had a more severe effect on mitochondrial fusion than loss of MFN2 at later time points **(Fig. 2B**, 30 and 40min).

Expression of ELMOD2 partially reverses mitochondrial fragmentation in MFN1- and MFN2-null MEFs

MEFs lacking MFN1 or MFN2 typically have a fragmented mitochondrial morphology, compared to WT MEFs which display a more tubular mitochondrial morphology (3) (**Figs 3A, 4A**). We previously demonstrated that overexpression of ARL2 led to a partial reversal of this fragmented phenotype. This reversal was even more marked following expression of the dominant activating mutant ARL2[Q70L] (4). Because ELMOD2 is an ARL2 GAP that also localizes to mitochondria and loss of ELMOD2 leads to mitochondrial fragmentation (1) (**Fig 1**), we asked whether increased expression of ELMOD2 can also reverse, in whole or part, the fragmentation resulting from the loss of mitofusins.

We began testing effects of ELMOD2 over-expression using the human protein (ELMOD2-myc/his) as it had been used in our previous biochemical analyses. However, we found that human ELMOD2 contains a large percentage of rare codons (53%), compared to mouse ELMOD2 (15%), which may contribute to its low levels of expression (**Fig S1A**). The graphs display the degree of commonality (% Max) or rarity (% Min) for each codon of human or mouse ELMOD2 when expressed in mice. These results were determined using codons.org which utilizes a previously published algorithm to determine codon rarity. A direct comparison of human and mouse ELMOD2 (ELMOD2-myc/DDK) under the same promoter revealed mouse ELMOD2 achieved substantially higher expression levels than the human protein in MEFs (**Fig S1B**). We did not pursue the cause of this difference but codon bias is a reasonable explanation. Consequently, we used mouse ELMOD2 for studies involving protein (over-)expression, though note that expression of human ELMOD2 yielded very similar results.

MFN2-null MEFs were transfected with a plasmid directing expression of ELMOD2-myc/DDK or empty vector and effect(s) on mitochondrial morphology were scored after 24 hr (**Fig 3**). MFN2-null MEFs that were not transfected or transfected with the empty vector predominantly (72%) showed a fragmented mitochondrial morphology, with most of the rest (23%) having short mitochondria and only a small portion (5%) of cells having tubular mitochondria. We included expression of MFN1-myc or MFN2-myc as positive controls. Expression of either mitofusin led to a dramatic reversal of mitochondrial fragmentation, especially expression of MFN2-myc which decreased the proportion of cells

with fragmented mitochondria to 1%. The majority of the MFN2-null MEFs expressing MFN2-myc were tubular (44%) or hyperfused (40%). Although the effect of ELMOD2-myc//DDK expression was not as complete as expression of the mitofusins, the effect was still obvious. The majority of MFN2-null MEFs expressing ELMOD2-myc/DDK displayed mitochondria with a short tube morphology (53%) with a smaller percentage (14%) displaying a tubular morphology similar to the typical shape observed in WT MEFs. Only 33% of cells expressing ELMOD2-myc/DDK have fragmented mitochondria, down from 72%. We also included expression of ARL2[Q70L] for comparison. As previously reported (4), expression of ARL2[Q70L] also partially reversed the mitochondrial fragmentation phenotype in these MEFs. The rescue effect of ARL[Q70L] appears to be somewhat stronger compared to ELMOD2-myc/DDK expression. When compared to ELMOD2-myc/DDK expression, there were a lower proportion of cells with fragmented or short mitochondria (24% and 31%, respectively), a larger proportion with tubular mitochondria (37%), and even a subset with hyperfused mitochondria (9%).

All ARF-family GAPs to date also demonstrate effector functions (5) so we tested whether this holds true also for ELMOD2 and its effects on mitochondrial morphology. The ELMOD2[R167K] mutant lacks the catalytic arginine previously shown to be necessary for GAP activity (6). ELMOD2[R167K]-myc/DDK expression in MFN2 null MEFs resulted in partial reversal of mitochondrial fragmentation that was almost identical to the effects observed following expression of ELMOD2-myc/DDK (**Fig 3**). Thus, the ability of ELMOD2 to partially rescue mitochondrial morphology in MFN2-null MEFs does not depend on its GAP activity, consistent with an effector functionality.

ELMOD2-myc/DDK also partially reversed mitochondrial fragmentation in MFN1-null MEFs (**Fig 4**). Almost all MFN1-null MEFs contained fragmented mitochondria (93%). Again, expression of the mitofusins leads to the most pronounced reversal of mitochondrial fragmentation, particularly MFN1-myc expression. MFN1-null MEFs expressing MFN1-myc had predominantly tubular (54%) mitochondria and only a very small fraction were fragmented (4%). Expression of ELMOD2-myc/DDK resulted in a large fraction of cells displaying mitochondria with a short tube phenotype (59%) and a

small fraction displaying a tubular morphology (9%). These results are similar to those in MFN2-null MEFs, although there are a slightly lower number of ELMOD2-expressing MFN1-null cells with a tubular mitochondrial morphology. ARL2[Q70L] also partial reversed fragmentation in these MEFs, but to a lesser extent compared to MFN2-null MEFs. Again, results following expression of ELMOD2[R167K] were nearly identical to expression of ELMOD2-myc/DDK.

We next tested the effect of ELMOD2-myc/DDK expression in MEFs null for both MFN1 and MFN2 –hereafter termed DKO (double knock-out) MEFs. The mitochondrial morphology in these MEFs is highly fragmented under normal conditions (3). Expression of MFN1-myc or MFN2-myc was able to partially reverse this fragmentation. However, expression of ELMOD2-myc/DDK had no noticeable effect on the mitochondrial morphology of DKO MEFs. The same was true of ELMOD2[R167K]-myc/DDK expression (**Fig 5A**). These results are the same as those previously reported for ARL2 (4). Thus, like ARL2, ELMOD2 requires the presence of at least one mitofusin to mediate its effects on mitochondrial morphology. Expression of either ELMOD2-myc/DDK, ELMOD2[R167K]-myc/DDK, or ARL2[Q70L] also had no effect on the mitochondrial morphology of OPA1-null MEFs (**Fig 5B**), further supporting a specific link between ELMOD2 and mitofusins. Expression of ELMOD2-myc/DDK in WT MEFs had no evident effect on mitochondrial morphology aside from a very modest increase in the fraction of cells with short mitochondria. The same was true for ELMOD2[R167K]-myc/DDK expression in WT MEFs. This is in contrast to expression of the mitofusins or ARL2[Q70L] which results in mitochondrial hyperfusion (**Fig 5C**). This result is also consistent with ELMOD2 acting as an effector of ARL2, as it is not uncommon for an activated, regulatory GTPase to have a stronger phenotype than does over-expression of its effector.

Lipid mediated transfections can be quite toxic to cells and even potentially generate secondary effects as a consequence. Thus, we included two additional controls in our study. We made use of lentiviral expression of ELMOD2 to compare the effects of lentiviral transduction to transient transfection, and we also included an ELMOD2 paralog, ELMOD3, for comparison. We transduced WT, MFN1-null,

MFN2-null, or MFN DKO MEFs with lentivirus expressing ELMOD3-myc or ELMOD2-myc (**Fig S2**) and quantified mitochondrial morphology. The results were very similar to those obtained using transient transfection, with ELMOD2-myc expression leading to a partial rescue of mitochondrial fragmentation in MFN1-null and MFN2-null MEFs, no effect on mitochondrial morphology in DKO MEFs, and a moderate increase in the fraction of short mitochondria in WT MEFs. In marked contrast, expression of ELMOD3-myc had no noticeable effects on mitochondrial morphology in any of the MEF lines. Thus, like ARL2, loss of ELMOD2 causes mitochondrial fragmentation and its increased expression partially reverses that fragmentation resulting from the loss of either MFN, but not both.

Expression of ARL2[Q70L] does not induce mitochondrial elongation in the absence of ELMOD2

The fact that ARL2 and ELMOD2 bind to each other, uniquely in each family localize to mitochondria, and yield very similar phenotypes when decreased in MEFs or over-expressed in MNF null MEFs all strongly suggest that they are acting in a common pathway with ELMOD2 acting "downstream" of ARL2. To test this model, we used our ELMOD2-null MEFs to ask whether dominant active ARL2, ARL2[Q70L], can still cause hyperfusion of mitochondria. Eight cell lines were used in this study: two ELMOD2-null lines, one each from two different guides, two different wild type lines, one parental and the other clonal post-CRISPR, and the same four lines after transduction with lentivirus directing expression of ELMOD2-myc. Each of these lines was transiently transfected with empty pcDNA3.1 vector (negative control) or one directing expression of ARL2[Q70L].

We have previously shown that expression of ARL2[Q70L] in HeLa cells promotes hyperfusion and elongation of mitochondria as well as partial reversal of mitochondrial fragmentation in MFN-null MEFs (4). Consistent with this, we found that expression of ARL2[Q70L] in WT MEFs led to a hyperfused mitochondrial morphology in an average of 48% of cells (**Fig 6A,B**). However, in ELMOD2-null MEFs, ARL2[Q70L] expression failed to promote mitochondrial elongation or hyperfusion. In fact, the morphology of mitochondria in ELMOD2-null MEFs expressing ARL2[Q70L] are indistinguishable

from cells transfected with the empty vector, with very few mitochondria appearing hyperfused (average of both lines = 1%). The effects of expression of ARL2[Q70L] in combination with expression of ELMOD2-myc in WT MEFs was similar to ARL2[Q70L] expression alone, with an average of 35% of cells having hyperfused mitochondria, although the combination also caused a slight increase in short and fragmented mitochondria. The presence of ELMOD2-myc in ELMOD2-null cells partially restored the ability of ARL2[Q70L] to promote mitochondrial elongation in these lines (average 31% hyperfused) although the combination, again, caused a slight increase in the proportion of cells with short (average 14%) and fragmented (average 16%) mitochondria compared to empty vector. These results show that the presence of ELMOD2 is necessary for ARL2[Q70L] to promote mitochondrial fusion, strongly suggesting that ELMOD2 is acting downstream of ARL2.

Negative control results were essentially identical to the results displayed in Figure 1 (**Fig 6A,C**). WT MEFs had predominantly tubular mitochondria (average 87%) while the mitochondria of ELMOD2-null MEFs were mostly short (average 38%) or fragmented (average 39%) with only an average of 24% appearing tubular. Transduction of ELMOD2-myc had little effect on mitochondrial morphology in WT MEFs, but increased the proportion of tubular mitochondria (average 74%) in ELMOD2-null MEFs, close to the proportion seen in WT cells.

Expression of ELMOD2 increases the rate of mitochondrial fusion in MFN2-null MEFs

As shown above (**Fig. 3, 4**), expression of ELMOD2-myc/DDK in MFN1- or MFN2-null MEFs results in elongation of mitochondria back towards morphologies seen in WT MEFs. As previously mentioned, alterations in mitochondrial morphology can be the result of changes in fission, fusion, or both. To begin to address which pathway is under regulation by ELMOD2, we tested effects of its absence on mitochondrial fusion using the previously described PAGFP assay.

ELMOD2 expression yielded a more pronounced effect in MFN2-null than in the MFN1-null MEFs so were used in this study. As is readily apparent from the images shown in **Figure 7A**, spread of

the PAGFP signal is far more extensive at 40 min post-photoactivation in MFN2-null cells expressing either ELMOD2-myc/his or ELMOD2[R167K]-myc/his. Quantification showing averages from at least 10 cells (**Fig. 7B**) confirms that ELMOD2 expression increases the rate of mitochondrial fusion and that loss of its GAP activity does not alter this effect. These results are consistent with those in Figure 3 lead us to the conclusion that ELMOD2 expression causes an increase in the rate of mitochondrial fusion, although this does not rule-out potential effects of ELMOD2 expression on mitochondrial fission. These data are also consistent with the model (see above) that ELMOD2 is acting downstream of ARL2 as it was previously shown to promote mitochondrial fusion and act from the inter-membrane space (IMS) to do so.

Attempts to quantify the localization of ELMOD2 in cultured cells have been unsuccessful

Given the similarities in actions of ELMOD2 to those of ARL2 and the model that they directly interact with each other to modulate mitochondrial fusion, we wanted to confirm the localization of ELMOD2 to the IMS, as we have done previously for ARL2. We have previously shown that ARL2 regulates mitochondrial morphology specifically from the IMS, through the use of a strong mitochondrial localization sequence (MLS), derived from Smac/Diablo, fused at the N-terminus to drive the exogenous protein to the IMS (4). This construct was sufficient to regulate mitochondrial morphologies while an N-terminal fusion of an MLS from ornithine carbamoyltransferase (OCT) that targets to the matrix or simply adding an HA-tag at the N-terminus to keep ARL2 out of mitochondria altogether failed to alter morphologies. We attempted to use the same strategies with ELMOD2 but found that the addition of any tag at the N-terminus of ELMOD2 (including a short HA tag) resulted in poor expression, with rapid degradation of the tagged ELMOD2. In addition, the exogenous ELMOD2 constructs that could be detected did not localize properly; *i.e.*, Smac-ELMOD2 only partially localized to mitochondria. As a result, the specific site of ELMOD2's activity in relation to mitochondrial morphology remains to be determined.

Studies of ELMOD2 are also complicated by the fact that it localizes to several cellular locations including the mitochondria, lipid droplets, and the ER (1,6,7). Additionally, ELMOD2 is expressed to only low levels in every cell line or tissue examined by immunoblot, it overexpresses poorly (particularly the human form as described above), and ELMOD2 antibodies lack the sensitivity required to monitor it at such low levels. The ELMOD2 antibody used throughout this paper detects endogenous mitochondrial ELMOD2 by immunofluorescence but is typically near or below the limit of detection in immunoblots. Our ELMOD2 antibody was raised in rabbits against purified, bacterially expressed ELMOD2 and characterized in our lab. We confirmed the specificity of the mitochondrial ELMOD2 staining by antigen competition (1).

ELMOD2, ARL2, MFN1-myc, MFN2-myc, myc-Miro1, and myc-Miro2 each display periodic, punctate staining at mitochondria

In our earlier studies of ARL2 at mitochondria, we used high resolution, structured illumination microscopy (SIM) and found that ARL2 localizes to discrete puncta along mitochondria, that align with MFN1-myc and MFN2-myc. Given the extensive functional similarities between ARL2 and ELMOD2 described above, as well as previously reported (1), we tested whether ELMOD2 shares this localization pattern. We utilized gated stimulated emission depletion (gSTED) microscopy instead of SIM, as gSTED affords even greater resolving power and is less prone to artifacts that can arise due to the image reconstruction required for SIM.

Imaging of endogenous ELMOD2 in COS7 cells by gSTED revealed that ELMOD2 staining is typically found at regularly-spaced puncta (**Fig 8**). The puncta typically repeat at intervals of 0.2-0.3μm, although there is some variation, likely due to variations in mitochondrial shape. As shown in previous work, ELMOD2 is also found at ER and lipid droplets so there is substantial non-mitochondrial staining that adds to background. Thus, to focus on mitochondrial ELMOD2 staining we used double labeling with well-established mitochondrial markers (*e.g.*, HSP60, cytochrome c, TOM20) to define the organelle

boundaries and then monitored ELMOD2 specific staining that fell within that boundary. We note that in contrast to ELMOD2 or ARL2, gSTED imaging of a number of mitochondrial proteins (HSP60, cytochrome c) appear in a diffuse (non-punctate) pattern within mitochondria.

We measured the average distance between ELMOD2 puncta over a total mitochondrial length of at least 100 μm per cell in 8 cells and determined the average distance between ELMOD2 puncta to be 0.265 μm. The distance between puncta was consistent within a single cell and when comparing multiple cells (**Fig S3**). We previously reported that mitochondrial ARL2 puncta repeat at 0.4 μm intervals when viewed by SIM. This difference may be due to the imaging modalities, so we also image ARL2 in COS7. When analyzed by gSTED, the ARL2 puncta repeated at an interval of 0.248μm, almost identical to the ELMOD2 pattern (**Fig 8**). To ensure that the punctate staining pattern we observed was not an artifact of gSTED imaging or deconvolution, we collected paired confocal images with each gSTED image and compared them (**Fig S4**). Observing the example mitochondria from Figure 8 by standard confocal microscopy, the ELMOD2 and ARL2 staining is clearly punctate, although the resolution (and therefore number of puncta) is lower compared to gSTED. This indicates that gSTED imaging improves our ability to image ARL2 and ELMOD2 puncta without the introduction of artifacts.

Although a number of multi-subunit protein complexes are known to exist inside mitochondria (*e.g.*, complexes I-V, MICOS, etc.) none of the components of these have been reported to display punctate staining with spacing similar to that seen for ELMOD2 and ARL2. We used SIM to image a number of other mitochondrial proteins to identify other candidates with similar spacing and found most do not. We repeated imaging a selection of these mitochondrial proteins by gSTED (cytochrome c, HSP60, TOM20) and found that, similar to the SIM results, these proteins either appear diffuse (cytochrome c, HSP60, **Fig S5**) or have punctate staining that does not have the same spacing as ELMOD2 (TOM20, **Fig S6**). We lack good antibodies directed against several key mitochondrial proteins so in some cases we had to use exogenous, epitope tagged protein expression. COS7 cells expressing low levels of MFN1-myc or MFN2-myc were co-stained for the myc epitope and ELMOD2, and imaged by

SIM. Punctate staining of MFN-myc was similar to that of ELMOD2 so we followed up using gSTED. ELMOD2 and each mitofusin displayed a very similar punctate staining pattern and the puncta often aligned (**Fig 9**). We also tested the localization of mitochondrial phospholipase D (mitoPLD), an outer mitochondrial membrane (OMM) protein involved in regulation of mitochondrial fusion, by expressing mitoPLD-GFP in COS7 cells. The mitoPLD-GFP signal was clearly punctate; however, there was no consistent overlap between mitoPLD-GFP puncta and ELMOD2 puncta (**Fig S6**).

To test whether the change from SIM to gSTED alters the previously observed association between ARL2 and the mitofusins, we transfected COS7 cells with MFN1-myc or MFN2-myc, co-stained for myc and ARL2, and imaged cells by gSTED. In both instances, there was fairly consistent overlap between the ARL2 and myc signals (**Fig S7**). Again, there is variation due to the curvature and thickness of the mitochondria, overlapping mitochondria, and non-mitochondrial ARL2 staining.

We also found two more examples of mitochondrial proteins that do share a similar staining pattern with ARL2, ELMOD2, and the mitofusins - Miro1 and Miro2. We transfected COS7 cells with myc-Miro1 or myc-Miro2, co-stained for myc and ELMOD2, and imaged the cells by gSTED. Much like the mitofusin results, the myc-Miro1 and myc-Miro2 signals showed regularly-spaced punctate staining which consistently aligned with ELMOD2 signal at mitochondria (**Fig 10**).

To quantify the apparent alignment of ARL2, ELMOD2, the mitofusins, and the miros, we measured the correlation coefficient between the green and red pixel intensities for every co-staining condition tested. Because ARL2 and ELMOD2 stain other cellular locations besides the mitochondria, we manually drew ROIs over all of the easily discernable mitochondria in the cells and limited analysis to this area. At least three cells were analyzed per condition. The average correlation coefficients between ELMOD2 and the negative controls were 0.007 (cytochrome c), -0.117 (HSP60), and 0.042 (TOM20) (**Fig S8**). The average correlation coefficient between ELMOD2 and mitoPLD-GFP, another protein that did not obviously align with ELMOD2 was 0.063 (**Fig S8**).These results show that there is no correlation

between the staining patterns in these samples and are consistent with the lack of alignment between ELMOD2 and these proteins. The correlation coefficients between the ELMOD2 and MFN-myc signals at mitochondria were 0.225 for MFN1-myc and 0.181 for MFN2-myc, noticeably higher than negative controls (**Fig S9**).The correlation coefficients between ARL2 and mitofusin puncta were 0.200 for MFN1-myc and 0.209 for MFN2-myc, both similar to the correlation between ELMOD2 and the mitofusin puncta and higher than negative controls (**Fig S9**). Finally, the correlation coefficient between ELMOD2 and the miros was 0.205 for myc-Miro1 and 0.235 for myc-Miro2, comparable to the correlations observed between ELMOD2, ARL2, and the mitofusins (**Fig S9**).

Discussion

We show that loss or overexpression of ELMOD2 has obvious effects on mitochondrial morphology. Loss of ELMOD2 via CRISPR knock-out leads to mitochondrial fragmentation (**Fig 1**) while overexpression of ELMOD2 reverses fragmentation in MFN1- or MFN2-null MEFs (**Figs 3, 4**). Furthermore, we provide evidence that these changes in mitochondrial morphology are at least partially a result of ELMOD2 regulating the rate of mitochondrial fusion – loss of ELMOD2 decreases the rate of fusion and vice versa for ELMOD2 overexpression (**Figs 2, 7**). Additionally, expression of ELMOD2[R167K] is equally capable of reversing mitochondrial fragmentation, suggesting that ELMOD2 does not require GAP activity to promote fusion (**Figs 3, 4, 7**). We also show that ARL2 cannot promote mitochondrial fusion without ELMOD2, placing ARL2 and ELMOD2 in the same pathway (**Fig 6**). Finally, we show by gSTED imaging that ELMOD2, ARL2, the mitofusins, and the miros localize to periodically-spaced puncta along mitochondria, distinct from the staining pattern of other mitochondrial proteins (**Figs 8-10**).

We have previously reported that loss of ELMOD2 via siRNA results in mitochondrial fragmentation (14). However, siRNA is inherently incomplete. In order to more completely remove ELMOD2, we knocked-out ELMOD2 using CRISPR-Cas9. MEFs lacking ELMOD2, displayed

fragmented mitochondria similar to our findings with siRNA (**Fig 1**). Additionally, we controlled for off-target effects by generating multiple clonal lines from multiple guides to ensure that that phenotype was consistent and by reversing the phenotype through expression of ELMOD2. Not only are these results in agreement with the siRNA data, but we've also shown that at least one cause of the mitochondrial fragmentation is a decrease in mitochondrial fusion (**Fig 2**). Altogether, these data suggest that ELMOD2 promotes mitochondrial fusion as loss of ELMOD2 results in a decrease in fusion and fragmentation.

Conversely, expression of ELMOD2 reverses mitochondrial fragmentation in MFN1- or MFN2-null MEFs and increases the rate of mitochondrial fusion (**Figs 3, 4, 7**). These results are in agreement with ELMOD2 promoting mitochondrial fusion. Importantly, ELMOD2 expression is *unable* to reverse mitochondrial fragmentation in OPA1-null or DKO MEFs (**Fig 5**). This means that ELMOD2 expression is capable of partially compensating for the loss of a single mitofusin, but not OPA1 or both mitofusins. Thus, the promotion of mitochondrial fusion by ELMOD2 requires the presence of either MFN1 or MFN2, suggesting that ELMOD2 functions upstream of the mitofusins. These results are highly similar to those reported for ARL2 which was also found to reverse mitochondrial fragmentation in MFN1- or MFN2-null MEFs but not OPA1-null or DKO MEFs (15), providing more evidence that ARL2 and ELMOD2 are acting in the same pathway to promote mitochondrial fusion.

Due to the wealth of data suggesting that ARL2 and ELMOD2 act in the same pathway, we tested this using the ELMOD2-null lines. We previously demonstrated that expression of ARL2[Q70L] leads to mitochondrial elongation (15). However, expression of ARL2[Q70L] in ELMOD2-null MEFs had no effect on mitochondrial morphology (**Fig 6**). This means that ELMOD2 is necessary for ARL2 to promote mitochondrial elongation, showing that ELMOD2 is acting downstream of ARL2 to regulate mitochondrial fusion. Furthermore, the results using ELMOD2[R167K] suggest that ELMOD2 is functioning as an effector in this pathway (rather than a GAP). ELMOD2[R167K] is equally capable of reversing fragmentation and enhancing fusion compared to wild-type ELMOD2, showing that ELMOD2 does not require GAP activity to promote mitochondrial fusion (**Figs 3, 4, 7**). This is not unusual, as all

other ARF family GAPs have been found to have effector functions (16). This is also consistent with the similarities in phenotypes between ARL2 and ELMOD2. If ELMOD2 were acting as a GAP, its loss would be predicted to lead to more active ARL2 (mitochondrial elongation) and its overexpression would be predicted to cause less active ARL2 (mitochondrial fragmentation), while, in fact, the opposite is true.

ELMOD2 and ARL2 are likely functioning as regulators of mitochondrial fusion. The fragmentation phenotype in the ELMOD2-null lines, while always more fragmented compared to WT MEFs, is variable, likely due to variations across different clonal lines (**Fig 1**). However, in all ELMOD2-null lines, the fragmentation phenotype is not as severe as phenotypes observed in MEFs lacking the key components of mitochondrial fusion (MFN1, MFN2, and OPA1 (**Figs 3-5**)). Similarly, ARL2 siRNA or expression of the dominant negative mutant ARL2[T30N], results in obvious mitochondrial fragmentation but not to the same degree as mitofusin or OPA1 loss (14). Notably, overexpression of ELMOD2 has no effect on the mitochondrial morphology of WT MEFs and overexpression of wild-type ARL2 also does not alter mitochondrial morphology in cells without fusion defects (14,15) (**Fig 5**). ARL2 expression only results in mitochondrial hyperfusion when it is constitutively active (ARL2[Q70L]) (15). Even in MFN1- and MFN2-null MEFs, expression of ELMOD2 or ARL2 results in an obvious, but partial reversal of mitochondrial fragmentation (**Figs 3, 4**). These data are evidence that ARL2 and ELMOD2 are likely not key proteins required for mitochondrial fusion but rather regulators which enhance this process.

The gSTED data show that ELMOD2, ARL2, the mitofusins, and the miros localize to puncta at mitochondria (**Figs 8-10**). These puncta have a periodicity unique to these proteins, repeating at an interval of 0.2-0.3 μm. We tested the localization of several known mitochondrial proteins with both soluble (HSP60, cytochrome c) and punctate (TOM20, mitoPLD) staining but none of these proteins shared the same spacing as ELMOD2 (**Figs S5, S6**). So, this staining is specific to ARL2, ELMOD2, the mitofusins, and the miros. We have previously suggested that ARL2 and the mitofusins could be part of a complex important for mitochondrial fusion (15). The data described here more accurately define to

spacing of these potential complexes and expand the number of proteins involved to include ELMOD2 and the miros. Because ELMOD2 interacts with ARL2, it follows that ARL2 and ELMOD2 are in the same complex. ARL2/ELMOD2 may then either directly or indirectly interact with the mitofusins and miros. Interestingly, mitoPLD, a regulator of mitochondrial fusion, does not appear to localize to this complex. This may be because mitoPLD promotes fusion by hydrolysis of cardiolipin to phosphatidic acid rather than through protein-protein interactions (31).

MFN1 and 2 are central to OMM fusion while Miro1 and 2 are essential for mitochondrial motility (4,5,32). Mitochondria must come in contact with each other in order to fuse, so motility necessarily precedes fusion; however, there are no established pathways connecting mitochondrial motility and fusion. The fact that both mitofusins and miros localize to the same puncta along mitochondria suggests such a link although more work is needed to confirm this. In addition, we have previously shown that ARL2[T30N] expression, ARL2 siRNA, or ELMOD2 siRNA result in perinuclear clustering of mitochondria (14), suggesting a defect in mitochondrial motility when ARL2 or ELMOD2 activity is lost.

Currently, there are few known regulators of mitochondrial fusion. Those that have been described typically act specifically on either MFN1 (such as MIB (33)) or MFN2 (Bax (34) and SMAD2 (35)). It appears that ARL2 and ELMOD2 are capable of acting through either mitofusin as expression of either partially reverses mitochondrial fragmentation in both MFN1- and MFN2-null MEFs. For both ARL2 and ELMOD2, the rescue is more pronounced in the MFN2-null MEFs but it is unclear whether this is due to a preferential activation of MFN1 or the fact that MFN1-null MEFs have a more severe fragmentation phenotype to begin with. ARL2 and ELMOD2 accumulate at mitochondria in MFN2-null but not MFN1-null MEFs (20), suggesting that ARL2 and ELMOD2 may behave, or at least localize, differently depending upon which mitofusin is lost.

Finally, all known regulators of mitochondrial fusion act from the cytosolic face of the mitochondria. However, we previously demonstrated that ARL2's regulation of mitochondrial morphology occurs specifically from the IMS (15). Although we were unable to determine ELMOD2's specific site of action, the fact that it interacts with ARL2 leads us to hypothesize that ELMOD2 is also acting from the IMS. High-resolution imaging is also in agreement with ELMOD2 localizing inside mitochondria. This localization is significant because it places ARL2 and ELMOD2 in a unique position between the OMM and IMM. In order for complete fusion to occur, fusion of the OMM and IMM must take place, thus, these processes must be coordinated. In yeast, the protein responsible for this coordination is Ugo1 (36). However, a protein(s) with a comparable function has not been identified in metazoan cells. The localization of ARL2 and ELMOD2 in the IMS places them in a position where it's possible for them to participate in crosstalk between the OMM and IMM.

In summary, we show that ELMOD2 promotes mitochondrial fusion and that its GAP activity is dispensable for this function. We also demonstrate that ELMOD2 acts downstream of ARL2 and upstream of the mitofusins. Additionally, we describe the unique staining pattern of ELMOD2, ARL2, the mitofusins, and the miros at mitochondria, suggestive of a possible complex involved in mitochondrial fusion. These findings demonstrate a novel mode of mitochondrial fusion regulation, expanding our understanding of mitochondrial morphology.

Acknowledgements

This work was supported by the NIH grant GM122568. The authors thank a number of colleagues for their gifts of key reagents used in these studies, including: Drs. David Chan (California Institute of Technology; Mfn-null MEFs, mitofusin plasmids), Pontus Aspenstrom (Karolinska Institute; miro plasmids), Michael Frohman (Stony Brook University; mitoPLD-GFP plasmid), Richard Youle (NIH; mito-PAGFP plasmid), and James Zheng (Emory University; mito-dsRed plasmid). This research project was supported in part by the Emory University Integrated Cellular Imaging Microscopy Core of the

Emory Neuroscience NINDS Core Facilities grant, 5P30NS055077. We thank Dr. Neil Anthony (Emory University) for assistance with image quantification as well as Christopher Ott, Geoff Daniels, and Dr. Gary Schools (Leica Microsystems Inc.) for assistance with acquisition of gSTED images.

References

1. Campello, S., and Scorrano, L. (2010) Mitochondrial shape changes: orchestrating cell pathophysiology. *EMBO reports* **11**, 678-684

2. Chen, H., Detmer, S. A., Ewald, A. J., Griffin, E. E., Fraser, S. E., and Chan, D. C. (2003) Mitofusins Mfn1 and Mfn2 coordinately regulate mitochondrial fusion and are essential for embryonic development. *The Journal of cell biology* **160**, 189-200

3. Eura, Y. (2003) Two Mitofusin Proteins, Mammalian Homologues of FZO, with Distinct Functions Are Both Required for Mitochondrial Fusion. *Journal of Biochemistry* **134**, 333-344

4. Koshiba, T., Detmer, S. A., Kaiser, J. T., Chen, H., McCaffery, J. M., and Chan, D. C. (2004) Structural basis of mitochondrial tethering by mitofusin complexes. *Science* **305**, 858-862

5. Rojo, M., Legros, F., Chateau, D., and Lombes, A. (2002) Membrane topology and mitochondrial targeting of mitofusins, ubiquitous mammalian homologs of the transmembrane GTPase Fzo. *Journal of cell science* **115**, 1663-1674

6. Zanna, C., Ghelli, A., Porcelli, A. M., Karbowski, M., Youle, R. J., Schimpf, S., Wissinger, B., Pinti, M., Cossarizza, A., Vidoni, S., Valentino, M. L., Rugolo, M., and Carelli, V. (2008) OPA1 mutations associated with dominant optic atrophy impair oxidative phosphorylation and mitochondrial fusion. *Brain* **131**, 352-367

7. Smirnova, E., Griparic, L., Shurland, D. L., and van der Bliek, A. M. (2001) Dynamin-related protein Drp1 is required for mitochondrial division in mammalian cells. *Molecular biology of the cell* **12**, 2245-2256

8. Watzlich, D., Vetter, I., Gotthardt, K., Miertzschke, M., Chen, Y. X., Wittinghofer, A., and Ismail, S. (2013) The interplay between RPGR, PDEdelta and Arl2/3 regulate the ciliary targeting of farnesylated cargo. *EMBO reports* **14**, 465-472

9. Francis, J. W., Goswami, D., Novick, S. J., Pascal, B. D., Weikum, E. R., Ortlund, E. A., Griffin, P. R., and Kahn, R. A. (2017) Nucleotide Binding to ARL2 in the TBCDARL2beta-Tubulin Complex Drives Conformational Changes in beta-Tubulin. *J Mol Biol* **429**, 3696-3716

10. Francis, J. W., Newman, L. E., Cunningham, L. A., and Kahn, R. A. (2017) A Trimer Consisting of the Tubulin-specific Chaperone D (TBCD), Regulatory GTPase ARL2, and beta-Tubulin Is Required for Maintaining the Microtubule Network. *The Journal of biological chemistry* **292**, 4336-4349

11. Tian, G., Thomas, S., and Cowan, N. J. (2010) Effect of TBCD and its regulatory interactor Arl2 on tubulin and microtubule integrity. *Cytoskeleton* **67**, 706-714

12. Muromoto, R., Sekine, Y., Imoto, S., Ikeda, O., Okayama, T., Sato, N., and Matsuda, T. (2008) BART is essential for nuclear retention of STAT3. *Int Immunol* **20**, 395-403

13. Ismail, S. A., Chen, Y. X., Rusinova, A., Chandra, A., Bierbaum, M., Gremer, L., Triola, G., Waldmann, H., Bastiaens, P. I., and Wittinghofer, A. (2011) Arl2-GTP and Arl3-GTP regulate a GDI-like transport system for farnesylated cargo. *Nature chemical biology* **7**, 942-949

14. Newman, L. E., Zhou, C. J., Mudigonda, S., Mattheyses, A. L., Paradies, E., Marobbio, C. M., and Kahn, R. A. (2014) The ARL2 GTPase is required for mitochondrial morphology, motility, and maintenance of ATP levels. *PloS one* **9**, e99270

15. Newman, L. E., Schiavon, C. R., Turn, R. E., and Kahn, R. A. (2017) The ARL2 GTPase regulates mitochondrial fusion from the intermembrane space. *Cellular logistics* **7**, e1340104

16. East, M. P., and Kahn, R. A. (2011) Models for the functions of Arf GAPs. *Semin Cell Dev Biol* **22**, 3-9

17. Bowzard, J. B., Cheng, D., Peng, J., and Kahn, R. A. (2007) ELMOD2 is an Arl2 GTPase-activating protein that also acts on Arfs. *The Journal of biological chemistry* **282**, 17568-17580

18. East, M. P., Bowzard, J. B., Dacks, J. B., and Kahn, R. A. (2012) ELMO domains, evolutionary and functional characterization of a novel GTPase-activating protein (GAP) domain for Arf protein family GTPases. *The Journal of biological chemistry* **287**, 39538-39553

19. Suzuki, M., Murakami, T., Cheng, J., Kano, H., Fukata, M., and Fujimoto, T. (2015) ELMOD2 is anchored to lipid droplets by palmitoylation and regulates adipocyte triglyceride lipase recruitment. *Molecular biology of the cell* **26**, 2333-2342

20. Newman, L. E., Schiavon, C. R., Zhou, C., and Kahn, R. A. (2017) The abundance of the ARL2 GTPase and its GAP, ELMOD2, at mitochondria are modulated by the fusogenic activity of mitofusins and stressors. *PloS one* **12**, e0175164

21. Karbowski, M., Cleland, M. M., and Roelofs, B. A. (2014) Photoactivatable green fluorescent protein-based visualization and quantification of mitochondrial fusion and mitochondrial network complexity in living cells. *Methods Enzymol* **547**, 57-73

22. Clarke, T. F. t., and Clark, P. L. (2008) Rare codons cluster. *PloS one* **3**, e3412

23. Zhang, Y., Liu, X., Bai, J., Tian, X., Zhao, X., Liu, W., Duan, X., Shang, W., Fan, H. Y., and Tong, C. (2016) Mitoguardin Regulates Mitochondrial Fusion through MitoPLD and Is Required for Neuronal Homeostasis. *Molecular cell* **61**, 111-124

24. Sharer, J. D., Shern, J. F., Van Valkenburgh, H., Wallace, D. C., and Kahn, R. A. (2002) ARL2 and BART enter mitochondria and bind the adenine nucleotide transporter. *Molecular biology of the cell* **13**, 71-83

25. Fransson, A., Ruusala, A., and Aspenstrom, P. (2003) Atypical Rho GTPases have roles in mitochondrial homeostasis and apoptosis. *The Journal of biological chemistry* **278**, 6495-6502

26. Huang, H., Gao, Q., Peng, X., Choi, S. Y., Sarma, K., Ren, H., Morris, A. J., and Frohman, M. A. (2011) piRNA-associated germline nuage formation and spermatogenesis require MitoPLD profusogenic mitochondrial-surface lipid signaling. *Developmental cell* **20**, 376-387

27. Karbowski, M., Arnoult, D., Chen, H., Chan, D. C., Smith, C. L., and Youle, R. J. (2004) Quantitation of mitochondrial dynamics by photolabeling of individual organelles shows that mitochondrial fusion is blocked during the Bax activation phase of apoptosis. *The Journal of cell biology* **164**, 493-499

28. Zhou, C., Cunningham, L., Marcus, A. I., Li, Y., and Kahn, R. A. (2006) Arl2 and Arl3 regulate different microtubule-dependent processes. *Molecular biology of the cell* **17**, 2476-2487

29. Song, Z., Chen, H., Fiket, M., Alexander, C., and Chan, D. C. (2007) OPA1 processing controls mitochondrial fusion and is regulated by mRNA splicing, membrane potential, and Yme1L. *The Journal of cell biology* **178**, 749-755

30. Zunino, R., Braschi, E., Xu, L., and McBride, H. M. (2009) Translocation of SenP5 from the nucleoli to the mitochondria modulates DRP1-dependent fission during mitosis. *The Journal of biological chemistry* **284**, 17783-17795

31. Choi, S. Y., Huang, P., Jenkins, G. M., Chan, D. C., Schiller, J., and Frohman, M. A. (2006) A common lipid links Mfn-mediated mitochondrial fusion and SNARE-regulated exocytosis. *Nature cell biology* **8**, 1255-1262

32. Boldogh, I. R., and Pon, L. A. (2007) Mitochondria on the move. *Trends Cell Biol* **17**, 502-510

33. Eura, Y., Ishihara, N., Oka, T., and Mihara, K. (2006) Identification of a novel protein that regulates mitochondrial fusion by modulating mitofusin (Mfn) protein function. *Journal of cell science* **119**, 4913-4925

34. Hoppins, S., Edlich, F., Cleland, M. M., Banerjee, S., McCaffery, J. M., Youle, R. J., and Nunnari, J. (2011) The soluble form of Bax regulates mitochondrial fusion via MFN2 homotypic complexes. *Molecular cell* **41**, 150-160

35. Kumar, S., Pan, C. C., Shah, N., Wheeler, S. E., Hoyt, K. R., Hempel, N., Mythreye, K., and Lee, N. Y. (2016) Activation of Mitofusin2 by Smad2-RIN1 Complex during Mitochondrial Fusion. *Molecular cell* **62**, 520-531

36. Anton, F., Fres, J. M., Schauss, A., Pinson, B., Praefcke, G. J., Langer, T., and Escobar-Henriques, M. (2011) Ugo1 and Mdm30 act sequentially during Fzo1-mediated mitochondrial outer membrane fusion. *Journal of cell science* **124**, 1126-1135

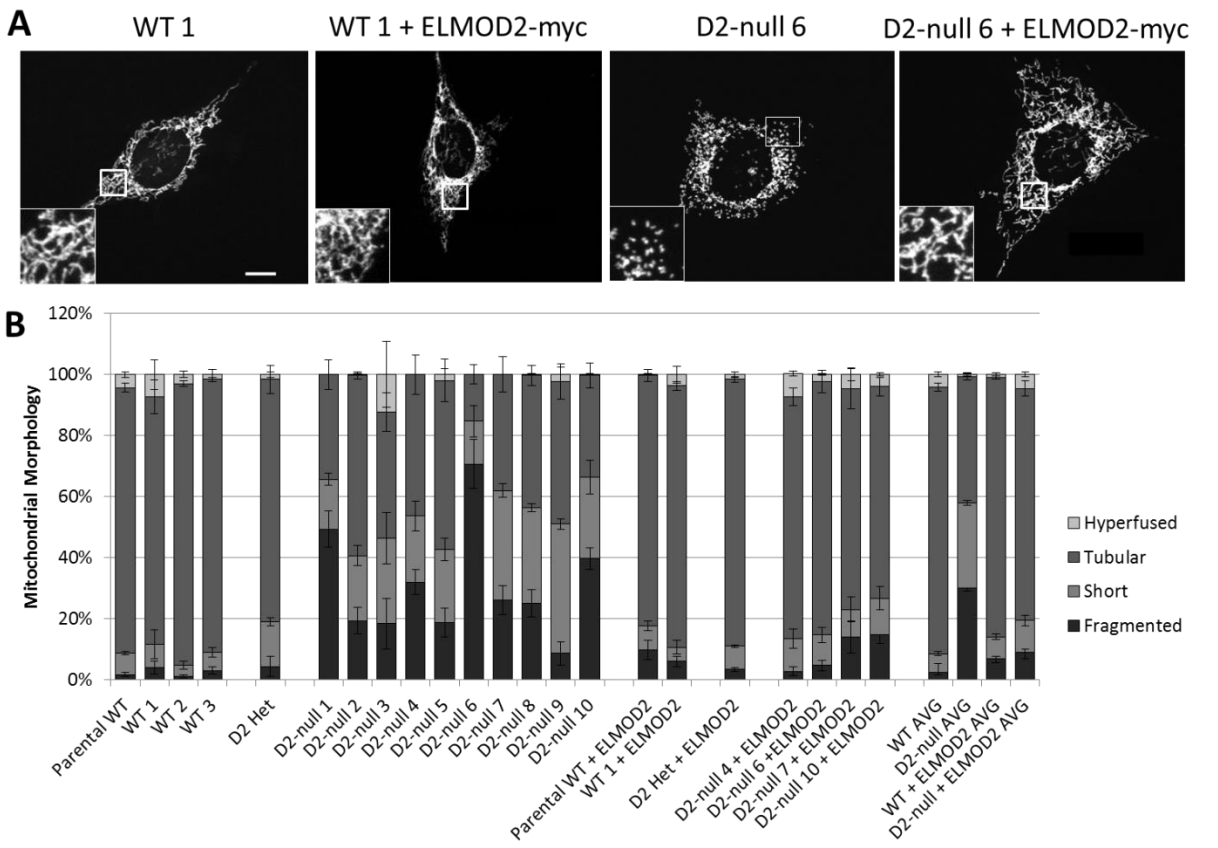

Figure 1: Knock-out of ELMOD2 causes mitochondrial fragmentation. Three clonal ELMOD2 WT, one heterozygously expressing ELMOD2, and ten ELMOD2-null MEFs were generated by CRISPR as described under Methods. The ELMOD2 het, two of the WT, and four of the ELMOD2-null lines were transduced with lentivirus expressing ELMOD2-myc also detailed under Methods (**A**) A selection of MEF lines were fixed 24 hours after plating and co-stained for myc (not shown) and HSP60. This figure shows one of the clonal ELMOD2 WT lines with and without expression of ELMOD2-myc and one of the ELMOD2-null lines also with and without expression of ELMOD2-myc. 2D projections of z-stacks are shown. Scale bar = 10 μm. (**B**) All of the cell lines generated by CRISPR were fixed and stained as described in A and scored for the presence of fragmented, short, tubular, or hyperfused mitochondria. N = 100 cells per condition. The bars in the far right section show average values across all WT MEFs, WT MEFs with ELMOD2-myc expression, ELMOD2-null MEFs, and ELMOD2-null MEFs with ELMOD2-myc expression. Error bars represent standard error of the mean (SEM) of three independent experiments.

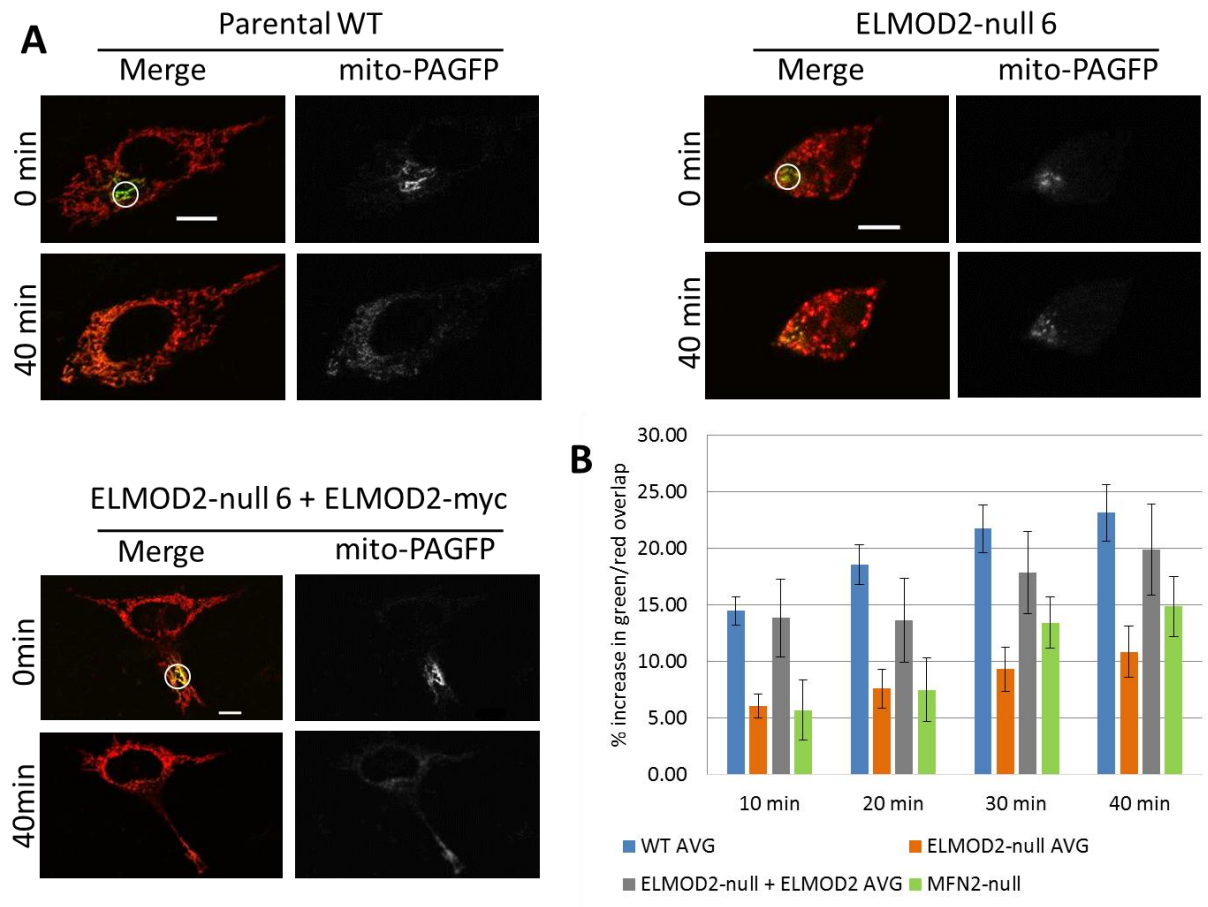

Figure 2: Loss of ELMOD2 decreases mitochondrial fusion. (**A**) Two WT lines, two ELMOD2-null lines, two ELMOD2-null lines expressing ELMOD2-myc (one of each is shown), and MFN2-null MEFs (not shown) were co-transfected with mito-dsRed and mito-PAGFP. 24hr after transfection, cells were photoactivated in the ROI shown and imaged over a period of 40min as described under Methods. Merged images of the mito-PAGFP signal (green) and mito-dsRed signal (red) are shown on the left while mito-PAGFP signal alone (gray) is shown on the right. Single z-planes are shown. Scale bar = 10 μm. (**B**) Mitochondrial fusion was indirectly quantified by calculating the increase in percentage of pixels positive for both red and green signal at each time-point. N = 10 cells per condition. Error bars represent SEM.

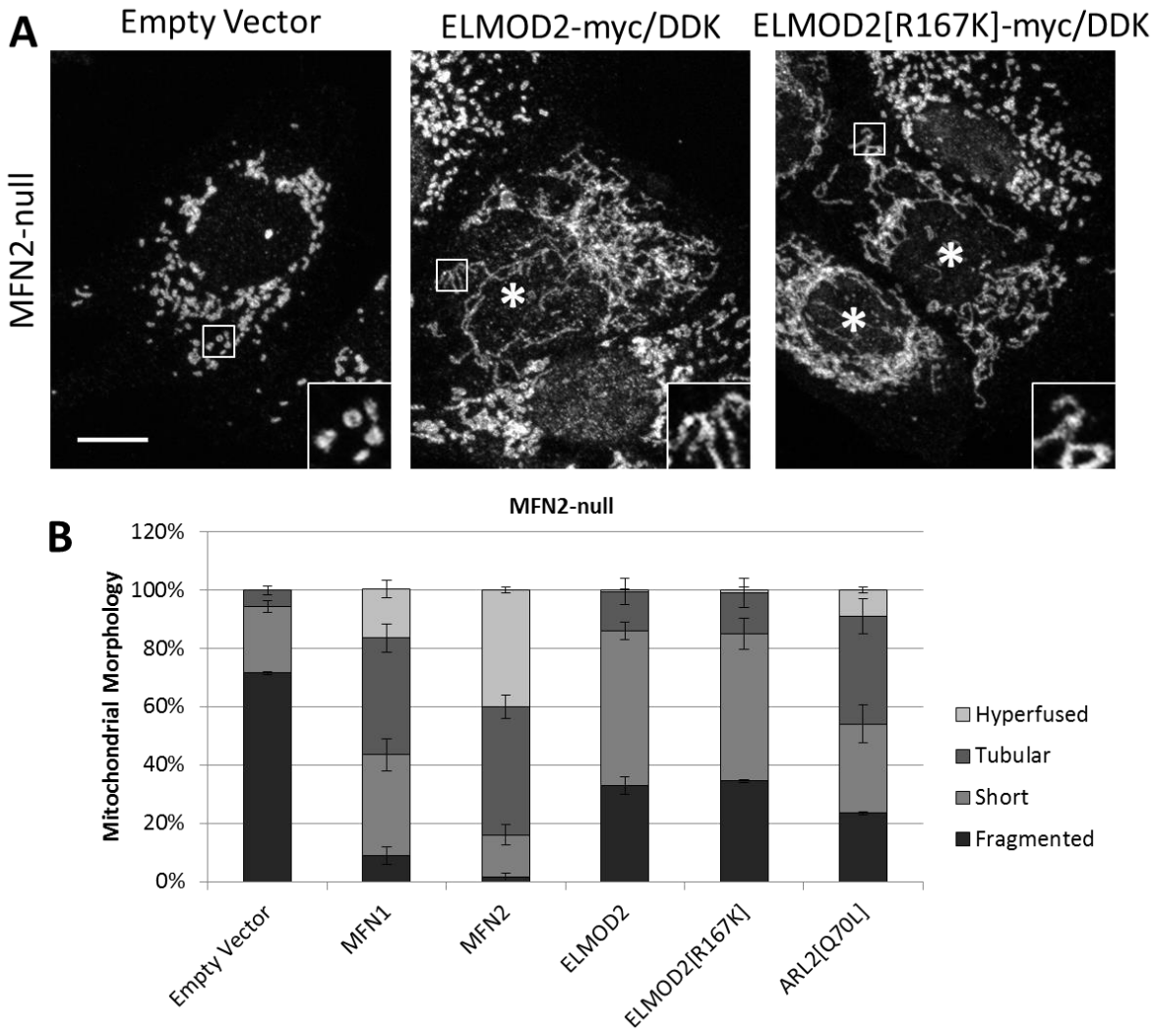

Figure 3: Expression of ELMOD2 or ELMOD2[R167K] partially reverses mitochondrial fragmentation in MFN2-null MEFs. (**A**) MFN2-null MEFs were transfected with pcDNA3.1 (empty vector, left), ELMOD2-myc/DDK (middle), or ELMOD2[R167K]-myc/DDK (right). Cells were fixed 24hr after transfection and co-stained for myc (not shown) and TOM20 as described under Methods. White asterisks indicate transfected cells. 2D projections of z-stacks are shown. Scale bar = 10 μm. (**B**) MFN2-null MEFs were transfected with pcDNA3.1, MFN1-myc, MFN2-myc, ELMOD2-myc/DDK, ELMOD2[R167K]-myc/DDK, or ARL2[Q70L] and fixed 24hr after transfection. Transfected cells were scored for the presence of fragmented, short, tubular, or hyperfused mitochondria. N=100 cells per condition. Error bars represent SEM of two independent experiments.

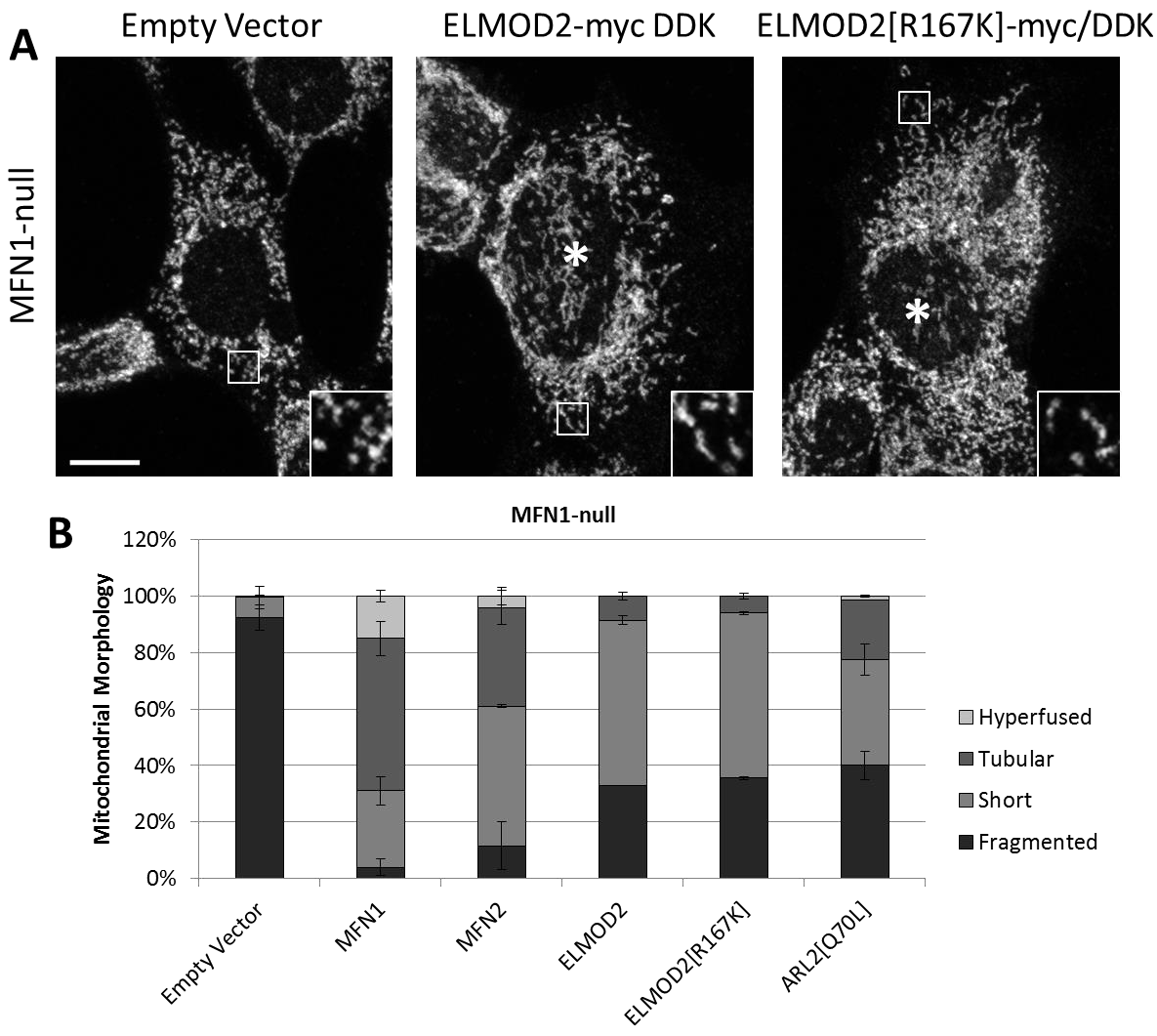

Figure 4: Expression of ELMOD2 or ELMOD2[R167K] partially reverses mitochondrial fragmentation in MFN1-null MEFs. (**A**) MFN1-null MEFs were transfected with pcDNA3.1 (empty vector, left), ELMOD2-myc/DDK (middle), or ELMOD2[R167K]-myc/DDK (right). Cells were fixed 24hr after transfection and co-stained for myc (not shown) and TOM20. White asterisks indicate transfected cells. 2D projections of z-stacks are shown. Scale bar = 10 μm. (**B**) MFN1-null MEFs were transfected with pcDNA3.1, MFN1-myc, MFN2-myc, ELMOD2-myc/DDK, ELMOD2[R167K]-myc/DDK, or ARL2[Q70L] and fixed 24hr after transfection. Transfected cells were scored for the presence of fragmented, short, tubular, or hyperfused mitochondria. N=100 cells per condition. Error bars represent SEM of two independent experiments.

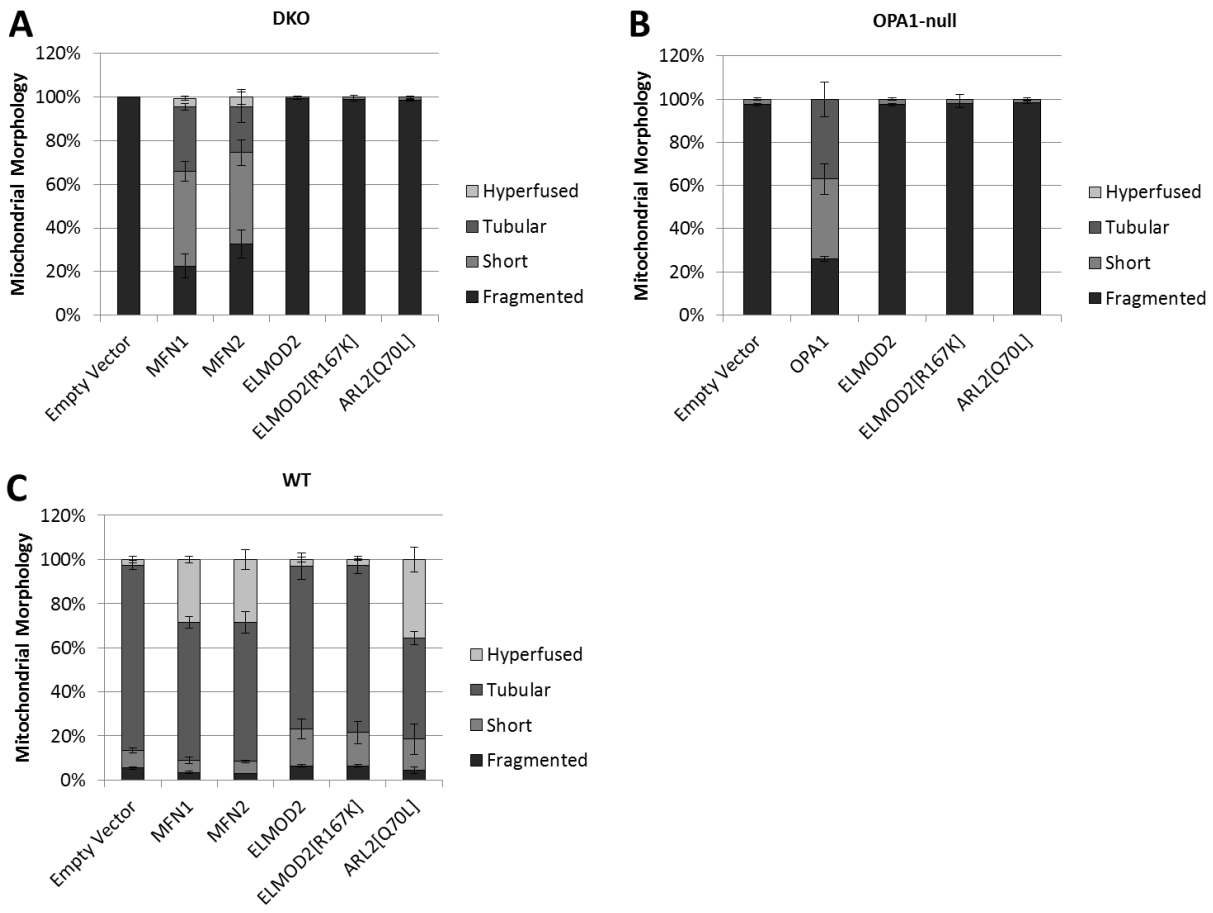

Figure 5: Expression of ELMOD2 or ELMOD2[R167K] does not affect the morphology of DKO, OPA1-null, or WT MEFs. (**A**) DKO MEFs were transfected with pcDNA3.1 (empty vector), MFN1-myc, MFN2-myc, ELMOD2-myc/DDK, ELMOD2[R167K]-myc/DDK, or ARL2[Q70L]. Cells were fixed 24hr after transfection and co-stained for myc and TOM20 or ARL2 and TOM20. Transfected cells were then scored for the presence of fragmented, short, tubular, or hyperfused mitochondria. N=100 cells per condition. Error bars represent SEM of two independent experiments. (**B**) Same as A except OPA1-null MEFs were transfected and OPA1-myc/his was used in place of MFN1-myc and MFN2-myc. (**C**) Same as A except WT MEFs were transfected.

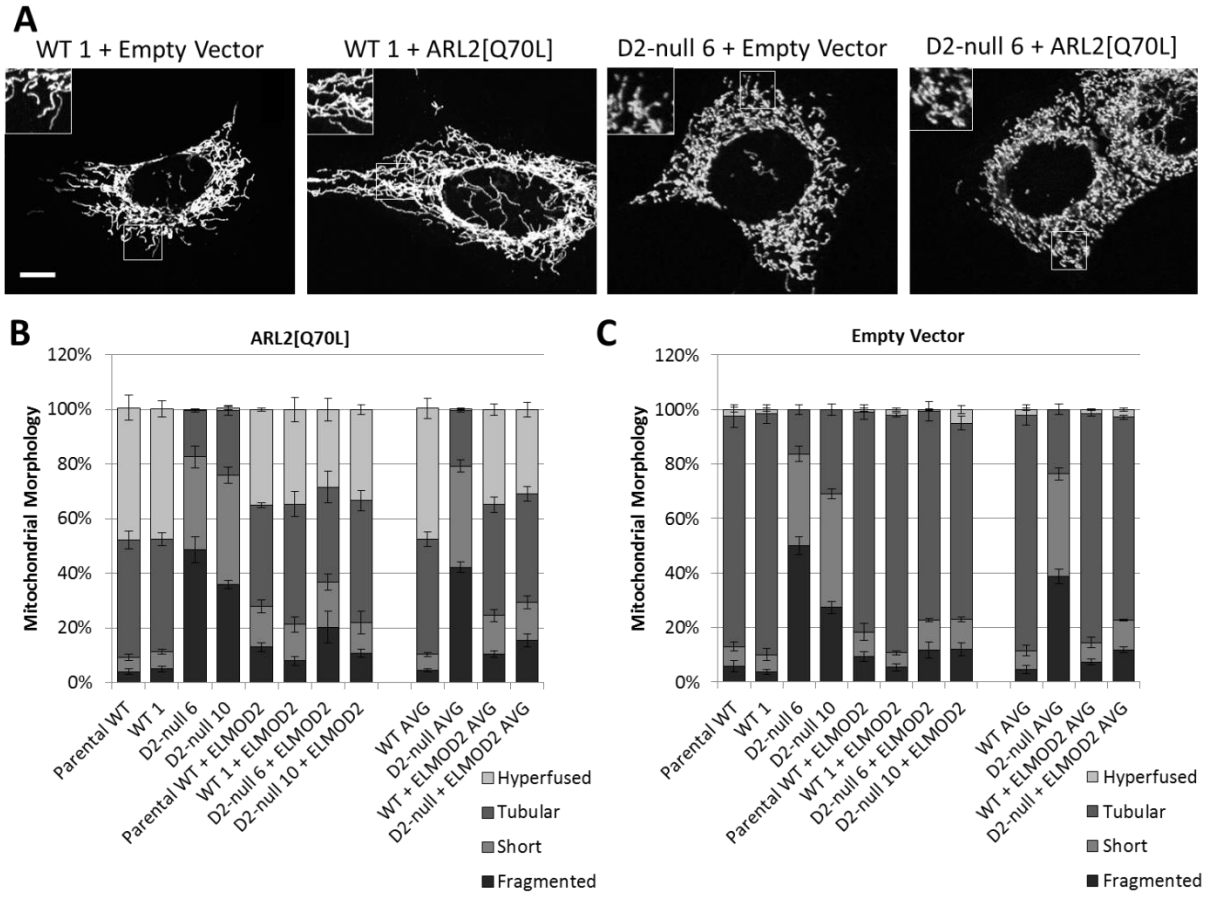

Figure 6: ARL2[Q70L] does not promote mitochondrial elongation in the absence of ELMOD2. (**A**) Selected CRISPR MEF lines were transfected with either pcDNA3.1 (empty vector) or ARL2[Q70L]. Cells were fixed 48hr after transfection and co-stained for ARL2 (not shown) or HSP60. 2D projections of z-stacks are shown. Scale bar = 10 μm. (**B**) Two WT and two ELMOD2-null MEF lines along with the same lines expressing ELMOD2-myc were transfected with pcDNA3.1 (empty vector). Cells were fixed and stained as described in A and scored for the presence of fragmented, short, tubular, or hyperfused mitochondria. N=100 cells per condition. The bars in the right section show average values across both WT MEFs, WT MEFs with ELMOD2-myc expression, ELMOD2-null MEFs, and ELMOD2-null MEFs with ELMOD2-myc expression. Error bars represent SEM of three independent experiments. (**C**) Same as B except MEFs were transfected with ARL2[Q70L].

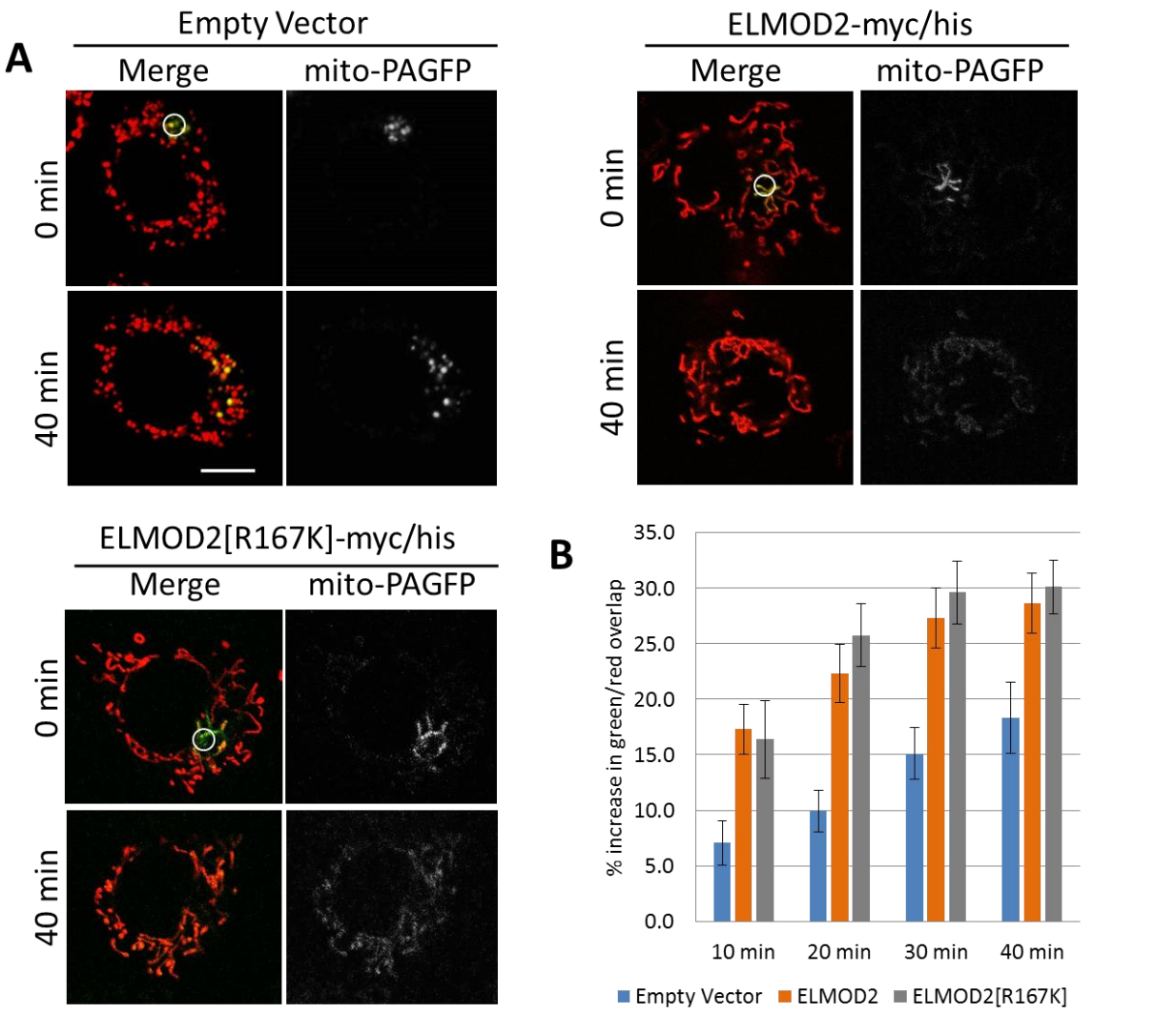

Figure 7: Expression of ELMOD2 or ELMOD2[R167K] increases mitochondrial fusion in MFN2-null MEFs. (**A**) MFN2-null MEFs were co-transfected with mito-dsRed and mito-PAGFP in combination with pcDNA3.1 (empty vector, top left), ELMOD2-myc/his (top right), or ELMOD2[R167K]-myc/his (bottom left). 24hr after transfection, cells were photoactivated in the ROI shown and imaged over a period of 40min as described under Methods. Merged images of the mito-PAGFP signal (green) and mito-dsRed signal (red) are shown on the left while mito-PAGFP signal alone (gray) is shown on the right. Single z-planes are shown. Scale bar = 10 µm. (**B**) Mitochondrial fusion was indirectly quantified by calculating the increase in percentage of pixels positive for both red and green signal at each time-point. N = 10 cells per condition. Error bars represent SEM.

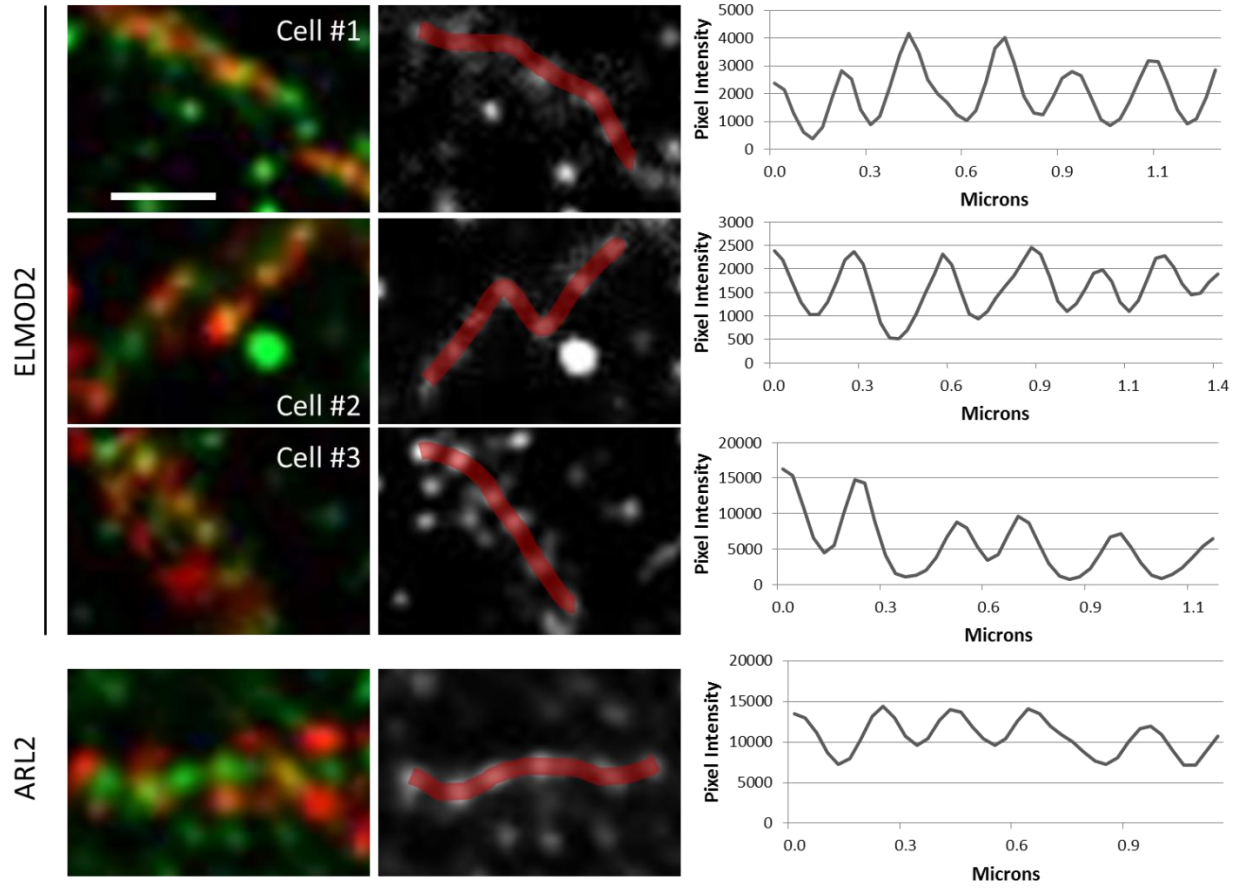

Figure 8: Mitochondrial ELMOD2 and ARL2 staining show the same periodic, punctate staining pattern when imaged by gSTED. COS7 cells were fixed and stained for ELMOD2 (top three rows) or ARL2 (bottom row) and imaged by gSTED as described under Methods. The left column shows example sections of mitochondria from four different cells co-stained for ELMOD2 or ARL2 (green) and a mitochondrial marker (red). The middle column shows line scans drawn in ImageJ over the ELMOD2 or ARL2 signal. These line scans were used to determine pixel intensities which are graphically displayed in the plot profiles in the right column. 2D projections of z-stacks are shown. Scale bar = 0.5 μm. The ELMOD2 and ARL2 signals alone are displayed in Figure S3.

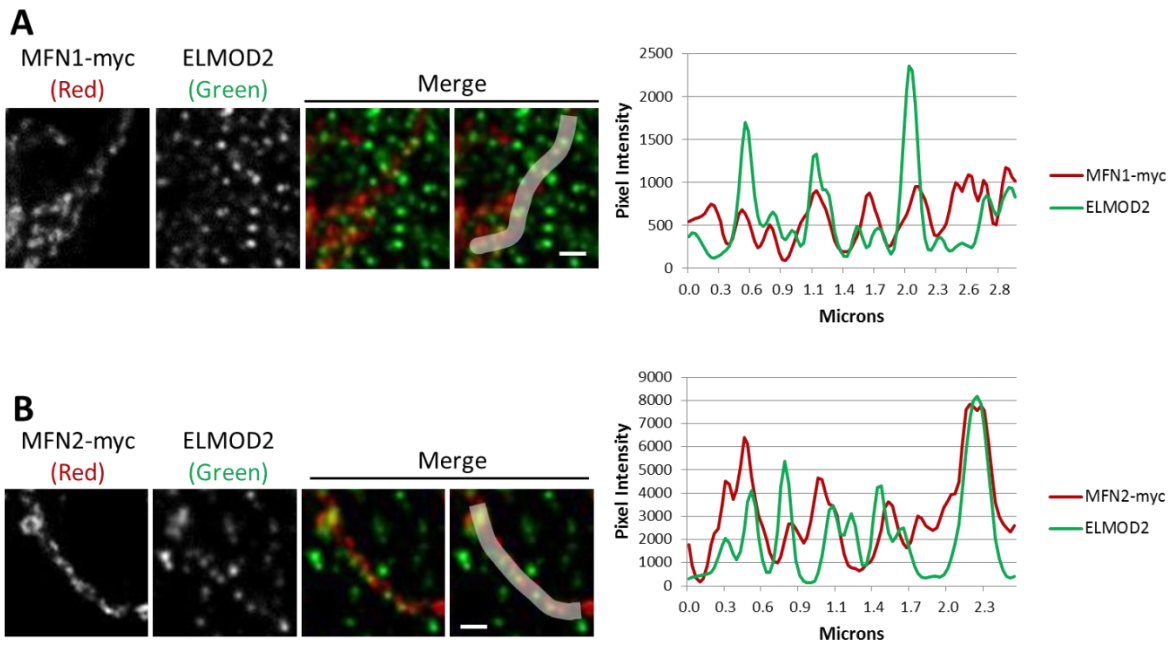

Figure 9: ELMOD2 puncta have a similar staining pattern when compared to MFN1-myc and MFN2-myc puncta at mitochondria. (**A**) COS7 cells were transfected with MFN1-myc. Cells were fixed 24hr after transfection, co-stained for myc (red) and ELMOD2 (green), and imaged by gSTED. A single mitochondrion is shown stained for myc (left), ELMOD2 (middle left), and merged (middle right). The far right image displays the merged image including the line scan drawn in ImageJ. The resulting plot profile showing pixel intensities for MFN1-myc and ELMOD2 is shown on the right. 2D projections of z-stacks are shown. Scale bar = 0.5 μm. (**B**) Same as A except cells were transfected with MFN2-myc and the plot profile shows pixel intensities for MFN2-myc and ELMOD2.

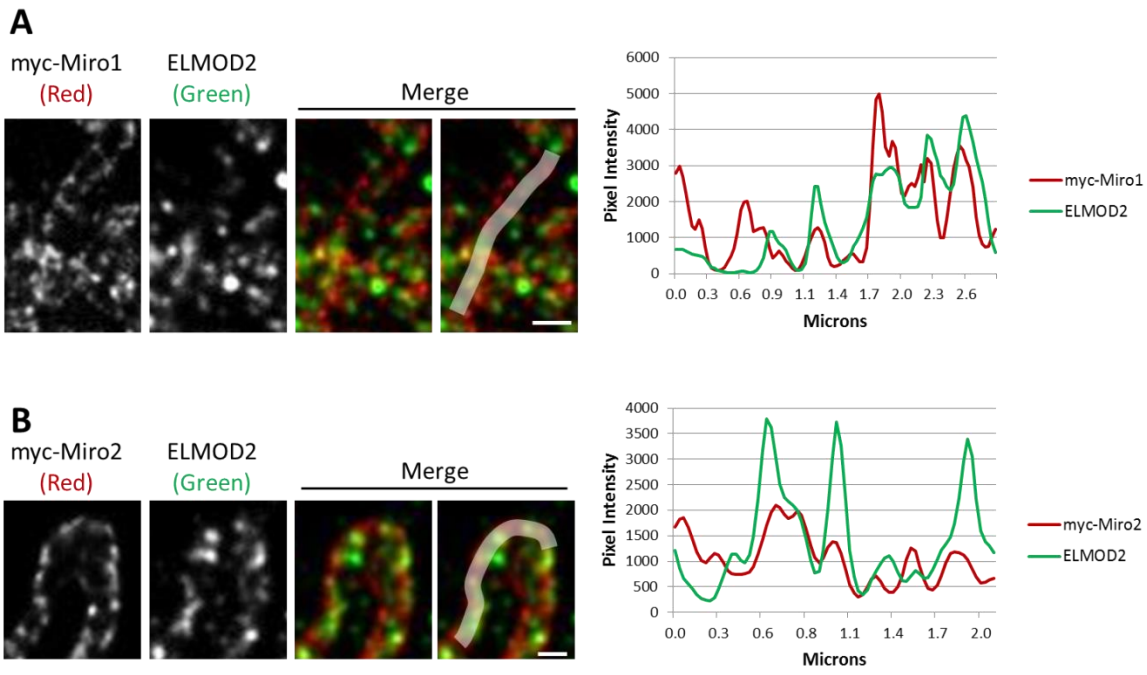

Figure 10: ELMOD2, myc-Miro1, and myc-Miro2 have similar punctate staining patterns at mitochondria. (**A**) COS7 cells were transfected with myc-Miro1. Cells were fixed 24hr after transfection, co-stained for myc (red) and ELMOD2 (green), and imaged by gSTED. A single mitochondrion is shown stained for myc (left), ELMOD2 (middle left), and merged (middle right). The far right image displays the merged image including the line scan drawn in ImageJ. 2D projections of z-stacks are shown. Scale bar = 0.5 μm. (**B**) Same as A except cells were transfected with myc-Miro2.

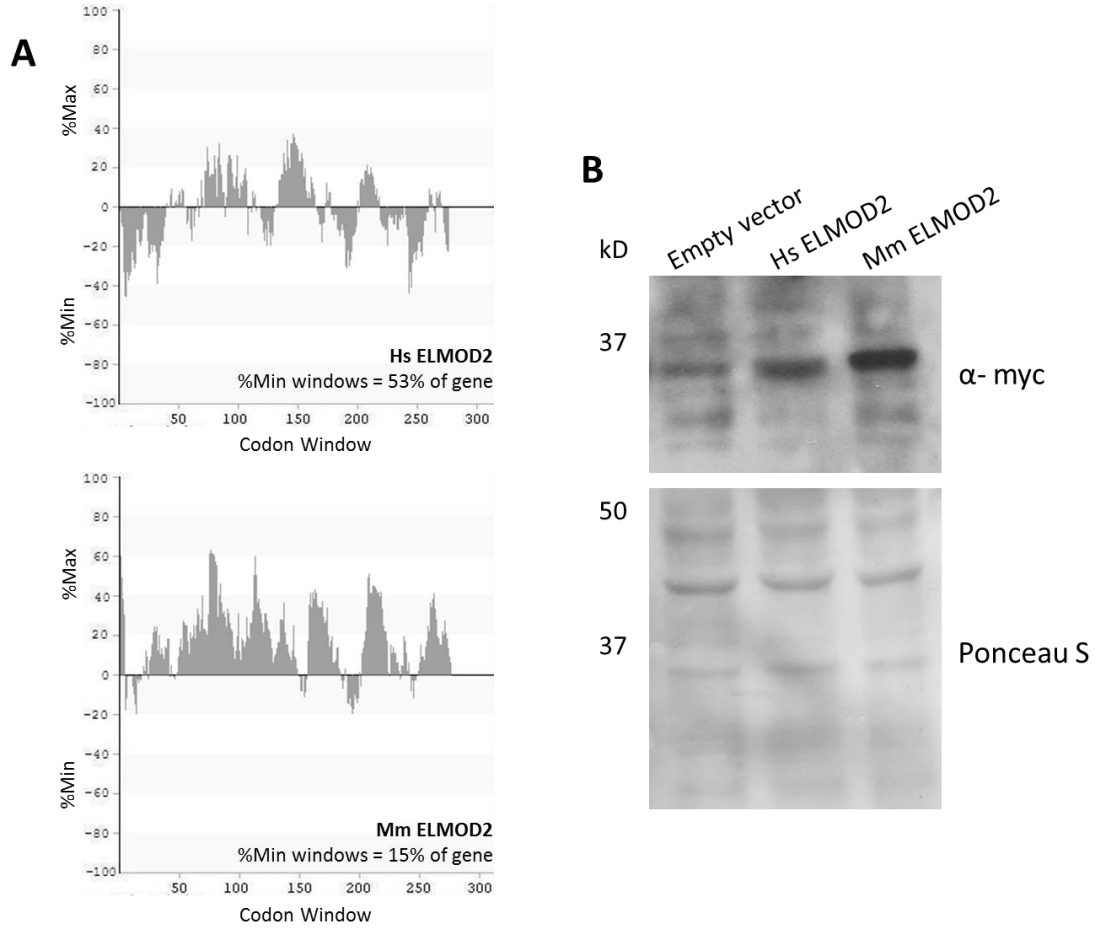

Figure S1: Mouse ELMOD2 expresses to higher levels than human ELMOD2. (**A**) The nucleotide sequences of human (top) and mouse (bottom) ELMOD2 were analyzed for rare codon usage. Analysis was carried out in the *Mus musculus* database on codons.org which utilizes a previously published algorithm. Nearly identical results were obtained using the *Homo sapiens* database. (**B**) Parental WT MEFs were transfected with empty vector (pcDNA3.1), human ELMOD2 (ELMOD2-myc/his), or mouse ELMOD2 (ELMOD2-myc/DDK). Cells were harvested and lysed 24hr after transfection. Cell lysates were separated by SDS-PAGE, transferred to nitrocellulose, and blotted for myc as described under Methods. Ponceau S staining was used to confirm equal protein loading.

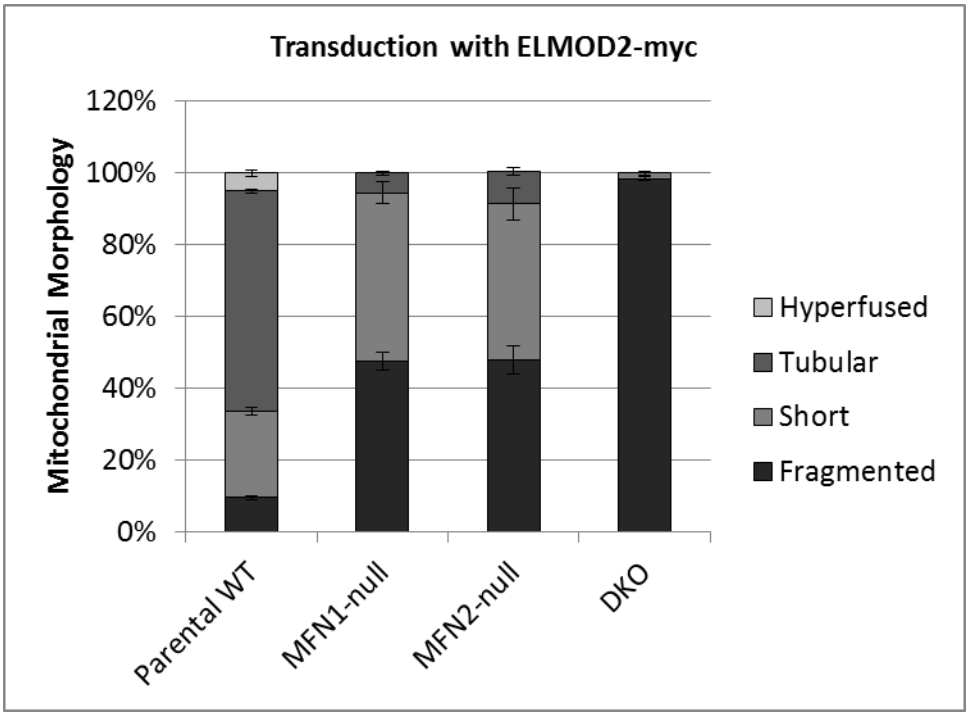

Figure S2: Lentiviral expression of ELMOD2 also partially reverses mitochondrial fragmentation in MFN1-null and MFN2-null MEFs. WT, MFN1-null, MFN2-null, or DKO MEFs were tranduced with lentivirus expressing ELMOD2-myc. Transduced cells were scored for the presence of fragmented, short, tubular, or hyperfused mitochondria. N=100 cells per condition. Error bars represent SEM of two independent experiments.

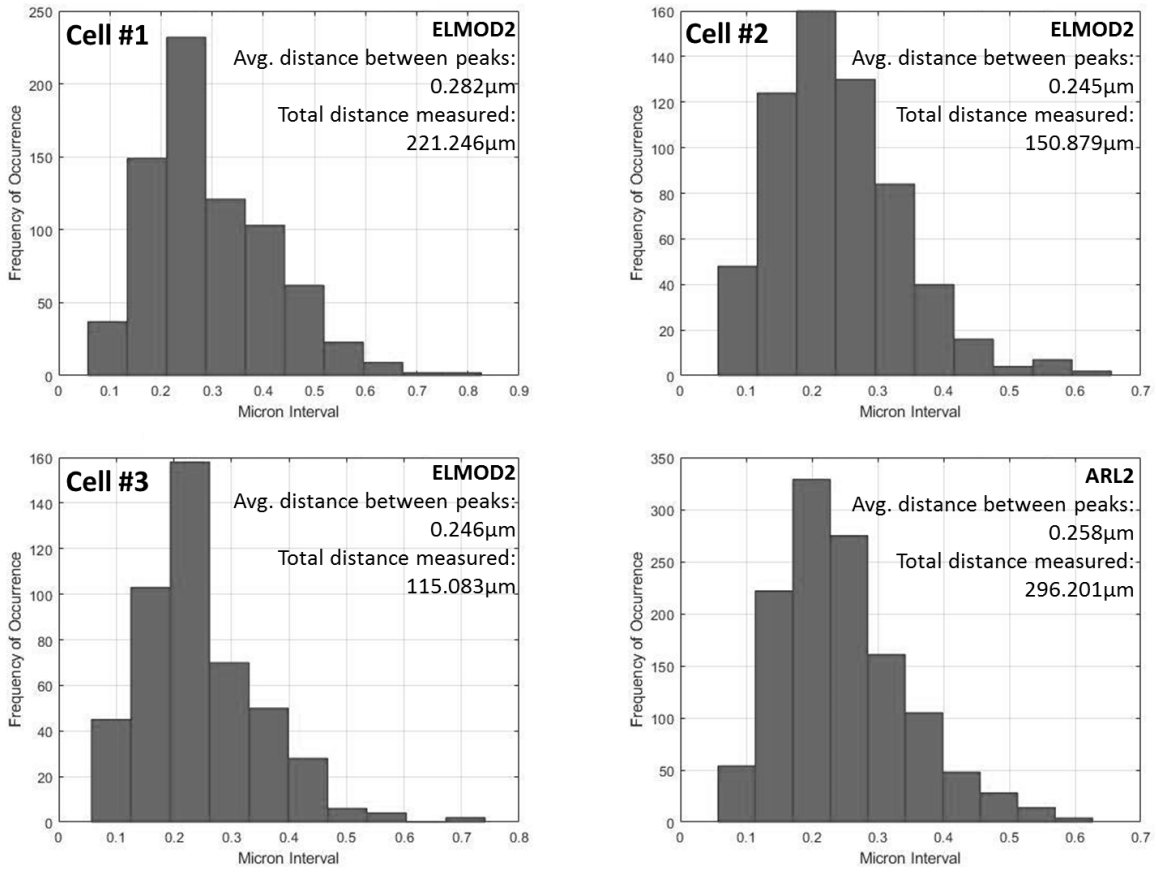

Figure S3: The periodicity of ELMOD2 and ARL2 staining at mitochondria is consistent. The pixel intensities of the ELMOD2 or ARL2 staining at mitochondria were quantified as described under Methods. These data were processed in MATLAB R2018a to determine the average distance between peaks in pixel intensity (distance between ELMOD2 or ARL2 puncta). Results for three different cells stained for ELMOD2 and one stained for ARL2 are displayed as histograms showing the frequency of each peak interval. The average distance between peaks for each cell is also displayed as well as the total ROI length (mitochondrial length) measured in each cell. The average peak distance when all cells were analyzed together was 0.265 µm for ELMOD2 (total 1344.459 µm ROI length) and 0.248 µm for ARL2 (total 450.699 µm ROI length).

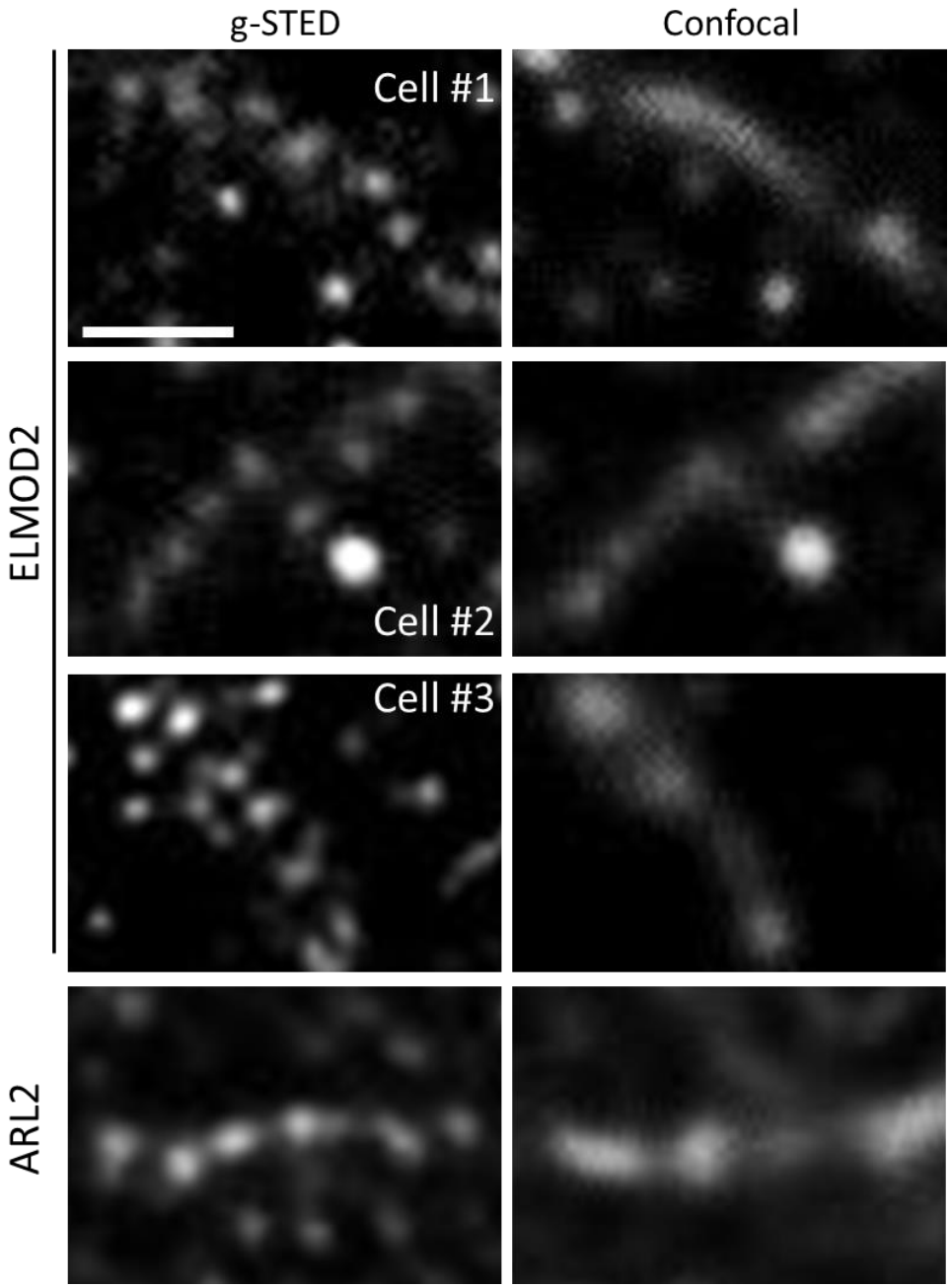

Figure S4: ELMOD2 and ARL2 puncta are less defined but still visible by confocal microscopy. The mitochondria from Figure 8 are shown when imaged by g-STED (left) and confocal (right) microscopy. Single channels are shown displaying endogenous ELMOD2 or ARL2 staining. 2D projections of z-stacks are shown. Aside from conversion to a maximum intensity projection, the confocal images were not manipulated in any way. Scale bar = 0.5 μm

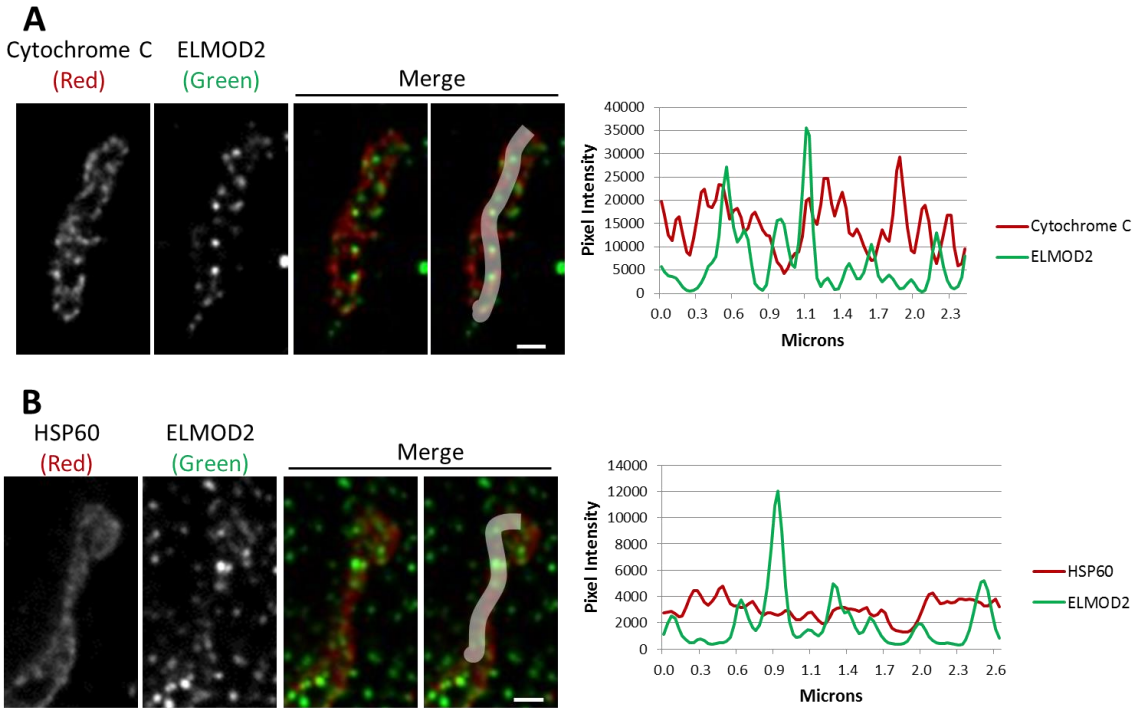

Figure S5: Cytochrome c and HSP60 do not share the same staining pattern as ELMOD2. (**A**) COS7 cells were fixed and co-stained for cytochrome c (red) and ELMOD2 (green) and imaged by gSTED. A single mitochondrion is shown stained for cytochrome c (left), ELMOD2 (middle left), and merged (middle right). The far right image displays the merged image including the line scan drawn in ImageJ. The resulting plot profile showing pixel intensities for cytochrome c and ELMOD2 is shown on the right. 2D projections of z-stacks are shown. Scale bar = 0.5 µm. (**B**) Same as A except cells were co-stained for HSP60 (red) and ELMOD2 (green) and the plot profile shows pixel intensities for HSP60 and ELMOD2.

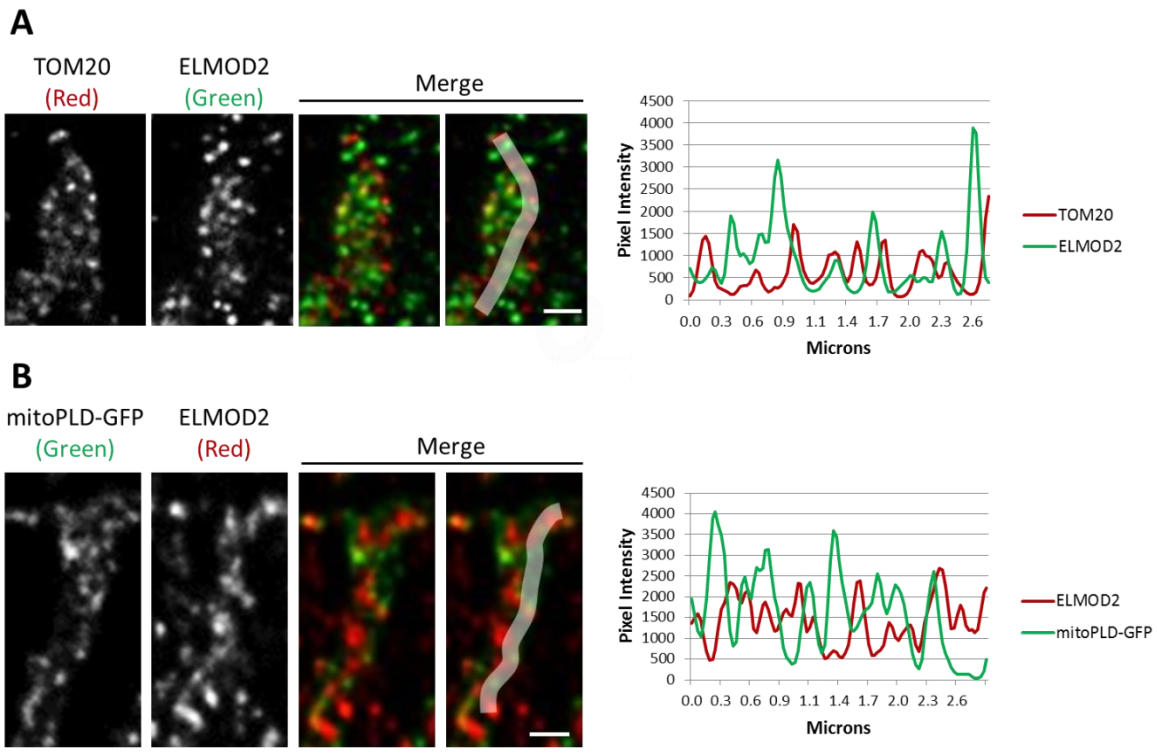

Figure S6: TOM20 and mitoPLD-GFP do not share the same staining pattern as ELMOD2. (**A**) COS7 cells were fixed and co-stained for TOM20 (red) and ELMOD2 (green) and imaged by gSTED. A single mitochondrion is shown stained for TOM20 (left), ELMOD2 (middle left), and merged (middle right). The far right image displays the merged image including the line scan drawn in ImageJ. The resulting plot profile showing pixel intensities for TOM20 and ELMOD2 is shown on the right. 2D projections of z-stacks are shown. Scale bar = 0.5 µm. (**B**) COS7 cells were transfected with mitoPLD-GFP (green). Cells were fixed 24hr after transfection, stained for ELMOD2 (red), and imaged by g-STED. A single mitochondrion is shown with mitoPLD-GFP signal (left), ELMOD2 signal (middle left), and merged (middle right). The far right image displays the merged image including the line scan drawn in ImageJ. The resulting plot profile showing pixel intensities for mitoPLD-GFP and ELMOD2 is shown on the right. 2D projections of z-stacks are shown. Scale bar = 0.5 µm.

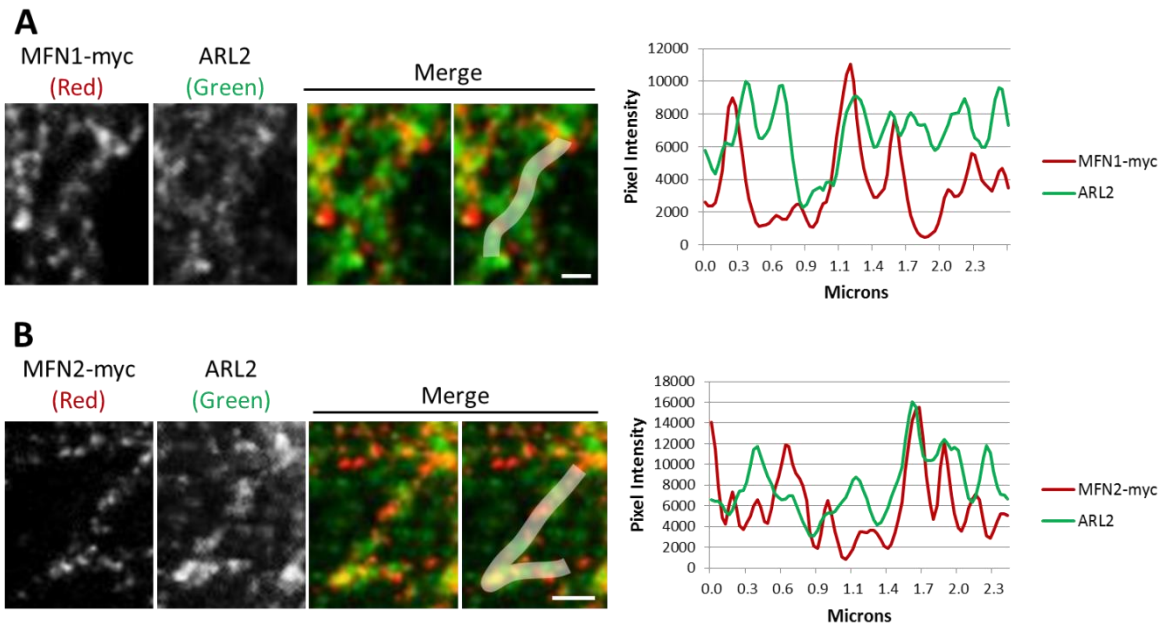

Figure S7: ARL2 puncta have a similar staining pattern when compared to MFN1-myc and MFN2-myc puncta at mitochondria. (**A**) COS7 cells were transfected with MFN1-myc. Cells were fixed 24hr after transfection, co-stained for myc (red) and ARL2 (green), and imaged by gSTED. A single mitochondrion is shown stained for myc (left), ARL22 (middle left), and merged (middle right). The far right image displays the merged image including the line scan drawn in ImageJ. The resulting plot profile showing pixel intensities for MFN1-myc and ARL2 is shown on the right. 2D projections of z-stacks are shown. Scale bar = 0.5 µm. (**B**) Same as A except cells were transfected with MFN2-myc and the plot profile shows pixel intensities for MFN2-myc and ARL2.

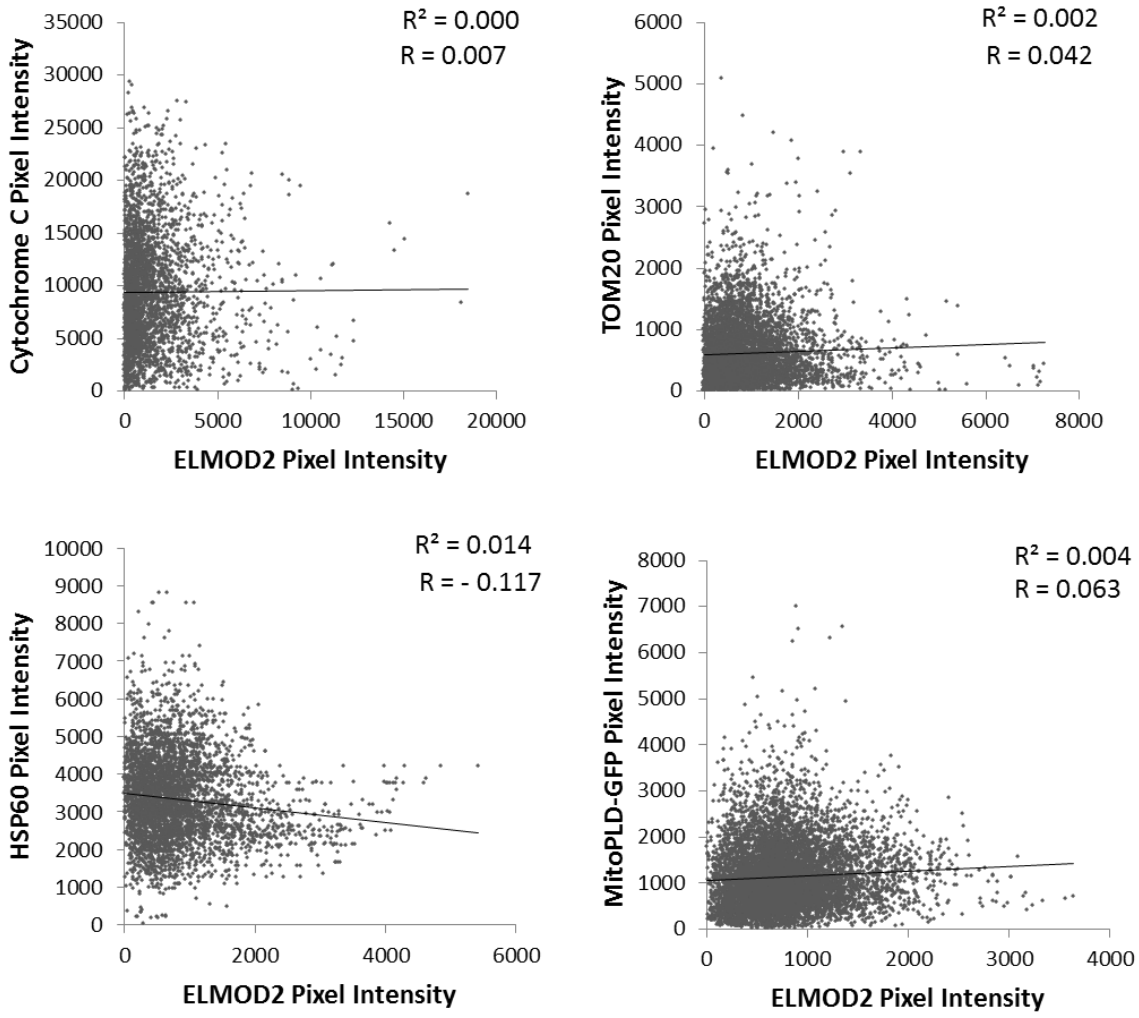

Figure S8: There is no correlation between ELMOD2 and several resident mitochondrial proteins. ROIs were drawn over mitochondria in ImageJ and pixel intensities in the green and red channels were measured as described under Methods. The correlations between the pixel intensities of the green and red channels are displayed as scatter plots for: cytochrome c+ELMOD2 (total ROI length = 507.015 μm), HSP60+ELMOD2 (345.249 μm), TOM20+ELMOD2 (452.637 μm), and mitoPLD-GFP+ELMOD2 (622.269 μm). For each of the scatter plots, the slope of the line of best fit is displayed as R^2 and the correlation coefficient is displayed as R.

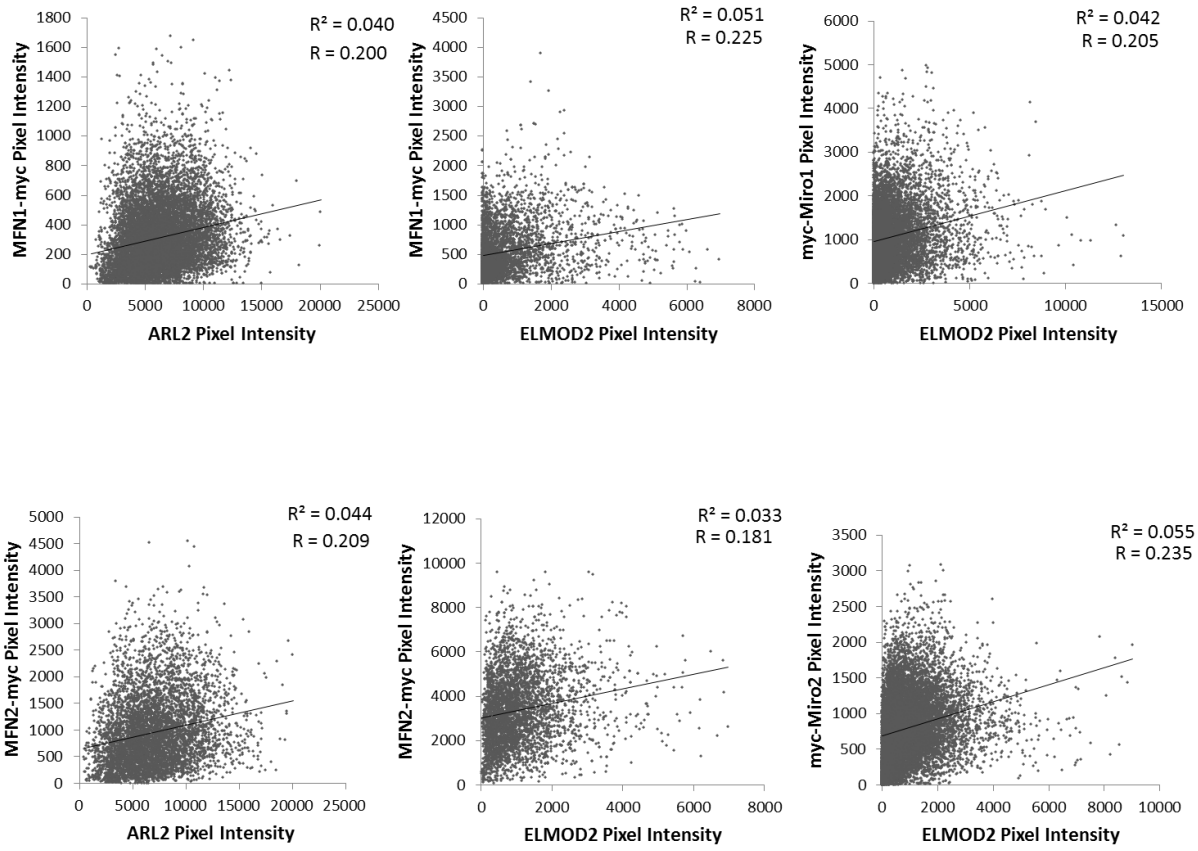

Figure S9: There is a moderate positive correlation between ELMOD2, ARL2, the mitofusins, and the miros. ROIs were drawn over mitochondria in ImageJ and pixel intensities in the green and red channels were measured as described under Methods. The correlations between the pixel intensities of the green and red channels are displayed as scatter plots for: MFN1-myc+ARL2 (total ROI length = 888.602 μm), MFN2-myc+ARL2 (463.500 μm), MFN1-myc+ELMOD2 (610.470 μm), MFN2-myc+ELMOD2 (704.008 μm), myc-Miro1+ELMOD2 (663.737 μm), and myc-Miro2+ELMOD2 (1038.740 μm). For each of the scatter plots, the slope of the line of best fit is displayed as R^2 and the correlation coefficient is displayed as R.

Chapter 5: Compositional complexity of rods and rings

This chapter was published as:

Cara R. Schiavon, Maxwell E. Griffin, Marinella Pirozzi, Raman Parashuraman, Wei Zhou, H.A. Jinnah, Daniel Reines, Richard A. Kahn. Compositional Complexity of Rods and Rings. Molecular Biology of the Cell. 2018.

Abstract

Rods and rings (RRs) are large linear- or circular-shaped structures typically described as polymers of IMPDH (inosine monophosphate dehydrogenase). They have been observed across a wide variety of cell types and species and can be induced to form by inhibitors of IMPDH. RRs are thought to play a role in the regulation of *de novo* guanine nucleotide synthesis, however, the function and regulation of RRs is poorly understood. Here we show that the regulatory GTPase, ARL2, a subset of its binding partners, and several resident proteins at the endoplasmic reticulum (ER), also localize to RRs. We also have identified two new inducers of RR formation, AICAR and glucose deprivation. We demonstrate that RRs can be disassembled if guanine nucleotides can be generated by salvage synthesis regardless of the inducer. Finally, we show that there is an ordered addition of components as RRs mature, with IMPDH first forming aggregates, followed by ARL2, and only later calnexin, a marker of the ER. These findings suggest that RRs are considerably more complex than previously thought and that the function(s) of RRs may include involvement of a regulatory GTPase, its effectors, and potentially contacts with intracellular membranes.

Introduction

The reversible formation of protein aggregates is increasingly understood to be important for a number of normal cellular processes, as well as pathological ones. Such aggregates form as a result of homo-polymerization of a single protein or they can contain much greater complexity in composition and size (Aguilera-Gomez & Rabouille, 2017). Such aggregates can be quite large and share the features of an organelle; *e.g.*, the nucleolus, Cajal bodies, P-bodies, U-bodies, eisosomes, purinosomes, G-bodies, loukomasomes, cytoophidia, and rods and rings (RRs). The functions of some complexes are known, such as assembly of ribosomes or spliceosomes at the nucleolus and Cajal bodies, respectively (Hebert & Poole, 2017; Nunez Villacis et al., 2018) or sites of RNA metabolism (P-bodies (Luo et al., 2018)), while others are less well-understood.

RRs are large, linear- or circular-shaped structures observable in a variety of mammalian cell lines under normal growth conditions and inducible in all cell lines tested (Willingham et al., 1987; Ji et al., 2006; Gunter et al., 2008; Noree et al., 2010; Ramer et al., 2010; Carcamo et al., 2011). RR induction is typically accomplished using the IMPDH (inosine monophosphate dehydrogenase) inhibitors mycophenolic acid (MPA) or ribavirin, which cause a rapid increase in the number and size of RRs (Ji et al., 2006; Carcamo et al., 2011; Thomas et al., 2012; Keppeke et al., 2016). RRs were first formally described following the observation that patients being treated for chronic hepatitis C infection with a combination of ribavirin and interferon α developed autoantibodies against structures, later named RRs (Covini et al., 2012; Keppeke et al., 2012). Such autoantibodies were found to react with IMPDH (Carcamo et al., 2011; Seelig et al., 2011), the rate-limiting enzyme in guanine nucleotide *de novo* synthesis that catalyzes the conversion of inosine monophosphate (IMP) to xanthosine monophosphate (XMP). IMPDH is by far the most commonly identified component of RRs, thus, the presence of IMPDH and induction in response to IMPDH inhibition are the hallmarks of RRs (Carcamo et al., 2014; Calise et al., 2015).

Cytoophidia are also large protein complexes linked to nucleotide metabolism and share a number of similarities with RRs (Gou et al., 2014; Aughey & Liu, 2015; Chang et al., 2015; J. L. Liu, 2016). The best established component of cytoophidia is CTP synthetase (CTPS) (Ingerson-Mahar et al., 2010; Noree et al., 2010; Carcamo et al., 2011; J. L. Liu, 2011), which catalyzes the conversion of uridine triphosphate (UTP) to cytidine triphosphate (CTP). Glutamine is a necessary cofactor in this reaction and glutamine analogs such as 6-diazo-5-oxo-L-norleucine (DON) and acivicin inhibit CTPS, leading to the formation of cytoophidia (Carcamo et al., 2011; Calise et al., 2014; Keppeke, Andrade, et al., 2015). These drugs also induce the formation of IMPDH-positive RRs (Carcamo et al., 2011; Calise et al., 2014; Keppeke, Calise, et al., 2015). Indeed, there is evidence of partial overlap between CTPS-positive and IMPDH-positive structures (Carcamo et al., 2011; Keppeke, Calise, et al., 2015) and these terms are sometimes used interchangeably. However, this overlap is not universal and IMPDH inhibitors do not

induce the formation of CTPS-positive structures (Keppeke, Calise, et al., 2015). For clarity, we will refer to IMPDH-positive structures as RRs and CTPS-positive structures as cytoophidia.

The function of RRs is unclear and even controversial. Because they are strongly induced upon inhibition of guanine nucleotide biosynthesis, a treatment expected to reduce the guanine nucleotide pool, RR formation has been thought of as a cellular response intended to increase guanine nucleotide synthesis (Carcamo et al., 2014). However, a recent study provided strong evidence that oligomerization of IMPDH does not change the enzymatic properties of the enzyme (Anthony et al., 2017). IMPDHs are abundant, soluble proteins that are normally found as tetramers (Gilbert et al., 1979) or octamers (Whitby et al., 1997). There are two isoforms of IMPDH in mammals, IMPDH1 and 2, which share 84% identity in primary sequence. Both are capable of converting IMP to XMP as well as forming homotetramers and homooctamers (Carr et al., 1993; Colby et al., 1999). Both isoforms have been reported to be present in RRs (Gunter et al., 2008).

We quite unexpectedly found strong and specific staining of RRs by a number of monoclonal antibodies to the regulatory GTPase ARL2 (ARF-like 2) (Clark et al., 1993). ARL2 is an essential and very highly conserved GTPase within the ARF superfamily, predicted to have been present in the last eukaryotic common ancestor and ubiquitous in eukaryotes (Clark et al., 1993; Li et al., 2004; Klinger et al., 2016). It localizes to several cellular locations including centrosomes (Zhou et al., 2006), the nucleus (Muromoto et al., 2008), and mitochondria (Newman et al., 2014; Newman, Schiavon, Turn, et al., 2017; Newman, Schiavon, Zhou, et al., 2017), though the clear majority is found in cytosol, as part of a heterotrimeric complex with the tubulin co-chaperone cofactor D and β-tubulin (Bhamidipati et al., 2000; Francis, Goswami, et al., 2017; Francis, Newman, et al., 2017). We have focused in recent years on defining the roles of ARL2 in tubulin biogenesis in cytosol (Francis, Goswami, et al., 2017; Francis, Newman, et al., 2017) and both mitochondrial fusion (Newman, Schiavon, Turn, et al., 2017; Newman, Schiavon, Zhou, et al., 2017) and ATP generation in mitochondria (Newman et al., 2014), though it has

also been linked to centrosome stability (Zhou et al., 2006) and transport of N-myristoylated protein cargos (Ismail et al., 2011; Watzlich et al., 2013).

Here we report a detailed characterization that extends our initial observation and leads us to the conclusion that RRs display much greater complexity in composition than suggested by the literature in this field. These results are likely to expand our understanding of the set of processes in which RRs are implicated.

Methods

Antibodies and reagents:

The following antibodies were purchased: Calnexin (Stressgen SPA-860), GRP78 (Stressgen SPA-826), SigmaR1 (Abcam AB89655), CTPS1 (Proteintech Group 15914-1-AP), Calreticulin (ThermoFisher PA-900), ELMOD3 (Sigma HPA012126), TGN46 (Abcam, AB16052), Acetylated tubulin (Sigma 6-11B-1), LC3 (Novus NB100-2220), α-tubulin (Sigma T9026), β-tubulin (Sigma T4026), and HSP60 (Stressgen ADI-SPA-807). IMPDH2 antibody was raised in rabbit against a peptide representing the FLAP region of IMPDH2 with an N-terminal cysteine appended (CDKHLSSQNRYFSEADKIK). Three mouse monoclonal ARL2 antibodies (3B4.B4, 15E11.B11, and 19F6.F11) were generated by the Emory University monoclonal antibody core facility using purified bacterially expressed human ARL2 as antigen. Rabbit polyclonal ARL2, ELMOD2, Cofactor D, ARL1, ARL3, ARF1, ARF3, ARF4, ARF6, BART, and ELMOD1, were raised against their corresponding human proteins and have been previously described (Cavenagh et al., 1996; Van Valkenburgh et al., 2001; Sharer et al., 2002; Zhou et al., 2006; Cunningham & Kahn, 2008; East et al., 2012; Newman et al., 2014). Rabbit polyclonal ARL13b antibody was provided by Dr. Tamara Caspary (Emory University). The following reagents were purchased: Mycophenolic acid (Sigma M5255), AICAR (Sigma A9978), DON (Sigma D2141), 3-Methyladenine (Sigma M9281), Bafilomycin (Sigma B1793), Metformin (Combi Blocks ST-9194), Nocodazole (VWR 102515-934), Latrunculin A (Sigma L5163), Cycloheximide

(Sigma 18079), Oligomycin (BioChemika 75352), Antimycin A (Sigma A8674), A-769662 (Abcam AB120335), Guanosine (Sigma G6264).

Cell lines:

The following cell lines were originally obtained from the ATCC: HeLa, NRK, IMCD3, MDCK, COS7, G361, and NIH3T3. The control MEFs used throughout these experiments were a generous gift from Dr. David Chan (California Institute of Technology) (Chen et al., 2003). The AMPK-null MEFs were obtained from Dr. Viollet (Laderoute et al., 2006). Normal control and HGprt mutant human primary fibroblasts were obtained and cultured as previously described (Fu et al., 2015).

Cell culture:

Cells were grown in DMEM (ThermoFisher 11965) supplemented with 10% fetal bovine serum (Atlanta Biologicals S11150) at 37°C in the presence of 5% CO_2. Cells are not cultured beyond 30 passages. Cell density, feeding, and plating schedules were maintained constant between conditions in every experiment, with a target of 70% cell density for data collection. Cells were screened for mycoplasma regularly by staining with Hoechst 33342 DNA dye, usually in conjunction with immunofluorescence experiments.

For glucose starvation experiments, cells were grown in DMEM and allowed to attach for at least 4 hr before exchanging medium. Cells were washed twice with PBS and medium exchanged for no glucose DMEM (ThermoFisher 11966) supplemented with 10% dialyzed fetal bovine serum. For MPA induction, cells were treated with 1 μM MPA dissolved in methanol or an equal volume of methanol. For AICAR induction, cells were treated with 1 mM AICAR dissolved in DMSO or an equal volume of DMSO. For DON experiments, cells were treated with 100 μM DON dissolved in water.

Transfection:

Cells at 90% density or higher were transfected in 6 well plates using a ratio of 2 µg Lipofectamine: 1 µg DNA. Sec61β plasmid (3 µg) was diluted in 250 µL Opti-MEM (ThermoFisher 31985). Lipofectamine 2000 (6 µg; ThermoFisher 11668) was diluted in a separate tube containing 250 µL Opti-MEM, vortexed briefly, and incubated at room temperature for 5 min. The tubes were mixed and incubated for 20 min. Cell culture medium was changed to 1.5 ml of Opti-MEM, and transfection complexes (500 µL) were added dropwise to the cells. After 4 hr, cells were trypsinized and re-plated onto coverslips, typically at a 1:4 split. Cells were fixed and processed for immunofluorescence 24 hr after transfection. The plasmid used to drive expression to visualize Sec61β, mCherry-Sec61β, was a gift from Gia Voeltz (University of Colorado, Addgene #49155).

Immunofluorescence:

Cells were grown on matrigel (BD Biosciences 356231) coated coverslips. Cells were fixed in a pre-warmed (37°C) solution of 4% paraformaldehyde in PBS (140 mM NaCl, 3 mM KCl, 10 mM Na_2HPO_4, 2 mM KH_2PO_4, pH 6.75) for 15 min at room temperature; and permeabilized with 0.1% (v/v) Triton X-100 in PBS for 10 min at room temperature. Coverslips were blocked for 1 hr at room temperature using filtered PBS containing 1% (w/v) BSA (Sigma A3059). Incubation with primary antibodies was carried out using blocking solution at 4°C overnight, followed by 4 x 5 minute washes in PBS. Secondary antibodies (1:500, Alexa fluorophores, ThermoFisher) were incubated in blocking solution for 1 hr at room temperature. When staining for actin, coverslips were incubated with rhodamine phalloidin (1:1000, ThermoFisher R415) in conjunction with secondary antibodies. Secondary antibody was removed by 2 x 5 minute washes in PBS. DNA was then stained with Hoechst 33342 for 4 min, followed by 2 x 5 minutes washes in PBS and mounting onto slides using Mowiol. Cells are regularly stained with secondary antibody only to ensure specificity of the primary antibodies.

Images were acquired using an Olympus FV1000 microscope and Olympus Fluoview v1.7 software, using 488 and 543 laser excitation and a 100x oil objective (1.45 NA). Z-stacks were acquired with a step

size of 0.37 μm, which were converted to maximum image intensity projections using ImageJ where indicated. The following antibody dilutions were used: IMPDH2 (1:10,000), mouse monoclonal ARL2 (1:100), rabbit polyclonal ARL2 (1:2,000), ELMOD2 (1:500), Cofactor D (1:1,000), Calnexin (1:1,000), GRP78 (1:100), SigmaR1 (1:100), CTPS1 (1:500), Calreticulin (1:100), ARL1 (1:1,000), ARL3 (1:2,000), ARF1 (1:1,000), ARF3 (1:1,000), ARF4 (1:1,000), ARF6 (1:1,000), ELMOD1 (1:1,000), ELMOD3 (1:500), BART (1:2,000), Cofactor A (1:1,000), Cofactor B (1:1,000), Cofactor C (1:1,000), Cofactor E (1:1,000), TGN46 (1:1,000), ARL13b (1:500), Acetylated tubulin (1:1,000), LC3 (1:200), α-tubulin (1:1,000), β-tubulin (1:1,000), HSP60 (1:5,000).

Antigen competition:

Coverslips were prepared for immunofluorescence and primary antibody diluted in blocking solution as described above. More dilute concentrations of primary antibody were used to facilitate competition. Mouse monoclonal ARL2 was used at a dilution of 1:1,000 and IMPDH2 was used at a dilution of 1:2,000,000. After diluting antibody, antigen was added at a ratio of 10 μg antigen per 1 μg antibody. For controls, an equal volume of blocking solution was added. The antigen/antibody mixtures and paired controls were incubated for 6 hr at 4°C with agitation, and then applied to coverslips. Immunofluorescence was then completed as described above.

Purification of human IMPDH2 expressed in *Saccharomyces cerevisiae* was carried out as described (McPhillips et al., 2004) in yeast strain DY3248 (MATa his3Δ1 leu2Δ0 ura3Δ0 MET15 LYS2 Δimd2::LEU2 Δimd3::kanMX4 [pYES2-IMPDH2-TAP (URA3)] with galactose induction. This strain is deleted for the yeast IMPDH genes and bears a 2μ plasmid with the human IMPDH2 coding region fused to a C-terminal TAP-tag expressed from the yeast GAL1 promoter to allow purification of human IMPDH oligomers free of the yeast proteins. Human ARL2 was purified from bacteria, as described previously (Clark et al., 1993).

Electron microscopy:

Samples for EM analyses were prepared using standard methods, as described previously (Rizzo et al., 2013). In brief, the cells were fixed with 4% paraformaldehyde and 0.05% glutaraldehyde for 30 min at room temperature for immunonanogold labeling or 1% glutaraldehyde for 2 hr for morphological analyses. For immunonanogold labelling the cells were permeabilized with 0.1% saponin in blocking solution (PBS containing 1% bovine serum albumin and 50 mM NH_4Cl) and incubated with antibodies to antigens of interest in the same solution at 4°C overnight (anti-IMPDH2 1:1000 and anti-ARL2 1:10), followed by secondary antibodies labeled with nanogold in the same solution for 2 hr at room temperature. The gold particles were then enhanced by nanogold enhancer (Nanoprobes) according to the manufacturer's instructions. The samples were then embedded in epon and ultra-thin sections (50–70 nm) were prepared. The samples were examined using a Tecnai 12 120kV microscope (FEI, The Netherlands). For quantification of the association of RRs with cellular organelles, the criteria used were the following: the membrane of the organelle should be within 20 nm of a RR and the length of this close association should be continuous for at least 50 nm.

Reproducibility/statistics:

Every experiment described has been independently repeated at least twice in at least three different cell lines. For quantification of immunofluorescence experiments, at least 100 cells per condition were analyzed per experiment. Error bars represent standard deviation (SD).

Results

RR size, shape, and quantity (both number per cell and prevalence within a cell population) are highly variable depending on the cell line under study. The fashion and extent to which different cell types elaborate RRs in the absence of any inducer (normal cell culture conditions) or in response to different drug treatments and growth conditions, also varies. We carried out experiments using a variety of cell lines to test the generalizability of our results. With the exception of electron microscopy data, each experiment was typically repeated in at least three different cell lines; including some combination

of HeLa, MEF (mouse embryo fibroblasts), NRK (normal rat kidney), IMCD3 (murine inner medullary collecting duct), human primary fibroblast, COS7 (African green monkey kidney), MDCK (Madin-Darby canine kidney), and NIH3T3 (mouse embryo fibroblast) cells. A summary of the results obtained in each is shown in Table I. The results displayed are representative of all cell lines tested unless otherwise noted.

The regulatory GTPase ARL2 localizes to RRs

Upon characterization of a number of new monoclonal antibodies specific to ARL2, we found that ARL2 localizes to large cellular structures matching the appearance of RRs. To confirm the identity of these ARL2-positive structures, we compared the ARL2 staining to that of IMPDH2, a well-established marker of RRs (Ji et al., 2006; Carcamo et al., 2011; Juda et al., 2014; Calise et al., 2015). When co-staining fixed cells with rabbit polyclonal antibodies directed against IMPDH2 and any of several mouse monoclonal antibodies raised against human ARL2, we observed very strong co-localization (**Figure 1**). Every ARL2-positive structure in every cell was IMPDH2-positive and *vice versa*, although the staining intensity of ARL2 varied across cell types. Three different monoclonal antibodies raised against bacterially expressed human ARL2 (3B4.B4, 15E11.B11, and 19F6.F11) yielded the same results. All of the ARL2 monoclonal staining displayed here was performed using the 3B4.B4 ARL2 mouse monoclonal antibody.

To further confirm the nature of the ARL2-positive structures as RRs, we treated cells with 1 μM mycophenolic acid (MPA) for 4 hr. Following addition of MPA, the size and quantity of ARL2-positive structures increased dramatically such that they were present in every cell, even in cell lines that display none of these structures under normal culture conditions, such as HeLa cells (**Figure 1**). The most intense ARL2 staining was observed in MPA-treated HeLa cells while the weakest (but still readily observable) was seen in MEFs (**Figure 1**). ARL2 co-localization with IMPDH2 at RR-shaped structures was observed in all cell lines tested, at endogenous structures (structures present under normal growth conditions), and under all induction conditions. ARL2 staining intensity is consistent regardless of the induction method;

however, the appearance of ARL2 at RRs can vary depending on the cell line. These variations are summarized in Table I. Additionally, RRs localized within the nucleus have been previously reported (Calise et al., 2014; Juda et al., 2014). We found that ARL2 localizes to both cytoplasmic and nuclear RRs (**Figure S1**), although ARL2 staining at nuclear RRs is sometimes difficult to discern due to ARL2 staining throughout the nucleus and the fact that nuclear RRs are typically shorter and finer than those observed in the cytosol. Thus, we conclude that ARL2 localizes to RRs based on its consistent co-localization with IMPDH2-positive and MPA-inducible structures in multiple cell types.

To confirm the specificity of both IMPDH2 and ARL2 antibody staining at RRs we carried out antigen competition using purified proteins. Prior incubation of the IMPDH2 antibody with purified, recombinant, human IMPDH2, followed by immunofluorescence staining of fixed cells resulted in near complete loss of IMPDH2 signal intensity at RRs compared to controls (**Figure S2**). Similarly, prior incubation of the ARL2 monoclonal antibody with purified ARL2 protein led to a corresponding decrease in ARL2 signal at RRs when the antibody was then used for immunofluorescence (**Figure S2**). This further confirms the specificity of the IMPDH2 and ARL2 signals we observe at RRs using our rabbit polyclonal IMPDH2 and mouse monoclonal ARL2 antibodies.

We also performed double labeling with mouse monoclonal and rabbit polyclonal antibodies, each directed against ARL2, and found complete overlap in staining at RRs, though less so at other structures (**Figure S3**). Indeed, our ARL2 monoclonal antibodies robustly stain RRs but react much more weakly than the polyclonal serum with cytosolic and mitochondrial ARL2 (**Figure S3**). This makes our ARL2 monoclonal antibodies quite useful for visualization of RRs as they display a clear preference for staining RRs over other structures. Reasons for this preferential staining of different structures between the antibodies is not understood, but the availability of both rabbit and mouse antibodies allowed us to perform double labeling with antibodies directed against many other antigens.

AICAR induces RR formation

To date, RR induction has been most commonly observed upon treatment of cells with drugs that either directly or indirectly inhibit IMPDH, *e.g.*, MPA that traps a covalent intermediate of IMPDH with covalently bound nucleotide and inhibits this key step in guanine nucleotide biosynthesis. Before we identified the ARL2-positive structures as RRs, we suspected the structures may be related to macroautophagy. To test this, we treated cells with 5-aminoimidazole-4-carboxamide ribonucleotide (AICAR) to promote autophagy via activation of AMP kinase (AMPK). Interestingly, we found that AICAR robustly induces the formation of RRs (**Figure 2**). AICAR is also an intermediate in the IMP pathway. It is the substrate for the enzyme just upstream of IMPDH, though it has not previously been reported to cause RR formation. All cells displayed at least one RR structure within 2 hr of AICAR treatment. RRs remained present in all AICAR-treated cells for at least 24 hr. However, the size of RRs differs when comparing AICAR- to MPA-treated cells, regardless of treatment time. With the exception of NRK cells, RRs induced by AICAR were smaller than those formed by MPA induction, although they are still larger than RRs observed in uninduced cells (**Figure 2**). In contrast to other cell types, in NRK cells, RRs induced by either AICAR or MPA were similar in size. NRK cells are also unusual in having almost no rings at all after treatment with MPA (**Figure 2**). Like with MPA treatment, AICAR induced RRs were always found to stain positively for both IMPDH2 and ARL2 (**Figure 2**).

As previously mentioned, AICAR is also a well-known activator of AMPK (Russell et al., 1999). To test if the induction of RRs with AICAR is a result of AMPK activation, we treated AMPK-null MEFs (MEFs lacking *ampk1* and *ampk2* (Laderoute et al., 2006)) with AICAR and compared RR induction to paired control MEFs. In both, AICAR was capable of dramatic RR induction (**Figure 3**), suggesting that RR induction with AICAR was independent of AMPK activation. Additionally, A-769662, another activator of AMPK (F. Liu et al., 2016), had no impact on RR size or quantity. Thus, it is likely that increasing AICAR levels act by altering the pools of one or more intermediates or products of the *de novo* and guanine nucleotide biosynthetic pathways which leads to RR formation.

Glucose starvation also induces RR formation

We recently showed that glucose starvation (cell culture in medium lacking glucose for up to 48 hr) caused changes in the staining intensity of ARL2 in mitochondria (Newman, Schiavon, Zhou, et al., 2017). Using the same regimen, we found that glucose starvation also increases the percentage of cells with RRs that stain positively for both IMPDH2 and ARL2 (**Figure 4**). Unlike MPA or AICAR, glucose starvation does not cause as robust an increase in the percentage of cells with RRs (**Figure 4B**). The proportion of cells which form RRs in response to glucose starvation varies greatly depending on the cell line. IMCD3 (**Figure 4B**), NRK, MDCK, and NIH3T3 show a moderate increase in the percentage of cells with at least one RR, compared to control conditions, while the fold increase is more dramatic in MEFs (**Figure 4B**). Several other cell lines (HeLa, COS7, G361, human fibroblasts) do not form RRs in response to glucose starvation. Notably, these are the same cell lines in which we have never observed RRs under normal growth conditions. In the rest of the cell lines tested, RRs can be observed in at least a small percentage of cells under normal growth conditions. In cell lines where glucose starvation has a strong effect on RR quantity, the fraction of cells with at least one RR never reaches 100% (*e.g.*, IMCD3 cells peak at ~75% (**Figure 4B**)).

RRs were also slower to form after switching to the no glucose medium, compared to drug treatments. Whereas 2 hr was sufficient for 100% of cells to display RRs following MPA or AICAR addition, an increase in RR quantity following glucose starvation was not evident until at least 6 hr after glucose removal and did not peak until 24 hr. In almost all cell lines in which glucose starvation induced RRs, we observed an increase in their number, but not size. MEFs were an exception, as glucose starvation increased both the quantity and size of RRs in this line, although they were still not as large as the RRs observed in MPA-treated MEFs.

The induction of RRs did not seem to be a generalized response to cell stress or growth inhibition. We tested a number of other drugs (3-methyladenine, bafilomycin, 2-deoxy glucose, metformin, oligomycin, antimycin A, cycloheximide, compound C, nocodazole, latrunculin A), as well as serum starvation, none of which influenced the size or quantity of RRs.

Guanosine fails to prevent RR formation in fibroblasts from Lesch-Nyhan disease patients

RR formation has been linked to guanine nucleotide metabolism in large part because the marker of RRs, IMPDH, is the rate limiting step in *de novo* synthesis of guanine nucleotides, and inhibitors of the enzyme are strong inducers of RRs. There also exists a salvage pathway in which guanine or guanosine can be imported from outside the cell and converted directly to GMP. Addition of guanosine has been shown to prevent or reverse the formation of constitutive or MPA-induced RRs (Calise et al., 2014; Calise et al., 2016). We recapitulated these findings in multiple cell lines (**Figure S4**). It has been suggested that guanosine feeds into the salvage pathway for guanine nucleotide production, compensating for the inhibition of the *de novo* pathway that results when cells are treated with IMPDH inhibitors. If so, this pathway would be diminished or lost in cells which have mutated hypoxanthine-guanine phosphoribosyltransferase (HGprt), the enzyme needed to convert guanine into GMP. Human cells with such mutations are available from patients with Lesch-Nyhan disease (LND) (Fu et al., 2015). Guanosine is normally converted first to guanine by purine nucleoside phosphorylase and then recycled into GMP by HGprt. Thus, if added guanosine prevents RR formation because of its ability to restore guanine nucleotides, we would predict that guanosine addition would have no such effect in LND fibroblasts, where guanosine incorporation into guanine nucleotides is defective.

Both normal and LND fibroblasts showed no RRs under control conditions and a robust induction of RRs following MPA treatment (**Figure 5**). Addition of 1 mM guanosine with MPA (1 μM) completely prevented RR formation in control human fibroblasts. However, when the same treatment was applied to LND fibroblasts, all cells formed obvious RRs, appearing identical to the MPA-only condition (**Figure 5**). This result suggests that it is not guanosine, but rather guanine nucleotides, which reverse RR formation following MPA.

It has been previously reported that interfering with *de novo* synthesis of guanine nucleotides by glutamine starvation or inhibition of dihydrofolate reductase, will induce the formation of RRs and that

the addition of guanosine completely reverses this effect (Calise et al., 2014; Calise et al., 2016). We found that guanosine is also capable of reversing RRs formed via AICAR treatment or glucose-starvation (**Figure S5**). These results support the hypothesis that RR formation is closely linked to guanine nucleotide pools regardless of induction methods, and that guanosine is able to prevent or reverse RR formation by generating guanine nucleotides via the purine salvage pathway.

ARL2 always co-localizes with IMPDH2 at RRs but not with CTPS1 at cytoophidia

Cytoophidia are similar to RRs in being large structures that form in response to glutamine analogs such as DON or acivicin (Carcamo et al., 2011; Calise et al., 2014; Keppeke, Andrade, et al., 2015). These drugs inhibit a range of enzymes which bind glutamine, including CTPS (Pinkus, 1977). Although there are several similarities between RRs and cytoophidia, there are also important differences. MPA never induced the formation of CTPS1-positive cytoophidia in HeLa cells and only rarely (~10% of cells) did so in NRK or IMCD3 cells (**Figure 6**). Unlike RRs, we never observed any cytoophidia under normal growth conditions in any of the cell lines tested and neither AICAR nor glucose starvation induced the formation of cytoophidia.

ARL2 only rarely co-localized with CTPS1. In NRK and IMCD3 cells, ARL2 and CTPS1 antibodies sometimes co-stained what appears to be the same rod-like structures, but in the same cell or others in the culture there were also many more structures positive for ARL2 or CTPS1, but negative for the other. HeLa cells serve as a striking example in which ARL2 and CTPS1-positive structures were often in close proximity but did not co-localize (**Figure 6**). This is in stark contrast to the consistent co-localization between ARL2 and IMPDH2 (**Figure 1**). The shape of cytoophidia was also obviously different compared to RRs in HeLa cells with cytoophidia being shorter, thicker, and lacking rings (**Figure 6**). We conclude that while RRs and cytoophidia often displayed a physical proximity, suggesting they may sometimes share an underlying substructure, they were clearly distinct structures and that ARL2 is a component of RRs but not cytoophidia.

A specific subset of ARL2 partners localize to RRs

We examined whether other members of the ARF family localized to RRs. Immunofluorescence using a rabbit polyclonal antibody directed against ARL3, the closest paralog of ARL2 sharing 53% identity (Li et al., 2004; Logsdon & Kahn, 2004), displayed localization to centrosomes as previously described (Zhou et al., 2006) but no co-localization at RRs in any of the cell lines tested (**Figure S6**). In agreement with those stark differences in immunolocalization results, we saw no evidence of cross reactivity in immunoblots when ARL2 and ARL3 antisera were used to probe the purified recombinant GTPases. Other members of the ARF family tested include ARL1, ARL13b, ARF1, ARF3, ARF4, and ARF6. None of these localized to RRs.

We next asked if known ARL2 binding partners were also present at RRs. We had earlier purified ELMOD2 from mammalian tissues as an ARL2 GTPase activating protein (GAP) and later showed that it is one of a three member family of paralogs in mammals, ELMOD1-3 (Bowzard et al., 2007; East et al., 2012). The ELMOD (cell EnguLfement and MOtility Domain) proteins each share a single (ELMO) domain with the three ELMO proteins in mammals (Chung et al., 2000; Gumienny et al., 2001), yet appear to have quite distinct functions, with only the ELMODs acting as GAPs for ARF family GTPases (Bowzard et al., 2007; East et al., 2012; Ivanova et al., 2014). Double labeling for ELMOD2 and ARL2 revealed clear co-localization at RRs (**Figure 7A**). This was evident in all cells examined, though less obviously so in HeLa cells. The staining of ELMOD2 at mitochondria and other sites made its presence at RRs less obvious compared to the ARL2 monoclonal antibodies, but every ARL2 positive RR (both endogenous and following induction) also stained positively for ELMOD2. The staining intensity of ELMOD2 at RRs was more intense following AICAR or glucose-starvation induction compared to MPA induction. In marked contrast, other members of the ELMOD family (ELMOD1 and ELMOD3) did not localize to RRs under any of these conditions (**Figure S6**).

We also observed that cofactor D co-localized with ARL2 at RRs (**Figure 7B**). Cofactor D exists in a 1:1:1 complex with ARL2 and β-tubulin and is one of several cofactors involved in αβ-tubulin biogenesis (Tian et al., 1996; Shern et al., 2003; Francis, Newman, et al., 2017). The other tubulin cofactors (cofactors A, B, C, and E) showed no evidence of staining at RRs (**Figure S6**). Like ELMOD2, cofactor D co-localization at RRs was observable in all cell lines tested with the exception of HeLa. Cofactor D staining was observable at RRs under control and all induction conditions with no obvious differences in staining intensity between the induction methods. Cytosolic cofactor D staining sometimes impedes visualization of cofactor D at RRs, although not to the same extent as ELMOD2. This may be because cofactor D staining usually appeared diffuse (as opposed to ELMOD2 which appeared punctate/mitochondrial), making the RR structures more easily discernible. β-tubulin did not localize to RRs by immunofluorescence, though we cannot exclude the possibility that some β-tubulin was present but key epitopes are masked in the trimer.

The ratio of rods to rings varies between cell types, though rods always outnumber rings. Rings are easier to identify as RRs because while rods might be mistaken for cilia or mitochondria, rings of this size are highly unusual in cells. For this reason, our figures more often show rings, even though they are fewer in number. We found no antibody that exhibited a clear preference in staining rods over rings or *vice versa*.

Binder of ARL2 (BART aka ARL2BP) was the first ARL2 partner identified, based upon its specific interaction with activated, GTP-bound ARL2 (Sharer & Kahn, 1999; Sharer et al., 2002; Bailey et al., 2009; Zhang et al., 2009). Like ARL2, BART is found predominantly in cytosol but also localizes to mitochondria (Sharer et al., 2002). Our rabbit polyclonal antibodies to BART found no evidence of staining of RRs. Thus, overall, these data demonstrate that there is a specific set of ARL2 binding partners, including ELMOD2 and cofactor D, that co-localized with ARL2 and IMPDH2 to RRs while others, ELMOD1/3, BART, and cofactors A/B/C/E, did not.

RRs are associated with an ER-derived membrane

The localization of ARL2, cofactor D, and ELMOD2 to RRs suggests that RRs are more complex than simple polymers of IMPDH. We examined the localization of well-established markers of various cellular organelles and found that several resident ER proteins co-localized with ARL2 at RRs. The most striking co-localization was observed with calnexin (**Figure 8A**), a transmembrane, resident endoplasmic reticulum protein which can escape and be found at the cell surface (Wiest et al., 1995; Wiest et al., 1997; Charonis et al., 2017). The next most prominent RR staining of a resident ER protein was another lumenal chaperone GRP78 (**Figure 8B**), which also can escape to the plasma membrane (Tsai et al., 2018). While its staining of RRs was comparable to that of calnexin, there was additional cytoplasmic staining that made RR staining with GRP78 antibodies less prominent. This was also seen for SigmaR1 (**Figure 8C**), another transmembrane, ER resident protein that is thought to accumulate in lipid rafts and at ER-mitochondria contact sites (Ruscher & Wieloch, 2015).

In contrast to the immunofluorescent localization of *endogenous* proteins described so far, we used exogenous expression of mCherry-tagged Sec61β due to the lack of an antibody capable of specifically staining the endogenous protein. mCherry-Sec61β also co-localized with RRs (**Figure S7**). Each of these proteins contains a transmembrane domain with the exception of GRP78 which resides in the ER lumen (Bole et al., 1986). The co-localization of these ER proteins at RRs was consistently observed in multiple cell lines, except for mCherry-Sec61β that had the weakest co-localization and was only observed in IMCD3 cells.

Co-localization of ER proteins at RRs was tested under control, glucose-starvation, and MPA-treatment conditions. Although co-localization between the previously listed ER proteins and RRs was observable under all of these conditions, the staining intensity was highest after glucose-starvation (with the exception of cells in which glucose-starvation does not induce RRs) (**Figure S8**).

In contrast to calnexin, GRP78, and SigmaR1, at least one other ER protein, calreticulin, did not localize to RRs (**Figure S9**). This finding raises the possibility that a sub-compartment of the ER associates with RRs. Other organelle markers that we tested included TGN46 (Golgi), HSP60 (mitochondria), α- and β-tubulin (microtubules), rhodamine phalloidin (actin), acetylated tubulin (primary cilia), and LC3 (autophagosomes) – none of which were observed at RRs (**Figure S9**). The presence of multiple transmembrane ER proteins at RRs suggests that the ER, or a membrane derived from the ER, is closely associated with RRs.

Ultrastructural data support the presence of ARL2 throughout RRs and association of RRs with a membrane

To further explore the association of both ARL2 and a membrane with RRs, we used transmission electron microscopy (EM) to visualize RRs in HeLa cells treated with MPA (1 μM) for 2 hr. As seen previously (Juda et al., 2014), RRs appeared as a collection of long, clustered filaments in longitudinal sections and as a bundle of filaments in cross section (**Figure 9A,C**, respectively). Using nanogold labelling with silver enhancement, in conjunction with the polyclonal IMPDH2 antibody, we observed localization of IMPDH2 throughout the RRs, as expected (**Figure 9D**). Immunolabeling throughout RRs was equally evident upon staining with a monoclonal ARL2 antibody, consistent with our immunofluorescence data (**Figure 9E**). It was also common to observe clusters of darkly staining glycogen granules adjacent to RRs (**Figure 9**), though we did not further explore this observation.

Intracellular membranes were often found to be in close apposition to rods by EM (**Figure 9**). These membranes appeared to be ER and mitochondria, based upon their morphologies, however, the membrane typically did not run along the entire length of the rod (**Figure 9B**). We quantified the fraction of RRs with closely apposed membranes and found about half to lie along ER and about a quarter were adjacent to a mitochondrion (**Figure 9F**).

Different components of RRs have different kinetics of recruitment.

We sought to monitor the assembly of RRs over time, to establish if it is an ordered process. We compared the kinetics of RR formation in 3 cell lines after addition of MPA (1 μM) over a 2 hr window, by co-staining for IMPDH2 and ARL2 **(Figure 10)**. The formation of RRs was quite consistent across cell lines, with MEFs progressing slightly faster than HeLa or NRK cells, but all 3 reaching their peak of 100% of cells with RRs within 1-2 hr after MPA addition (**Figure 10A,B**). Within 5 min of MPA treatment, IMPDH2-positive structures were observed in a small percentage of cells (**Figure 10A)**. At this time they were dispersed throughout the cytosol, appearing to have a punctate morphology, and were far more numerous and much smaller in size than mature RRs. The same was true in MEFs and NRK cells except the morphology appeared less punctate and more like small, extremely thin rods. The size and number of RRs per cell changed over time, with the number of structures per cell decreasing and the size and thickness of the structures increasing (**Figure 10A**). Visual inspection of such time course data also suggests that IMPDH2 staining was more diffuse prior to, or at early time points after, MPA addition, consistent with the mass movement of IMPDH2 from the soluble fraction into RRs. Such a change in localization is suggestive of the lack of need for new protein synthesis, although not formally tested here.

ARL2 appears to recruit to RRs after IMPDH2. Co-staining of ARL2 and IMPDH2 over time revealed that ARL2 was not recruited to RRs until ~20 min after MPA addition, while IMPDH2-positive structures were evident at 5 and 10 min (**Figure 10A,C**). The accumulation of ARL2 at RRs appears to coincide with the change in RR morphology from a punctate (or very thin rod) shape to the more typical RR shape; *i.e.*, ARL2 co-localization is rarely visible at punctate structures but almost always visible at RR-shaped structures. This difference between IMPDH2 and ARL2 staining and the change in morphology were most dramatic between 10 and 20 min. At later times the two proteins stained indistinguishably.

In contrast to IMPDH2 or ARL2, calnexin recruitment to RRs was slower and only ~40% of cells showed calnexin at RRs after 45 min in MPA, at which point ARL2 was seen at RR in more than 80% of cells **(Figure 11)**. Thus, these time course data are consistent with an ordered and sequential addition of

components, with IMPDH the first protein to polymerize, ARL2 arriving slightly later, and calnexin recruitment still later.

Discussion

We provide evidence that a number of proteins not directly involved in nucleotide metabolism are present at RRs. They appear to be recruited to RRs with a high degree of specificity and in an ordered fashion, consistent with them playing specific roles. We demonstrate that the regulatory GTPase ARL2 is a component of RRs, based upon its co-localization with IMPDH2 in every cell line tested and the coordinated increases in each upon treatment with each of the inducers of RR formation, most notably MPA (**Figure 1**). We also describe for the first time two treatments that promote RR formation, AICAR and glucose deprivation, which also contain ARL2. Among the other newly identified proteins found to co-localize at RRs are a number of ER proteins, leading us to propose a role for the ER in RR biology. These newly discovered components of RRs and means of induction also allow us to draw clear distinctions between RRs and cytoophidia.

The localization of ARL2 to RRs was observed in every cell line tested, although with variability in the staining intensity (**Table I**). ARL2 localization was also evident at the EM level, in which ARL2 could be seen throughout the RRs (**Figure 9**). In contrast, other members of the ARF family, including the closest paralog to ARL2, ARL3, were not found at RRs (**Figure S5**). Specificity was also evident in the ARL2 interacting partners present in RRs, ELMOD2 and cofactor D (**Figure 7**), as others were not found there (ELMOD1, ELMOD3, BART, other tubulin cofactors). We have focused in recent years on defining the roles of ARL2 in tubulin biogenesis (Francis, Goswami, et al., 2017; Francis, Newman, et al., 2017), mitochondrial fusion (Newman, Schiavon, Turn, et al., 2017; Newman, Schiavon, Zhou, et al., 2017), and ATP generation in mitochondria (Newman et al., 2014). ELMOD2 appears to work together with ARL2 in the mitochondrial intermembrane space to affect fusion. ARL2 function has also been linked to centrosome stability (Zhou et al., 2006) and transport of N-myristoylated protein cargos (Ismail

et al., 2011; Watzlich et al., 2013). Given this diversity of ARL2 actions there are several potential functional links to RRs to be examined. It is also possible that inclusion of ARL2 (and cofactor D/ELMOD2) in RRs may serve to sequester it away from other sites and actions, in what has been termed "higher order signaling" (Francis et al., 2016).

Surprisingly, a number of ER-resident, membrane proteins were also found associated with RRs (**Figure 8**). The co-staining of IMPDH2 with these ER proteins leads us to propose a role for the ER, or a sub-compartment derived from it, in RR biology. We found that calnexin, GRP78, SigmaR1, and Sec61β all co-localize with IMPDH2 at RRs (**Figure 8**). With the exception of GRP78, each is a transmembrane protein, so their localization to RRs strongly implies that there is a membrane component associating with RRs. Because calreticulin, another common ER marker, does not co-localize with RRs we speculate that only a sub-compartment of the ER interacts with RRs. Previous reports have not found RRs associated with membrane when visualized using EM (Ji et al., 2006; Thomas et al., 2012; Juda et al., 2014), and we too find examples of RR that are not proximal to a membrane. Although the membrane proteins (*e.g.*, calnexin) appear to co-localize along the entire length of RRs when visualized by immunofluorescence, this is not the case for membranes seen in our EM images. We cannot currently explain this apparent difference, though they may arise during sample preparation required by the different techniques of staining. It is also possible that these differences are amplified by using MPA to induce the RRs observed by EM as the staining intensity of ER- associated proteins is more intense in RRs induced by glucose-starvation (**Figure S8**). This was also true of ELMOD2, which has been reported to partially localize to the ER (Suzuki et al., 2015). On the other hand, IMPDH2, ARL2, and cofactor D (all primarily cytosolic proteins) showed no such difference in staining intensity when comparing induction conditions.

These newly described components of RRs are recruited in an ordered fashion. Only IMPDH2 was seen in the earliest stages of RR formation, followed by ARL2 recruitment as RRs begin to coalesce into larger structures, and finally calnexin was added at the fully-formed RRs (**Figures 10, 11**).These data are consistent with a model in which RRs draw from a soluble pool of IMPDH, coalesce, and mature with

the addition of the signaling and membrane proteins identified here. The diffuse, cytosolic staining of IMPDH2 seen in untreated cells decreases over time, consistent with re-localization of a large fraction of total cellular IMPDH from the cytosol into RRs (**Figure 10)**, though drawing quantitative conclusions from immunofluorescence data of soluble proteins is challenging. The observation that ARL2 is recruited after initiation of RR formation suggests that it is not required for the initial oligomerization of IMPDH but may play a role in the elongation or stabilization of nascent RRs. The differences in the timing of protein recruitment to RRs and consistency of these differences across the three cell lines tested (HeLa, MEFs, and NRK) suggest that the formation of RRs is a conserved and carefully regulated process.

Two other conditions were also found to induce RR formation, AICAR and glucose starvation, though to varying degrees depending on the cell line (**Figures 2, 4**). RRs are most often experimentally induced via direct IMPDH binding inhibitors, but they can also be induced by glutamine starvation (Calise et al., 2014), serine starvation, glycine addition (Calise et al., 2016), glutamine analogs (Carcamo et al., 2011; Calise et al., 2014; Keppeke, Calise, et al., 2015), and inhibition or knock-down of dihydrofolate reductase (Calise et al., 2016). It is hypothesized that these other inducers of RRs inhibit *de novo* purine synthesis either by inhibiting enzymes involved in this pathway (glutamine analogs) or by depriving the pathway of necessary substrates (glutamine, serine/glycine). However, purine synthesis inhibition is not necessarily required for RR formation as RRs have been observed following treatments that do not inhibit *de novo* purine synthesis (Chang et al., 2015; Keppeke et al., 2018) and even under normal growth conditions (Willingham et al., 1987; Gunter et al., 2008; Ramer et al., 2010; Carcamo et al., 2011; Chang et al., 2015). It's possible that alterations in intracellular purine pools (due to interruption of purine synthesis, innate differences in cellular metabolism, or other factors) serve as the trigger for RR formation. To our knowledge, this is the first report of AICAR-mediated induction of RR formation. AICAR is commonly used as an activator of AMP kinase (AMPK). AMPK activation does not appear to be the mechanism of AICAR's effect here because RR formation was independent of AMPK (**Figure 3**). AICAR is an intermediate in the purine synthesis pathway upstream of IMP. Thus, the robust induction of

RRs upon the addition of AICAR may be linked to its role as a metabolite in *de novo* purine synthesis, possibly by inhibiting the *de novo* pathway via allosteric inhibition or by altering intracellular purine pools.

Our data further strengthen the links between RR and nucleotide metabolism as we found that guanosine prevents or reverses RR formation (Ji et al., 2006; Calise et al., 2014; Calise et al., 2016) in a process that is dependent upon the purine salvage pathway. We have demonstrated that guanosine reverses or prevents RR formation by its conversion to GMP via HGprt in the purine salvage pathway as previously shown (Ji et al., 2006). In previous studies, guanosine always resulted in a complete reversal or prevention of RR formation in all cell lines and RR induction conditions tested (Calise et al., 2014; Calise et al., 2016). Consistent with this, we found that guanosine was capable of reversing RR formation in combination with any of the inducers (MPA, DON, AICAR, and glucose-starvation), and in every cell line tested, with the important exception of human fibroblasts lacking functional HGprt (**Figure 5, S3, S4**). This demonstrates that RR reversal with guanosine is dependent on HGprt-mediated purine salvage. These results also strengthen the link between RR formation and nucleotide pools, suggesting that RRs form in response to a decrease in guanine nucleotides which guanosine can alleviate via the salvage pathway.

Glucose-starvation had the mildest and most variable effect on RR formation in different cell lines compared to other inducers tested (summarized in **Table I**). There is one report of glucose depletion inducing CTPS filament (cytoophidia) formation in *S. cerevisiae* (Noree et al., 2010), but there are no reports of increases in RRs in mammalian cells. Glucose plays a part in a myriad of metabolic and energetic pathways, offering many ways in which glucose-starvation may induce RR formation. Ribose-5-phosphate, generated from glucose via the pentose phosphate pathway, is a precursor for purine nucleotide synthesis. The folate cycle, which has been previously linked to RR formation (Calise et al., 2016), also relies on glucose, as serine, one of the necessary substrates in this cycle, is synthesized from

glucose. Overall, these data broaden our understanding of the ways in which RRs can be induced and strengthen the possibility that RRs are linked to other cellular pathways.

The terms RRs and cytoophidia have been used synonymously, and some reports show partial overlap between IMPDH and CTPS in what appear to be a common structure (Ramer et al., 2010; Carcamo et al., 2011; Carcamo et al., 2014; Keppeke, Calise, et al., 2015). We examined the co-localization between ARL2 and cytoophidia, using CTPS1 as a marker. ARL2 rarely co-localizes with CTPS1 in NRK and IMCD3 cells and never does so in HeLa cells (**Figure 6**). These results reveal that ARL2 localizes specifically to RRs and highlights a clear difference between RRs and cytoophidia. Although RRs and cytoophidia may be related, most evidence indicates that they are distinct structures. IMPDH inhibitors, the most common method of RR induction, do not induce cytoophidia (Keppeke, Calise, et al., 2015). Our results with MPA induction are in agreement with those findings (**Figure 6**). Neither glucose-starvation nor AICAR induced the formation of cytoophidia although each led to RR formation. Glutamine analogs such as DON and acivicin induce cytoophidia due to their inhibition of CTPS (Carcamo et al., 2011; Calise et al., 2014; Keppeke, Andrade, et al., 2015). These drugs also induce the formation of RRs, however, this is likely due to the fact that multiple enzymes involved in *de novo* purine synthesis require glutamine as a cofactor, making them sensitive to these drugs. Guanosine is capable of reversing RR formation but has no effect on cytoophidia (Keppeke, Calise, et al., 2015). Cytoophidia are also smaller than RRs and lack ring-shaped structures (**Figure 6**). Loukomasomes, another large cellular structure similar in appearance to RRs have been reported (Noble et al., 2016). However, these structures also appear to be distinct from RRs despite their similar shape. Thus, our data argue strongly that RRs and cytoophidia are not the same structures, although they may have some related roles as both are linked to nucleotide metabolism which may explain the partial overlap observed between CTPS and IMPDH but not ARL2.

In summary, we describe evidence of the specific, ordered recruitment of ARL2, a subset of its effectors, and ER-derived membranes to RRs. We have recently described roles for ARL2 and TBCD in

αβ-tubulin biogenesis (Francis, Goswami, et al., 2017; Francis, Newman, et al., 2017) and for ARL2 and ELMOD2 in mitochondrial fusion (Newman et al., 2014; Newman, Schiavon, Zhou, et al., 2017), with others demonstrating roles of ARL2 in transport of myristoylated cargo proteins (Jaiswal et al., 2016). Whether any of these processes are linked to RRs is unclear. We speculate that the recruitment of ARL2 and related proteins into RRs could serve a role in inhibiting the actions of this GTPase at other sites via its sequestration into these very large and reversible structures. The specificity with which ARL2, ELMOD2, and cofactor D are each recruited to RRs and the universal roles that regulatory GTPases in the ARF and RAS superfamilies play in cell signaling are consistent with a model linking RRs to some aspect of cell signaling; though we currently lack mechanistic details. With additional components of RRs now elucidated, we are in a better position to understand the function of this fascinating structure and its interaction with cellular organelles.

Acknowledgments

This work was supported by grants from the NIH (GM122568, RAK; GM120271 to DR). The authors thank a number of colleagues for their gifts of key reagents used in these studies, including: Drs. Tamara Caspary (Emory Univ; Arl13b antibody), David Chan (CalTech; mouse embryonic fibroblasts), Gia Voeltz (Univ Colorado at Boulder; plasmid directing expression of mCherry-Sec61β), Juan Carlos Zabala (Universidad de Cantabria; antibodies to cofactors A/B/C/E). The collection, validation, and distribution of human fibroblasts from LND patients is supported by NIH R56 NS102980 (HAJ). This research project was supported in part by the Emory University Integrated Cellular Imaging Microscopy Core of the Emory Neuroscience NINDS Core Facilities grant, 5P30NS055077. The Eurobioimaging Facility at the Institute of Protein Biochemistry is funded by grants from MIUR, Government of Italy.

References

Aguilera-Gomez, A., & Rabouille, C. (2017). Membrane-bound organelles versus membrane-less compartments and their control of anabolic pathways in Drosophila. *Dev Biol, 428*(2), 310-317. doi:10.1016/j.ydbio.2017.03.029

Anthony, S. A., Burrell, A. L., Johnson, M. C., Duong-Ly, K. C., Kuo, Y. M., Simonet, J. C., Michener, P., Andrews, A., Kollman, J. M., & Peterson, J. R. (2017). Reconstituted IMPDH polymers accommodate both catalytically active and inactive conformations. *Mol Biol Cell*. doi:10.1091/mbc.E17-04-0263

Aughey, G. N., & Liu, J. L. (2015). Metabolic regulation via enzyme filamentation. *Crit Rev Biochem Mol Biol, 51*(4), 282-293. doi:10.3109/10409238.2016.1172555

Bailey, L. K., Campbell, L. J., Evetts, K. A., Littlefield, K., Rajendra, E., Nietlispach, D., Owen, D., & Mott, H. R. (2009). The structure of binder of Arl2 (BART) reveals a novel G protein binding domain: implications for function. *J Biol Chem, 284*(2), 992-999. doi:10.1074/jbc.M806167200

Bhamidipati, A., Lewis, S. A., & Cowan, N. J. (2000). ADP ribosylation factor-like protein 2 (Arl2) regulates the interaction of tubulin-folding cofactor D with native tubulin. *J Cell Biol, 149*(5), 1087-1096.

Bole, D. G., Hendershot, L. M., & Kearney, J. F. (1986). Posttranslational association of immunoglobulin heavy chain binding protein with nascent heavy chains in nonsecreting and secreting hybridomas. *J Cell Biol, 102*(5), 1558-1566.

Bowzard, J. B., Cheng, D., Peng, J., & Kahn, R. A. (2007). ELMOD2 is an Arl2 GTPase-activating protein that also acts on Arfs. *J Biol Chem, 282*(24), 17568-17580. doi:10.1074/jbc.M701347200

Calise, S. J., Carcamo, W. C., Krueger, C., Yin, J. D., Purich, D. L., & Chan, E. K. (2014). Glutamine deprivation initiates reversible assembly of mammalian rods and rings. *Cell Mol Life Sci, 71*(15), 2963-2973. doi:10.1007/s00018-014-1567-6

Calise, S. J., Keppeke, G. D., Andrade, L. E., & Chan, E. K. (2015). Anti-rods/rings: a human model of drug-induced autoantibody generation. *Front Immunol, 6*, 41. doi:10.3389/fimmu.2015.00041

Calise, S. J., Purich, D. L., Nguyen, T., Saleem, D. A., Krueger, C., Yin, J. D., & Chan, E. K. (2016). 'Rod and ring' formation from IMP dehydrogenase is regulated through the one-carbon metabolic pathway. *J Cell Sci, 129*(15), 3042-3052. doi:10.1242/jcs.183400

Carcamo, W. C., Calise, S. J., von Mühlen, C. A., Satoh, M., & Chan, E. K. L. (2014). Chapter Two - Molecular Cell Biology and Immunobiology of Mammalian Rod/Ring Structures. In W. J. Kwang (Ed.), *International Review of Cell and Molecular Biology* (Vol. Volume 308, pp. 35-74): Academic Press.

Carcamo, W. C., Satoh, M., Kasahara, H., Terada, N., Hamazaki, T., Chan, J. Y., Yao, B., Tamayo, S., Covini, G., von Muhlen, C. A., & Chan, E. K. (2011). Induction of cytoplasmic rods and rings structures by inhibition of the CTP and GTP synthetic pathway in mammalian cells. *PLoS One, 6*(12), e29690. doi:10.1371/journal.pone.0029690

Carr, S. F., Papp, E., Wu, J. C., & Natsumeda, Y. (1993). Characterization of human type I and type II IMP dehydrogenases. *J Biol Chem, 268*(36), 27286-27290.

Cavenagh, M. M., Whitney, J. A., Carroll, K., Zhang, C., Boman, A. L., Rosenwald, A. G., Mellman, I., & Kahn, R. A. (1996). Intracellular distribution of Arf proteins in mammalian cells. Arf6 is uniquely localized to the plasma membrane. *J Biol Chem, 271*(36), 21767-21774.

Chang, C. C., Lin, W. C., Pai, L. M., Lee, H. S., Wu, S. C., Ding, S. T., Liu, J. L., & Sung, L. Y. (2015). Cytoophidium assembly reflects upregulation of IMPDH activity. *J Cell Sci, 128*(19), 3550-3555. doi:10.1242/jcs.175265

Charonis, A. S., Michalak, M., Groenendyk, J., & Agellon, L. B. (2017). Endoplasmic reticulum in health and disease: the 12th International Calreticulin Workshop, Delphi, Greece. *J Cell Mol Med, 21*(12), 3141-3149. doi:10.1111/jcmm.13413

Chen, H., Detmer, S. A., Ewald, A. J., Griffin, E. E., Fraser, S. E., & Chan, D. C. (2003). Mitofusins Mfn1 and Mfn2 coordinately regulate mitochondrial fusion and are essential for embryonic development. *J Cell Biol, 160*(2), 189-200. doi:10.1083/jcb.200211046

Chung, S., Gumienny, T. L., Hengartner, M. O., & Driscoll, M. (2000). A common set of engulfment genes mediates removal of both apoptotic and necrotic cell corpses in C. elegans. *Nat Cell Biol, 2*(12), 931-937.

Clark, J., Moore, L., Krasinskas, A., Way, J., Battey, J., Tamkun, J., & Kahn, R. A. (1993). Selective amplification of additional members of the ADP-ribosylation factor (ARF) family: cloning of additional human and Drosophila ARF-like genes. *Proc Natl Acad Sci U S A, 90*(19), 8952-8956.

Colby, T. D., Vanderveen, K., Strickler, M. D., Markham, G. D., & Goldstein, B. M. (1999). Crystal structure of human type II inosine monophosphate dehydrogenase: implications for ligand binding and drug design. *Proc Natl Acad Sci U S A, 96*(7), 3531-3536.

Covini, G., Carcamo, W. C., Bredi, E., von Muhlen, C. A., Colombo, M., & Chan, E. K. (2012). Cytoplasmic rods and rings autoantibodies developed during pegylated interferon and ribavirin therapy in patients with chronic hepatitis C. *Antivir Ther, 17*(5), 805-811. doi:10.3851/imp1993

Cunningham, L. A., & Kahn, R. A. (2008). Cofactor D functions as a centrosomal protein and is required for the recruitment of the gamma-tubulin ring complex at centrosomes and organization of the mitotic spindle. *J Biol Chem, 283*(11), 7155-7165. doi:10.1074/jbc.M706753200

East, M. P., Bowzard, J. B., Dacks, J. B., & Kahn, R. A. (2012). ELMO domains, evolutionary and functional characterization of a novel GTPase-activating protein (GAP) domain for Arf protein family GTPases. *J Biol Chem, 287*(47), 39538-39553. doi:10.1074/jbc.M112.417477

Francis, J. W., Goswami, D., Novick, S. J., Pascal, B. D., Weikum, E. R., Ortlund, E. A., Griffin, P. R., & Kahn, R. A. (2017). Nucleotide Binding to ARL2 in the TBCDARL2beta-Tubulin Complex Drives

Conformational Changes in beta-Tubulin. *J Mol Biol, 429*(23), 3696-3716. doi:10.1016/j.jmb.2017.09.016

Francis, J. W., Newman, L. E., Cunningham, L. A., & Kahn, R. A. (2017). A Trimer Consisting of the Tubulin-specific Chaperone D (TBCD), Regulatory GTPase ARL2, and beta-Tubulin Is Required for Maintaining the Microtubule Network. *J Biol Chem, 292*(10), 4336-4349. doi:10.1074/jbc.M116.770909

Francis, J. W., Turn, R. E., Newman, L. E., Schiavon, C., & Kahn, R. A. (2016). Higher order signaling: ARL2 as regulator of both mitochondrial fusion and microtubule dynamics allows integration of 2 essential cell functions. *Small Gtpases, 7*(4), 188-196. doi:10.1080/21541248.2016.1211069

Fu, R., Sutcliffe, D., Zhao, H., Huang, X., Schretlen, D. J., Benkovic, S., & Jinnah, H. A. (2015). Clinical severity in Lesch-Nyhan disease: the role of residual enzyme and compensatory pathways. *Mol Genet Metab, 114*(1), 55-61. doi:10.1016/j.ymgme.2014.11.001

Gilbert, H. J., Lowe, C. R., & Drabble, W. T. (1979). Inosine 5'-monophosphate dehydrogenase of Escherichia coli. Purification by affinity chromatography, subunit structure and inhibition by guanosine 5'-monophosphate. *Biochem J, 183*(3), 481-494.

Gou, K. M., Chang, C. C., Shen, Q. J., Sung, L. Y., & Liu, J. L. (2014). CTP synthase forms cytoophidia in the cytoplasm and nucleus. *Exp Cell Res, 323*(1), 242-253. doi:10.1016/j.yexcr.2014.01.029

Gumienny, T. L., Brugnera, E., Tosello-Trampont, A. C., Kinchen, J. M., Haney, L. B., Nishiwaki, K., Walk, S. F., Nemergut, M. E., Macara, I. G., Francis, R., Schedl, T., Qin, Y., Van Aelst, L., Hengartner, M. O., & Ravichandran, K. S. (2001). CED-12/ELMO, a novel member of the CrkII/Dock180/Rac pathway, is required for phagocytosis and cell migration. *Cell, 107*(1), 27-41.

Gunter, J. H., Thomas, E. C., Lengefeld, N., Kruger, S. J., Worton, L., Gardiner, E. M., Jones, A., Barnett, N. L., & Whitehead, J. P. (2008). Characterisation of inosine monophosphate dehydrogenase expression

during retinal development: differences between variants and isoforms. *Int J Biochem Cell Biol, 40*(9), 1716-1728. doi:10.1016/j.biocel.2007.12.018

Hebert, M. D., & Poole, A. R. (2017). Towards an understanding of regulating Cajal body activity by protein modification. *RNA Biol, 14*(6), 761-778. doi:10.1080/15476286.2016.1243649

Ingerson-Mahar, M., Briegel, A., Werner, J. N., Jensen, G. J., & Gitai, Z. (2010). The metabolic enzyme CTP synthase forms cytoskeletal filaments. *Nat Cell Biol, 12*(8), 739-746. doi:10.1038/ncb2087

Ismail, S. A., Chen, Y. X., Rusinova, A., Chandra, A., Bierbaum, M., Gremer, L., Triola, G., Waldmann, H., Bastiaens, P. I., & Wittinghofer, A. (2011). Arl2-GTP and Arl3-GTP regulate a GDI-like transport system for farnesylated cargo. *Nat Chem Biol, 7*(12), 942-949. doi:10.1038/nchembio.686

Ivanova, A. A., East, M. P., Yi, S. L., & Kahn, R. A. (2014). Characterization of recombinant ELMOD (cell engulfment and motility domain) proteins as GTPase-activating proteins (GAPs) for ARF family GTPases. *J Biol Chem, 289*(16), 11111-11121. doi:10.1074/jbc.M114.548529

Jaiswal, M., Fansa, E. K., Kösling, S. K., Mejuch, T., Waldmann, H., & Wittinghofer, A. (2016). Novel biochemical and structural insights into the interaction of myristoylated cargo with Unc119 and their release by Arl2/3. *Journal of Biological Chemistry*. doi:10.1074/jbc.M116.741827

Ji, Y., Gu, J., Makhov, A. M., Griffith, J. D., & Mitchell, B. S. (2006). Regulation of the interaction of inosine monophosphate dehydrogenase with mycophenolic Acid by GTP. *J Biol Chem, 281*(1), 206-212. doi:10.1074/jbc.M507056200

Juda, P., Smigova, J., Kovacik, L., Bartova, E., & Raska, I. (2014). Ultrastructure of cytoplasmic and nuclear inosine-5'-monophosphate dehydrogenase 2 "rods and rings" inclusions. *J Histochem Cytochem, 62*(10), 739-750. doi:10.1369/0022155414543853

Keppeke, G. D., Andrade, L. E., Grieshaber, S. S., & Chan, E. K. (2015). Microinjection of specific anti-IMPDH2 antibodies induces disassembly of cytoplasmic rods/rings that are primarily stationary and stable structures. *Cell Biosci, 5*(1), 1. doi:10.1186/2045-3701-5-1

Keppeke, G. D., Calise, S. J., Chan, E. K., & Andrade, L. E. (2015). Assembly of IMPDH2-based, CTPS-based, and mixed rod/ring structures is dependent on cell type and conditions of induction. *J Genet Genomics, 42*(6), 287-299. doi:10.1016/j.jgg.2015.04.002

Keppeke, G. D., Chang, C. C., Peng, M., Chen, L. Y., Lin, W. C., Pai, L. M., Andrade, L. E. C., Sung, L. Y., & Liu, J. L. (2018). IMP/GTP balance modulates cytoophidium assembly and IMPDH activity. *Cell Div, 13*, 5. doi:10.1186/s13008-018-0038-0

Keppeke, G. D., Nunes, E., Ferraz, M. L., Silva, E. A., Granato, C., Chan, E. K., & Andrade, L. E. (2012). Longitudinal study of a human drug-induced model of autoantibody to cytoplasmic rods/rings following HCV therapy with ribavirin and interferon-alpha. *PLoS One, 7*(9), e45392. doi:10.1371/journal.pone.0045392

Keppeke, G. D., Prado, M. S., Nunes, E., Perazzio, S. F., Rodrigues, S. H., Ferraz, M. L., Chan, E. K., & Andrade, L. E. (2016). Differential capacity of therapeutic drugs to induce Rods/Rings structures in vitro and in vivo and generation of anti-Rods/Rings autoantibodies. *Clin Immunol, 173*, 149-156. doi:10.1016/j.clim.2016.10.004

Klinger, C. M., Spang, A., Dacks, J. B., & Ettema, T. J. (2016). Tracing the Archaeal Origins of Eukaryotic Membrane-Trafficking System Building Blocks. *Mol Biol Evol, 33*(6), 1528-1541. doi:10.1093/molbev/msw034

Laderoute, K. R., Amin, K., Calaoagan, J. M., Knapp, M., Le, T., Orduna, J., Foretz, M., & Viollet, B. (2006). 5'-AMP-activated protein kinase (AMPK) is induced by low-oxygen and glucose deprivation

conditions found in solid-tumor microenvironments. *Mol Cell Biol, 26*(14), 5336-5347. doi:10.1128/mcb.00166-06

Li, Y., Kelly, W. G., Logsdon, J. M., Jr., Schurko, A. M., Harfe, B. D., Hill-Harfe, K. L., & Kahn, R. A. (2004). Functional genomic analysis of the ADP-ribosylation factor family of GTPases: phylogeny among diverse eukaryotes and function in C. elegans. *FASEB J, 18*(15), 1834-1850. doi:10.1096/fj.04-2273com

Liu, F., Jin, R., Liu, X., Huang, H., Wilkinson, S. C., Zhong, D., Khuri, F. R., Fu, H., Marcus, A., He, Y., & Zhou, W. (2016). LKB1 promotes cell survival by modulating TIF-IA-mediated pre-ribosomal RNA synthesis under uridine downregulated conditions. *Oncotarget, 7*(3), 2519-2531. doi:10.18632/oncotarget.6224

Liu, J. L. (2011). The enigmatic cytoophidium: compartmentation of CTP synthase via filament formation. *Bioessays, 33*(3), 159-164. doi:10.1002/bies.201000129

Liu, J. L. (2016). The Cytoophidium and Its Kind: Filamentation and Compartmentation of Metabolic Enzymes. *Annu Rev Cell Dev Biol, 32*, 349-372. doi:10.1146/annurev-cellbio-111315-124907

Logsdon, J., J. M., & Kahn, R. A. (2004). The Arf Family Tree. In R. A. Kahn (Ed.), *Arf Family GTPases* (pp. 1-22). Dordrecht: Kluwer Academic Publishers.

Luo, Y., Na, Z., & Slavoff, S. A. (2018). P-Bodies: Composition, Properties, and Functions. *Biochemistry, 57*(17), 2424-2431. doi:10.1021/acs.biochem.7b01162

McPhillips, C. C., Hyle, J. W., & Reines, D. (2004). Detection of the mycophenolate-inhibited form of IMP dehydrogenase in vivo. *Proc Natl Acad Sci U S A, 101*(33), 12171-12176. doi:10.1073/pnas.0403341101

Muromoto, R., Sekine, Y., Imoto, S., Ikeda, O., Okayama, T., Sato, N., & Matsuda, T. (2008). BART is essential for nuclear retention of STAT3. *Int Immunol, 20*(3), 395-403. doi:10.1093/intimm/dxm154

Newman, L. E., Schiavon, C. R., Turn, R. E., & Kahn, R. A. (2017). The ARL2 GTPase regulates mitochondrial fusion from the intermembrane space. *Cell Logist, 7*(3), e1340104. doi:10.1080/21592799.2017.1340104

Newman, L. E., Schiavon, C. R., Zhou, C., & Kahn, R. A. (2017). The abundance of the ARL2 GTPase and its GAP, ELMOD2, at mitochondria are modulated by the fusogenic activity of mitofusins and stressors. *PLoS One, 12*(4), e0175164. doi:10.1371/journal.pone.0175164

Newman, L. E., Zhou, C. J., Mudigonda, S., Mattheyses, A. L., Paradies, E., Marobbio, C. M., & Kahn, R. A. (2014). The ARL2 GTPase is required for mitochondrial morphology, motility, and maintenance of ATP levels. *PLoS One, 9*(6), e99270. doi:10.1371/journal.pone.0099270

Noble, J. W., Hunter, D. V., Roskelley, C. D., Chan, E. K., & Mills, J. (2016). Loukoumasomes Are Distinct Subcellular Structures from Rods and Rings and Are Structurally Associated with MAP2 and the Nuclear Envelope in Retinal Cells. *PLoS One, 11*(10), e0165162. doi:10.1371/journal.pone.0165162

Noree, C., Sato, B. K., Broyer, R. M., & Wilhelm, J. E. (2010). Identification of novel filament-forming proteins in Saccharomyces cerevisiae and Drosophila melanogaster. *J Cell Biol, 190*(4), 541-551. doi:10.1083/jcb.201003001

Nunez Villacis, L., Wong, M. S., Ferguson, L. L., Hein, N., George, A. J., & Hannan, K. M. (2018). New Roles for the Nucleolus in Health and Disease. *Bioessays, 40*(5), e1700233. doi:10.1002/bies.201700233

Pinkus, L. M. (1977). Glutamine binding sites. *Methods Enzymol, 46*, 414-427.

Ramer, M. S., Cruz Cabrera, M. A., Alan, N., Scott, A. L., & Inskip, J. A. (2010). A new organellar complex in rat sympathetic neurons. *PLoS One, 5*(5), e10872. doi:10.1371/journal.pone.0010872

Rizzo, R., Parashuraman, S., Mirabelli, P., Puri, C., Lucocq, J., & Luini, A. (2013). The dynamics of engineered resident proteins in the mammalian Golgi complex relies on cisternal maturation. *J Cell Biol, 201*(7), 1027-1036. doi:10.1083/jcb.201211147

Ruscher, K., & Wieloch, T. (2015). The involvement of the sigma-1 receptor in neurodegeneration and neurorestoration. *J Pharmacol Sci, 127*(1), 30-35. doi:10.1016/j.jphs.2014.11.011

Russell, R. R., 3rd, Bergeron, R., Shulman, G. I., & Young, L. H. (1999). Translocation of myocardial GLUT-4 and increased glucose uptake through activation of AMPK by AICAR. *Am J Physiol, 277*(2 Pt 2), H643-649.

Seelig, H. P., Appelhans, H., Bauer, O., Bluthner, M., Hartung, K., Schranz, P., Schultze, D., Seelig, C. A., & Volkmann, M. (2011). Autoantibodies against inosine-5'-monophosphate dehydrogenase 2--characteristics and prevalence in patients with HCV-infection. *Clin Lab, 57*(9-10), 753-765.

Sharer, J. D., & Kahn, R. A. (1999). The ARF-like 2 (ARL2)-binding protein, BART. Purification, cloning, and initial characterization. *J Biol Chem, 274*(39), 27553-27561.

Sharer, J. D., Shern, J. F., Van Valkenburgh, H., Wallace, D. C., & Kahn, R. A. (2002). ARL2 and BART enter mitochondria and bind the adenine nucleotide transporter. *Mol Biol Cell, 13*(1), 71-83. doi:10.1091/mbc.01-05-0245

Shern, J. F., Sharer, J. D., Pallas, D. C., Bartolini, F., Cowan, N. J., Reed, M. S., Pohl, J., & Kahn, R. A. (2003). Cytosolic Arl2 is complexed with cofactor D and protein phosphatase 2A. *J Biol Chem, 278*(42), 40829-40836. doi:10.1074/jbc.M308678200

Suzuki, M., Murakami, T., Cheng, J., Kano, H., Fukata, M., & Fujimoto, T. (2015). ELMOD2 is anchored to lipid droplets by palmitoylation and regulates adipocyte triglyceride lipase recruitment. *Mol Biol Cell, 26*(12), 2333-2342. doi:10.1091/mbc.E14-11-1504

Thomas, E. C., Gunter, J. H., Webster, J. A., Schieber, N. L., Oorschot, V., Parton, R. G., & Whitehead, J. P. (2012). Different characteristics and nucleotide binding properties of inosine monophosphate dehydrogenase (IMPDH) isoforms. *PLoS One, 7*(12), e51096. doi:10.1371/journal.pone.0051096

Tian, G., Huang, Y., Rommelaere, H., Vandekerckhove, J., Ampe, C., & Cowan, N. J. (1996). Pathway leading to correctly folded beta-tubulin. *Cell, 86*(2), 287-296.

Tsai, Y. L., Ha, D. P., Zhao, H., Carlos, A. J., Wei, S., Pun, T. K., Wu, K., Zandi, E., Kelly, K., & Lee, A. S. (2018). Endoplasmic reticulum stress activates SRC, relocating chaperones to the cell surface where GRP78/CD109 blocks TGF-beta signaling. *Proc Natl Acad Sci U S A.* doi:10.1073/pnas.1714866115

Van Valkenburgh, H., Shern, J. F., Sharer, J. D., Zhu, X., & Kahn, R. A. (2001). ADP-ribosylation factors (ARFs) and ARF-like 1 (ARL1) have both specific and shared effectors: characterizing ARL1-binding proteins. *J Biol Chem, 276*(25), 22826-22837. doi:10.1074/jbc.M102359200

Watzlich, D., Vetter, I., Gotthardt, K., Miertzschke, M., Chen, Y. X., Wittinghofer, A., & Ismail, S. (2013). The interplay between RPGR, PDEdelta and Arl2/3 regulate the ciliary targeting of farnesylated cargo. *EMBO Rep, 14*(5), 465-472. doi:10.1038/embor.2013.37

Whitby, F. G., Luecke, H., Kuhn, P., Somoza, J. R., Huete-Perez, J. A., Phillips, J. D., Hill, C. P., Fletterick, R. J., & Wang, C. C. (1997). Crystal structure of Tritrichomonas foetus inosine-5'-monophosphate dehydrogenase and the enzyme-product complex. *Biochemistry, 36*(35), 10666-10674. doi:10.1021/bi9708850

Wiest, D. L., Bhandoola, A., Punt, J., Kreibich, G., McKean, D., & Singer, A. (1997). Incomplete endoplasmic reticulum (ER) retention in immature thymocytes as revealed by surface expression of "ER-resident" molecular chaperones. *Proc Natl Acad Sci U S A, 94*(5), 1884-1889.

Wiest, D. L., Burgess, W. H., McKean, D., Kearse, K. P., & Singer, A. (1995). The molecular chaperone calnexin is expressed on the surface of immature thymocytes in association with clonotype-independent CD3 complexes. *Embo J, 14*(14), 3425-3433.

Willingham, M. C., Richert, N. D., & Rutherford, A. V. (1987). A novel fibrillar structure in cultured cells detected by a monoclonal antibody. *Exp Cell Res, 171*(2), 284-295.

Zhang, T., Li, S., Zhang, Y., Zhong, C., Lai, Z., & Ding, J. (2009). Crystal structure of the ARL2-GTP-BART complex reveals a novel recognition and binding mode of small GTPase with effector. *Structure, 17*(4), 602-610. doi:10.1016/j.str.2009.01.014

Zhou, C., Cunningham, L., Marcus, A. I., Li, Y., & Kahn, R. A. (2006). Arl2 and Arl3 regulate different microtubule-dependent processes. *Mol Biol Cell, 17*(5), 2476-2487. doi:10.1091/mbc.E05-10-0929

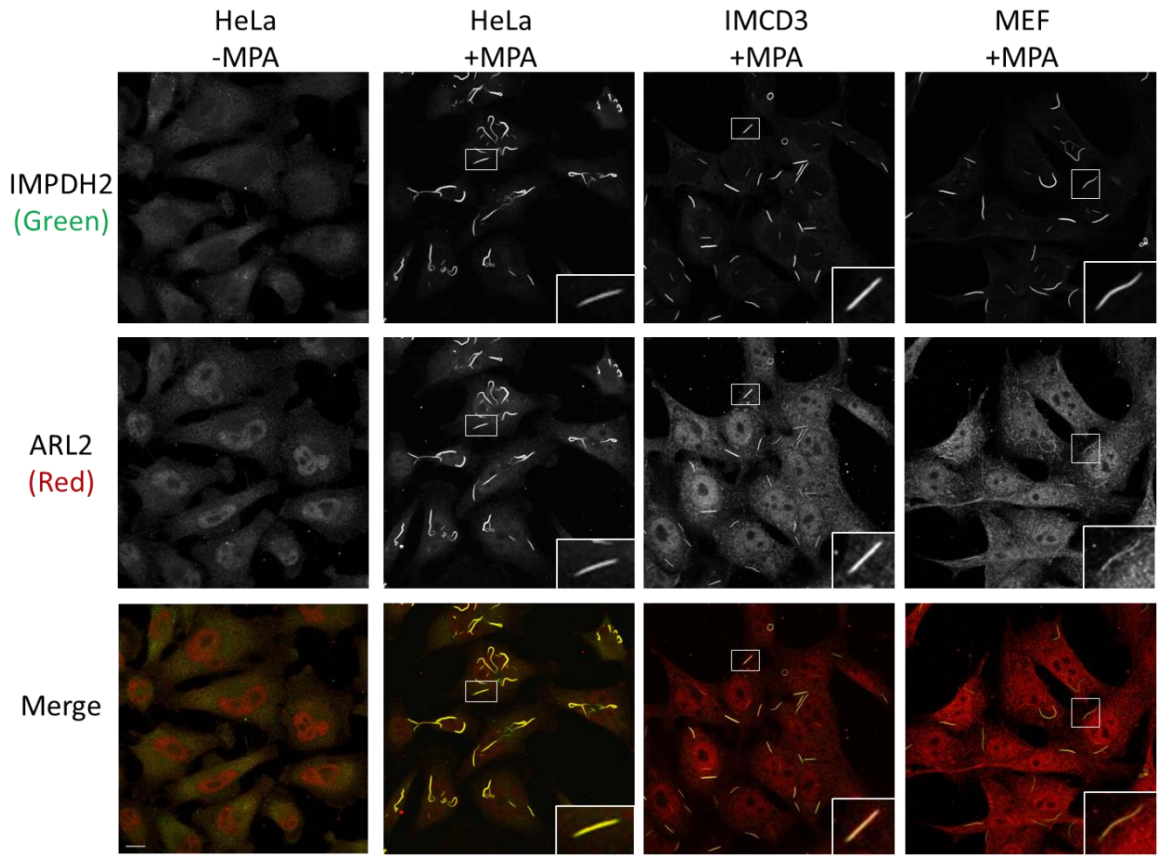

Figure 1: ARL2 localizes to IMPDH2-positive structures that are inducible with MPA. HeLa (first two columns), IMCD3 (third column), and MEF (last column) cell lines were treated with either vehicle control (-MPA) or 1 μM MPA (+MPA) for 4 hr. Cells were then fixed and co-stained for IMPDH2 (top row) and ARL2 (middle row), as described under Methods. 2D projections of z-stacks are shown. Scale bar in lower left panel = 10 μm and is the same for each image. Insets show zoomed-in versions of individual rods.

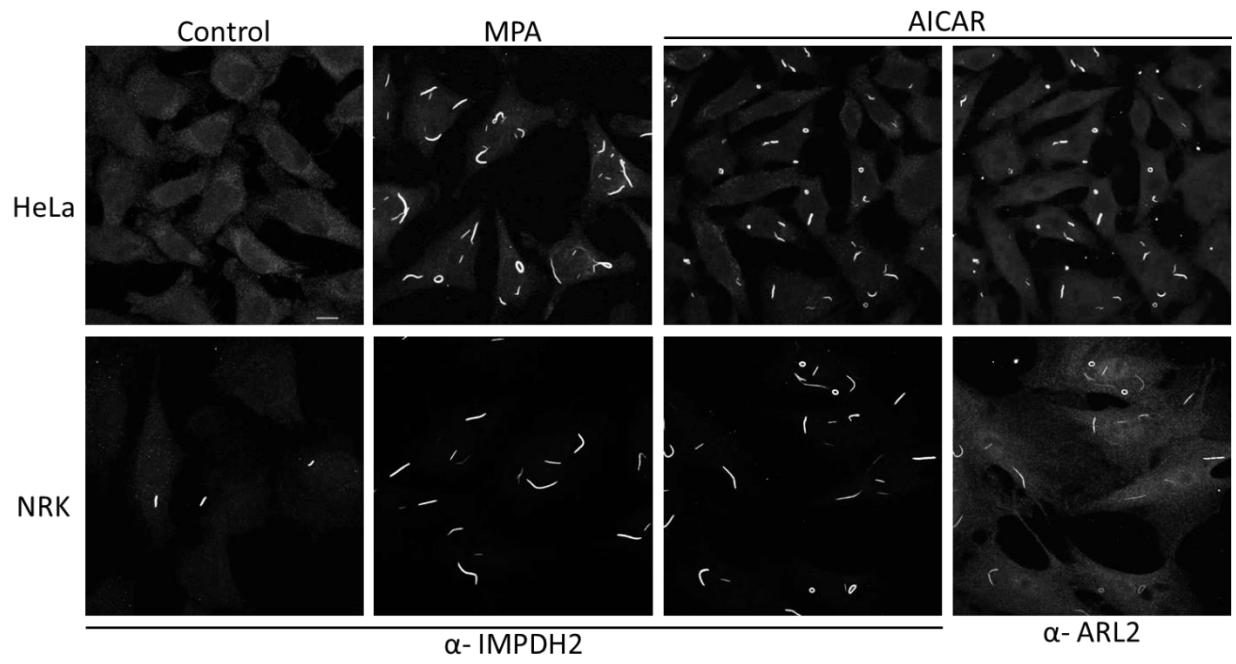

Figure 2: AICAR induces RR formation. HeLa (top row) or NRK (bottom row) cells were treated with either vehicle control (left-most column), 1 μM MPA (second column), or 1 mM AICAR (right two columns) for 2 hr. Cells were then fixed and co-stained for IMPDH2 and ARL2. Only the IMPDH2 staining is shown in the two left-most columns, while both IMPDH2 (third column) and ARL2 (fourth column) co-staining are shown on the two columns to the right. 2D projections of z-stacks are shown. Scale bar = 10 μm.

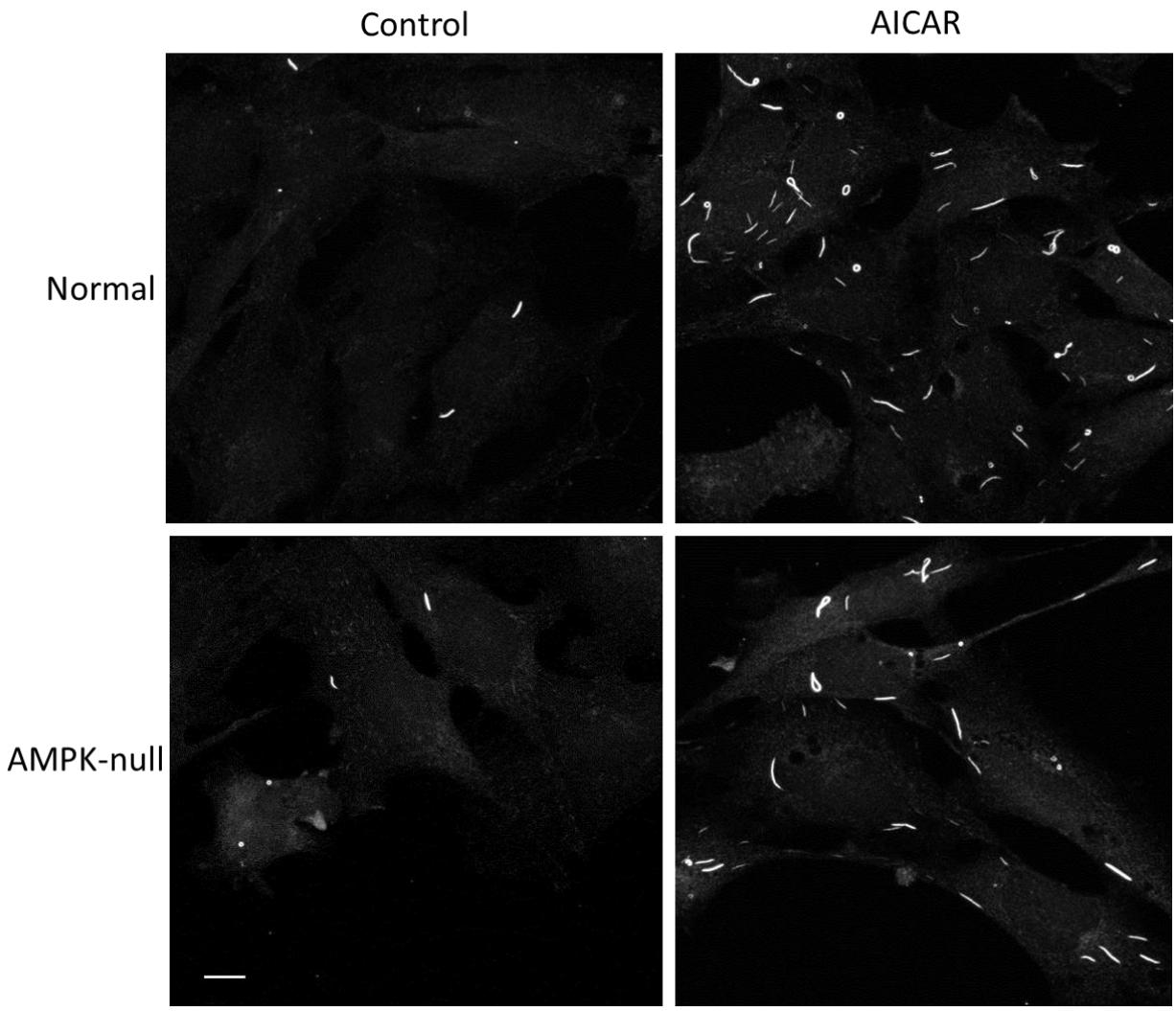

Figure 3: AICAR is capable of inducing RR formation in AMPK-null MEFs. AMPK-null MEFs (bottom) and paired control MEFs (top) were treated with vehicle control (left) or 1 mM AICAR (right) for 2 hr. Cells were then fixed and stained for IMPDH2. 2D-projections of z-stacks are shown. Scale bar = 10 μm.

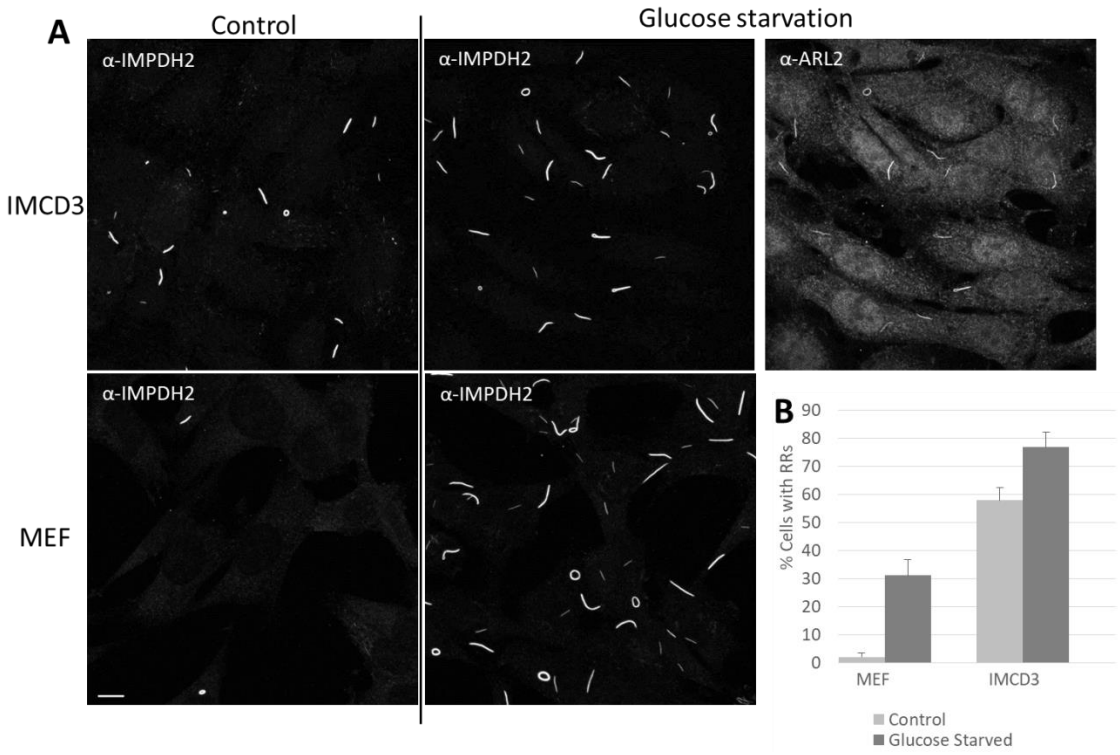

Figure 4: Glucose starvation increases the percentage of cells with RRs. (**A**) IMCD3 (top row) or MEF (bottom row) cell lines were grown in either normal medium (left) or glucose-free medium (middle) for 24 hr. Cells were then fixed and co-stained for IMPDH2 (left and middle) and ARL2 (right). 2D projections of z-stacks are shown. Scale bar = 10 μm. (**B**) Cells treated as described in A were scored for the presence of RRs. The percentage of cells with at least one RR is shown. N=200 for each cell line and condition. Scale bars represent standard deviation of two independent experiments.

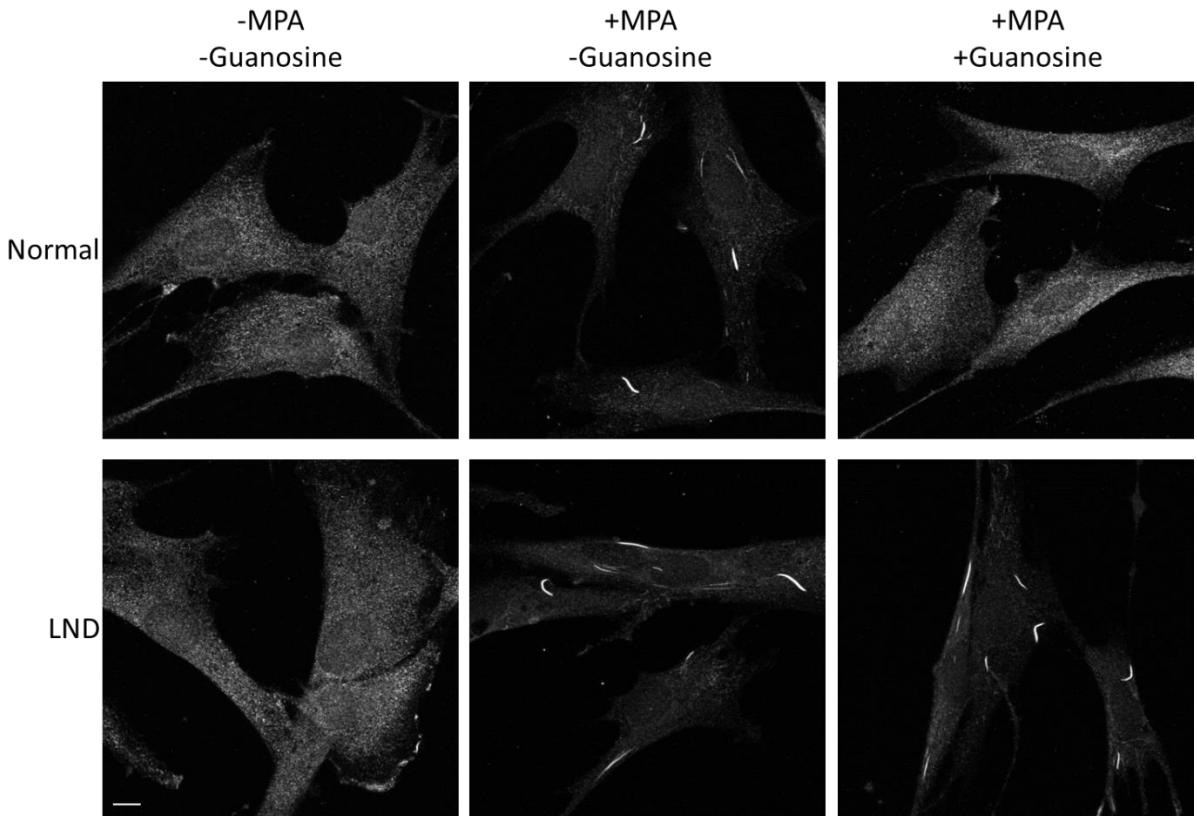

Figure 5: Guanosine does not prevent RR formation in LND fibroblasts. Normal human fibroblasts (top) and fibroblasts derived from patients with LND (bottom) were treated with vehicle control (left), 1 μM MPA (middle), or 1 μM MPA + 1 mM guanosine (right) for 4 hr. Cells were then fixed and stained for IMPDH2. 2D-projections of z-stacks are shown. Scale bar = 10 μm.

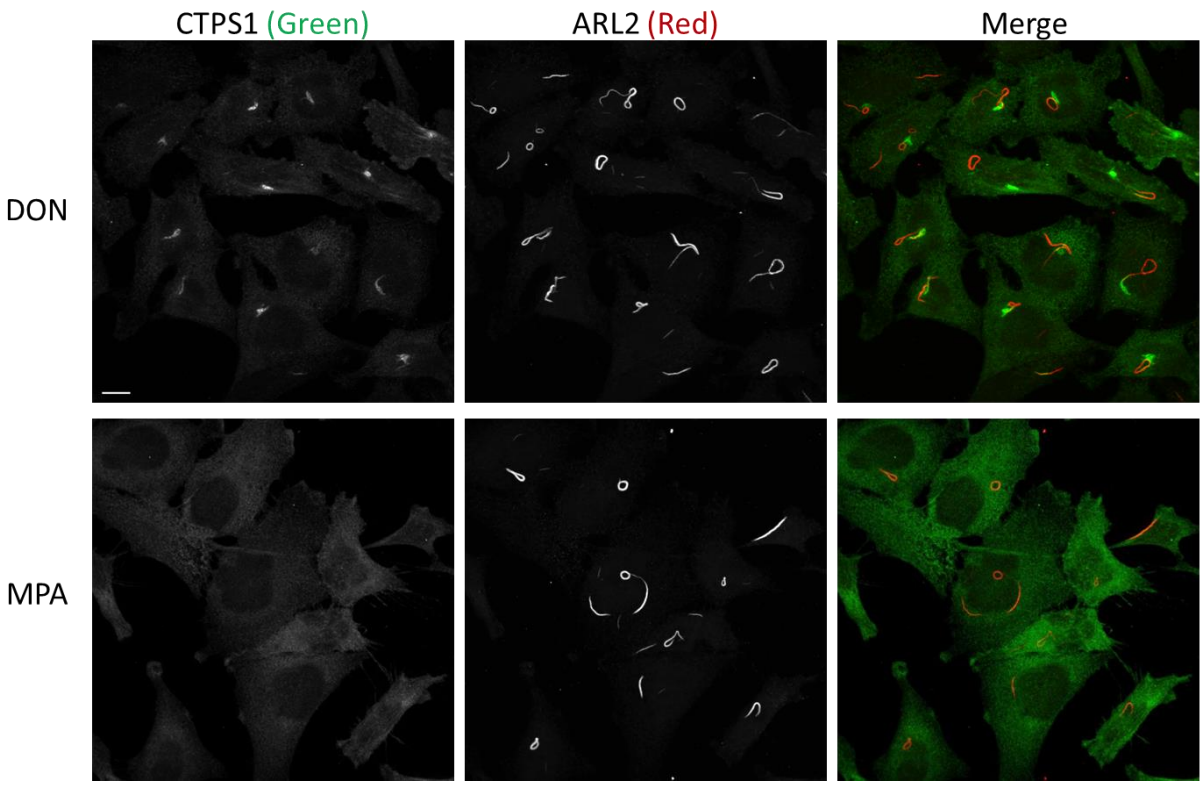

Figure 6: ARL2 does not localize to CTPS1-positive structures which are induced with DON but does co-localize with IMPDH2-positive RRs. HeLa cells were treated with either 100 μM DON (top) or 1 μM MPA (bottom) for 24 hr. Cells were then fixed and co-stained for CTPS1 (left) and ARL2 (middle). 2D projections of z-stacks are shown. Scale bar = 10 μm.

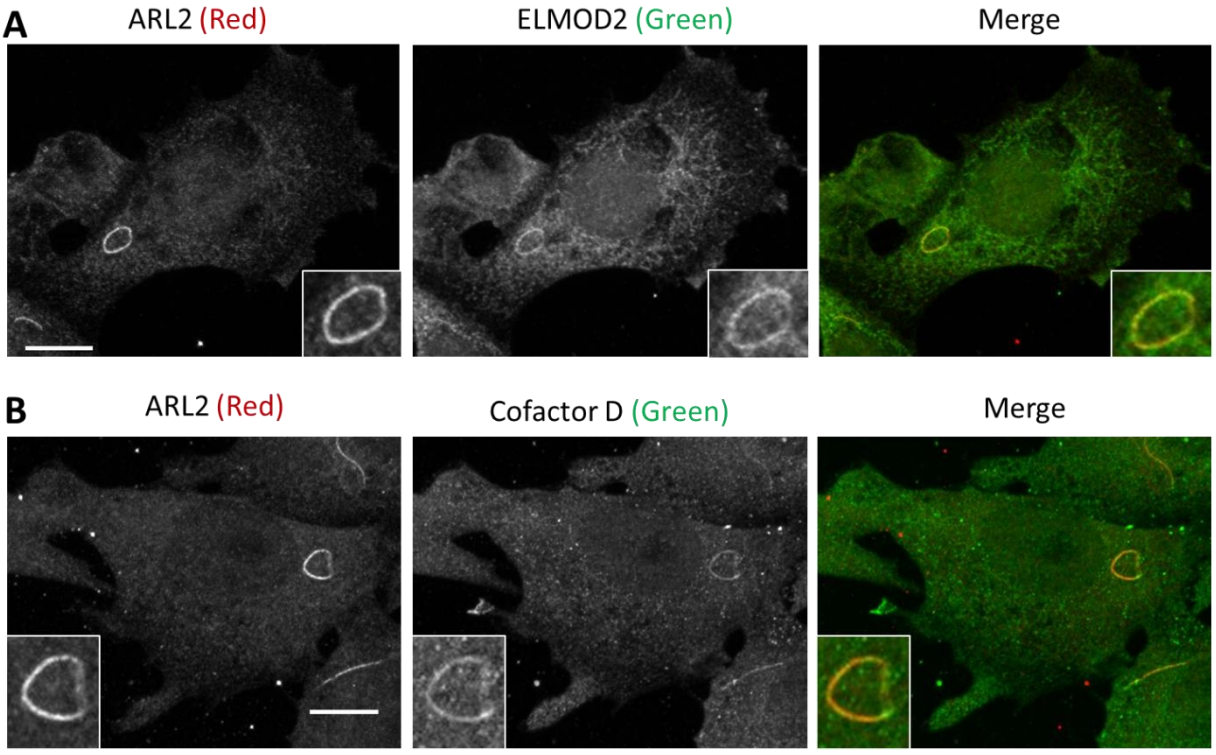

Figure 7: A subset of ARL2 binding partners localize to RRs. (**A**) MEFs were grown under glucose-starvation conditions for 48 hr, then fixed and co-stained for ARL2 (left) and ELMOD2 (middle). (**B**) MEFs were treated with 1 μM MPA for 2 hr, then fixed and co-stained for ARL2 (left) and Cofactor D (middle). In each case, 2D projections of z-stacks are shown. Scale bar = 10 μm. Insets show zoomed-in versions of individual rings.

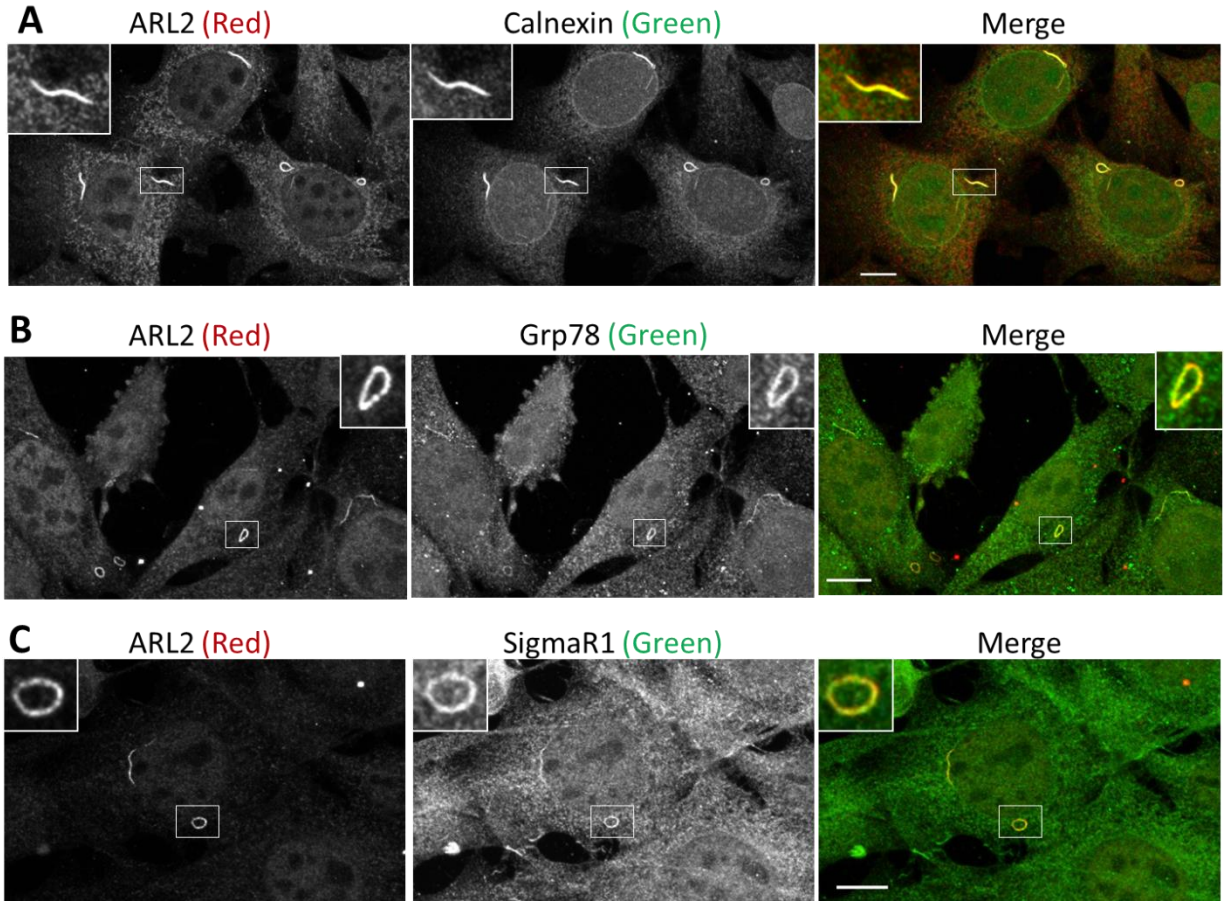

Figure 8: Three different ER membrane proteins also co-localize with RRs. MEFs were grown under glucose starvation conditions for 24 hr, then fixed and co-stained for ARL2 (left) and (**A**) calnexin (top middle), (**B**) GRP78 (middle) or (**C**) SigmaR1 (bottom middle). 2D projections of z-stacks are shown. Scale bar = 10 μm. Insets show zoomed-in versions of individual rods for A and rings for B and C.

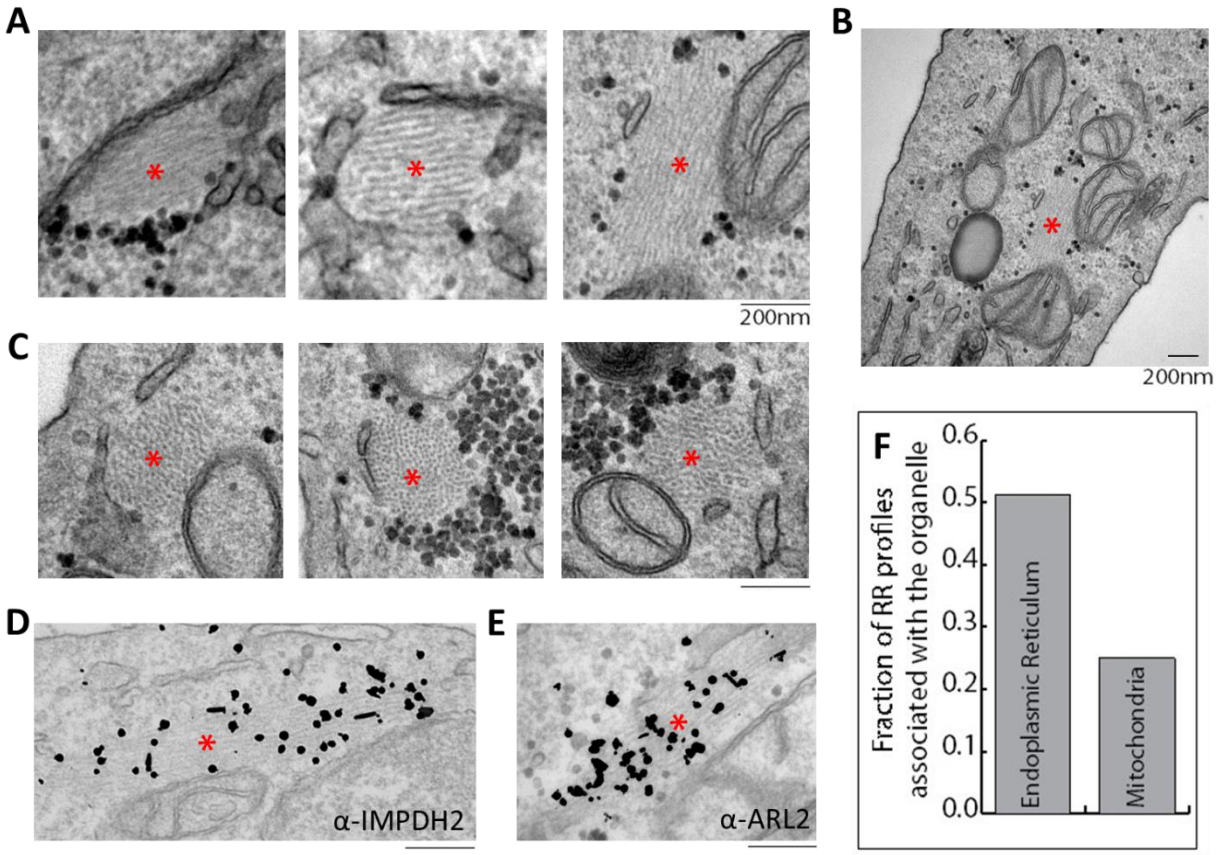

Figure 9: The filamentous nature of RRs is evident by EM staining and ARL2 and IMPDH2 co-localize to RRs as seen by immunogold staining. HeLa cells were induced with 1 μM MPA for 2 hr and processed for EM, as described under Methods. All scale bars = 200nm. (**A**) Longitudinal sections of RRs. The RRs are indicated by an asterisk (*). (**B**) A zoomed-out image of the RR shown in the far-right image from A. (**C**) Transverse sections of RRs. Labelling scheme is the same as A. (**D**) Immuno-EM showing localization of IMPDH2 using IMPDH2 antibody coupled to nanogold particles. The asterisk marks the RR while the black particles indicate the IMPDH2 localization. (**E**) Same as D except using ARL2 antibody to show localization of ARL2. (**F**) The fraction of RRs that were associated with the ER or mitochondrial membranes were counted in randomly acquired EM images of the RRs and plotted. N=45.

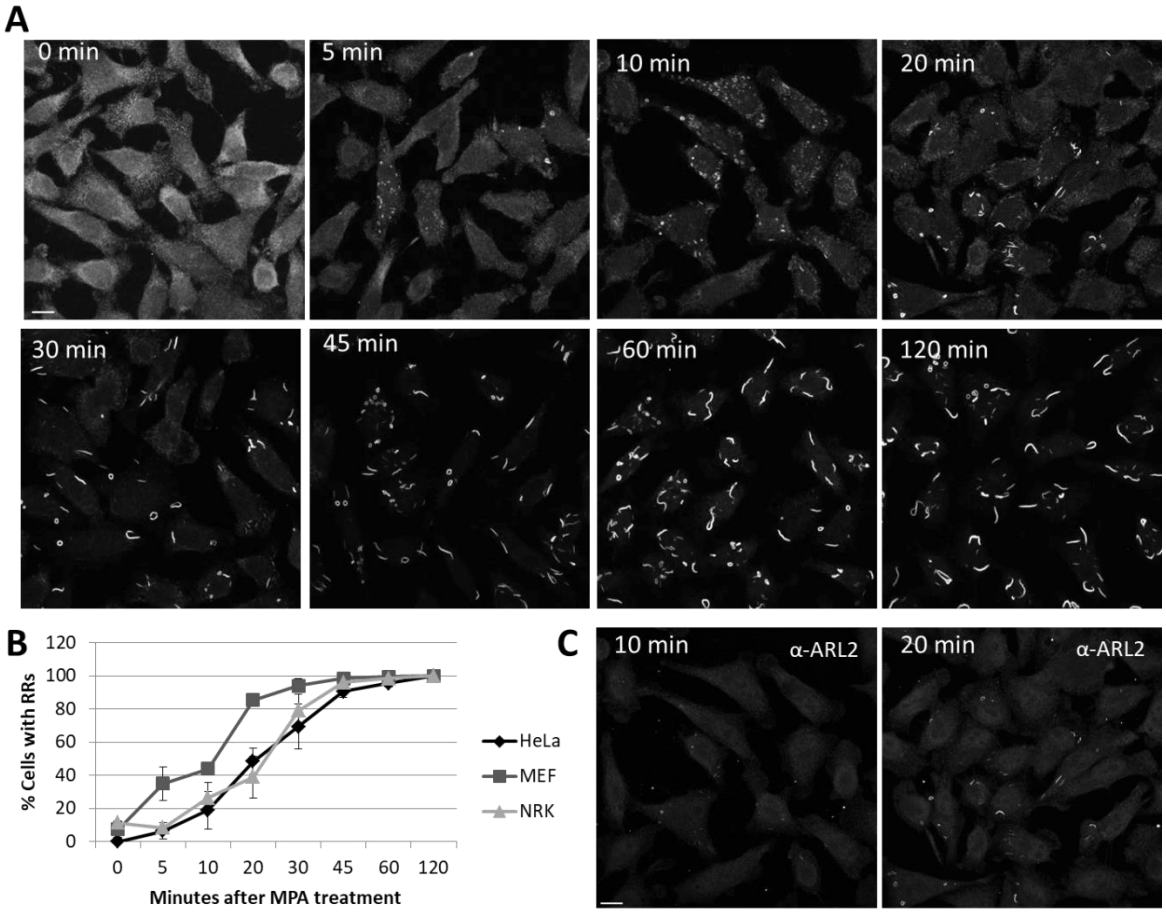

Figure 10: RRs increase in size and quantity over time after induction with MPA. HeLa, MEF, or NRK cells (HeLa cells are pictured) were fixed at the times shown after addition of MPA (1 μM). Cells were then co-stained for IMPDH2 and ARL2. (**A**) IMPDH2 staining is shown. Images were collected and processed identically at every step for each time-point. 2D projections of z-stacks are shown. Scale bar = 10 μm. (**B**) Cells treated as described in A were scored for the presence of RRs based on IMPDH2 staining. The percentage of cells with at least one RR is shown. N=100 for each time-point and cell line. Error bars represent standard deviation between two independent experiments. (**C**) ARL2 staining is shown at the 10 and 20 min time-points (same fields shown in panel A). 2D projections of z-stacks are shown. Scale bar = 10 μm.

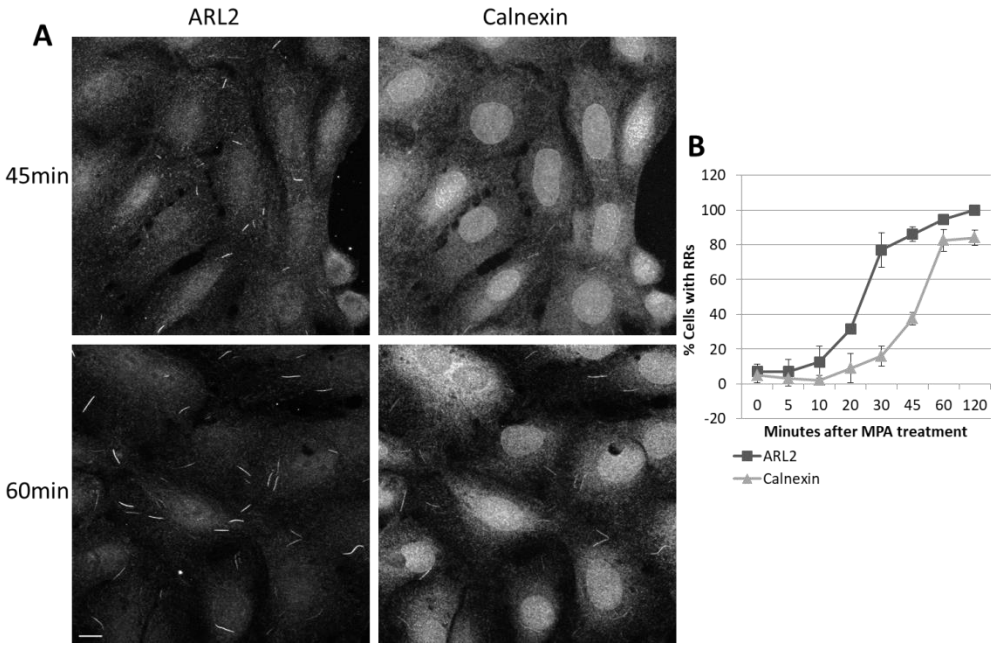

Figure 11: Calnexin recruits to RRs well after IMPDH2 and ARL2. (**A**) HeLa, MEF, or NRK cells (NRK cells are pictured) were fixed at different times after addition of MPA (1 μM). Cells were then co-stained for ARL2 and calnexin, as described under Methods. ARL2 (left) and calnexin (right) at 45 min (top) and 60 min (bottom) are shown. 2D projections of z-stacks are shown. Scale bar = 10 μm. (**B**) NRK cells treated as described in A were scored for the presence of RRs based on ARL2 or calnexin staining. The percentage of cells with at least one RR is shown. N=100 for each time-point. Error bars represent standard deviation between two independent experiments.

Table I: Summary of results from multiple different cell lines and their responses to different inducers of RRs, reversal by guanosine, and co-localization of different antigens with IMPDH2 or ARL2. Conditions of cell culture or the antibodies used in double labeling are shown on the left. Cell lines are listed along the top. A plus (+) indicates the presence of RRs or co-localization at RRs, additional plus signs (+++) indicates a stronger signal than seen in other cells, and a minus sign (-) indicates the absence of RRs or of co-localization at RRs. For RR co-localization, the inducer that leads to the strongest staining intensity is indicated in parentheses. ND = not done. Citations to relevant literature are included in the right most column.

	Cell lines									
Conditions and antigens tested	**HeLa**	**MEF**	**NRK**	**IMCD3**	**hFB**	**hFB - LND**	**MDCK**	**NIH3T3**	**COS7**	**Relevant literature**
RRs present without inducers	-	+	+	+++	-	-	+++	+	-	(Willingham et al., 1987; Gunter et al., 2008; Ramer et al., 2010; W. C. Carcamo et al., 2011; Chang et al., 2015)
RRs induced by:										
MPA	+++	+++	++	+++	++	++	ND	ND	+	(Ji et al., 2006; Gunter et al., 2008; Thomas et al., 2012; Calise et al., 2014; Chang et al., 2015; Keppeke, Andrade, et al., 2015; Calise et al., 2016; Keppeke et al., 2016)
Glucose starvation	-	+++	+	++	-	-	++	+	-	(Noree et al., 2010)
AICAR	++	++	+++	+++	++	++	ND	ND	ND	
DON	+++	+++	++	++	++	++	ND	ND	ND	(W. C. Carcamo et al., 2011; Calise et al., 2014; Chang et al., 2015; Keppeke, Andrade, et al., 2015; Keppeke, Calise, et al., 2015)
Guanosine reversal	+++	+++	ND	+++	+++	-	ND	ND	ND	(Gunter et al., 2008; Calise et al., 2014; Keppeke, Calise, et al., 2015; Calise et al., 2016)
Co-localization at RRs:										
ARL2 (MPA)	+++	+	++	++	+++	+++	++	+	+++	
ELMOD2 (glucose starvation)	+	++	+	+	ND	ND	+	+	ND	
Cofactor D (MPA)	-	+	+	+	ND	ND	ND	ND	ND	
Calnexin (glucose starvation)	+	++	++	++	ND	ND	ND	ND	ND	
GRP78 (glucose starvation)	ND	++	ND	+	ND	ND	ND	ND	ND	
SigmaR1 (glucose starvation)	ND	++	ND	+	ND	ND	ND	ND	ND	
Sec61β (glucose starvation)	ND	ND	ND	+	ND	ND	ND	ND	ND	
CTPS1 (DON)	-	ND	+/-	+/-	ND	ND	ND	ND	ND	(W. C. Carcamo et al., 2011; Chang et al., 2015; Keppeke, Calise, et al., 2015)

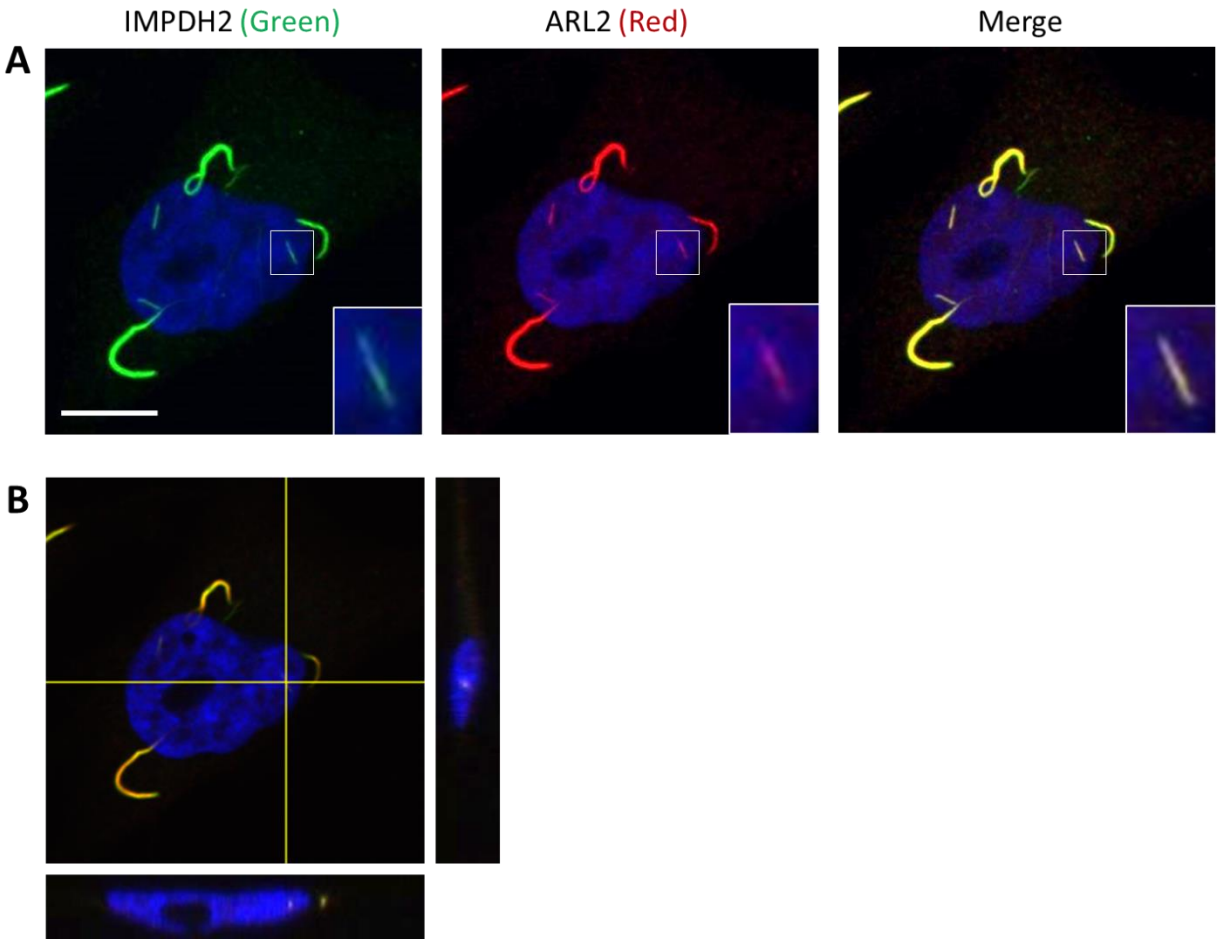

Figure S1: ARL2 localizes to nuclear RRs. (**A**) HeLa cells were treated with 1 µM MPA for 4 hr, fixed, and co-stained for IMPDH2 (green) and ARL2 (red). Cell nuclei were stained with Hoechst dye (blue). 2D projections of z-stacks are shown. Scale bar = 10 µm. Insets show one of several nuclear rods. (**B**) A single z-section of the merged image from A is shown accompanied by reconstructed x-z and y-z orthogonal sections showing the position of the nuclear rod in relation to the nuclear stain.

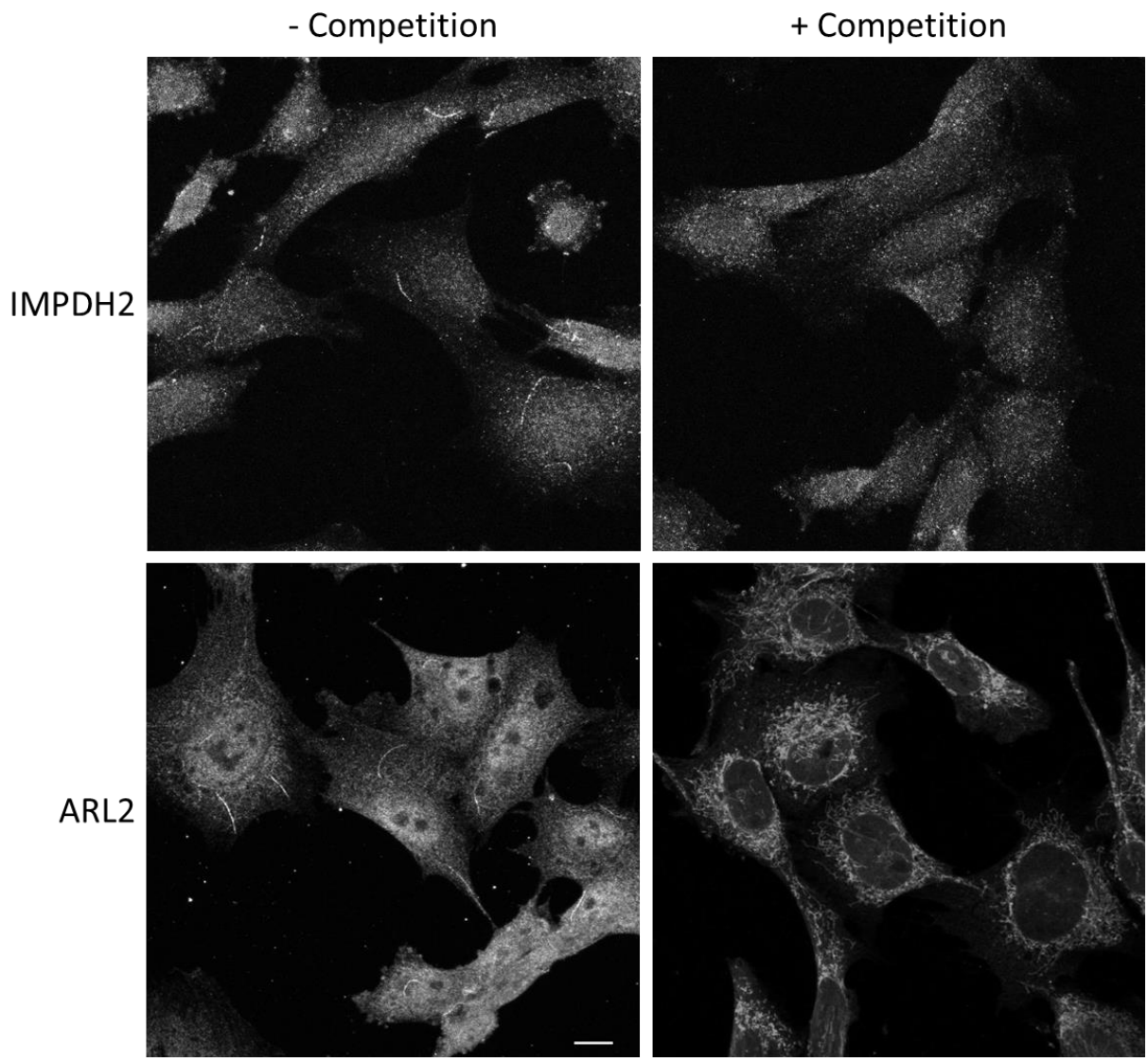

Figure S2: IMPDH2 and ARL2 staining at RRs is lost with antigen competition. MEFs were treated with 1 μM MPA for 2 hr, then fixed and stained. Antigen competition was performed as described under Methods. Top: cells were stained with IMPDH2 polyclonal antibody with (right) or without (left) pre-incubation with purified IMPDH2 protein. Bottom: cells were stained with ARL2 monoclonal antibody with (right) or without (left) pre-incubation with purified, recombinant ARL2. 2D-projections of z-stacks are shown. Scale bar = 10 μm.

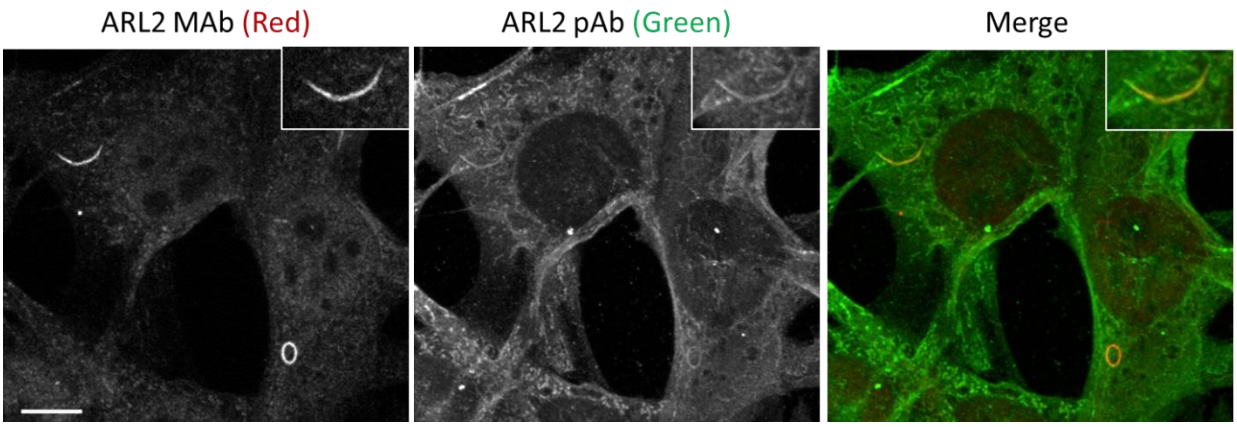

Figure S3: ARL2 monoclonal and polyclonal antibodies display different staining intensities for RRs and other organelles. MEFs were glucose-starved for 48 hr and co-stained with our mouse monoclonal ARL2 antibody (left) and our rabbit polyclonal ARL2 antibody (middle). 2D-projections of z-stacks are shown. Scale bar = 10 μm.

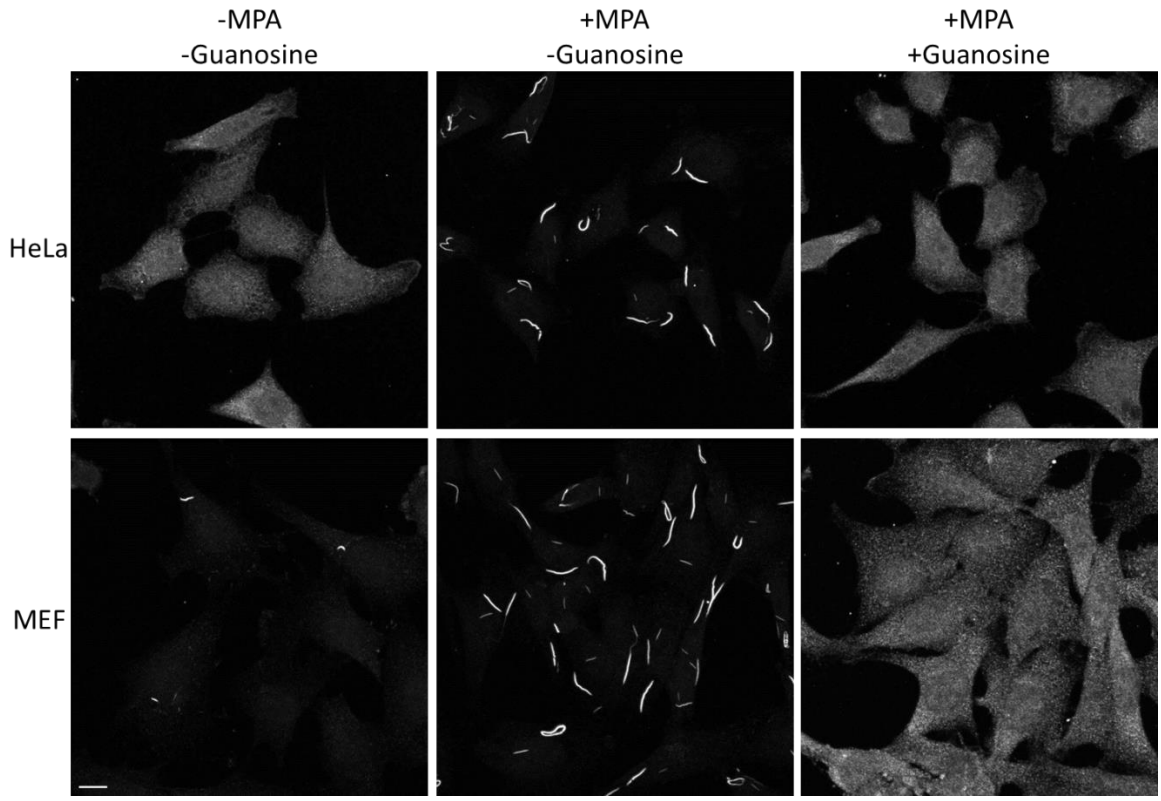

Figure S4: Guanosine prevents MPA-induced RR formation. HeLa cells (top) or MEFs (bottom) were incubated for 4 hr in either vehicle control (left), 1 µM MPA (middle), or 1 µM MPA + 1 mM guanosine (right). Cells were then fixed and stained for IMPDH2. 2D-projections of z-stacks are shown. Scale bar = 10 µm.

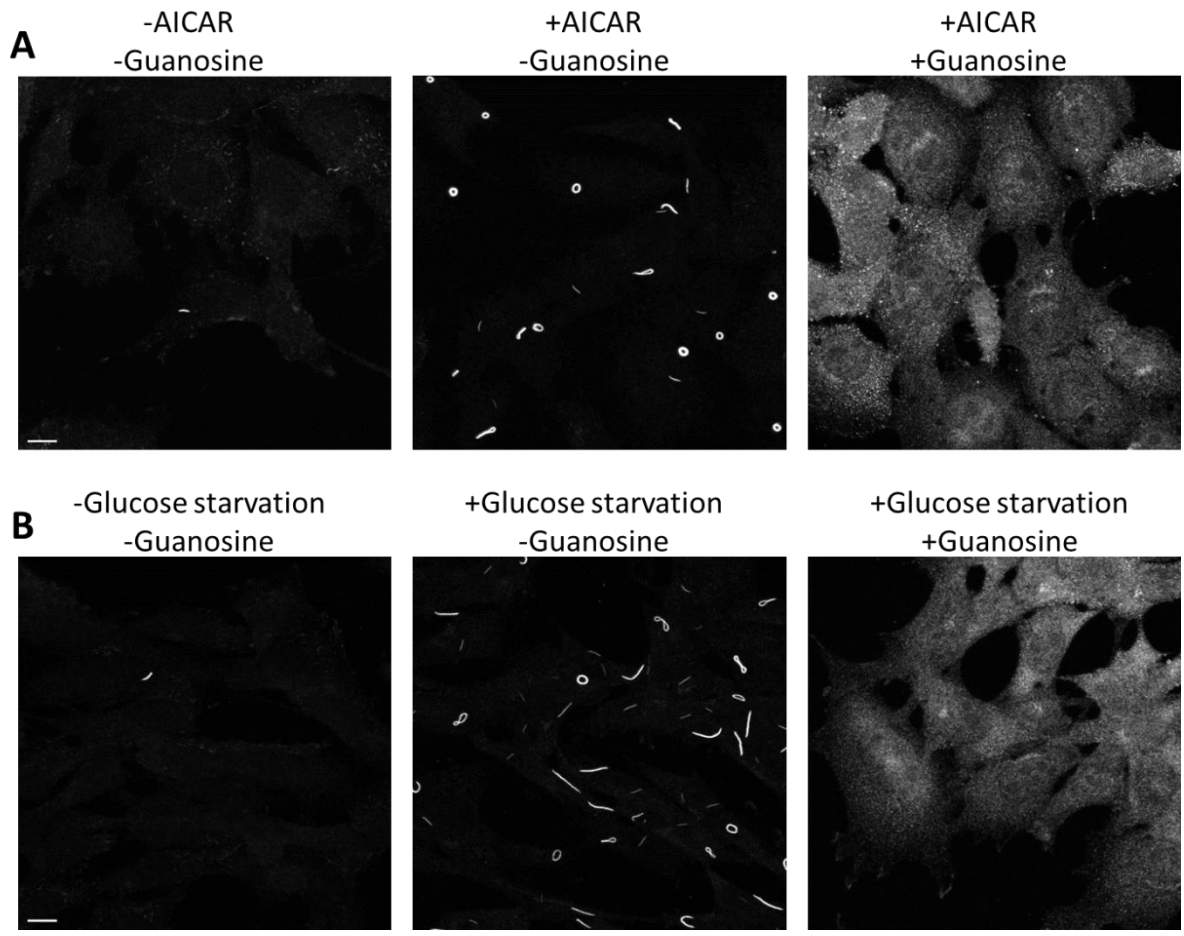

Figure S5: Guanosine reverses RR formation induced by AICAR or glucose-starvation. (**A**) MEFs were incubated in vehicle control for 22 hr (left), 1 mM AICAR for 22 hr (middle), or 1 mM AICAR for 18 hr followed by 1 mM AICAR + 1 mM guanosine for 4 hr (right). Cells were then fixed and stained for IMPDH2. 2D-projections of z-stacks are shown. Scale bar = 10 μm. (**B**) MEFs were incubated in normal medium for 22 hr (left), glucose-free medium for 22 hr (middle), or glucose-free medium for 18 hr followed by glucose-free medium + 1 mM guanosine for 4 hr (right). Cells were then fixed and stained for IMPDH2. 2D-projections of z-stacks are shown. Scale bar = 10 μm.

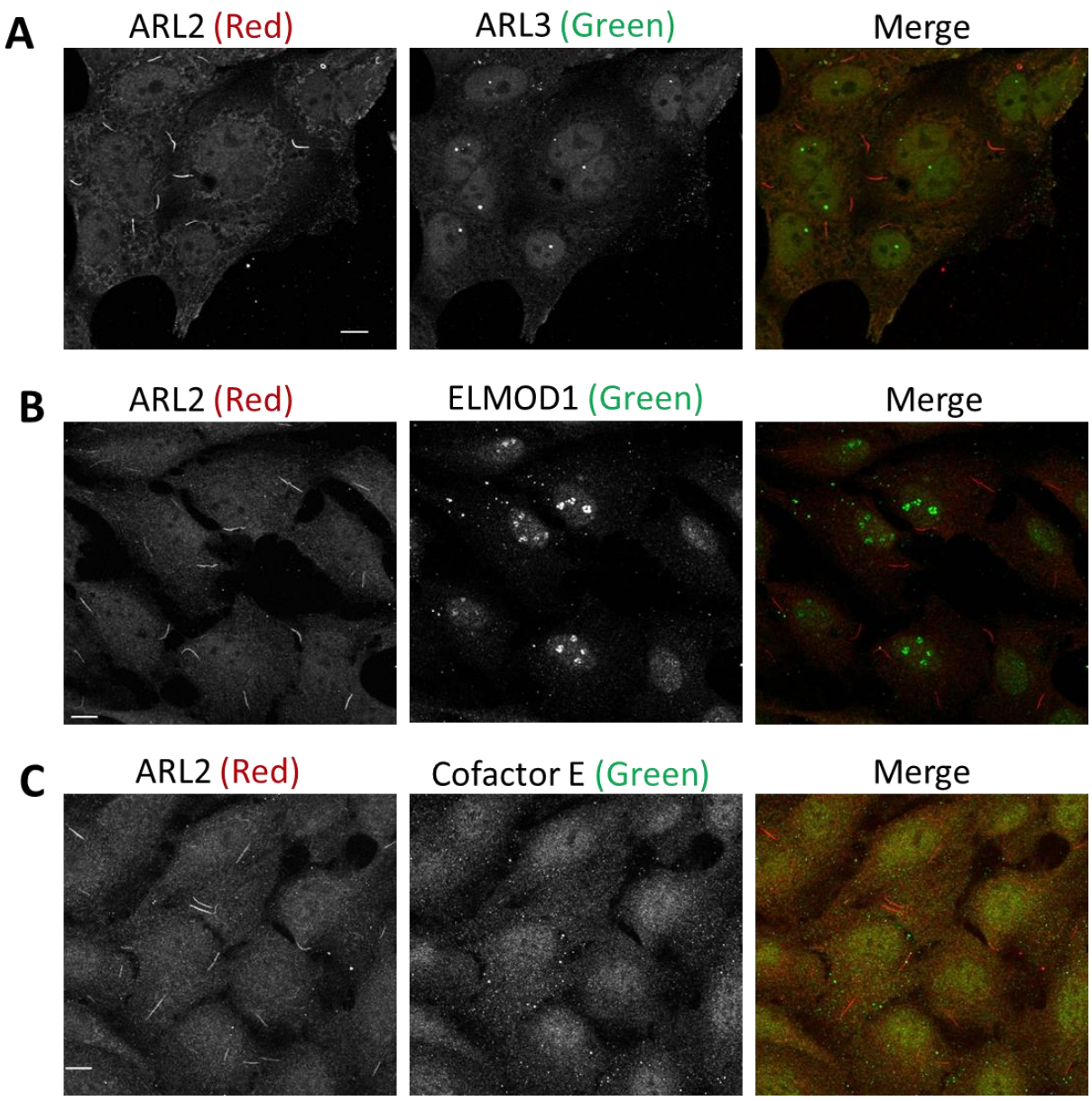

Figure S6: ARL3, ELMOD1, and Cofactor E do not co-localize with ARL2 at RRs. (**A**) IMCD3 cells were treated with 1 μM MPA for 2 hr, fixed, and co-stained for ARL2 (left) and ARL3 (middle). 2D-projections of z-stacks are shown. Scale bar = 10 μm. (**B**) NRK cells were treated with 1 μM MPA for 2 hr, fixed, and co-stained for ARL2 (left) and ELMOD1 (middle). 2D-projections of z-stacks are shown. Scale bar = 10 μm. (**C**) NRK cells were treated with 1 μM MPA for 2 hr, fixed, and co-stained for ARL2 (left) and Cofactor E (middle). 2D-projections of z-stacks are shown. Scale bar = 10 μm.

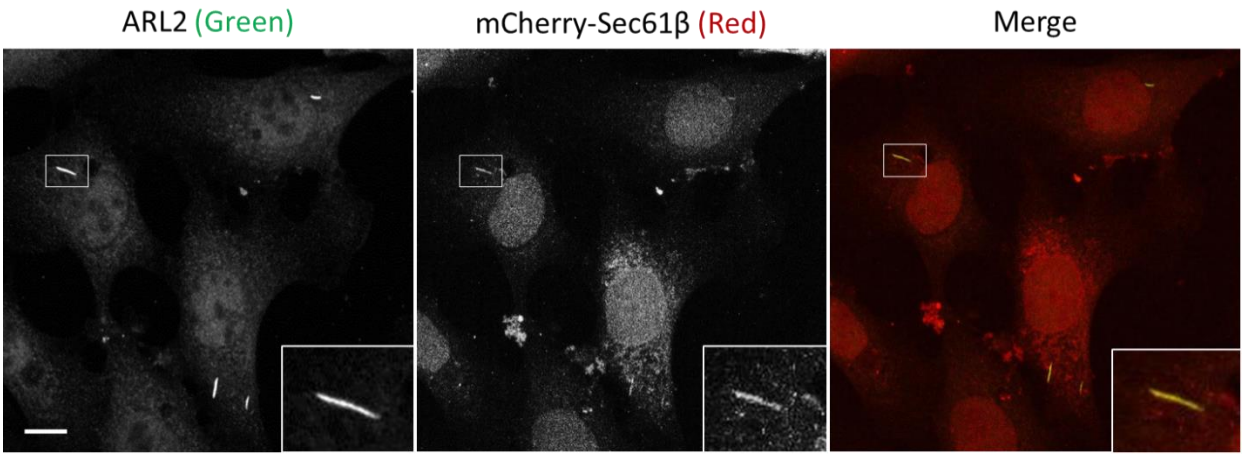

Figure S7: mCherry-Sec61β co-localizes with RRs. IMCD3 cells were transfected with plasmid expressing mCherry-Sec61β (middle) as described under Methods, then fixed and stained for ARL2 (left). 2D-projections of z-stacks are shown. Scale bar = 10 μm. Inset shows a zoomed-in version of an individual rod.

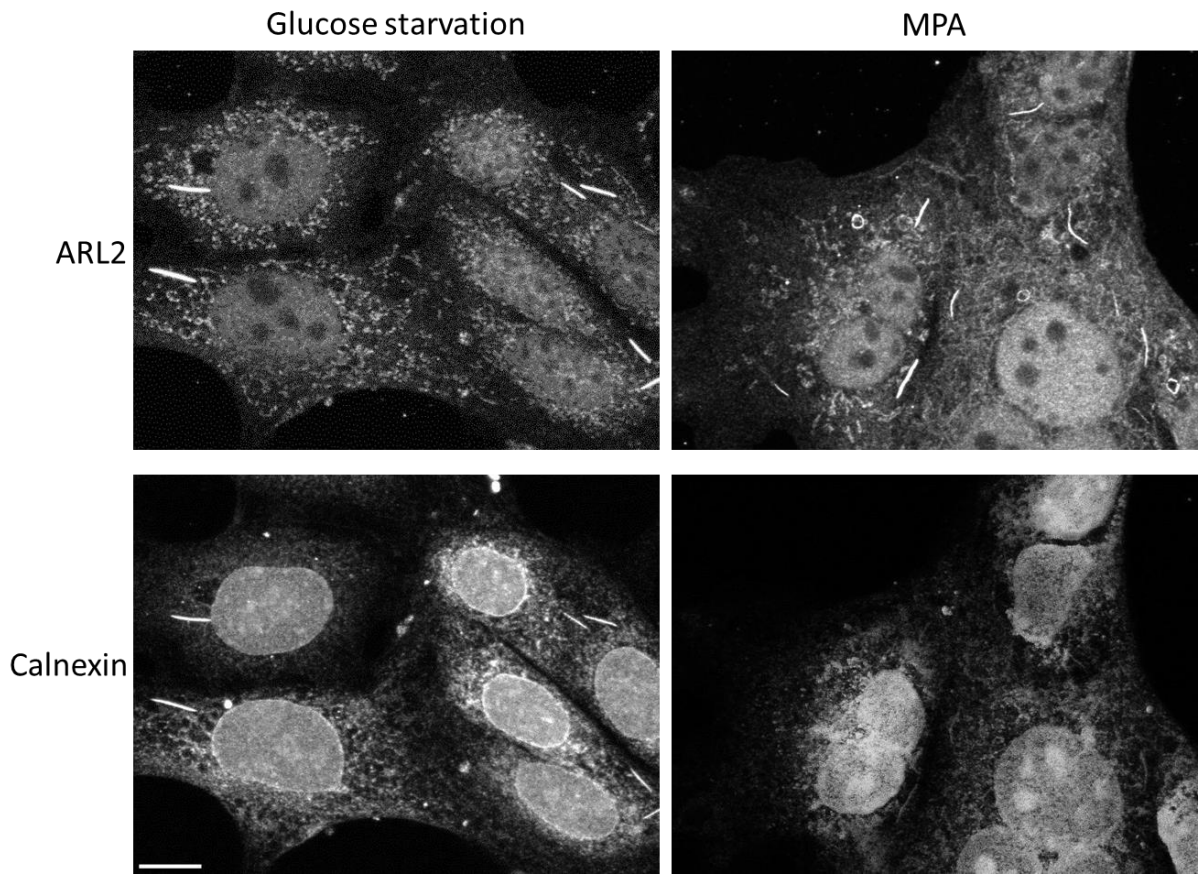

Figure S8: Calnexin staining at RRs is more apparent after glucose starvation than MPA-treatment. IMCD3 cells were grown under glucose starvation conditions for 24 hr (left) or treated with 1 μM MPA for 2 hr (right), fixed, and co-stained for ARL2 (top) and calnexin (bottom). Images were collected and processed the same at every step for both conditions. 2D-projections of z-stacks are shown. Scale bar = 10 μm.

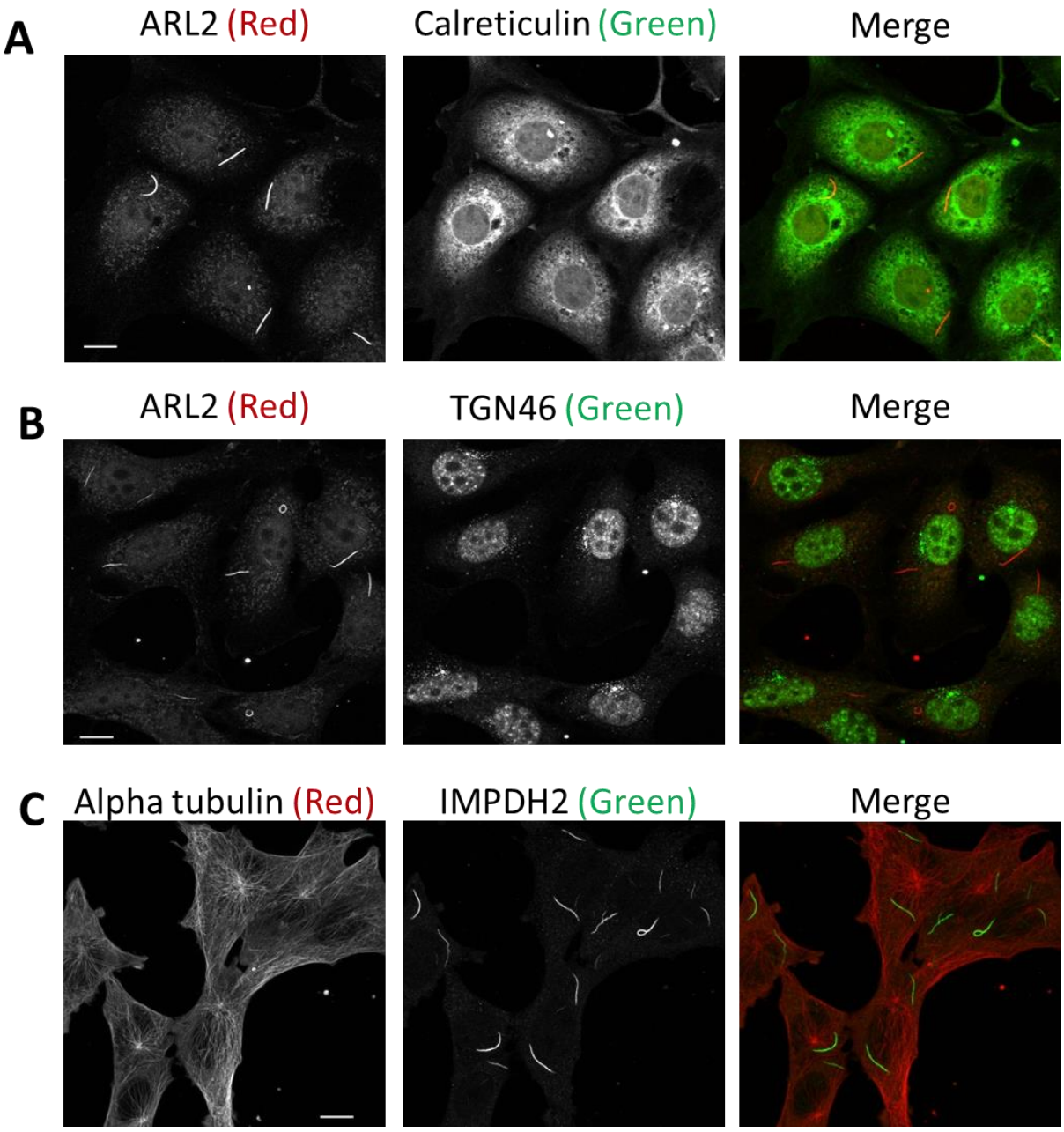

Figure S9: Calreticulin, TGN46, and α-tubulin do not co-localize with ARL2 or IMPDH2 at RRs. (**A**) IMCD3 cells were glucose-starved for 24 hr, fixed, and co-stained for ARL2 (left) and calreticulin (middle). 2D-projections of z-stacks are shown. Scale bar = 10 μm. (**B**) IMCD3 cells were glucose-starved for 24 hr, fixed, and co-stained for ARL2 (left) and TGN46 (middle). 2D-projections of z-stacks are shown. Scale bar = 10 μm. (**C**) MEFs were treated with 1 μM MPA for 2 hr, fixed, and co-stained for α-tubulin (left) and IMPDH2 (middle). 2D-projections of z-stacks are shown. Scale bar = 10 μm.

Chapter 6: Discussion

Summary

Mitochondria

Mitochondria are essential organelles involved in a variety of cellular processes. The function of mitochondria is directly impacted by their shape which is highly dynamic. Some of the key players in mitochondrial fission and fusion have been identified and characterized (1-5). While some regulatory mechanisms have also been elucidated (6-12), our understanding of the regulation of mitochondrial morphology remains sparse. Work from our lab previously identified ARL2 and ELMOD2 as potential novel regulators of mitochondrial morphology (13-15).

In chapter 2, Laura Newman and I developed a method to study the function of ARL2 localized to specific compartments of mitochondria. We utilized N-terminal tags derived from OCT or SMAC to drive ARL2 or GFP to the matrix or IMS, respectively. Because the matrix and IMS are very small cellular compartments, overexpression may saturate these areas. To address this, we used a series of truncated pCMV promoters (14,16,17) to attenuate expression of ARL2 or GFP. The combination of truncated promoters and mitochondrial localization tags has proved to be a useful tool in our studies of ARL2's role in mitochondria. They may also be useful to other researchers for similar studies and we have placed the plasmids in Addgene for this purpose.

In chapter 3, Laura Newman and I followed up on the observation that the endogenous, mitochondrial staining of ARL2 and ELMOD2 noticeably changed in intensity under a variety of conditions. With a few exceptions, ARL2 and ELMOD2 responded the same way to changes in growth conditions, providing further evidence of ARL2 and ELMOD2 functioning in the same pathway at mitochondria. We observed an increase in the staining intensity of ARL2 and ELMOD2 following serum or glucose starvation, increased time after plating (ARL2 only), treatment with several mitochondrial poisons (also ARL2 only) and loss of MFN2 (MFN2-null or DKO MEFs). We also observed a decrease in the mitochondrial staining intensity of ARL2 and ELMOD2 as cells became more dense. These

changes in staining intensity suggest that ARL2 and ELMOD2 may be subject to regulated import into mitochondria in response to certain stressors. These observations (particularly changes related to density and time after plating) also proved valuable in our imaging studies of ARL2 and ELMOD2, allowing us modulate mitochondrial staining intensity based on growth conditions. The increase in ARL2 and ELMOD2 staining under glucose or serum starvation conditions (two conditions that lead to mitochondrial elongation) in particular may suggest a role for ARL2 and ELMOD2 in stress-induced hyperfusion (SIMH). The fact that ARL2 and ELMOD2 staining increases in response to loss of MFN2 specifically is also interesting given that MFN2 has additional signaling functions in addition to its role in mitochondrial fusion. This provides further evidence that ARL2 and ELMOD2 are involved not only in the regulation of mitochondrial morphology, but in signaling between mitochondria and other parts of the cell.

In chapter 4, I focused on the role of ELMOD2 in mitochondrial morphology. Before this work, we established that ARL2 promotes mitochondrial fusion from the IMS upstream of the mitofusins. We also observed by SIM that ARL2 and the mitofusins localize to regularly-spaced puncta along mitochondria. In my studies of ELMOD2 I found that ELMOD2 also functions upstream of the mitofusins to promote fusion. I also confirmed that ELMOD2 is indeed acting downstream of ARL2 in this pathway. This adds to our understanding of a novel regulatory mechanism for mitochondrial fusion. Whereas previous studies focused on ARL2 individually, the addition of ELMOD2 provides the beginnings of a true pathway. Importantly, ARL2 and ELMOD2 are, so far, the only proteins found to regulate the mitofusins from within the mitochondria and are the only ones that regulate both MFN1 and MFN2. I also further studied the mitochondrial localization of ELMOD2 by gated stimulated depletion (gSTED) microscopy. I found that ELMOD2 aligns to puncta with the same periodicity as ARL2 and that these puncta align with the mitofusins. Additionally, I showed that ELMOD2 puncta also align with the miros. These data suggest ARL2, ELMOD2, and the mitofusins may form a novel complex involved in mitochondrial fusion and that the miros may also be a part of this complex, linking regulation of

mitochondrial morphology to mitochondrial motility. Such a complex has never been described before and could change the way we understand mitochondrial morphology and motility. This chapter also includes a description of the challenges in studying ELMOD2. There are several issues including low endogenous expression levels, limited sensitivity of the available antibodies, and ELMOD2's instability as a result of tagging at the N-terminus. Also, any N-terminal tagged ELMOD2 that manages to express does not localize properly (*i.e.* SMAC-ELMOD2 only partially localizes to mitochondria). Despite these challenges, the studies of ELMOD2 in mitochondria were possible thanks to my selection of the proper cell lines and growth conditions, use of mouse ELMOD2 in place of human ELMOD2 to improve expression levels, and other protocol optimizations.

Rods and Rings

IMPDH is the primary component of RRs and inhibition of IMPDH leads to robust induction of RR formation. For these reasons, RRs are thought to be involved in guanine nucleotide metabolism because IMPDH catalyzes the rate-limiting step in *de novo* synthesis of guanine nucleotides. Aside from this, little is known about the components or functions of RRs. The only confirmed proteins at RRs are IMPDH and perhaps CTPS, although results with CTPS are inconsistent (18). To date, RRs have been induced either through direct IMPDH inhibition or treatments that indirectly impede IMPDH function by inhibiting the pathway upstream of IMPDH.

In chapter 5, I detailed my study of RRs. Upon observing that ELMOD2 and ARL2 localize to large cellular structures, I confirmed that these structures are RRs. I observed that TBCD (tubulin binding cofactor D) localizes to RRs as well. Until now, RRs have typically been described as polymers of IMPDH. The fact that ARL2 and a subset of its binding partners localize to RRs is exciting because this suggests that RRs are more complicated than simple IMPDH polymers and that they may be linked to cell signaling and regulation by other parts of the cell. It is particularly interesting that ARL2, a GTPase regulated by GDP/GTP, localizes to RRs which appear to be very important for guanine nucleotide

metabolism. One reason ARL2 localizes to RRs could be to sense alterations in guanine nucleotide pools and signal to other parts of the cell accordingly.

I also observed that several resident ER proteins localize to RRs and that a membrane can be seen along the edge of a high percentage of RRs by EM. This adds a further layer of complexity to RRs, suggesting that the ER or a membrane derived from the ER can be associated with RRs. Notably, no one has reported an association between RRs and a membrane before. This not only adds to the list of proteins that associate with RRs but implies that RRs interact directly with other organelles such as the ER. I also demonstrated that RRs can be induced by treatment with AICAR or glucose starvation. This is the first time either of these conditions were shown to affect RR formation. AICAR is a metabolite upstream of IMP (we confirmed that the activity of AICAR is independent of AMPK), so it's likely that it causes an alteration in nucleotide pools that promotes RR formation. Glucose impacts many pathways within the cell (including nucleotide synthesis), so there are various possible ways that glucose starvation impacts RR formation. Each of these inducers are significant because neither of them inhibit IMPDH. Not only are these novel mechanisms of RR induction, they provide a way to promote RR formation without IMPDH inhibition, potentially allowing for the study of uninhibited IMPDH activity within RRs.

In this chapter I also demonstrated compelling evidence that guanine nucleotide pools are a primary factor in RR formation. Reversal or prevention of RR formation following addition of guanosine has been previously demonstrated (19-22). By using fibroblasts from patients with loss of function mutations in HGPRT (the enzyme necessary for salvage of guanosine), I showed that guanosine can only prevent RR formation when the salvage pathway is functional, meaning that the salvage pathway can compensate for inhibition of the *de novo* pathway.

Finally, I demonstrated further evidence that cytoophidia and RRs are different structures. I showed that ARL2 only consistently co-localizes with RRs and not cytoophidia (consistent with ARL2 associating with proteins involved in guanine nucleotide synthesis as opposed to pyrimidine synthesis)

and that AICAR and glucose starvation induce RR formation but not cytoophidia formation. These results in combination with data from others showing that various RR inducers do not induce cytoophidia and that cytoophidia and RRs do not consistently overlap (18) suggest that RRs and cytoophidia are different, but possibly related, structures. This is important because RRs and cytoophidia are often described as the same structures. The understanding that they are not the same structure will be fundamental to determining the roles of both RRs and cytoophidia.

Future directions

Mitochondria

There are still outstanding questions concerning ELMOD2 and the pathway it acts in at mitochondria and other areas of the cell. At mitochondria specifically, the precise location that ELMOD2 acts from has not been determined. Because ELMOD2 appears to be inside mitochondria based on high resolution imaging, and ARL2 acts from the IMS, we hypothesize that ELMOD2 also acts from the IMS. We attempted to confirm this using the tools developed in chapter 2, but N-terminal tagging of ELMOD2 leads to rapid degradation of the protein. To address this, it may be possible to use expression of a truncated ELMOD2 (ELMOD2's MLS is predicted to be near its N-terminus) or mitochondrial fractionation to more precisely determine ELMOD2's location of action.

Determining ELMOD2's sub-mitochondrial location would be part of further fleshing out the pathway involving ELMOD2, ARL2, and mitochondrial fusion. We still do not know whether ARL2/ELMOD2 interact directly or indirectly with the mitofusins, and if the interaction is indirect, what protein(s) they're acting through. We also don't know what acts upstream of ARL2 or what other proteins may be part of the potential complex involved in regulation of mitochondrial fusion. In an attempt to identify other components of this complex, I used the APEX2 protein proximity assay developed by Alice Ting (23-25). The results of this screen did not turn up likely candidates, but the results are available if they ever become relevant in the future. Another potential approach to identify other proteins involved in

this complex or pathway is crosslinking co-immunoprecipitation with ARL2, ELMOD2, or the mitofusins. However, this would be technically challenging due to the low levels of expression and multiple localization sites. For proteins that we suspect may be part of a complex with ARL/ELMOD2 such as the mitofusins or miros, other approaches such as proximity ligation assays can be carried out to determine whether or not the interaction between ARL2/ELMOD2 with these proteins is direct or indirect.

The ELMOD2-null MEFs will likely serve as a powerful tool to understand the role of ELMOD2 at mitochondria as well as other cellular locations. These cells have already been used to confirm that ELMOD2 is functioning downstream of ARL2 at mitochondria (chapter 4). There are a wide variety of assays that assess mitochondrial morphology and function that can be used to test these cells. Additionally, ELMOD2's localization is not limited to mitochondria. Rachel Turn is currently characterizing the ELMOD2-null MEFs and has found several obvious phenotypes aside from mitochondrial fragmentation. In our future studies, it will be important to tease apart the functions of ELMOD2 at different cellular locations. Expression of ELMOD2 that localizes to specific locations (via tagging) or is excluded from certain locations (via truncations or mutations) in these MEFs will help us to address this. Continued study of these MEFs will likely teach us more about the role of ELMOD2 at various parts of the cell and how cell signaling between these parts is regulated.

Rods and Rings

RRs have not been extensively studied, so there are many questions remaining. One question is: what role do RRs play and how do they accomplish it? There is evidence supporting a link between RRs and guanine nucleotide metabolism; however, the fact that the ER, ARL2, and a subset ARL2 binding partners localize to RRs suggests that RRs are considerably more complex than previously thought. The more we know about the make-up of RRs, the more we'll be able to understand their role in the cell. Thus, determining other components of RRs would be extremely informative. There have not yet been extensive

attempts to determine the components of RRs and there are various ways this question could be tackled (protein proximity assays, co-immunoprecipitation, etc.).

We also do not know the mechanism(s) by which RRs are regulated. There is strong evidence supporting the link between RRs and nucleotide metabolism, particularly guanine nucleotide pools. It has been suggested that RRs form in response to a decrease in guanine nucleotides in an attempt to ramp-up guanine nucleotide synthesis (26). However, my results using AICAR and glucose starvation make things less clear (chapter 5). There is no obvious reason that AICAR addition or glucose starvation would impair the function of IMPDH or decrease guanine nucleotide pools. In fact, when we analyzed the nucleotide levels in cells treated with AICAR compared to controls or MPA-treated cells, there was large drop in guanine nucleotides in MPA-treated cells but no change in guanine nucleotide levels in AICAR-treated cells compared to controls. This suggests that the trigger for RR formation is more complicated than a simple drop in guanine nucleotide levels.

The finding that the ER or an ER-derived membrane associates with RRs is entirely novel. We do not know the exact nature of the membrane or how and why the membrane associates with RRs. We observed that the membrane appears to only associate with mature RRs nearly an hour after induction begins (chapter 5). This suggests that the membrane is not necessary for the initiation of RR formation but may be involved in RR stability. Also, our IF and EM data are not consistent in terms of either the percentage of RRs adjacent to ER or what portion of RRs are associated with a membrane (chapter 5). It will be important to hash out these inconsistencies (perhaps through high-resolution IF) to better understand the role of the membrane at RRs.

Finally, although we have determined that ARL2 and some of its binding partners localize to RRs, we do not know what role they play there. I tested the localization of many other ARF family members and ARL2 binding partners and found no evidence of co-localization with RRs (chapter 5), suggesting that there is specificity to the interaction between RRs and ARL2/ELMOD2/TBCD. ARL2 recruits to

RRs before the membrane but after RRs begin to take on a more mature shape (chapter 5). This implies that ARL2 is not necessary for the nucleation or initial formation of RRs but may be involved in RR elongation, recruitment of other RR components, association of the membrane, and/or RR stability. Some preliminary *in vitro* data from the Reines lab suggests that ARL2 promotes the oligomerization of IMPDH providing more support for the idea that ARL2 promotes RR elongation and/or stability. However, more work is needed to confirm these roles as well as any other potential functions of ARL2, ELMOD2, and TBCD at RRs. Further *in vitro* studies such as reconstitution of RR formation may help us understand more. We also have ELMOD2-null cells, ELMOD2 and ARL2 siRNA, and dominant mutants of ARL2 which will be helpful tools in understanding the role of ARL2 and its binding partners at RRs.

Concluding remarks

Although the key components involved in mitochondrial morphology have been characterized, much remains unknown about the regulation of these proteins. The understanding of how mitochondrial shape is regulated is important for our fundamental understanding of how mitochondria work, which is applicable to diseases associated with mutations in specific mitochondrial proteins as well as more complex diseases linked to mitochondrial dysfunction (27-37). Similarly, although there are hypotheses about the function and regulation of RRs, very little is known about the role RRs play in the cell and what pathway(s) they're involved in. This is despite the fact that RRs are a conserved feature across species and cell types (19,38-45) and form in response to some commonly prescribed drugs (20,22,38,39,46,47).

My studies of ARL2 and ELMOD2 have elucidated the role of ELMOD2 in mitochondrial fusion, further describing a new regulatory mechanism of mitochondrial fusion, possibly involving a novel protein complex (chapter 4). Laura Newman and I have set up the beginnings of a pathway that regulates both mitofusins from the IMS – a pathway with a site of action that has never been proposed before. I have also more extensively studied the potential complex of ARL2, ELMOD2, the mitofusins, and miros providing more compelling evidence of its existence and expanded upon its components and periodicity.

I have also completed studies of RRs concluding that their composition and regulation are considerably more complex than previously appreciated (chapter 5). Before my studies, RRs were described as simple polymers of IMPDH with little in the way of function aside from the possibility of gunanine nucleotide regulation. I have expanded this understanding, showing that RRs include ARL2, a specific subset of its binding partners, ER-associated proteins, and likely other components. I have also demonstrated that RR regulation is more complicated than simple IMPDH inhibition or a drop in guanine nucleotides. These findings change the way that RRs are understood especially in the context of signaling between RRs and other parts of the cell which will likely be very important in future studies of RRs by our lab and others.

It's likely significant that ARL2 and ELMOD2 localize to both mitochondria and RRs. Our lab and others have previously documented the various cellular locations and functions of ARL2 and ELMOD2 (**Figure 1**). We have previously suggested that the variety of ARL2 locations and functions is a result of ARL2's role in "higher order signaling" (48). Meaning that ARL2 is important for mediating cross-talk between disparate organelles to maintain cellular homeostasis. Expanding the role of ARL2 and ELMOD2 in mitochondrial fusion as well as describing an entirely new cellular localization for ARL2, ELMOD2, and TBCD further strengthens this idea. Ultimately, the more we understand about ARL2, other ARF GTPases, and their effectors, the better we will understand the basic biology of the cell which will be broadly applicable to our understanding of human health and disease.

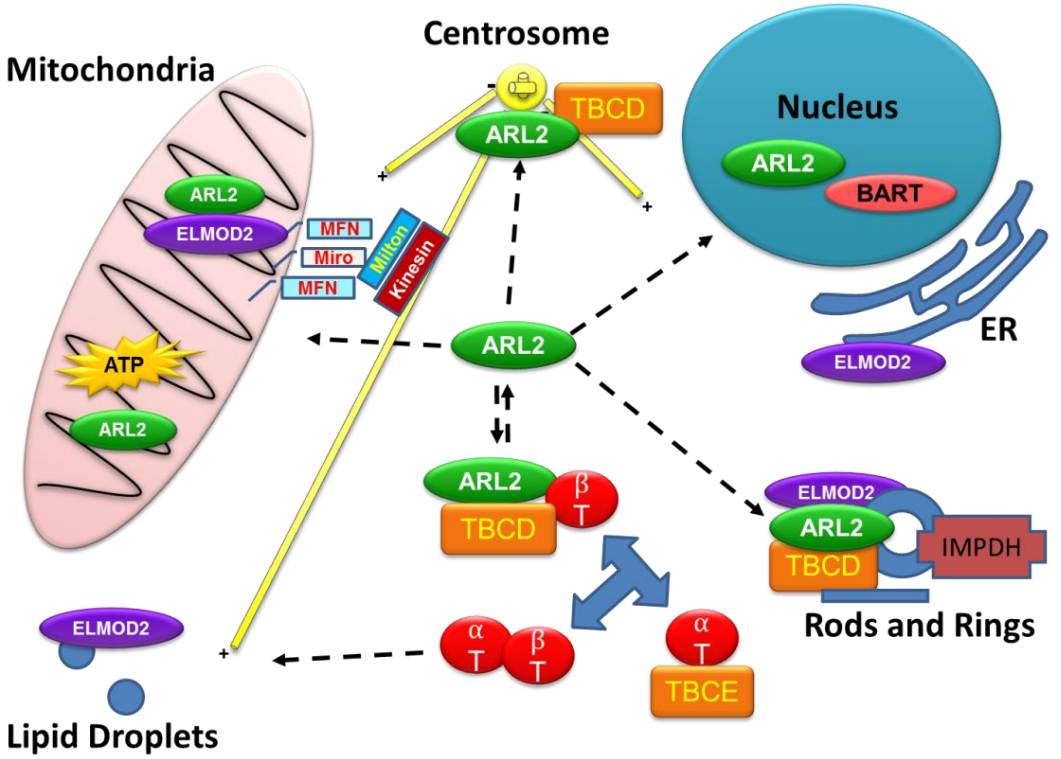

Figure 1: Currently established cellular locations of ARL2 and ELMOD2. ARL2 has been previously observed at mitochondria, the centrosome, cytosol, and the nucleus (13,14,49-51). The majority of ARL2 is in the cytosol where it interacts with TBCD (tubulin binding cofactor D) to regulate microtubule folding (49,51). ARL2 and TBCD are also involved in centrosome stability (50). ARL2 also plays a role at mitochondria regulating mitochondrial morphology and motility via the mitofusins and is also important for ATP production (13,14). ELMOD2 has been found to localize to the mitochondria, ER, and lipid droplets (13,17,52). My research has expanded our understanding of the role of ELMOD2 at mitochondria, placing it in a pathway downstream of ARL2 and upstream of the mitofusins, regulating mitochondrial fusion. It also shows a further association between ARL2, ELMOD2, the mitofusins, and the miros suggesting a role for ARL2 and ELMOD2 in mitochondrial motility. I have also determined another cellular localization for ARL2, ELMOD2, and TBCD – RRs. However, the role of these proteins at RRs remains undetermined. Adapted from Francis et al. (48).

References

1. Chen, H., Detmer, S. A., Ewald, A. J., Griffin, E. E., Fraser, S. E., and Chan, D. C. (2003) Mitofusins Mfn1 and Mfn2 coordinately regulate mitochondrial fusion and are essential for embryonic development. *The Journal of cell biology* **160**, 189-200
2. Eura, Y. (2003) Two Mitofusin Proteins, Mammalian Homologues of FZO, with Distinct Functions Are Both Required for Mitochondrial Fusion. *Journal of Biochemistry* **134**, 333-344
3. Koshiba, T., Detmer, S. A., Kaiser, J. T., Chen, H., McCaffery, J. M., and Chan, D. C. (2004) Structural basis of mitochondrial tethering by mitofusin complexes. *Science* **305**, 858-862
4. Zanna, C., Ghelli, A., Porcelli, A. M., Karbowski, M., Youle, R. J., Schimpf, S., Wissinger, B., Pinti, M., Cossarizza, A., Vidoni, S., Valentino, M. L., Rugolo, M., and Carelli, V. (2008) OPA1 mutations associated with dominant optic atrophy impair oxidative phosphorylation and mitochondrial fusion. *Brain* **131**, 352-367
5. Smirnova, E., Griparic, L., Shurland, D. L., and van der Bliek, A. M. (2001) Dynamin-related protein Drp1 is required for mitochondrial division in mammalian cells. *Molecular biology of the cell* **12**, 2245-2256
6. Tanaka, A., Cleland, M. M., Xu, S., Narendra, D. P., Suen, D. F., Karbowski, M., and Youle, R. J. (2010) Proteasome and p97 mediate mitophagy and degradation of mitofusins induced by Parkin. *The Journal of cell biology* **191**, 1367-1380
7. Eura, Y., Ishihara, N., Oka, T., and Mihara, K. (2006) Identification of a novel protein that regulates mitochondrial fusion by modulating mitofusin (Mfn) protein function. *Journal of cell science* **119**, 4913-4925
8. Hoppins, S., Edlich, F., Cleland, M. M., Banerjee, S., McCaffery, J. M., Youle, R. J., and Nunnari, J. (2011) The soluble form of Bax regulates mitochondrial fusion via MFN2 homotypic complexes. *Molecular cell* **41**, 150-160

9. Kumar, S., Pan, C. C., Shah, N., Wheeler, S. E., Hoyt, K. R., Hempel, N., Mythreye, K., and Lee, N. Y. (2016) Activation of Mitofusin2 by Smad2-RIN1 Complex during Mitochondrial Fusion. *Molecular cell* **62**, 520-531

10. Shutt, T., Geoffrion, M., Milne, R., and McBride, H. M. (2012) The intracellular redox state is a core determinant of mitochondrial fusion. *EMBO reports* **13**, 909-915

11. Pyakurel, A., Savoia, C., Hess, D., and Scorrano, L. (2015) Extracellular regulated kinase phosphorylates mitofusin 1 to control mitochondrial morphology and apoptosis. *Molecular cell* **58**, 244-254

12. Lee, J. Y., Kapur, M., Li, M., Choi, M. C., Choi, S., Kim, H. J., Kim, I., Lee, E., Taylor, J. P., and Yao, T. P. (2014) MFN1 deacetylation activates adaptive mitochondrial fusion and protects metabolically challenged mitochondria. *Journal of cell science* **127**, 4954-4963

13. Newman, L. E., Zhou, C. J., Mudigonda, S., Mattheyses, A. L., Paradies, E., Marobbio, C. M., and Kahn, R. A. (2014) The ARL2 GTPase is required for mitochondrial morphology, motility, and maintenance of ATP levels. *PloS one* **9**, e99270

14. Newman, L. E., Schiavon, C. R., Turn, R. E., and Kahn, R. A. (2017) The ARL2 GTPase regulates mitochondrial fusion from the intermembrane space. *Cellular logistics* **7**, e1340104

15. Muromoto, R., Sekine, Y., Imoto, S., Ikeda, O., Okayama, T., Sato, N., and Matsuda, T. (2008) BART is essential for nuclear retention of STAT3. *Int Immunol* **20**, 395-403

16. Morita, E., Arii, J., Christensen, D., Votteler, J., and Sundquist, W. I. (2012) Attenuated protein expression vectors for use in siRNA rescue experiments. *BioTechniques* **0**, 1-5

17. Suzuki, M., Murakami, T., Cheng, J., Kano, H., Fukata, M., and Fujimoto, T. (2015) ELMOD2 is anchored to lipid droplets by palmitoylation and regulates adipocyte triglyceride lipase recruitment. *Molecular biology of the cell* **26**, 2333-2342

18. Keppeke, G. D., Calise, S. J., Chan, E. K., and Andrade, L. E. (2015) Assembly of IMPDH2-based, CTPS-based, and mixed rod/ring structures is dependent on cell type and conditions of induction. *Journal of genetics and genomics = Yi chuan xue bao* **42**, 287-299

19. Gunter, J. H., Thomas, E. C., Lengefeld, N., Kruger, S. J., Worton, L., Gardiner, E. M., Jones, A., Barnett, N. L., and Whitehead, J. P. (2008) Characterisation of inosine monophosphate dehydrogenase expression during retinal development: differences between variants and isoforms. *The international journal of biochemistry & cell biology* **40**, 1716-1728

20. Calise, S. J., Carcamo, W. C., Krueger, C., Yin, J. D., Purich, D. L., and Chan, E. K. (2014) Glutamine deprivation initiates reversible assembly of mammalian rods and rings. *Cellular and molecular life sciences : CMLS* **71**, 2963-2973

21. Calise, S. J., Purich, D. L., Nguyen, T., Saleem, D. A., Krueger, C., Yin, J. D., and Chan, E. K. (2016) 'Rod and ring' formation from IMP dehydrogenase is regulated through the one-carbon metabolic pathway. *Journal of cell science* **129**, 3042-3052

22. Keppeke, G. D., Andrade, L. E., Grieshaber, S. S., and Chan, E. K. (2015) Microinjection of specific anti-IMPDH2 antibodies induces disassembly of cytoplasmic rods/rings that are primarily stationary and stable structures. *Cell & bioscience* **5**, 1

23. Fernandez-Suarez, M., Chen, T. S., and Ting, A. Y. (2008) Protein-protein interaction detection in vitro and in cells by proximity biotinylation. *Journal of the American Chemical Society* **130**, 9251-9253

24. Hung, V., Udeshi, N. D., Lam, S. S., Loh, K. H., Cox, K. J., Pedram, K., Carr, S. A., and Ting, A. Y. (2016) Spatially resolved proteomic mapping in living cells with the engineered peroxidase APEX2. *Nature protocols* **11**, 456-475

25. Lam, S. S., Martell, J. D., Kamer, K. J., Deerinck, T. J., Ellisman, M. H., Mootha, V. K., and Ting, A. Y. (2015) Directed evolution of APEX2 for electron microscopy and proximity labeling. *Nature methods* **12**, 51-54

26. Liu, J. L. (2016) The Cytoophidium and Its Kind: Filamentation and Compartmentation of Metabolic Enzymes. *Annual review of cell and developmental biology* **32**, 349-372

27. Kashatus, J. A., Nascimento, A., Myers, L. J., Sher, A., Byrne, F. L., Hoehn, K. L., Counter, C. M., and Kashatus, D. F. (2015) Erk2 Phosphorylation of Drp1 Promotes Mitochondrial Fission and MAPK-Driven Tumor Growth. *Molecular cell* **57**, 537-551

28. Chen, L., Gong, Q., Stice, J. P., and Knowlton, A. A. (2009) Mitochondrial OPA1, apoptosis, and heart failure. *Cardiovasc Res* **84**, 91-99

29. Shen, T., Zheng, M., Cao, C., Chen, C., Tang, J., Zhang, W., Cheng, H., Chen, K. H., and Xiao, R. P. (2007) Mitofusin-2 is a major determinant of oxidative stress-mediated heart muscle cell apoptosis. *The Journal of biological chemistry* **282**, 23354-23361

30. Ashrafian, H., Docherty, L., Leo, V., Towlson, C., Neilan, M., Steeples, V., Lygate, C. A., Hough, T., Townsend, S., Williams, D., Wells, S., Norris, D., Glyn-Jones, S., Land, J., Barbaric, I., Lalanne, Z., Denny, P., Szumska, D., Bhattacharya, S., Griffin, J. L., Hargreaves, I., Fernandez-Fuentes, N., Cheeseman, M., Watkins, H., and Dear, T. N. (2010) A mutation in the mitochondrial fission gene Dnm1l leads to cardiomyopathy. *PLoS genetics* **6**, e1001000

31. Song, M., Mihara, K., Chen, Y., Scorrano, L., and Dorn, G. W., 2nd. (2015) Mitochondrial fission and fusion factors reciprocally orchestrate mitophagic culling in mouse hearts and cultured fibroblasts. *Cell metabolism* **21**, 273-285

32. Lin, M. T., and Beal, M. F. (2006) Mitochondrial dysfunction and oxidative stress in neurodegenerative diseases. *Nature* **443**, 787-795

33. Abou-Sleiman, P. M., Muqit, M. M., and Wood, N. W. (2006) Expanding insights of mitochondrial dysfunction in Parkinson's disease. *Nat Rev Neurosci* **7**, 207-219

34. Stuppia, G., Rizzo, F., Riboldi, G., Del Bo, R., Nizzardo, M., Simone, C., Comi, G. P., Bresolin, N., and Corti, S. (2015) MFN2-related neuropathies: Clinical features, molecular pathogenesis and therapeutic perspectives. *J Neurol Sci*

35. Carelli, V., Ross-Cisneros, F. N., and Sadun, A. A. (2004) Mitochondrial dysfunction as a cause of optic neuropathies. *Prog Retin Eye Res* **23**, 53-89

36. Gottlieb, E., and Tomlinson, I. P. (2005) Mitochondrial tumour suppressors: a genetic and biochemical update. *Nat Rev Cancer* **5**, 857-866

37. Serasinghe, M. N., Wieder, S. Y., Renault, T. T., Elkholi, R., Asciolla, J. J., Yao, J. L., Jabado, O., Hoehn, K., Kageyama, Y., Sesaki, H., and Chipuk, J. E. (2015) Mitochondrial Division Is Requisite to RAS-Induced Transformation and Targeted by Oncogenic MAPK Pathway Inhibitors. *Molecular cell* **57**, 521-536

38. Carcamo, W. C., Satoh, M., Kasahara, H., Terada, N., Hamazaki, T., Chan, J. Y., Yao, B., Tamayo, S., Covini, G., von Muhlen, C. A., and Chan, E. K. (2011) Induction of cytoplasmic rods and rings structures by inhibition of the CTP and GTP synthetic pathway in mammalian cells. *PloS one* **6**, e29690

39. Ji, Y., Gu, J., Makhov, A. M., Griffith, J. D., and Mitchell, B. S. (2006) Regulation of the interaction of inosine monophosphate dehydrogenase with mycophenolic Acid by GTP. *The Journal of biological chemistry* **281**, 206-212

40. Willingham, M. C., Richert, N. D., and Rutherford, A. V. (1987) A novel fibrillar structure in cultured cells detected by a monoclonal antibody. *Experimental cell research* **171**, 284-295

41. Chen, K., Zhang, J., Tastan, O. Y., Deussen, Z. A., Siswick, M. Y., and Liu, J. L. (2011) Glutamine analogs promote cytoophidium assembly in human and Drosophila cells. *Journal of genetics and genomics = Yi chuan xue bao* **38**, 391-402

42. Ramer, M. S., Cruz Cabrera, M. A., Alan, N., Scott, A. L., and Inskip, J. A. (2010) A new organellar complex in rat sympathetic neurons. *PloS one* **5**, e10872

43. Noree, C., Sato, B. K., Broyer, R. M., and Wilhelm, J. E. (2010) Identification of novel filament-forming proteins in Saccharomyces cerevisiae and Drosophila melanogaster. *The Journal of cell biology* **190**, 541-551

44. Liu, J. L. (2010) Intracellular compartmentation of CTP synthase in Drosophila. *Journal of genetics and genomics = Yi chuan xue bao* **37**, 281-296

45. Ingerson-Mahar, M., Briegel, A., Werner, J. N., Jensen, G. J., and Gitai, Z. (2010) The metabolic enzyme CTP synthase forms cytoskeletal filaments. *Nature cell biology* **12**, 739-746

46. Keppeke, G. D., Prado, M. S., Nunes, E., Perazzio, S. F., Rodrigues, S. H., Ferraz, M. L., Chan, E. K., and Andrade, L. E. (2016) Differential capacity of therapeutic drugs to induce Rods/Rings structures in vitro and in vivo and generation of anti-Rods/Rings autoantibodies. *Clin Immunol* **173**, 149-156

47. Thomas, E. C., Gunter, J. H., Webster, J. A., Schieber, N. L., Oorschot, V., Parton, R. G., and Whitehead, J. P. (2012) Different characteristics and nucleotide binding properties of inosine monophosphate dehydrogenase (IMPDH) isoforms. *PloS one* **7**, e51096

48. Francis, J. W., Turn, R. E., Newman, L. E., Schiavon, C., and Kahn, R. A. (2016) Higher order signaling: ARL2 as regulator of both mitochondrial fusion and microtubule dynamics allows integration of two essential cell functions. *Small GTPases*, 0

49. Bhamidipati, A., Lewis, S. A., and Cowan, N. J. (2000) ADP ribosylation factor-like protein 2 (Arl2) regulates the interaction of tubulin-folding cofactor D with native tubulin. *The Journal of cell biology* **149**, 1087-1096

50. Shern, J. F., Sharer, J. D., Pallas, D. C., Bartolini, F., Cowan, N. J., Reed, M. S., Pohl, J., and Kahn, R. A. (2003) Cytosolic Arl2 is complexed with cofactor D and protein phosphatase 2A. *The Journal of biological chemistry* **278**, 40829-40836

51. Tian, G., Thomas, S., and Cowan, N. J. (2010) Effect of TBCD and its regulatory interactor Arl2 on tubulin and microtubule integrity. *Cytoskeleton* **67**, 706-714

52. East, M. P., Bowzard, J. B., Dacks, J. B., and Kahn, R. A. (2012) ELMO domains, evolutionary and functional characterization of a novel GTPase-activating protein (GAP) domain for Arf protein family GTPases. *The Journal of biological chemistry* **287**, 39538-39553